Fingerprinting the effect of airborne particulate matter via *in vitro* toxicoproteomics

Ngoc Quang Vuong

Thesis submitted to the Faculty of Graduate and Postdoctoral Studies
in partial fulfillment of the requirements for the degree of

Doctorate in Philosophy in Biochemistry
with specialization in Environmental Toxicology

Department of Biochemistry, Microbiology and Immunology
Faculty of Medicine
University of Ottawa

uOttawa

L'Université canadienne
Canada's university

Abstract

It is a challenge to assess the toxicity of environmental air particulate matter (PM) because PM composition is complex and variable, due to source contribution and atmospheric transformation. The goal of this study is to establish an *in vitro* model that can fingerprint the cytotoxic effects of airborne PM and their associated toxicity mechanisms. For this purpose, the cytotoxic effects of different reference and environmental particles on A549 human lung epithelial cells were characterized using multiple endpoint assays (cytokine release, LDH release, BrdU incorporation, cellular ATP and resazurin reduction) and proteomic analyses (2D-GE and MALDI-TOF-TOF-MS/MS). The results of this study demonstrated that proteomic analyses can distinguish the influences of different (carbon black and titanium dioxide) and similar (cristobalite and α-quartz) particles on various pathways in A549 cells (e.g., cell death and cell proliferation); and the cytotoxicity assays were capable of differentiating the phenotypic outcomes of the particles, which were complementary and supportive to pathway analyses. The ability of *in vitro* toxicoproteomics to differentiate the toxicity of environmental particles was tested on Ottawa urban dust (EHC-93) and its water-insoluble and soluble fractions. Findings from both cytotoxicity assays and proteomic analyses consistently indicated that the insoluble materials explained most of the toxic effects of the total PM. Interestingly, the toxic potency of EHC-93 total was not equal to the sum of its insoluble and soluble fractions, implying inter-component interactions between insoluble and soluble materials that may be reflected through synergistic or antagonistic *in vitro* responses. The insoluble and soluble fractions uniquely altered the expression patterns of the proteins involved in pathways such as cell death, cell proliferation and inflammation. For example, the insoluble and soluble fractions oppositely

altered the expression of the proteins (e.g., TREM1, PDIA3, PKM and ENO1) involved in an inflammatory response pathway in A549 cells, and the insoluble fraction was more potent than the soluble fraction in increasing secretion of pro-inflammatory cytokines MCP-1 and IL-8 from A549 cells. In essence, i*n vitro* toxicoproteomics is a valuable tool in relating the physicochemical characteristics of ambient air particles to their biological reactivity through understanding their mechanisms of toxicity.

Acknowledgements

First and foremost, I would like to thank my supervisor and collaborator/advisor, Drs. Renaud Vincent and Premkumari Kumarathasan, for the opportunity to conduct my Ph.D. study in their laboratories. This Ph.D. thesis would not have materialized if it was not for the opportunity that they gave me. I really appreciated the guidance and vision that they provided me to get through the obstacles in my study, as well as for the time and space that provided to me to think and to learn to become a scientist.

Secondly, I wanted to thank my Thesis Advisory Committee members Drs. Ajoy Basak, Alain Stintzi (also my co-supervisor), Subramanian Karthikeyan for their time and effort that they put in to assess my works and attended all the TAC meetings. Their feedback and suggestions were crucial in shaping my project.

Thirdly, I wanted to thank my collaborators and colleagues Drs. Dalibor Breznan, Errol Thomson, Susantha Mohottalage, and Marianne Ariganello for the expertise and insightful comments that they provided in my experimental works and/or writings that led to the successful publication of my works. I especially wanted to thank Dalibor for being there with me through thick and thin, and all the constructive criticism that he provided towards my writing and presentation, and thank you for being a constant motivating friend! I also wanted to thank the friendships and technical supports that were provided by Ms. Christine McKinnon-Roy and Alexandra Star, and Mr. Alain Filiatreault and Francesco DeRose.

Finally and importantly, I wanted to thank my wife (Arpornrad Sae-Wu), my parents (Hong Phan and Loc Vuong) and my sister (Nhung Vuong) for their constant support throughout my study.

Table of contents

List of abbreviations

2D-GE	Two-dimensional gel electrophoresis
A549	Type II alveolar human lung epithelial cell line
ACGIH	American Conference for Governmental Industrial Hygienists
ACN	Acetonitrile
ANOVA	Analysis of variance
APCI	Atmospheric-pressure chemical ionization
ATP	Adenosine triphosphate
BAP	Benzo(a)pyrene
BrdU	5-bromo-2'-deoxyuridine
CAAQS	Canadian Ambient Air Quality Standards
CARA	Clean Air Regulatory Agenda
CB	Carbon black
CID	Collision induce dissociation
CR	Cristobalite
DEP	Diesel emission particle
DMEM	Dulbecco's Modified Eagle's Medium
EC	Elemental carbon
ECD	Electron capture dissociation
EDX	Energy dispersive X-ray spectroscopy
EHC-93	Ottawa ambient PM collected from the Environmental Health Center in 1993
EI	Electron impact
ELISA	Enzyme-linked immunosorbent assay
ESI	Electrospray ionization
ETD	Electron transfer dissociation
FAB	Fast atom bombardment
FBS	Fetal bovine serum
FC	Fold-change
FWER	Familywise error rate
GI	Gastrointestinal
IARC	International Agency for Research on Cancer
ICP	Inductively coupled plasma
IPA	Ingenuity pathway analysis
IPG	Immobilized pH gradient
LDH	Lactate dehydrogenase
LTQ	Linear quadrupole ion trap
m/z	Mass to charge ratio
MALDI	Matrix-assisted laser desorption/ionization
MI	Min-U-Sil 5
MOWSE	Molecular weight search
MS	Mass spectrometry
MS/MS	Tandem mass spectrometry
MW	Molecular weight

NGS	Next generation sequencing
O_3	Ozone
PAGE	Polyacrylamide gel electrophoresis
PAH	Polycyclic aromatic hydrocarbon
pI	Isoelectric point
PM	Particulate matter
PM10	Particulate matter with aerodynamic diameter less than 10 μm
PM2.5	Particulate matter with aerodynamic diameter less than 2.5 μm
PMF	Peptide mass fingerprint
pXRD	Powder X-ray diffraction
Q/m	Charge to mass ratio
RNS	Reactive nitrogen species
ROS	Reactive oxygen species
RT-PCR	Reverse transcription-polymerase chain reaction
SA	Surface area
SDS	Sodium dodecyl sulfate
SEM	Scanning electron microscopy
SiO_2	Silica
SO_2	Sulphur dioxide
TCDD	2,3,7,8-tetrachlorodibenzo-p-dioxin
TFA	Trifluoroacetic acid
TiO_2	Titanium dioxide
TLV	Threshold limit value
TOF	Time of flight
TOF-TOF	Double time of flight
WHO	World Health Organization
XRE	Xenobiotic response element

List of figures

List of tables

Chapter I. Introduction

Environmental air particulate matter (PM) is a complex mixture of particles that consist of a wide range of sizes and physicochemical properties. Episodic rises in the level of airborne PM are known to cause adverse health effects, where the effects of the PM are associated with the physicochemical properties of its constituents. Thus, it is essential to identify the toxic components in ambient air PM and determine their mechanisms of effects in order to develop regulatory measures to reduce the negative health effects of air pollution. However, it is a challenge to fulfill this need because the particle composition in different geographical locations varies, depending on the local sources of release. Furthermore, it is also difficult to collect a sufficient quantity of PM that can be used for various *in vivo*, *in vitro* and physicochemical assessments. Thus, it is rare to find a study that can identify the toxic components of air particles and elucidate their pathways of effects. The goal of this Ph.D. research project is to establish an *in vitro* toxicoproteomic approach that can disentangle the toxic effects of airborne PM. In this study, a human lung epithelial cell line (A549) was used as a model to assess the cytotoxic effects of occupational health relevant particles such as titanium dioxide, carbon black, cristobalite and Min-U-Sil 5, and Ottawa urban air particles (EHC-93) and its fractionated water-soluble and insoluble components. The cytotoxic effects of these particles were assessed via multiple cytotoxicity assays (i.e., LDH release, BrdU incorporation, cellular ATP and resazurin reduction) and proteomic analyses (i.e., two-dimensional gel electrophoresis and MALDI-TOF-TOF-MS/MS). The results of this study demonstrate that *in vitro* toxicoproteomics is a valuable approach that is useful to investigate the molecular mechanisms that delineate the cytotoxic effects of airborne PM.

I.1. London Fog.

A classic example of air pollution is the London smog of December 1952. At the time, coal was heavily used as a heating source. The combustion of coal released black soot, tar and sulphur dioxide (SO_2) in the air, which created a thick layer of smog that spread through the city and persisted over a period of four days (December 5 to 8, 1952) (Scott, 1953). During this period, the levels of smoke and SO_2 were measured at 4.46 mg/m^3 and 1.339 parts per million, respectively, which were about 40 and 20 times higher than normal (Scott, 1953). These increases in the levels of smoke and SO_2 were correlated with a drastic increase of deaths in the city (Scott, 1953). The death toll in the aftermath of this event rose above 12000, and the reported causes of death were almost exclusively due to respiratory and cardiovascular complications such as lung cancer, bronchitis, pneumonia, pulmonary tuberculosis and heart diseases (Bell and Davis, 2001; Scott, 1953). This tragic event provided unequivocal evidence that air pollution is toxic and a serious health concern. Since then, the London Fog has been the cornerstone of air pollution research and development of regulatory guidelines on ambient air particulate matter.

I.2. Categorization of airborne particles based on physicochemical properties.

The environmental air contains a mixture of gases and particles with a wide range of origins, sizes and physicochemical properties. This study focused mainly on the toxic effects of environmental air particles. The level and composition of particles vary in an environment depending on the time of day, season and geographical location. These particles originate either from nature or human occurrences. The natural sources of ambient air particles include microorganisms, animals, plants, trees and stones (due to erosion), and occasional natural

disasters such as forest fires and volcanic eruptions. Most of the naturally occurring PM are endotoxins from bacteria (e.g., lipopolysaccharides), allergens from trees (e.g., pollens), and eroded mineral (e.g., silica) and metal (e.g., iron) particles from stones and rocks. Most man-made airborne pollutants are derived from farming, mining, construction, automobile exhausts and industrial releases, and domestic combustion of wood, gas, coal and oil. The three main types of anthropogenic airborne particles that are associated with adverse health outcomes are metals (e.g., zinc, iron and copper), minerals (e.g., asbestos and silica) and carbonaceous materials (e.g., pesticides, elemental carbon and polycyclic aromatic hydrocarbons) (see section I.4.).

Epidemiological and toxicological studies generally categorize ambient air particles into several groups based on their physical sizes: >PM10 are coarse particles that have aerodynamic diameter > 10 μm, PM10 and PM2.5 are small particles with cut-off aerodynamic diameters < 10 and 2.5 μm, and ultrafine particles are those particles with at least one dimension < 100 nm (also known as nano- or ultrafine particles). The reason to categorize the particles based on size is because physical size is an important parameter that dictates the deposition behavior and the potency of PM. The levels of PM10 and PM2.5 have been found to associate with adverse health outcomes in humans. For example, the levels of PM10 correlate positively with morbidity or mortality due to respiratory illnesses and lung cancer (Hales et al., 2012; Pope, 1989), and the levels of PM2.5 associated with morbidity and mortality due to cardiovascular diseases and/or lung cancer (Burnett et al., 2000; Dockery et al., 1993; Pope et al., 2011). According to World Health Organization (WHO) air quality guidelines in 2005, the annual mean levels of PM10 and PM2.5 should not exceed 20 and 10 $\mu g/m^3$ to meet healthy standard, and the 24-hour mean levels of PM10 and PM2.5 should not exceed 50 and 25 $\mu g/m^3$. The Canadian Ambient Air Quality Standards (CAAQS)

are more stringent than WHO, and are mainly focused on PM2.5. The new 2015 standard of CAAQS under section of 54 and 55 of the *Canadian Environmental Protection Act 1999* is to keep the level of outdoor PM2.5 below 10 and 28 μg/m^3 on annual and 24-hour bases, respectively(http://www.ec.gc.ca/default.asp?lang=En&n=56D4043B-1&news=A4B2C28A-2DFB-4BF4-8777-ADF29B4360BD).

Size is an important determinant of particle toxicity owed mainly to the basis of physics. First, physical size dictates the probability of distribution and penetration of particles in the respiratory tract (Raabe et al., 1988). Generally, most coarse particles are filtered out by the nose and nasal cavity (Landahl and Black, 1947; Landahl and Tracewell, 1949), while smaller particles are capable of penetrating deeper in the respiratory tract (Raabe et al., 1988). Second, smaller particles are present in greater number per mass unit as compared to larger particles. Third, smaller particles have greater surface area per mass unit, which permits greater surface interaction with the cells (see Figure 1 for a schematic illustration). For instance, inhalation of ultrafine carbon black (CB) particles (14 nm diameter) induced significantly greater pulmonary inflammatory and toxicity responses in rats as compared to its larger counterpart (260 nm diameter), based on mass (Sager and Castranova, 2009). However, when the doses were equalized based on surface area, the effects of the smaller CB particles were only slightly greater than the larger CB particles (non-significant difference) (Sager and Castranova, 2009). Similar observations were also found with other particles such as titanium dioxide (Oberdorster et al., 1994) and metallic nickel (Serita et al., 1999). The results of these studies suggest that surface area is a better dose metric to evaluate the toxic potency of a particle, especially a nano-particle, as compared to the conventional mass dose metric. In addition, these studies challenge the

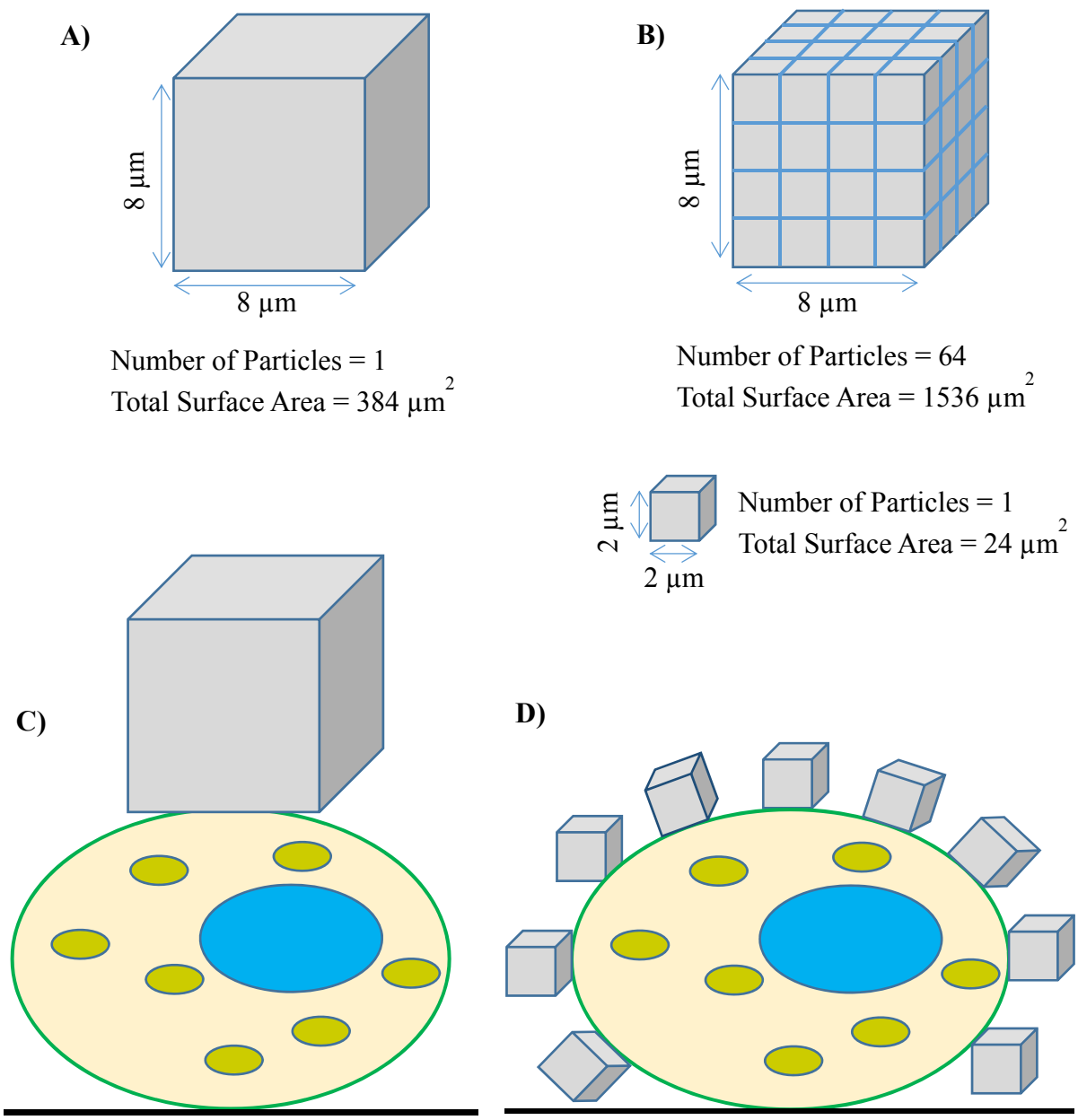

Figure I – 1. A schematic diagram that demonstrates the relationship between size and surface area of the particles.
Drawing of an 8 µm cubic particle (A). Drawings of a 2 µm cubic particle and an 8 µm cubic particle that was cut into 64 equal particles that are 2 µm in size (B). The interaction between a cell and one 8 µm cubic particle is illustrated (C). The interaction between a cell and nine 2 µm cubic particles is illustrated (D).

conventional mass dose metric that has been used to establish the threshold limit value (TLV) of a particle or substance.

It should be noted that size is not the only property that dictates the toxic potency of a particle. The shape, surface charge or surface coating can also contribute to its overall toxicity (Johnston et al., 2009; Oberdorster et al., 2005; Sun et al., 2015a; Zhang et al., 2012). Furthermore, the chemical properties of particles also play an important role in determining toxicity. The toxicity of particles with different chemical properties will be discussed later in Section I.4. In essence, the physicochemical properties of a particle contribute to its overall toxic potency.

I.3. Destinations of inhaled particles in a body.

Epidemiological studies indicate that exposure to environmental air pollution causes non-accidental morbidity and mortality (Burnett et al., 2000; Goldberg et al., 2013; Hales et al., 2012; Scott, 1953). Early studies focused on investigating the adverse health effects of air pollution in the respiratory and cardiovascular system, because the respiratory tract is the main route of entry of airborne PM into an organism. However, more recent data indicates that environmental air particles can also affect extra-pulmonary organs, such as brain, liver, spleen and kidney (see section I.3.3. below).

I.3.1. General entry, deposition and clearance of inhaled particles.

Upon nosal inhalation, the majority of the coarse particles greater than 1 μm can be filtered out by the nose and nasal cavity (Landahl and Black, 1947; Landahl and Tracewell, 1949). Most of the deposited particles in the nasal cavity can be quickly cleared from the nose by the action of nasal mucociliary clearance (Merkus et al., 1998; Proctor et al., 1973),

which allows the trapped particles to be sent to the gastrointestinal (GI) tract for excretion or directly expelled from the nose. Thus, inhaling through the nose helps to filter out a significant amount of particles that would not have been filtered out by mouth inhalation. Those inhaled particles that were not captured or filtered out by the nose can then enter the lower respiratory tract (tracheobronchial airways and lungs). There, deposited particles are cleared by the action of the mucociliary escalator, which sends the particles to the GI tract (Clarke and Pavia, 1980; Ferin, 1972). The deposited particles can also trigger inflammatory responses in the local tissue that recruit leukocytes such as neutrophils (Harmsen et al., 1987) and macrophages (Harmsen et al., 1985) to uptake the particles and move to the mucociliary escalator or local lymphatic nodes for clearance (Ferin, 1972). Although the clearance mechanisms of the respiratory tract are efficient, there is a limit to their clearance capacity. Therefore, exposures to high levels of environmental air PM can cause negative health effects (see sections I.3.2. and I.3.3. below).

I.3.2. Adverse effects of PM in the respiratory pulmonary system.

Exposure to air pollution is known to associate with the development or exacerbation of respiratory illnesses, such as bronchitis (Liu et al., 2014; Scott, 1953; Stocks, 1959), asthma (Canova et al., 2012; MacIntyre et al., 2014; Su et al., 2013), pulmonary fibrosis (Johannson et al., 2014) and lung cancer (Liu et al., 2014; Merlo et al., 1991; Pope et al., 2011; Siemiatycki et al., 1989; Stocks, 1959). The development or exacerbation of these respiratory illnesses can be explained by the toxic effects of the particles retained in the respiratory tract (see Section I.4. for more detail). As the respiratory tract is directly linked to the circulatory system, it is not a surprise that air pollution is also associated with adverse cardiopulmonary functions, such as hypertension, palpitation, atherosclerosis, myocardial

infarction and stroke (Chen et al., 2013). A plausible pathway that can explain how airborne particles can affect the cardiopulmonary system is the spill-over of the respiratory system to the circulation (Kumarathasan et al., 2015; Sun et al., 2008). For instance, Kumarathasan and colleagues recently reported that exposing rats to EHC-93 Ottawa urban dust via nose-only inhalation can induce inflammatory responses in the respiratory tract and can elevate the levels of plasma carboxyhemoglobin, endothelin-1, reactive oxygen species (ROS) and reactive nitrogen species (RNS) (Kumarathasan et al., 2015). Thus, exposures to airborne PM have been linked to the development or exacerbation of cardiopulmonary diseases.

I.3.3. Effects of air particles in extra-pulmonary organs.

More recent data indicates that the toxic effects of environmental air particles can extend beyond the cardiopulmonary system. For example, exposures to air pollution have also been associated with non-pulmonary complications, such as declined cognitive function (Ailshire and Crimmins, 2014; Jedrychowski et al., 2014; Julvez et al., 2007; Tonne et al., 2014) and increased risk of diabetes mellitus (Brook et al., 2013; Rao et al., 2015; Vora et al., 2014). A possible pathway to explain such systemic effects of environmental air PM is the translocation of the deposited particles away from the respiratory tract. For example, Oberdorster and colleagues demonstrated that inhalation of ultrafine TiO_2 particles leads to the accumulation of TiO_2 in the lymph nodes of rats (Oberdorster et al., 1994). Similarly, Kreyling et al., showed that inhaled 15 and 80 nm iridium particles (insoluble) translocate from the respiratory tract to the liver, spleen, heart and brain of rats (Kreyling et al., 2002). In addition, a recent study from our laboratory demonstrated that exposing rats to EHC-93 Ottawa urban dust and/or ozone (nose-only inhalation) can alter the expression of genes in various organs, including lung, heart, liver, kidney, spleen, pituitary and cerebral hemisphere

(Thomson et al., 2013). These findings support epidemiological data that the effects of environmental air particles indeed extend beyond the respiratory tract.

I.4. Toxic effects of different airborne particles.

Identifying the drivers of toxic potency and determining the mechanisms of their effects in airborne PM is important and useful in the development of regulatory measures to reduce the negative health effects of air pollution. Most of the anthropogenic particles fall into three main categories, namely, metal, mineral and carbonaceous material. This section will briefly review the impacts of some particles in these categories and some of their underpinning mechanisms of toxicity.

I.4.1. Metals.

Epidemiological studies from U.S. and Canadian cities showed that there is a strong correlation between the levels of metals in environmental air PM and negative health effects in humans (Burnett et al., 2000; Laden et al., 2000). Examples of the respirable metal particles that can be found in environmental air are Zn, Ni, Fe, Cu, Al, Mn, Pb, Co and Cd, and the levels of these metals vary depending on the local sources of emission (Thomson et al., 2015; Thomson et al., 2016; Vincent et al., 2001; Zhang et al., 2016). Some of these metals, such as Pb and Cd, are non-essential metals and they are known to be toxic to human. For example, Cd is classified as a human carcinogen by the International Agency for Research on Cancer (IARC) (IARC monographs volume 58, 1993). Inhalation of Cd causes lung cancer, as this metal can cause oxidative damage to DNA (e.g., single strand DNA breaks) (Hassoun and Stohs, 1996). Interestingly, essential metals such as Zn, Cu and Fe that act as cofactors for proper folding and/or activity of a broad number of proteins can also

cause adverse health effects at high levels. Since these metals can be found in ambient air particles collected from Ottawa (Vincent et al., 1997) and other locations in Canada (Thomson et al., 2016), they pose a potential health risk to the public. For example, human exposure to Zn dust or fumes can lead to pneumonitis or metal fume fever (Cooper, 2008). Our laboratory has identified that Zn is a water-soluble component in Ottawa urban dust (EHC-93) that can induce inflammation and lung injury in rats (Adamson et al., 2000). Each metal may possess specific mechanisms that lead to toxicity or carcinogenicity. However, the most common mechanism of toxicity for most metals is their ability to generate ROS or RNS through the Fenton reaction (Li et al., 2008; Trachootham et al., 2008). The Fenton reaction is the generation of hydroxyl radical from hydrogen peroxide in the presence of a metal (e.g., $Fe^{2+} + H_2O_2 \rightarrow Fe^{3+} + HO\bullet + HO^-$) (Fenton 1894). Increases in the level of ROS or RNS in cells can ultimately lead to oxidative modification of lipids (Esterbauer et al., 1991), proteins (Kobayashi et al., 2006) and DNA (Valko et al., 2006).

I.4.2. Minerals.

Minerals are abundantly present in the environment, and many minerals have been used in a broad range of applications worldwide. Unfortunately, excessive exposures to a number of mineral particles via inhalation are known to cause serious adverse health effects. For example, silica (SiO_2) is a known occupationally hazardous respirable particle. Chronic exposure to silica is primarily an occupational hazard for sand blasters, miners, brick workers and construction workers. However, silica (sand) is a common component in ambient air; hence, excessive exposure to silica particle is a general public health concern. According to IARC, silica is a group 1 human carcinogen (IARC, 1997), and the American Conference for Governmental Industrial Hygienists (ACGIH) indicated that silica has a low threshold limit

value (TLV) of 0.025 mg/m^3 (ACGIH, 2001). Exposure to silica is known to cause formation of scar tissue in the lungs, a condition known as silicosis (Cassel et al., 2008; Lee et al., 2013). The cytotoxicity of silica is likely due to its ability to activate the NLRP3 inflammasome (Cassel et al., 2008; Dostert et al., 2008; Hornung et al., 2008), stimulate the production of ROS (Cassel et al., 2008; Dostert et al., 2008), as well as trigger apoptotic and necrotic cell death (Cassel et al., 2008; Chao et al., 2001; Iyer et al., 1996; Joshi and Knecht, 2013).

Titanium dioxide (TiO_2) is a naturally occurring oxidized mineral form of titanium. Historically, TiO_2 was loosely used as a "negative control" for many toxicological studies because it was found to be relatively inert and was not considered as an occupational hazardous material (TLV = 10 mg/m^3) (ACGIH, 2001). However, the vastly increased application of TiO_2 in a number of products, including cosmetics, foods and medicines warranted more rigorous investigations of the safety of this mineral, especially nano-sized TiO_2 particles. Recent studies found that the toxicity of TiO_2 depends on various physicochemical parameters of the particles, including size, aggregation state, crystal phase and surface modification (Johnston et al., 2009).

I.4.3.Carbonaceous materials.

Soot or black carbon is an undesirable product of uncontrolled and incomplete combustion of organic materials such as wood, coal, diesel and cigarettes that results in the generation of varying amounts of elemental and organic carbon. These carbonaceous materials can cause adverse health effects in humans and animals. The toxic effects of organic carbon pollutants known as polycyclic aromatic hydrocarbons (PAHs) have been heavily investigated due to their presence in cigarette smoke and several well recognized

historic events. For example, Percivall Pott, an English surgeon, was the first to notice the high incident of scrotum cancer in chimney sweepers in London all the way back in mid 1700, and suggested a positive relationship between occupational cancer and environmental carcinogen (Brown and Thornton, 1957). The Seveso disaster in July 1976 in Italy was an accident from the Industrie Chimiche Meda Societa Azionaria that dispersed kilogram quantities of 2,3,7,8-tetrachlorodibenzo-*p*-dioxin (TCDD) and TCDD-like substances in the air (Bertazzi et al., 1998; Walsh, 1977). It resulted in the death of thousands of animals, the sacrifice of thousands more suspected exposed-animals (to prevent food chain contamination), and several hundred people suffered from skin lesions or chloracne (a painful and skin disfiguring condition due to chronic inflammation) (Bertazzi et al., 1998). Another incident is the use of TCDD in an attempted assassination of Viktor Yushchenko in 2004, who was campaigning for a Ukrainian presidential election. Although the dioxin poisoning did not kill him, he suffered severe inflammation in the liver, pancreas and intestines (Sterling and Hanke, 2005). He also suffered excruciating back pain over a month and developed chloracne that permanently disfigured him (Sterling and Hanke, 2005).

PAHs and TCDD are known to bind to the aryl hydrocarbon receptor (AHR) in the cytosol of cells. Upon ligand binding, the AHR undergo conformational changes to expose its nuclear localization sequence and translocate to the nucleus (Ikuta et al., 1998). There, the AHR dissociates from its inhibitory chaperones (Hsp90, P23 and ARA9) (Perdew, 1988; Kazlauskas et al., 1999; Ikuta et al., 1998; Carver et al., 1998; Seok et al., 2017) and binds to its transcription partner (ARNT) (Reyes et al., 1992; Seok et al., 2017). The ligand-AHR/ARNT complex activate various genes through binding to their promoter regions such as the xenobiotic response element (XRE) (Reyes et al., 1992) of xenobiotic metabolizing enzymes including cytochrome P450 1A1 (CYP1A1) and CYP1B1. The activated AHR

(ligand-AHR/ARNT complex) also binds directly to the promoter region of the antioxidant response element (ARE) of nuclear factor erythroid 2 p45-related factors (NRF2) (Beischlag et al., 2008), which can activate various antioxidant enzymes. Interestingly, the activation of NF-κB can also be induced by activated AHR or overexpression of AHR (Tsay et al., 2013). Finally, the activated AHR regulates itself by stimulating the expression of the AHR repressor (AHRR) (Gradin et al., 1999; Hankinson et al., 1985), where the AHRR competes with AHR to dimerize with ARNT (Gradin et al., 1999; Mimura et al., 1999). In summary, activation of the AHR can stimulate a large set of genes that have diverse functions in the cell. An earlier study from our laboratory showed that ambient air PM from various environments contain PAHs, and the particles from these environments can stimulate the expression of CYP1A1, as measured by the CAT-Tox [L] assay in HepG2 cell line (Vincent et al., 1997).

Accumulated data over the years suggest that the AHR plays an important role in carcinogenicity. Chronic exposure of animals to a low level of TCDD has is known to cause neoplasm (Kociba et al., 1979; Kociba et al., 1978; Van Miller et al., 1977). An organic extract of airborne particulate matter from Sapporo, Japan induced the expression of CYP1A1 and tumour development in $AHR^{+/+}$ mice upon dermal application; the extract neither induced the expression of CYP1A1 nor caused the development of dermal carcinoma in $AHR^{-/-}$ mice (Matsumoto et al., 2007). The levels of CYP1A1 protein in human lung tissues in smokers and ex-smokers are 2.6 and 3.2 times higher than never-smokers, respectively (Lin et al., 2003b). Similarly, the protein and mRNA levels of AHR (Lin et al., 2003b), CYP1A1 and CYP1B1 (Lin et al., 2003a) are higher in lung carcinoma cells as compared to normal cells. A few possible mechanisms have been proposed as to how the AHR mediates PAH-induced carcinogenicity. One of the mechanisms is that the activation of

AHR can increase the production of DNA adducts through up-regulation of CYP1A1 and CYP1B1. These enzymes convert PAHs into reactive intermediates (such as dihydrodiol epoxides) that can bind covalently to DNA and cause subsequent gene mutation (Denissenko et al., 1996; Puisieux et al., 1991).

AHR-independent mechanisms can also generate DNA adducts from PAHs (Kondraganti et al., 2003). Another possible mechanism for AHR to promote tumourigenesis is its ability to regulate NF-kB, a key protein that modulates the inflammatory response. However, the role of AHR in mediating pro-inflammatory responses is not clear. For example, transgenic mice that express the constitutively active form of AHR in keratinocytes were found to develop inflammatory skin lesions (Tauchi et al., 2005). On the other hand, AHR knockout mice were observed to have heightened lung inflammatory response to cigarette smoke (Thatcher et al., 2007). Thus, more investigation is required to clarify the role of AHR in the inflammatory response. Regardless of whether AHR can mediate PAH-induced pro-inflammatory response, ample evidence has shown that exposure to PAHs can stimulate pro-inflammatory responses. For example, it has been reported that benzo[a]pyrene (BAP) or diesel exhaust particles (which also contain BAP) can stimulate the expression (mRNA) and secretion (peptide) of the pro-inflammatory interleukin-8 (IL8) in cells in the respiratory system, such as macrophages (Podechard et al., 2008), bronchial epithelial cells (Kawasaki et al., 2001) and lung epithelial cells (Pei et al., 2002). In short, PAHs are air pollutants that have carcinogenic properties.

While the toxic and carcinogenic effects of PAHs in humans and animals have been well documented, information on the health effect of elemental carbon (EC) is much less clear. Aside from a few reports showing that there is a positive correlation between the level of EC in ambient air and cardiovascular health risk in humans (Bell, 2012; Levy et al., 2012;

Schneider et al., 2010) or animals (Wagner et al., 2014), there is very little data on the toxicology of EC. However, the toxicity of man-made EC powder known as carbon black (CB) has been used as a surrogate for EC in previous studies (Donaldson and Stone, 2003). Carbon black is an industrial product generated from controlled pyrolysis of hydrocarbons that produces mainly elemental carbon, where only trace amounts of PAHs and inorganic materials could be found (MJ et al., 2003; Watson and Valberg, 2001). Carbon black should not be confused with black carbon (soot), which is an undesired by-product of uncontrolled combustion that contains varying amounts of EC, organic materials and metals (Long et al., 2013; Watson and Valberg, 2001). Carbon black is commonly used as a black pigment in automobile tires, rubbers, paint, coating and printing inks. Exposure to CB is known to aggravate pulmonary inflammation in humans (Zhang et al., 2014) and mice following inhalation (Saputra et al., 2014; Zhang et al., 2014), and it causes toxicity to cells *in vitro* (Lee et al., 2011; Mroz et al., 2007; Sahu et al., 2014; Yamawaki and Iwai, 2006).

I.5. Factors that influence the final toxicological outcomes of ambient air particles.

Examining and comparing the adverse health effects of ambient air particles from different environments is complicated and requires careful interpretation. For example, the combined toxic effect of two particles in a cell or animal is often not equal to the sum of the effects of two individual particles. Moreover, a particle can be modified in the atmosphere by pressure, heat, UV light or the presence of other particles. Finally, the susceptibility in a population can vary depending on the age, genetic makeup and health state of the individuals in question. This section will briefly review the notable factors that can contribute to the final adverse health outcomes of exposure to urban air particles.

I.5.1. Interaction effect.

When two or more particles are acting in an organism, which represents a more realistic exposure scenario outside of a laboratory, their effects as a whole are often unpredictable because the particles themselves can interact with each other or the biological effects can interact in the organism to antagonize or synergize the final effect. Antagonism occurs when the total toxic effect of two or more particles is less than the sum toxic effects the individual particles. An example of an antagonistic effect is arsenic and selenium, where the combined poisonous doses of As and Se together can neutralize the toxic effects of the individual agents (Kenyon et al., 1997; Levander, 1977; Moxon, 1938). Synergism occurs when the combined toxic effect of two or more particles is greater than the sum toxicities of the individual particles. An example of a synergistic effect is that the use of paraquat (a herbicide) and maneb (a fungicide) together, but not alone, increases the risk of developing Parkinson's disease in humans (Costello et al., 2009; Wang et al., 2011). In addition, treating mice with these two agents together enhances the development of Parkinson's disease (Desplats et al., 2012; Gupta et al., 2010). In our laboratory, we demonstrated that ozone (O_3) or Ottawa urban dust (EHC-93) caused only mild or no injury to rat lungs, respectively; co-exposure of rats to these two pollutants caused significantly greater lung injury than either to O_3 or EHC-93 alone (Adamson et al., 1999; Bouthillier et al., 1998; Vincent et al., 1997a). Therefore, the toxic effect of a complex mixture of airborne PM cannot be predicted.

I.5.2. Atmospheric transformation.

When a particle is emitted into the air, its physical and chemical properties can be modified by light, temperature, pressure, humidity and/or interactions with gases and with other PMs in the atmosphere. For example, Zielinska and colleagues have shown that there is

a difference in toxicity in animals that were exposed to diesel emission particles (DEPs) in their pristine form versus atmospheric-transformed DEPs, where the aged DEPs were found more toxic than their pristine counterparts (Zielinska et al., 2010). Another example came directly from the results in the present study, which show that the cytotoxic potency of EHC-93 Ottawa urban dust as a whole is less than its water-insoluble components, where the water-soluble materials have been stripped off (see Figure V – 2 in Chapter 5). In addition, Sun et al. demonstrated that the inflammatory effects of amorphous nanosilica particles can be reduced through calcination and metal doping (Sun et al., 2015). Thus, the toxic effects of ambient particles can be modified in the atmosphere, which has the capacity to alter the physicochemical properties of the particles.

I.5.3. Biological susceptibilities.

It has been established that the effects of environmental air pollution within a population are not homogeneous due to a number of biological factors, which include age, health state and genetic makeup. For example, Pope reported that the levels of PM10 near a steel mill in Utah Valley were more strongly correlated with hospital admissions due to bronchitis and asthma in children than in adults (Pope, III, 1989). On the other hand, increased concentration of ambient particles was found to increase mortality in elderly individuals suffering from chronic coronary artery diseases (Goldberg et al., 2001). These observations suggested that the susceptibility of humans to air pollutants can depend on their age and/or developmental state. Furthermore, individuals with pre-existing health complications, such as asthma, lung cancer, heart disease or diabetes are at greater risk than their healthy counterparts (Bell and Davis, 2001; Brook et al., 2013; Brook et al., 2010; Goldberg et al., 2000; Goldberg et al., 2001; Goldberg et al., 2013; Hales et al., 2012; Pope

et al., 2009; Pope et al., 2011). All these observations demonstrate that biological factors such as age, health state, lifestyle and genetic makeup are important determinants in PM susceptibility.

I.6. Clean Air Regulatory Agenda.

The federal government of Canada has recognized that emissions from industrial and transportation-based sources are associated with adverse impacts on health and environment. In 2006, they launched a Clean Air Regulatory Agenda (CARA) project that committed to protect the health and environment of Canadians. The main role of our group in this program was to obtain and characterize PM of different sizes from various industrial sites in Canada associated with defined sources of emission (e.g., steel mill in Hamilton, petrochemical refinery in Montreal, and aluminum smelter in Shawinigan), and then characterize their *in vitro* cytotoxic potencies. However, ambient air PM is a complex mixture of particles with a wide range of sizes and physicochemical properties. The composition of the suspended ambient air particles varies in different geographical locations, depending on the local sources of release (Burnett et al., 2000; Thomson et al., 2015; Thomson et al., 2016). Due to such variation in particle composition, it is difficult to disentangle the drivers of toxic potency in ambient air PM and investigate their mechanisms of adverse health effects. The goal of my Ph.D. work was to test the feasibility of an *in vitro* toxicoproteomic platform for profiling the cellular responses to conventional particulate matter of occupational health relevance (e.g., carbon black, titanium dioxide, silica) and to an urban dust that has been used worldwide for toxicological studies (e.g., EHC-93 Ottawa urban dust). This platform

will eventually be applied to assess the toxic effects of environmental air PM sampled from different locations in Canada.

I.7. *In vitro* toxicology: Assessment of the cytotoxic potency of particulate matter

The toxic effects of airborne particulate matter are best examined in humans and animals, as the results provide a direct answer to particle toxicity. Unfortunately, *in vivo* toxicological assessments can be complicated or difficult to perform for various reasons, such as ethics, cost, susceptibility variation among individuals (as mentioned above) and availability of material. Thus, a vast amount of studies have used *in vitro* approaches to evaluate the toxicity of environmental air particles. It is understood that the *in vitro* results may not be directly correlated to the physiological responses of humans and animals to PM. However, *in vitro* models are still embraced across different fields of study as they can provide mechanistic details on cellular responses to the substance(s) in question. Moreover, *in vitro* methods pose few or no ethical problems, are relatively inexpensive to perform, require smaller amounts of test material/substance and they could be conducted in an automated and/or high-throughput manner, enabling the screening of many different particles simultaneously. The goal of this study is to establish an *in vitro* approach that can differentiate the potency and pathways of effects of environmental air particles that would be useful for the purpose of regulatory toxicology.

I.7.1. Cellular models used in toxicological studies.

The cytotoxic effects of respirable particles have been examined using various cell lines and primary cells from the respiratory or cardiovascular system, such as monocytes, macrophages, and bronchial and alveolar epithelial cells. The A549 human lung epithelial

cell line is one of the frequently used cell lines to examine the cytotoxic effect of environmental air particles. The A549 cells are derived from a solid lung tumor in a 58 year old Caucasian male that was explanted in 1972 (Giard et al., 1973). They possess the characteristics of type II alveolar epithelial lung cells that can produce, store in lamellar bodies, and secrete lung surfactant (Lieber et al., 1976). Type II alveolar epithelial cells are cuboidal cells that take up about 5 % of the total alveolar surface, but comprise 60 % of alveolar epithelial cells (Crapo et al., 1982). Type II cells are responsible for replacing injured type I cells via proliferation and differentiation (Barkauskas et al., 2013; Evans et al., 1973). Thus, A549 cells are a useful *in vitro* model to examine the toxic effects of air pollution. In this study, A549 cells were used to investigate the cytotoxic effects of various airborne particles.

I.7.2. Cytotoxicity assays.

The cytotoxic potencies of respirable particles have been traditionally assessed using various endpoint assays, such as lactate dehydrogenase (LDH) release, 5-bromo-2'-deoxyuridine (BrdU) incorporation, cellular ATP content and resazurin reduction assays. The LDH release assay quantifies the loss of LDH from the cytosol of the cells, which reflects the level of cell membrane damage or cell lysis by dead or dying cells (i.e., apoptosis or necrosis). The BrdU incorporation assay measures the rate of BrdU (an analog of thymidine) incorporated into the DNA of proliferating cells. The ATP assay assesses the level of cellular ATP that reflects the extent of mitochondrial injury, plasma membrane damage and/or loss of metabolic energy in the cells. In the resazurin reduction assay, viable cells reduce a non-fluorescent redox dye, resazurin (dark blue in color), to a fluorescent reaction product, resorufin (pink in color), and nonviable cells lose metabolic capacity to convert the indicator

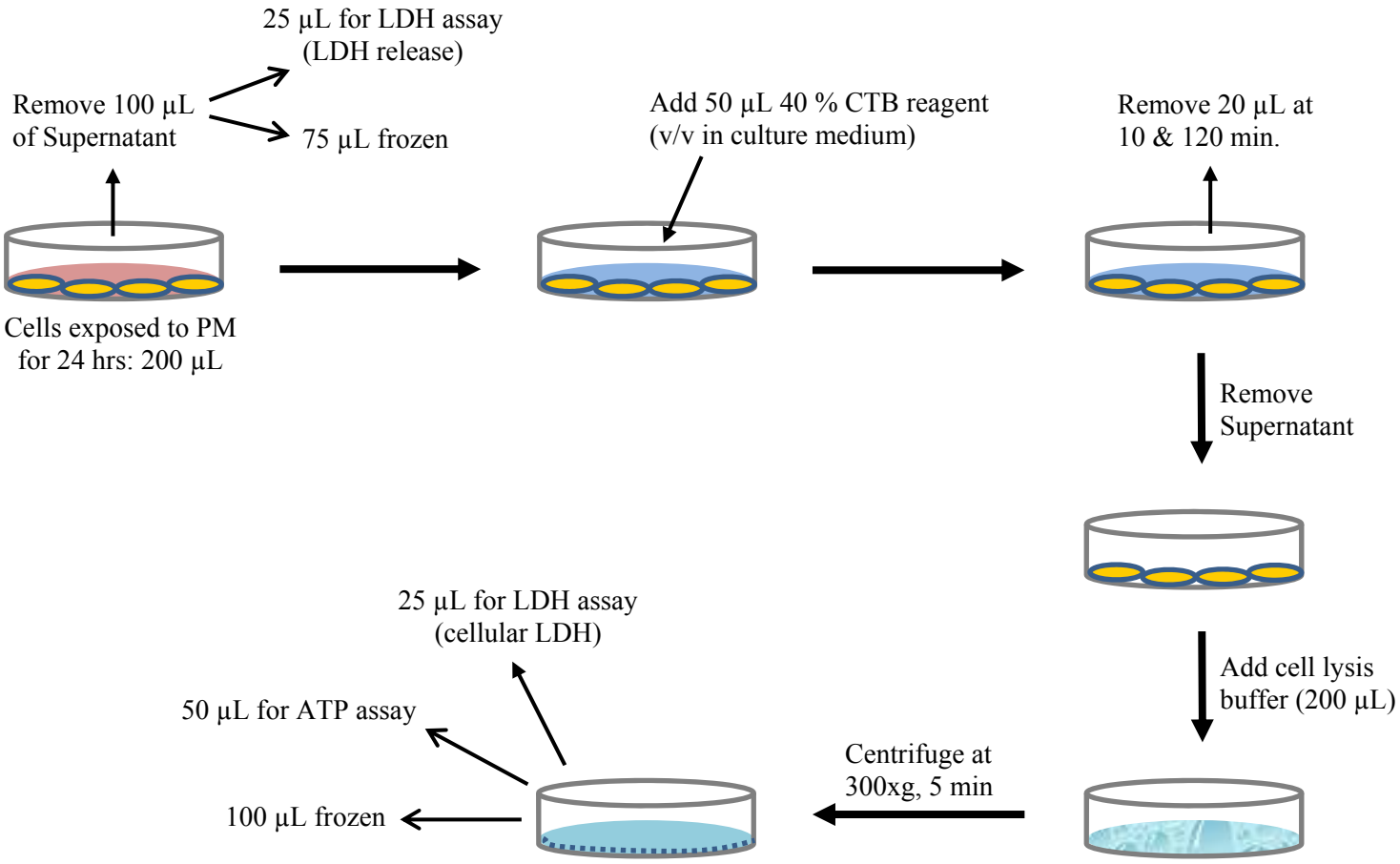

Figure I – 2. Schematic diagram of the integrated cytotoxicity bioassay.

dye. Mitochondrial, cytosolic and microsomal enzymes have been implicated in the reduction of resazurin (Gonzalez and Tarloff, 2001). These assays are attractive to researchers because they can be applied in a high through-put manner to assess the cellular phenotypic outcomes of particle toxicity. However, the majority of the toxicological studies in the literature used only one or two of these assays. Our laboratory recently adopted the use of all four of these assays to better understand the toxic effects of particles *in vitro* (Breznan et al., 2013; Breznan et al., 2016; Kumarathasan et al., 2014; Thomson et al., 2015; Thomson et al., 2016), where three assays were integrated into a sequential cytotoxicity bioassay that allowed the same particle-exposed cells to be examined directly (Figure I – 2).

I.7.3. Genomics.

Physiological changes in the cells can be controlled at the transcriptional level. Thus, assessing changes in the expression of genes in cells can provide a molecular basis to PM toxicity (Vincent et al., 1997b). It is known that exposure to airborne particles can alter the expression of genes in cells, animals and humans. The rapid development of genomic methods such as real-time polymerase chain reaction (RT-PCR), microarrays and next generation sequencing (NGS) has enabled toxicologists to characterize the toxic effects of airborne PM in great detail. For example, Kovats et al. recently used NGS to assess the presence of pathogenic particles that can be found in the resuspended ambient air particles in a Hungarian horse stable. The results of their study revealed that as many as 384 species of pathogen can be found (Kovats et al., 2016). Sellamuthu and colleagues have used a microarray approach to assess the cytotoxicity mechanisms of α-quartz (Min-U-Sil 5) in A549 cells, and their results showed that the particle perturbed the expression of genes that are involved in cellular growth and proliferation, cell death, inflammatory response and cell

cycle (Sellamuthu et al., 2011). Our laboratory is equipped with a robotic platform that can conduct RT-PCR in a high-throughput manner. We have used this platform to show that inhalation of ozone and/or EHC-93 provoked a similar pattern of gene expression in pathways such as anti-oxidant response, xenobiotic metabolism and inflammation in various tissues in rats such as lung, heart, liver, kidney, spleen, pituitary and cerebral hemispheres (Thomson et al., 2013). Therefore, different genomic methods can be used to examine various impacts of airborne particles in the environment, as well as to obtain detailed mechanisms of particle toxicity. The caveat in interpreting genomic data is that gene expression does not always translate into protein expression, which dictates cellular functions.

I.7.4. Proteomics.

Proteins are the functional products of the genome, and their expression is tightly regulated to serve different biological processes. Investigating changes in the cell proteome can provide clues to the molecular basis of cellular toxicity. There are different methods to assess the expression of proteins, depending on the purpose of the study. Immuno-based assays such as western blot, enzyme-linked immunosorbent assay (ELISA) or multiplex immunoassays are useful to determine the production of specific peptides/biomarkers. For example, our laboratory has utilized Bio-plex immunoassays to assess the release of various peptides/cytokines, such as IL-1, IL-8, IL-6, VEGF, TNF and EDN-1, from macrophages or A549 cells in response to respirable particles (Breznan et al., 2016; Chauhan et al., 2004; Chauhan et al., 2005; Thomson et al., 2015; Thomson et al., 2016). Such assays are sensitive and can be applied in a high-throughput manner, but they require prior knowledge about the

peptide sequence for the production of antibodies. These assays are expensive and only have a limited capacity.

Protein separation by two dimensional gel electrophoresis (2D-GE) followed by mass spectrometry (MS) is a basic method used in quantification and identification of proteins in complex biological matrices, and shot-gun proteomic analyses are common alternatives to gel-based proteomic procedures. Some of the shot-gun proteomic analysis methods include direct analysis of digests of cell lysates using MALDI TOF-MS or LC-MS, which can provide detailed proteomic information. The advantage of 2D-GE is that it is a relatively inexpensive approach that provides high content data.

I.7.5.Two-dimensional gel electrophoresis (2D-GE).

2D-GE is a basic proteomic method that can capture the levels of protein expression in cells by separating proteins based on their isoelectric point (pI) and molecular weight (MW). The concept of 2D gel electrophoresis has been around since 1950s (Poulik and Smithies, 1958; Smithies and Poulik, 1956), where the proteins in a sample were separated by starch gel and filter paper electrophoresis. However, such 2D electrophoresis method was rarely applied until the technique was improved by introducing the isoelectric focusing step to separate the proteins in a sample according to their pI on an immobile pH gradient, followed by their MW in an polyacrylamide gel (Kenrick and Margolis, 1970). Since most proteins have a unique pI and MW, each spot in such a 2D gel generally corresponds to an individual protein form, although overlays are expected. Later in 1970, it was possible to determine that there are 20 and 30 – 35 proteins in the S30 and S50 ribosomal subunits, respectively, of *E. coli* (Kaltschmidt and Wittmann, 1970), and since these early experiments, the use of 2D gel electrophoresis began to spread rapidly. With the recent

advancement in mass spectrometry (MS), researchers can characterize a small amount of protein, such as a sample from a spot in a 2D gel, and such a protein can be identified by comparing its MS spectrum to an existing library of proteins' spectra that have been previously identified. Furthermore, the increase and/or decrease in protein expression in cells following a treatment can also be examined by 2D-GE. For example, 2D-GE and MS analyses have been used to assess changes to the proteome of cells that were exposed to various materials, such as silica (Yang et al., 2010), polystyrene (Morbt et al., 2009), chlorinated benzenes (Morbt et al., 2011) and uranium (Malard et al., 2005). Our laboratory has previously analyzed the proteins expressed in A549 cells by 2D-GE, where protein spots from 2D gels were picked and then identified by MALDI-TOF-MS (Kumarathasan et al., 2005). Thus, 2D-GE can be used to investigate the mechanisms by which particulate matter affect cellular pathways.

I.7.6. Mass spectrometry (MS).

Mass spectrometry is an analytical method that separates ionized molecules based on mass to charge ratio (m/z), which is useful to identify organic and biological molecules. The fundamental principle of MS is based on the pioneering works of Eugen Goldstein, Wilhelm Wien and Joseph John Thomson in separate studies in the late 1800s and early 1900s. In 1886, when Goldstein examined the properties of the cathode rays (later known as electrons), which move from the cathode (negatively charged) to the anode (positively charged) in a discharge tube under low pressure, he noticed that there are also positively charged rays that move from the anode to and through a perforated cathode (Goldstein, 1886). Thereby, he called these positively charged anode rays "Kanalstrahlen" or canal rays, since they can pass through the canals in the cathode plate. It was later identified that these canal rays are

positively charged molecules that were generated by the cathode rays (electrons) that knock off an electron from the gas molecules in the discharge tube. In 1898, Wilhelm Wien used a magnetic or electric field to deflect the canal rays that came through the holes in the cathode plate; such deflection was useful to separate these canal rays (positively charged ions) based on their charge to mass ratio (Q/m). Wien's work was latter refined by Sir Joseph John Thomson, who developed the first mass spectrometer and recorded the first mass spectrograph, showing that neon gas consisted of more than one isotope, which identified the existence of ^{20}Ne and ^{22}Ne (Thomson, 1913). In 1918 and 1919, Arthur Jeffrey Dempster and Francis William Aston (a student of Thomson), respectively, were the first to independently construct the mass spectrometers that today's instruments were built upon (Borman et al., 2003).

Nowadays, various MS instruments have been developed for different purposes. All MS instruments consist of three principal components: ionizer, analyzer and detector. The ionizer causes ionization of molecules in a sample, the analyzer separates the ionized molecules, and the detector detects ionized molecules that come out of the analyzer. The ionizer is a chamber where the sample is placed or injected. The sample molecules can be ionized in this chamber with various techniques, such as matrix-assisted laser desorption/ionization (MALDI), electrospray ionization (ESI), electron impact (EI), fast atom bombardment (FAB), atmospheric-pressure chemical ionization (APCI) or inductively coupled plasma (ICP) ionization. The goal of all these techniques is common, that is to strip an electron from each sample molecule to generate a positively charged ion. Most ionized molecules carry a 1+ charge because it is more difficult (i.e., requires more energy) to remove a second electron in a particle. Once the ions are generated, the positively charged plates present in the ionization chamber propel the positively charged ions through a narrow

slit to generate a beam of ions that is directed into the analyzer. The ionized molecules can then be separated in an analyzer based on a technique such as time-of-flight (TOF), Orbitrap, quadrupole, linear quadrupole ion trap (LTQ), or a combination of the techniques above (e.g., LTQ Orbitrap and Q-TOF). The detector does not vary significantly from one instrument to another, as its function is to detect the separated ionized molecules and to record their levels of abundance. The outputs from the detector are then computerized into a mass spectrum that shows the m/z and intensity values of different particles in a sample. In the case that an ionized molecule carries a 2+ charge, it can be easily identified, because it produces a peak that is half of the m/z value of the peak that corresponds to the same molecule that carries a 1+ charge. However, the 2+ peak is much smaller than the 1+ peak.

The use of MS has gained significant momentum in various biological science fields such as proteomics and lipidomics in recent years due to the rapid development in MS technology and bioinformatics. To determine the identity of a protein by MS, the protein is typically digested by a protease such as trypsin into a predictable set of peptides based on the known cleavage sites of the enzyme, which are arginine and lysine for trypsin. The digested peptides are then subjected to ionization in a mass spectrometer to generate a set of ions with specific m/z and intensity that can be recorded as a mass spectrum, a peptide mass fingerprint (PMF) spectrum. The accuracy of protein identification took a leap forward when tandem mass spectrometry (MS/MS) was introduced into protein sequencing (Cody et al., 1985; Hunt et al., 1986). This technique is based on the inducible and predictable fragmentation of the parent ions into a unique set of daughter ions with specific m/z and intensity values. Since a number of “unique” peptide segments in a protein can produce a very specific MS/MS spectrum, such a spectrum can be used to fingerprint the identity of a protein. There have been various techniques developed to cause fragmentation of ionized

peptides for MS/MS analysis. Examples of some of these techniques are voltage lift (Suckau et al., 2003), collision-induced dissociation (CID) (Hunt et al., 1986), electron-transfer dissociation (ETD) (Syka et al., 2004) and electron-capture dissociation (ECD) (Zubarev et al., 1998). The identity of an unknown peptide can be determined by comparing its MS/MS spectrum to that of the MS/MS spectra of known peptides in databases such as SwissProt and RefSeq, using Mascot search engine.

Our laboratory has demonstrated that MALDI-TOF-MS is a useful tool to determine the identities of protein spots that can be visualized from 2D gels (Kumarathasan et al., 2005). MALDI is a soft ionization technique that uses a laser beam to ionize a sample that has been co-crystallized with a matrix molecule (e.g., α-cyano-4-hydroxy-cinnamic acid) on a metal plate. The function of the matrix is to absorb the energy from the laser beam and transfer it to the peptides in the sample to assist the ionization process. Upon ionization, the peptides are desorbed from the surface and they can be sent to an analyzer using a positively charged anode plate. A MALDI is typically coupled to a time of flight (TOF) analyzer that separates the sample molecules based on the time it takes for different molecules to travel in the analyzer to reach the detector. As the smaller peptides travel faster than the larger peptides, the time of flight is inversely proportional to the mass of the peptide. The MALDI-TOF-TOF-MS/MS instrument in our laboratory has the full capacity to perform tandem mass spectrometry (using voltage lift technique), which was utilized in this study to determine the identities of protein spots in 2D gels.

Objective

The objective of this study is to establish an *in vitro* toxicoproteomic model that can distinguish the effects of airborne particles with various physicochemical properties.

Hypothesis

Previous studies demonstrated that exposure of cells, animals or humans to environmental air PM typically generates a distinct pattern of mRNA and protein expression that is dictated by the physicochemical composition of the particles. Thus, I hypothesized that proteomic and/or genomic analyses would be useful to determine the characteristic effects of particle toxicity.

Specific aims

The main goal of this study was to develop an *in vitro* toxicoproteomic approach that is sensitive enough to discriminate the cellular responses to respirable particles that are similar or different in physicochemical properties. This approach is outlined in Figure I – 3, where the cytotoxic effects of PM in the A549 human lung epithelial cells are examined by multiple cytotoxicity assays (LDH release, BrdU incorporation, cellular ATP and resazurin reduction assays) and proteomic analyses (e.g., 2D-GE and MALDI-TOF-TOF-MS/MS). Initially, the responses of A549 cells will be characterized against several occupational health-relevant particles with low complexity (i.e., carbon black, titanium dioxide and silica). Upon success, the same experimental approach will be used to examine a more complex sample of urban air particles (i.e., EHC-93 Ottawa urban dust). To meet the objective of my study, I propose to carry out the following specific aims:

Aim #1: To establish a proteomic platform that uses 2D-GE and MALDI-TOF-TOF-MS/MS to assess changes in the proteome of A549 cells following carbon black and titanium dioxide exposures. The purpose of this aim is to assess whether 2D-GE and MALDI-TOF-TOF-MS/MS can distinguish cellular responses to two occupational health-relevant particles that are different in cytotoxic potencies and physicochemical properties, and identify their mechanisms of particle toxicity. This work is documented in two manuscripts published in Journal of Proteomics and Data in Brief, which can be found in Chapter IIa: "Proteomic changes in human lung epithelial cells (A549) in response to carbon black and titanium dioxide exposures" and Chapter IIb: "Human lung epithelial cell A549 proteome data after treatment with titanium dioxide and carbon black".

Aim #2: To examine changes in the proteome of A549 cells following exposures to two crystalline silica particles (α-quartz and cristobalite) using the 2D-GE and MALDI-TOF-TOF-MS/MS. The purpose of this aim is to test if the developed *in vitro* toxicoproteomic platform is capable of differentiating cellular responses to two occupational health-relevant particles that are similar in cytotoxic potencies and physicochemical properties at the molecular level. This work is documented in a manuscript that has been published in Journal of Applied Toxicology, which can be found in Chapter III: "Responses of A549 human lung epithelial cells to cristobalite and α-quartz exposures assessed by toxicoproteomics and gene expression analysis".

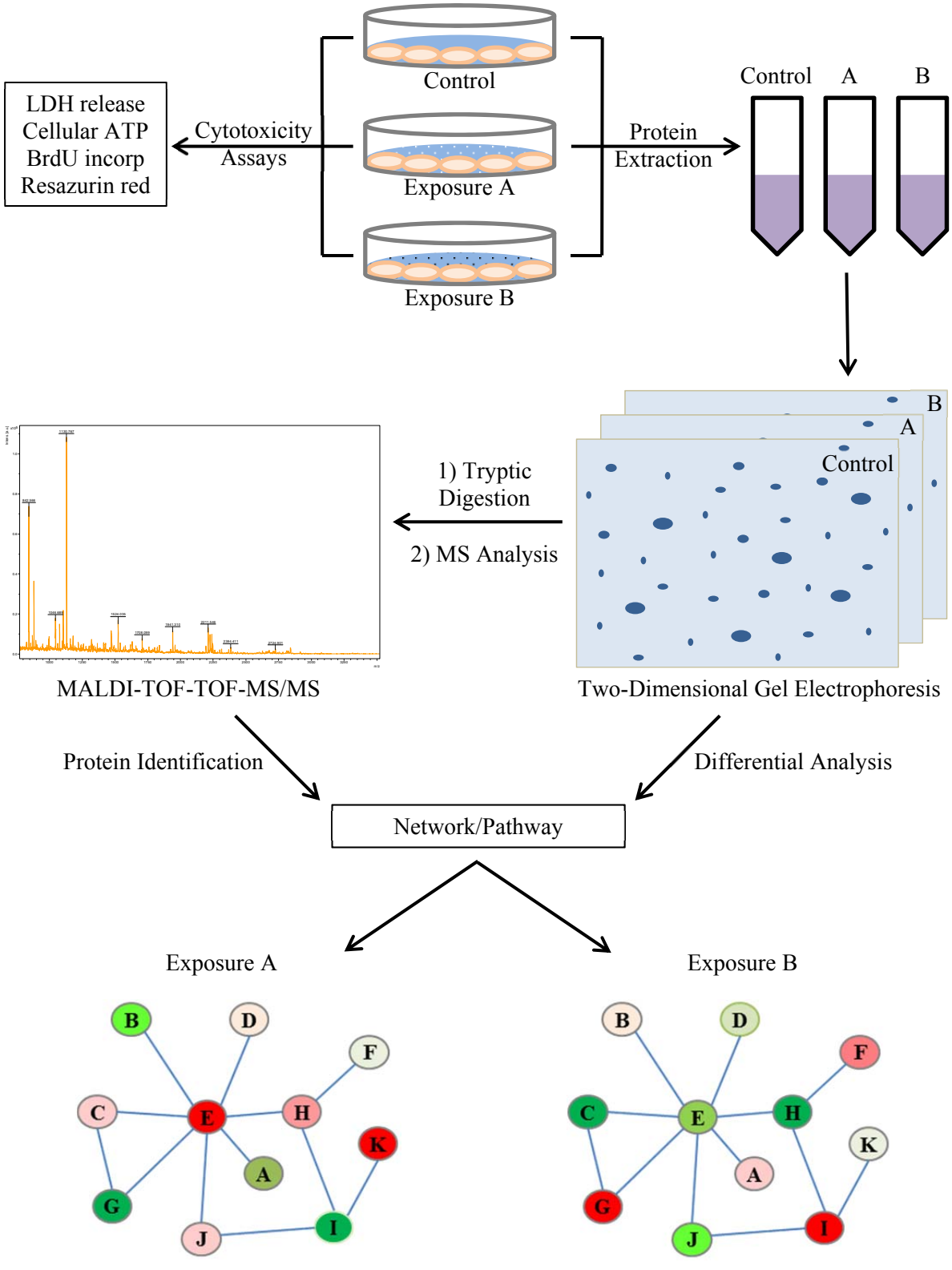

Figure I – 3. A graphical abstract of an *in vitro* toxicoproteomic approach.

Aim #3: To use the established *in vitro* toxicoproteomic model to examine changes in the proteome of A549 cells following exposures to Ottawa urban dust (EHC-93) and its water-soluble and -insoluble fractions. The purpose of this aim is to test if toxicoproteomics can distinguish the pathways of cellular toxicity in response to complex mixtures of urban air particles (i.e., total, insoluble and soluble fractions) that are different in cytotoxic potencies and physicochemical characteristics. This work is documented in a manuscript that has been submitted to Particle and Fibre Toxicology, which can be found in Chapter IV: "*In vitro* toxicoproteomic analysis of A549 human lung epithelial cells exposed to urban air particulate matter and its water-soluble and insoluble fractions".

References

Adamson,I.Y., Prieditis,H., Hedgecock,C. and Vincent,R. (2000). Zinc is the toxic factor in the lung response to an atmospheric particulate sample. Toxicol Appl Pharmacol 166:111-119.

Adamson,I.Y., Vincent,R., and Bjarnason,S.G. (1999). Cell injury and interstitial inflammation in rat lung after inhalation of ozone and urban particulates. Am J Respir Cell Mol Biol 20:1067-1072.

Ailshire,J.A. and Crimmins,E.M. (2014). Fine particulate matter air pollution and cognitive function among older US adults. Am J Epidemiol 180:359-366.

Amatullah,H., North,M.L., Akhtar,U.S., Rastogi,N., Urch,B., Silverman,F.S., Chow,C.W., Evans,G.J. and Scott,J.A. (2012). Comparative cardiopulmonary effects of size-fractionated airborne particulate matter. Inhal Toxicol 24:161-171.

Barkauskas,C.E., Cronce,M.J., Rackley,C.R., Bowie,E.J., Keene,D.R., Stripp,B.R., Randell,S.H., Noble,P.W., and Hogan,B.L. (2013). Type 2 alveolar cells are stem cells in adult lung. J Clin Invest 123:3025-3036.

Bell,M.L. and Davis,D.L. (2001). Reassessment of the lethal London fog of 1952: novel indicators of acute and chronic consequences of acute exposure to air pollution. Environ Health Perspect (Suppl 3):389-94.

Bell,M.L., Ebisu,K., Leaderer,B.P., Gent,J.F., Lee,H.J., Koutrakis,P., Wang,Y., Dominici,F. and Peng,R.D. (2014). Associations of PM(2).(5) Constituents and Sources With Hospital Admissions: Analysis of Four Counties in Connecticut and Massachusetts (USA) for Persons >/= 65 Years of Age. Environ. Health Perspect 122:138-144.

Borman,S., Russell,H., and Slaga,T.J. (2003). A mass spec timeline. Today's Chemist at Work 47-49.

Bouchon,A., Facchetti,F., Weigand,M.A. and Colonna,M. (2001) TREM-1 Amplifies inflammation and is a crucial mediator of septic shock. Nature 410:1103-1107.

Bouthillier,L., Vincent,R., Goegan,P., Adamson,I.Y., Bjarnason,S., Stewart,M., Guenette,J., Potvin,M., and Kumarathasan,P. (1998). Acute effects of inhaled urban particles and ozone: lung morphology, macrophage activity, and plasma endothelin-1. Am J Pathol 153:1873-1884.

Breznan,D., Karthikeyan,S., Phaneuf,M., Kumarathasan,P., Cakmak,S., Denison,M.S., Brook,J.R., and Vincent,R. (2016). Development of an integrated approach for comparison of in vitro and in vivo responses to particulate matter. Part Fibre Toxicol 13:41.

Brook,R.D., Cakmak,S., Turner,M.C., Brook,J.R., Crouse,D.L., Peters,P.A., van Donkelaar,A., Villeneuve,P.J., Brion,O., Jerrett,M., Martin,R.V., Rajagopalan,S., Goldberg,M.S., Pope,C.A., III and Burnett,R.T. (2013). Long-term fine particulate matter exposure and mortality from diabetes mellitus in Canada. Diabetes Care 36:3313-20.

Brown,J.R. and Thornton,J.L. (1957). Percivall Pott (1714-1788) and Chimney Sweepers' Cancer of the Scrotum. Br J Ind Med 14:68–70.

Burnett,R.T., Brook,J., Dann,T., Delocla,C., Philips,O., Cakmak,S., Vincent,R., Goldberg,M.S., and Krewski,D. (2000). Association between particulate- and gas-phase components of urban air pollution and daily mortality in eight Canadian cities. Inhal Toxicol 12(Suppl 4):15-39.

Canova,C., Dunster,C., Kelly,FJ, Minelli C, Shah PL, Caneja C, Tumilty MK, Burney P. (2012). PM10-induced hospital admissions for asthma and chronic obstructive pulmonary disease: the modifying effect of individual characteristics. Epidemiology 23:607-15.

Carver,L.A., LaPres,J.J., Jain,S., Dunham,E.E. and Bradfield,C.A. (1998). Characterization of the Ah receptor-associated protein, ARA9. J Biol Chem 273:33580–33587.

Cassel,S.L., Eisenbarth,S.C., Iyer,S.S., Sadler,J.J., Colegio,O.R., Tephly,L.A., Carter,A.B., Rothman,P.B., Flavell,R.A., and Sutterwala,F.S. (2008). The Nalp3 inflammasome is essential for the development of silicosis. Proc Natl Acad Sci USA 105:9035-9040.

Chao,S.K., Hamilton,R.F., Pfau,J.C., and Holian,A. (2001). Cell surface regulation of silica-induced apoptosis by the SR-A scavenger receptor in a murine lung macrophage cell line (MH-S). Toxicol Appl Pharmacol 174:10-16.

Chauhan,V., Breznan,D., Goegan,P., Nadeau,D., Karthikeyan,S., Brook,J.R., and Vincent,R. (2004). Effects of ambient air particles on nitric oxide production in macrophage cell lines. Cell Biol Toxicol 20:221-239.

Chauhan,V., Breznan,D., Thomson,E., Karthikeyan,S., and Vincent,R. (2005). Effects of ambient air particles on the endothelin system in human pulmonary epithelial cells (A549). Cell Biol Toxicol 21:191-205.

Chen,R., Zhang,Y., Yang,C., Zhao,Z., Xu,X., and Kan,H. (2013). Acute effect of ambient air pollution on stroke mortality in the China air pollution and health effects study. Stroke 44:954-960.

Chu,B., Wang,J., Wang,Y., and Yang,G. (2015). Knockdown of PKM2 induces apoptosis and autophagy in human A549 alveolar adenocarcinoma cells. Mol Med Rep 12:4358-4363.

Clarke,S.W. and Pavia,D. (1980). Lung mucus production and mucociliary clearance: methods of assessment. Br J Clin Pharmacol 9:537-546.

Cody,R.B.Jr, Amster,I.J. and McLafferty FW. (1985). Peptide mixture sequencing by tandem Fourier-transform mass spectrometry. Proc Natl Acad Sci USA 82:6367-70.

Crapo,J.D., Barry,B.E., Gehr,P., Bachofen,M., and Weibel,E.R. (1982). Cell number and cell characteristics of the normal human lung. Am Rev Respir Dis 126:332-337.

Dockery,D.W., Pope,C.A., III, Xu,X., Spengler,J.D., Ware,J.H., Fay,M.E., Ferris,B.G., Jr., and Speizer,F.E. (1993). An association between air pollution and mortality in six U.S. cities. N Engl J Med 329:1753-1759.

Dostert,C., Petrilli,V., Van,B.R., Steele,C., Mossman,B.T., and Tschopp,J. (2008). Innate immune activation through Nalp3 inflammasome sensing of asbestos and silica. Science 320:674-677.

Evans,M.J., Cabral,L.J., Stephens,R.J., and Freeman,G. (1973). Renewal of alveolar epithelium in the rat following exposure to NO2. Am J Pathol 70:175-198.

Fenton,H.J.H. (1894). Oxidation of tartaric acid in presence of iron. J Chem Soc, Trans 65:899–911.

Ferin,J. (1972). Observations concerning alveolar dust clearance. Ann N Y Acad Sci 200:66-72.

Fujii,T., Hayashi,S., Hogg,J.C., Vincent,R. and van Eeden,S.F. (2001). Particulate matter induces cytokine expression in human bronchial epithelial cells. Am J Respir Cell Mol Biol 25:265-271.

Gan,W.Q., FitzGerald,J.M., Carlsten,C., Sadatsafavi,M. and Brauer,M. (2013). Associations of ambient air pollution with chronic obstructive pulmonary disease hospitalization and mortality. Am. J. Respir. Crit. Care Med. 187:721-727.

Giard,D.J., Aaronson,S.A., Todaro,G.J., Arnstein,P., Kersey,J.H., Dosik,H., and Parks,W.P. (1973). In vitro cultivation of human tumors: establishment of cell lines derived from a series of solid tumors. J Natl Cancer Inst 51:1417-1423.

Goldberg,M.S., Burnett,R.T., Bailar,J.C., III, Tamblyn,R., Ernst,P., Flegel,K., Brook,J., Bonvalot,Y., Singh,R., Valois,M.F., and Vincent,R. (2001). Identification of persons with cardiorespiratory conditions who are at risk of dying from the acute effects of ambient air particles. Environ. Health Perspect. 109(Suppl 4):487-494.

Goldberg,M.S., Burnett,R.T., Stieb,D.M., Brophy,J.M., Daskalopoulou,S.S., Valois,M.F., and Brook,J.R. (2013). Associations between ambient air pollution and daily mortality among elderly persons in Montreal, Quebec. Sci Total Environ 463-464C:931-942.

Goldstein,E. (1886). Über eine noch nicht untersuchte Strahlungsform an der Kathodeinducirter Entladungen. Berlin Akd. Monatsber II, 691.

Gonzalez,R.J. and Tarloff,J.B. (2001). Evaluation of hepatic subcellular fractions for alamar blue and MTT reductase activity. Toxicol In Vitro 15:257-259.

Guan,L., Rui,W., Bai,R., Zhang,W., Zhang,F. and Ding,W. (2016). Effects of size-fractionated particulate matter on cellular oxidant radical generation in human bronchial epithelial BEAS-2B cells. Int J Environ Res Public Health 13:483.

Hales,S., Blakely,T., and Woodward,A. (2012). Air pollution and mortality in New Zealand: cohort study. J Epidemiol Community Health 66:468-473.

Harmsen,A.G., Mason,M.J., Muggenburg,B.A., Gillett,N.A., Jarpe,M.A., and Bice,D.E. (1987). Migration of neutrophils from lung to tracheobronchial lymph node. J Leukoc Biol 41:95-103.

Harmsen,A.G., Muggenburg,B.A., Snipes,M.B., and Bice,D.E. (1985). The role of macrophages in particle translocation from lungs to lymph nodes. Science 230:1277-1280.

Hassoun,E.A. and Stohs,S.J. (1996). Cadmium-induced production of superoxide anion and nitric oxide, DNA single strand breaks and lactate dehydrogenase leakage in J774A.1 cell cultures. Toxicology 112:219-226.

Hornung,V., Bauernfeind,F., Halle,A., Samstad,E.O., Kono,H., Rock,K.L., Fitzgerald,K.A., and Latz,E. (2008). Silica crystals and aluminum salts activate the NALP3 inflammasome through phagosomal destabilization. Nat Immunol 9:847-856.

Huang,Q., Zhang,J., Peng,S., Tian,M., Chen,J. and Shen,H. (2014). Effects of water soluble PM2.5 extracts exposure on human lung epithelial cells (A549): A proteomic study. J. Appl. Toxicol. 34:675-687.

Huang,W., Zhu,T., Pan,X., Hu,M., Lu,S.E., Lin,Y., Wang,T., Zhang,Y. and Tang,X. (2012). Air pollution and autonomic and vascular dysfunction in patients with cardiovascular disease: interactions of systemic inflammation, overweight, and gender. Am J Epidemiol 176:117-126.

Hunt,D.F., Yates,J.R., III, Shabanowitz,J., Winston,S., and Hauer,C.R. (1986). Protein sequencing by tandem mass spectrometry. Proc Natl Acad Sci U S A 83:6233-6237.

Hussain,S., Thomassen,L.C., Ferecatu,I., Borot,M.C., Andreau,K., Martens,J.A., Fleury,J., Baeza-Squiban,A., Marano,F., and Boland,S. (2010). Carbon black and titanium dioxide nanoparticles elicit distinct apoptotic pathways in bronchial epithelial cells. Part Fibre Toxicol 7:10.

IARC (1997). IARC working group on the evaluation of carcinogenic risks to humans: Silica, some silicates, coal dust and para-aramid fibrils. Lyon, 15-22 October 1996. IARC Monogr. Eval. Carcinog. Risks Hum. 68, 1-475.

Ikuta,T., Eguchi,H., Tachibana,T., Yoneda,Y. and Kawajiri,K. (1998). Nuclear localization and export signals of the human aryl hydrocarbon receptor. J. Biol. Chem. 273, 2895–2904.

Iyer,R., Hamilton,R.F., Li,L., and Holian,A. (1996). Silica-induced apoptosis mediated via scavenger receptor in human alveolar macrophages. Toxicol Appl Pharmacol 141:84-92.

Jedrychowski WA, Perera FP, Camann D, Spengler J, Butscher M, Mroz E, Majewska R, Flak E, Jacek R, Sowa A. (2015). Prenatal exposure to polycyclic aromatic hydrocarbons and cognitive dysfunction in children. Environ Sci Pollut Res Int 22:3631-9.

Johannson,K.A., Vittinghoff,E., Lee,K., Balmes,J.R., Ji,W., Kaplan,G.G., Kim,D.S., and Collard,H.R. (2014). Acute exacerbation of idiopathic pulmonary fibrosis associated with air pollution exposure. Eur Respir J 43:1124-1131.

Johnston,H.J., Hutchison,G.R., Christensen,F.M., Peters,S., Hankin,S., and Stone,V. (2009). Identification of the mechanisms that drive the toxicity of TiO_2 particulates: the contribution of physicochemical characteristics. Part Fibre Toxicol 6:33.

Julvez,J., Ribas-Fito,N., Torrent,M., Forns,M., Garcia-Esteban,R. and Sunyer,J. (2007). Maternal smoking habits and cognitive development of children at age 4 years in a population-based birth cohort. Int J Epidemiol 36:825-832.

Kazlauskas,A., Poellinger,L. and Pongratz,I. (1999). Evidence that the co-chaperone p23 regulates ligand responsiveness of the dioxin (Aryl hydrocarbon) receptor. J Biol Chem 274:13519–13524.

Kreyling,W.G., Semmler,M., Erbe,F., Mayer,P., Takenaka,S., Schulz,H., Oberdorster,G., and Ziesenis,A. (2002). Translocation of ultrafine insoluble iridium particles from lung epithelium to extrapulmonary organs is size dependent but very low. J Toxicol Environ Health A 65:1513-1530.

Kumarathasan,P., Blais,E., Saravanamuthu,A., Bielecki,A., Mukherjee,B., Bjarnason,S., Guenette,J., Goegan,P., and Vincent,R. (2015). Nitrative stress, oxidative stress and plasma endothelin levels after inhalation of particulate matter and ozone. Part Fibre Toxicol 12:28.

Kumarathasan,P., Mohottalage,S., Goegan,P., and Vincent,R. (2005). An optimized protein in-gel digest method for reliable proteome characterization by MALDI-TOF-MS analysis. Anal Biochem 346:85-89.

Laden,F., Neas,L.M., Dockery,D.W., and Schwartz,J. (2000). Association of fine particulate matter from different sources with daily mortality in six U.S. cities. Environ Health Perspect 108:941-947.

Landahl,H.D. and Black,S. (1947). Penetration of air-borne particulates through the human nose. J Ind Hyg Toxicol 29:269-277.

Landahl,H.D. and Tracewell,T. (1949). Penetration of air-borne particulates through the human nose. J Ind Hyg Toxicol 31:55-59.

Lieber,M., Smith,B., Szakal,A., Nelson-Rees,W., and Todaro,G. (1976). A continuous tumor-cell line from a human lung carcinoma with properties of type II alveolar epithelial cells. Int J Cancer 17:62-70.

Liu,L., Yu,L.Y., Mu,H.J., Xing,L.Y., Li,Y.X. and Pan,G.W. (2014). Shape of concentration-response curves between long-term particulate matter exposure and morbidities of chronic bronchitis: a review of epidemiological evidence. J Thorac Dis 6:S720-S727.

Malard,V., Prat,O., Darrouzet,E., Berenguer,F., Sage,N., and Quemeneur,E. (2005). Proteomic analysis of the response of human lung cells to uranium. Proteomics. 5:4568-4580.

MacIntyre,E.A., Brauer,M., Melén,E., Bauer,C.P., Bauer,M., Berdel,D., Bergström,A., Brunekreef,B., Chan-Yeung,M., Klümper,C., Fuertes,E., Gehring,U., Gref,A., Heinrich,J., Herbarth,O., Kerkhof,M., Koppelman,G.H., Kozyrskyj,A.L., Pershagen,G., Postma,D.S., Thiering,E., Tiesler,C.M., Carlsten,C. (2014). GSTP1 and TNF Gene variants and associations between air pollution and incident childhood asthma: the traffic, asthma and genetics (TAG) study. Environ Health Perspect 122:418-24.

Merkus,F.W., Verhoef,J.C., Schipper,N.G., and Marttin,E. (1998). Nasal mucociliary clearance as a factor in nasal drug delivery. Adv Drug Deliv Rev 29:13-38.

Merlo,F., Costantini,M., Reggiardo,G., Ceppi,M., and Puntoni,R. (1991). Lung cancer risk among refractory brick workers exposed to crystalline silica: a retrospective cohort study. Epidemiology 2:299-305.

Morbt,N., Mogel,I., Kalkhof,S., Feltens,R., Roder-Stolinski,C., Zheng,J., Vogt,C., Lehmann,I., and von,B.M. (2009). Proteome changes in human bronchoalveolar cells following styrene exposure indicate involvement of oxidative stress in the molecular-response mechanism. Proteomics 9:4920-4933.

Morbt,N., Tomm,J., Feltens,R., Mogel,I., Kalkhof,S., Murugesan,K., Wirth,H., Vogt,C., Binder,H., Lehmann,I., and von,B.M. (2011). Chlorinated benzenes cause concomitantly oxidative stress and induction of apoptotic markers in lung epithelial cells (A549) at nonacute toxic concentrations. J Proteome Res 10:363-378.

Mutze K, Vierkotten S, Milosevic J, Eickelberg O and Konigshoff M (2015) Enolase 1 (ENO1) and Protein Disulfide-Isomerase Associated 3 (PDIA3) Regulate Wnt/Beta-Catenin-Driven Trans-Differentiation of Murine Alveolar Epithelial Cells. Dis Model Mech 8:877-890.

Oberdorster,G., Ferin,J., and Lehnert,B.E. (1994). Correlation between particle size, in vivo particle persistence, and lung injury. Environ Health Perspect 102(Suppl 5):173-179.

Oberdorster,G., Maynard,A., Donaldson,K., Castranova,V., Fitzpatrick,J., Ausman,K., Carter,J., Karn,B., Kreyling,W., Lai,D., Olin,S., Monteiro-Riviere,N., Warheit,D., and Yang,H. (2005). Principles for characterizing the potential human health effects from exposure to nanomaterials: elements of a screening strategy. Part Fibre Toxicol 2:8.

Peng RD, Dominici F, Pastor-Barriuso R, Zeger S L and Samet J M (2005) Seasonal Analyses of Air Pollution and Mortality in 100 US Cities. Am J Epidemiol 161:585-594.

Perdew,G.H. (1988). Association of the Ah receptor with the 90-kDa heat shock protein. J Biol Chem 263:13802–13805.

Pisani C, Gaillard J C, Nouvel V, Odorico M, Armengaud J and Prat O (2015) High-Throughput, Quantitative Assessment of the Effects of Low-Dose Silica Nanoparticles on Lung Cells: Grasping Complex Toxicity With a Great Depth of Field. BMC Genomics 16:315.

Pope,C.A., III (1989). Respiratory disease associated with community air pollution and a steel mill, Utah Valley. Am J Public Health 79:623-628.

Pope CA, III, Burnett R T, Krewski D, Jerrett M, Shi Y, Calle E E and Thun M J (2009) Cardiovascular Mortality and Exposure to Airborne Fine Particulate Matter and Cigarette Smoke: Shape of the Exposure-Response Relationship. Circulation 120:941-948.

Pope, C.A., III, Burnett, R.T., Turner, M.C., Cohen, A., Krewski, D., Jerrett, M., Gapstur, S.M., and Thun, M.J. (2011). Lung cancer and cardiovascular disease mortality associated with ambient air pollution and cigarette smoke: shape of the exposure-response relationships. Environ Health Perspect 119:1616-1621.

Prieditis,H. and Adamson,I.Y. (2002). Comparative Pulmonary Toxicity of Various Soluble Metals Found in Urban Particulate Dusts. Exp Lung Res 28:563-576.

Proctor,D.F., Andersen,I.B., and Lundqvist,G. (1973). Clearance of Inhaled Particles From the Human Nose. Arch Intern Med 131:132.

Raabe,O.G., Al-Bayati,M.A., Teague,S.V., and Rasolt,A. (1988). Regional deposition of inhaled monodisperse coarse and fine aerosol particles in small laboratory animals. Ann Occup Hyg 32:53-63.

Rao X, Patel P, Puett R and Rajagopalan S (2015) Air Pollution As a Risk Factor for Type 2 Diabetes. Toxicol Sci 143:231-241.

Reich M, Liefeld T, Gould J, Lerner J, Tamayo P and Mesirov J P (2006) GenePattern 2.0. Nat Genet 38:500-501.

Reyes,H., Reisz-Porszasz,S. and Hankinson,O. (1992). Identification of the Ah receptor nuclear translocator protein (Arnt) as a component of the DNA binding form of the Ah receptor. Science 256:1193–1195.

Roskoski R, Jr. (2012) ERK1/2 MAP Kinases: Structure, Function, and Regulation. Pharmacol Res 66:105-143.

Sager,T.M. and Castranova,V. (2009). Surface area of particle administered versus mass in determining the pulmonary toxicity of ultrafine and fine carbon black: comparison to ultrafine titanium dioxide. Part Fibre Toxicol 6:15.

Sakamoto N, Hayashi S, Gosselink J, Ishii H, Ishimatsu Y, Mukae H, Hogg J C and van Eeden S F (2007) Calcium Dependent and Independent Cytokine Synthesis by Air Pollution Particle-Exposed Human Bronchial Epithelial Cells. Toxicol Appl Pharmacol 225:134-141.

Schenk M, Bouchon A, Seibold F and Mueller C (2007) TREM-1--Expressing Intestinal Macrophages Crucially Amplify Chronic Inflammation in Experimental Colitis and Inflammatory Bowel Diseases. J Clin Invest 117:3097-3106.

Schneider A, Hampel R, Ibald-Mulli A, Zareba W, Schmidt G, Schneider R, Ruckerl R, Couderc J P, Mykins B, Oberdorster G, Wolke G, Pitz M, Wichmann H E and Peters A (2010) Changes in Deceleration Capacity of Heart Rate and Heart Rate Variability Induced by Ambient Air Pollution in Individuals With Coronary Artery Disease. Part Fibre Toxicol 7:29.

Scott,J.A. (1953). Fog and deaths in London, December 1952. Public Health Rep 68:474-479.

Seok,S.H., Lee,W., Jiang,L., Molugu,K., Zheng,A., Li,Y., Park,S., Bradfield,C.A. and Xing,Y. (2017). Structural hierarchy controlling dimerization and target DNA recognition in the AHR transcriptional complex. Proc Natl Acad Sci U S A 114:5431-5436.

Serita,F., Kyono,H., and Seki,Y. (1999). Pulmonary clearance and lesions in rats after a single inhalation of ultrafine metallic nickel at dose levels comparable to the threshold limit value. Ind Health 37:353-363.

Siemiatycki,J., Dewar,R., Lakhani,R., Nadon,L., Richardson,L., and Gerin,M. (1989). Cancer risks associated with 10 inorganic dusts: results from a case-control study in Montreal. Am J Ind Med 16:547-567.

Snow SJ, De Vizcaya-Ruiz A, Osornio-Vargas A, Thomas R F, Schladweiler M C, McGee J and Kodavanti U P (2014) The Effect of Composition, Size, and Solubility on Acute Pulmonary Injury in Rats Following Exposure to Mexico City Ambient Particulate Matter Samples. J Toxicol Environ Health A 77:1164-1182.

Sterling,J.B. and Hanke,C.W. (2005). Dioxin toxicity and chloracne in the Ukraine. J Drugs Dermatol 4:148-150.

Stocks,P. (1959). Cancer and bronchitis mortality in relation to atmospheric deposit and smoke. Br Med J 1(5114):74-9.

Su,M.W., Tsai,C.H., Tung,K.Y., Hwang,B.F., Liang,P.H., Chiang,B.L., Yang,Y.H., and Lee,Y.L. (2013). GSTP1 is a hub gene for gene-air pollution interactions on childhood asthma. Allergy 68:1614-1617.

Suckau,D., Resemann,A., Schuerenberg,M., Hufnagel,P., Franzen,J., and Holle,A. (2003). A novel MALDI LIFT-TOF/TOF mass spectrometer for proteomics. Anal Bioanal Chem 376:952-965.

Sun,B., Pokhrel,S., Dunphy,D.R., Zhang,H., Ji,Z., Wang,X., Wang,M., Liao,Y.P., Chang,C.H., Dong,J., Li,R., Madler,L., Brinker,C.J., Nel,A.E., and Xia,T. (2015a). Reduction of Acute Inflammatory Effects of Fumed Silica Nanoparticles in the Lung by Adjusting Silanol Display through Calcination and Metal Doping. ACS Nano 9:9357-9372.

Sun,H., Zhu,A., Zhang,L., Zhang,J., Zhong,Z., and Wang,F. (2015b). Knockdown of PKM2 Suppresses Tumor Growth and Invasion in Lung Adenocarcinoma. Int J Mol Sci 16:24574-24587.

Sun,Q., Yue,P., Ying,Z., Cardounel,A.J., Brook,R.D., Devlin,R., Hwang,J.S., Zweier,J.L., Chen,L.C., and Rajagopalan,S. (2008). Air pollution exposure potentiates hypertension through reactive oxygen species-mediated activation of Rho/ROCK. Arterioscler Thromb Vasc Biol 28:1760-1766.

Suzuki Y, Imai Y, Nakayama H, Takahashi K, Takio K and Takahashi R (2001) A Serine Protease, HtrA2, Is Released From the Mitochondria and Interacts With XIAP, Inducing Cell Death. Mol Cell 8:613-621.

Syka,J.E., Coon,J.J., Schroeder,M.J., Shabanowitz,J., and Hunt,D.F. (2004). Peptide and protein sequence analysis by electron transfer dissociation mass spectrometry. Proc Natl Acad Sci U S A 101:9528-9533.

Thomson,E.M., Breznan,D., Karthikeyan,S., Mackinnon-Roy,C., Charland,J.P., Dabek-Zlotorzynska,E., Celo,V., Kumarathasan,P., Brook,J.R., and Vincent,R. (2015). Cytotoxic and inflammatory potential of size-fractionated particulate matter collected repeatedly within a small urban area. Part Fibre Toxicol 12:24.

Thomson,E.M., Breznan,D., Karthikeyan,S., Mackinnon-Roy,C., Vuong,N.Q., Dabek-Zlotorzynska,E., Celo,V., Charland,J.P., Kumarathasan,P., Brook,J.R., and Vincent,R. (2016). Contrasting biological potency of particulate matter collected at sites impacted by distinct industrial sources. Part Fibre Toxicol 13:65.

Thomson E, Kumarathasan P, Goegan P, Aubin R A and Vincent R (2005) Differential Regulation of the Lung Endothelin System by Urban Particulate Matter and Ozone. Toxicol Sci 88:103-113.

Thomson EM, Vladisavljevic D, Mohottalage S, Kumarathasan P and Vincent R (2013) Mapping Acute Systemic Effects of Inhaled Particulate Matter and Ozone: Multiorgan Gene Expression and Glucocorticoid Activity. Toxicol Sci 135:169-181.

Thomson,J.J. (1913). Rays of positive electricity. Proceedings of the Royal Society A 89:1-20.

Tonne C, Elbaz A, Beevers S and Singh-Manoux A (2014) Traffic-Related Air Pollution in Relation to Cognitive Function in Older Adults. Epidemiology 25:674-681.

Verma V, Rico-Martinez R, Kotra N, King L, Liu J, Snell T W and Weber R J (2012) Contribution of Water-Soluble and Insoluble Components and Their Hydrophobic/Hydrophilic Subfractions to the Reactive Oxygen Species-Generating Potential of Fine Ambient Aerosols. Environ Sci Technol 46:11384-11392.

Vincent,R., Bjarnason,S.G., Adamson,I.Y., Hedgecock,C., Kumarathasan,P., Guenette,J., Potvin,M., Goegan,P., and Bouthillier,L. (1997a). Acute pulmonary toxicity of urban particulate matter and ozone. Am J Pathol 151:1563-1570.

Vincent,R., Goegan,P., Johnson,G., Brook,J.R., Kumarathasan,P., Bouthillier,L., and Burnett,R.T. (1997b). Regulation of promoter-CAT stress genes in HepG2 cells by suspensions of particles from ambient air. Fundam Appl Toxicol 39:18-32.

Vincent,R., Kumarathasan,P., Goegan,P., Bjarnason,S.G., Guenette,J., Berube,D., Adamson,I.Y., Desjardins,S., Burnett,R.T., Miller,F.J., and Battistini,B. (2001). Inhalation toxicology of urban ambient particulate matter: acute cardiovascular effects in rats. Res Rep Health Eff Inst 5-54.

Vora R, Zareba W, Utell M J, Pietropaoli A P, Chalupa D, Little E L, Oakes D, Bausch J, Wiltshire J and Frampton M W (2014) Inhalation of Ultrafine Carbon Particles Alters Heart Rate and Heart Rate Variability in People With Type 2 Diabetes. Part Fibre Toxicol 11:31.

Vuong NQ, Goegan P, De R F, Breznan D, Thomson E M, O'Brien J S, Karthikeyan S, Williams A, Vincent R and Kumarathasan P (2016a) Responses of A549 Human Lung Epithelial Cells to Cristobalite and Alpha-Quartz Exposures Assessed by Toxicoproteomics and Gene Expression Analysis. J Appl Toxicol 37:721-731.

Vuong NQ, Goegan P, Mohottalage S, Breznan D, Ariganello M, Williams A, Elisma F, Karthikeyan S, Vincent R and Kumarathasan P (2016b) Human Lung Epithelial Cell A549 Proteome Data After Treatment With Titanium Dioxide and Carbon Black. Data Brief 8:687-691.

Vuong NQ, Goegan P, Mohottalage S, Breznan D, Ariganello M, Williams A, Elisma F, Karthikeyan S, Vincent R and Kumarathasan P (2016c) Proteomic Changes in Human Lung Epithelial Cells (A549) in Response to Carbon Black and Titanium Dioxide Exposures. J Proteomics 149:53-63.

Yang W, Zheng Y, Xia Y, Ji H, Chen X, Guo F, Lyssiotis C A, Aldape K, Cantley L C and Lu Z (2012) ERK1/2-Dependent Phosphorylation and Nuclear Translocation of PKM2 Promotes the Warburg Effect. Nat Cell Biol 14:1295-1304.

Yi S, Zhang F, Qu F and Ding W (2014) Water-Insoluble Fraction of Airborne Particulate Matter (PM10) Induces Oxidative Stress in Human Lung Epithelial A549 Cells. Environ Toxicol 29:226-233.

Zanobetti A, Franklin M, Koutrakis P and Schwartz J (2009) Fine Particulate Air Pollution and Its Components in Association With Cause-Specific Emergency Admissions. Environ Health 8:58.

Zhang,Y., Ji,X., Ku,T., Li,G., and Sang,N. (2016). Heavy metals bound to fine particulate matter from northern China induce season-dependent health risks: A study based on myocardial toxicity. Environ. Pollut 216:380-390.

Zhang,Y., Xu,D., Li,W., Yu,J., and Chen,Y. (2012). Effect of Size, Shape, and Surface Modification on Cytotoxicity of Gold Nanoparticles to Human HEp-2 and Canine MDCK Cells. Hindawi 2012:1-7.

Zubarev,R.A., Kelleher,N.L., and McLafferty,F.W. (1998). Electron Capture Dissociation of Multiply Charged Protein Cations. A Nonergodic Process. J Am Chem Soc 120:3265-3266.

Chapter IIa. Proteomic changes in human lung epithelial cells (A549) in response to carbon black and titanium dioxide exposures

This manuscript was published in Journal of Proteomics.

Vuong NQ, Goegan P, Mohattalage S, Breznan D, Ariganello M, Williams A, Elisma F, Karthikeyan S, Vincent R and Kumarathasan P. Proteomic changes in human lung epithelial cells (A549) in response to carbon black and titanium dioxide exposures. Journal of Proteomics. 2016 Oct 21;149:53-63.

Received: 1 December 2015
Received in revised form: 12 March 2016
Accepted: 26 March 2016
Available online: 12 April 2016

Ngoc Vuong wrote the manuscript, analyzed all the results (including cytotoxicity assays, 2D-GE, MALDI-TOF-MS, bioinformatics and pathway analyses), and performed most experimental works.

Abstract

This study combined cytotoxicity assays with proteomic analysis to characterize the unique biological responses of the A549 human lung epithelial cell line to two physicochemically distinct respirable particles titanium dioxide (TiO_2) and carbon black (CB). Cellular LDH, ATP, BrdU incorporation and resazurin reduction indicated that CB was more potent than TiO_2. Proteomic analysis was done using 2D-GE and MALDI-TOF-TOF-MS. Proteomic changes reflected common and particle-specific responses. Particle-specific proteomic responses were associated with cell death (necrosis and apoptosis), viability and proliferation pathways. Our results suggested that these pathways were consistent with the cytotoxicity data. For instance, increased expressions of anti-proliferative proteins LMNA and PA2G4 were in agreement with the decreased BrdU incorporation in A549 cells after exposure to CB. Similarly, increased expression of HSPA5 that is associated with ATPase activity was consistent with decreased cellular ATP levels in these cells. These findings reveal that proteomic changes can explain the cellular cytotoxicity characteristics of the particles. In essence, our results demonstrate that the *in vitro* toxicoproteomic approach is a promising tool to gain insight into molecular mechanisms underlying particle exposure-specific cytotoxicity.

IIa.1. Introduction

Airborne particulate matter (PM) is a complex mixture of inorganic and organic compounds. Inhalation of airborne PM has been linked to the development or exacerbation of respiratory illnesses such as bronchitis (Scott, 1953; Stocks, 1959; Liu et al., 2014), asthma (MacIntyre et al., 2014; Su et al., 2013; Canova et al., 2012), cystic fibrosis (Goeminne et al., 2013; Farhat et al., 2013) and lung cancer (Merlo et al., 1991; Pope, III et al., 2011; Siemiatycki et al., 1989; Kachuri et al., 2013; Stocks, 1959).Toxicity of urban air particles and their associated adverse health outcomes can vary with particle composition. Insight into particle exposure-specific molecular mechanisms can provide a biological basis of particle toxicity. In this study, we focused on an *in vitro* toxicoproteomic approach that can distinguish the toxic effects of two particles that are chemically and physically different.

Carbon black (CB) is a manufactured product containing predominantly (95%) elemental carbon (EC) with negligible amounts of inorganic and organic materials (Wang MJ et al., 2003; Watson and Valberg, 2001) and should not be confused with black carbon (soot) that contains varying amounts of EC, organic materials and metals (Long et al., 2013; Watson and Valberg, 2001). Recent reports have implied that exposure to EC can have a negative impact on the cardiovascular system (Bell, 2012; Levy et al., 2012; Schneider et al., 2010; Wagner et al., 2014). Yet, toxicity mechanisms underpinning EC exposure-related adverse cardiovascular effects are not clear, and CB has been used as a surrogate for EC in *in vitro* and *in vivo* toxicity studies (Lee et al., 2011; Mroz et al., 2007; Sahu et al., 2014; Saputra et al., 2014; Yamawaki and Iwai, 2006; Zhang et al., 2014). Meanwhile, titanium dioxide (TiO_2) is typically used as a “negative control” in many particle toxicology studies due to its relative low toxicity properties both *in vivo* and *in vitro*. Nevertheless, recent

studies have reported that the toxicity of TiO_2 could depend on physicochemical parameters such as size, aggregation, crystal phase and surface modifications (Johnston et al., 2009).

Cytotoxicity of particles has traditionally been assessed by endpoint assays such as resazurin reduction, cellular ATP, lactate dehydrogenase (LDH) release and 5-bromo-2′-deoxyuridine (BrdU) incorporation. These assays are attractive to researchers because they can be applied in a high-throughput manner to estimate the toxic potency of respirable particles. One of the drawbacks of these cytotoxic assays is that they do not reveal detailed information at the molecular level. In recent years, proteomic-based approaches have gained momentum in toxicology based on their ability to delineate the molecular mechanism underlying the toxicity of PM (Ge et al., 2015; Kumarathasan P et al., 2012). Protein separation by two-dimensional gel electrophoresis (2D-GE) followed by protein identification by mass spectrometry (MS) or tandem mass spectrometry (MS/MS) is a classical proteomic approach used to quantify and identify proteins in complex biological matrices. While shot-gun proteomic analyses (using MALDI-TOF-TOF/MS/MS or LC/MS/MS) are proposed alternatives to gel-based proteomic procedures, the advantage of 2D-GE is that it is relatively in-expensive and can provide high content data. Recent studies have used 2D-GE to identify proteomic changes in cells to help characterize the toxicity caused by exposure to particles (Ge et al., 2011; Ge et al., 2015; Hosp et al., 2015; Malard et al., 2005; Morbt et al., 2011; Peng et al., 2014; Yang et al., 2010).

In this study, in order to understand particle-specific cellular changes we exposed a human lung epithelial cell line (A549) to two chemically and physically different respirable materials, CB and TiO_2 particle. We then used a toxicoproteomic approach by conducting traditional cytotoxicity assays along with proteomics to identify the molecular signature of particle toxicity.

IIa.2. Materials and methods

IIa.2.1. Materials.

Culture flasks (T-25 and T-75), 96-well plate and plastic cell scrapers were obtained from Corning Inc. (Corning, NY). Dulbecco's Modified Eagle's Medium (DMEM) and fetal bovine serum (FBS) were purchased from HyClone (Logan, UT). Gentamicin, trifluoroacetic acid, α-cyano-4-hydroxy-cinnamic acid, Tris-HCl, NaCl, Tween-20 and Tween-80 were obtained from Sigma-Aldrich (Oakville, ON). Iodoacetamide, bis-acrylamide, ammonium persulfate, glycerol, immobilized pH gradient strips, Criterion Cassette (13.3 × 8.7 cmW × L), Tris/Glycine/SDS buffer, and BioSafe Coomassie Blue were purchased from Bio-Rad (Mississau-ga, ON). Trypsin, resazurin reduction (CellTiter-Blue®) and lactate dehydrogenase (LDH) cytotoxicity assay kits (CytoTox-96®) were from Promega Corporation (Madison, WI), ATP assay kit (ViaLight™ Plus) was purchased from Lonza Corporation (Rockland, ME), and 5-bromo-2′-deoxyuridine (BrdU) cell proliferation ELISA (chemilumines-cent) assay kit was obtained from Roche Diagnostics (Laval, QC). All water used was deionized/demineralized (N16 MΩ resistivity).

IIa.2.2. Particles preparation

TiO_2 (SRM-154b) obtained from the National Institute of Standards and Technology (Gaithersburg, MD) was subjected to three successive washes with methanol and then phosphate buffered saline (PBS) to remove possible soluble metals and organic contaminants before use in the experiments (Vincent et al., 1997). Carbon black (Cas#1333-86-4) obtained from Cabot Corporation (Boston, MA) was used as received. Particles were resuspended at 10 mg/mL in particle buffer (0.19 % NaCl and 25 μg/mL Tween-80) (Nadeau et al., 1996),

vortexed (30 s), sonicated (20 min on ice), homoge-nized with a Dounce Homogenizer (25 strokes), and then heated (56 °C, 1 h). The particles were stored at −40 °C until use.

IIa.2.3. Cell culture and particle exposure

The A549 cell line (American Type Culture Collection - CCL-185; human, epithelial, lung carcinoma) was sub-cultured in DMEM supplemented with 50 μg/mL gentamycin and 10 % FBS. The cells were maintained in T-75 flasks in a humidified atmosphere at 37 °C containing 5 % CO_2 and 95 % air. For experiments, the cells were seeded at 1.5 × 106 cells (T-25), 3.75 × 106 cells (T-75) or 2.0 × 104 cells/well (96-well plate for cytotoxicity assays) and incubated for 24 h, resulting in approximately 75% confluence prior to dosing with particles. The final volume of culture medium was 5 mL (T-25), 15 mL (T-75) or 200 μL/well (96-well plate). Solutions of particles were prepared by thawing the frozen stocks to aqueous solutions, sonicating on ice (20 min) then diluting in the culture medium to make up dosing concentrations of 0, 60, 140 and 200 μg/cm^2. The cells were exposed to the particles by replacing the existing culture medium with the particle solutions, and the flasks/plates were returned to the incubator and allowed to incubate for 24 h. To harvest the exposed cells, the medium in each flask was removed and the cells were detached from the flasks using a plastic scraper. The cell sus-pension was collected in cell culture medium and centrifuged at 350 ×g for 5 min, and the supernatant was removed. The cell pellet was then washed twice with PBS. The final cell pellet was aspirated dry and stored frozen at −80 °C until further use. The integrated cytotoxicity bioassay which combined endpoints of cell viability (resazurin reduction assay), cellular membrane integrity (intracellular LDH content) and energy metabolism (ATP assay) were conducted in 96-well plates as described in our

previous study (Kumarathasan et al., 2014). The cell proliferation (BrdU incorporation) assay was conducted in a separate 96-well plate.

IIa.2.4. Protein extraction

The cell pellets were solubilized in a protein extraction/rehydration buffer from Bio-Rad (8 M urea, 2 % CHAPS, 50 mM dithiothreitol, 0.2 % Biolyte 3/10), where the volume depends on the number of cells in the pellet to achieve 1–2 μg/μL, and 1×10^6 A549 cells was experimentally estimated to yield about 200 μg of protein. The samples were vortexed (30 s), sonicated (10 min), vortexed (30 s) and centrifuged (15,000 ×g, 10 min). The extracted protein in the supernatant was collected, and the concentration of protein in each extract was determined immediately using the Coomassie Plus Protein assay kit (Thermo Scientific). The extracted protein samples were stored at −80 °C until use.

IIa.2.5. Two-dimensional gel electrophoresis (2D-GE)

2D-GE was conducted as described in our previous study (Kumarathasan et al., 2005). Briefly, an appropriate quantity of protein was suspended in a total volume of 200 μL of extraction buffer, and applied to an immobilized pH gradient (IPG) strips (11 cm, pH 3–10 or pH 5–8) in a clean disposable rehydration tray and allowed to incubate for 1 h at room temperature. The IPG strip was then overlaid with mineral oil and allowed to continue incubating overnight (16–20 h). The IPG strip was then moved to an isoelectric focusing tray, overlaid with mineral oil and subjected to isoelectric focusing using a PROTEAN IEF cell (BioRad). The focusing conditions were as follows: stage 1: linear ramp to 250 V for 20 min; stage 2: linear ramp to 8000 V for 2.5 h; stage 3: rapid ramp for 20,000 V h. The strip was then stored at −80 °C until use. The focused IPG strip was thawed and gently agitated for 10 min in equilibration buffer 1 (6 M urea, 2 % SDS, 375 mM Tris-HCl, 20 % glycerol,

130 mM dithiothreitol, 0.001 % bromophenol blue). Then each strip was gently agitated for another 10 min in equilibration buffer 2 (6 M urea, 2 % SDS, 375 mM Tris-HCl, 20 % glycerol, 135 mM iodoacetamide, 0.001 % bromophenol blue). The strip was then placed on a 12 % SDS-PAGE gel casted in a 1.0 mm thick Criterion Cassette (13.3 × 8.7 cm W × L) and subjected to electrophoresis at 200 V for 65 min. Following electrophoresis, the gel was removed from the Criterion Cassette, washed for 30 min in water, stained in BioSafe Coomassie Blue (Bio-Rad) overnight (16–20 h), destained twice in water, and then imaged with a standard scanner.

To overcome the typical warping and distortion issues from gel to gel near the extremities of the pH and the molecular weight range, a common area (Figure IIa – 2; pH 5.1–7.8 and 100 – 20 kDa) that clearly shows the protein spots across all experimental gels was selected to assess the proteome differences among the treatments. The protein spots within the gels were matched and quantified with PDQuest™ Advance V8.0.1 (Bio-Rad), where spot volume was quantified using the available "Local regression model (LOESS)" algorithm in PDQuest. The reported normalized spot volume for each protein was used to compare its level of expression across the treatments. Three gels representing three biological repeats were generated for each group in this experiment to assess the particle-induced changes in the proteome of A549 cells.

IIa.2.6. In-gel digest, preparing protein spots for identification

To identify the protein in each spot of interest, a large set of preparative gels (10–12 gels) were prepared with 175 μg of protein/gel as described above. The gels were then stained with Biosafe Coomassie blue and imaged. The spots in preparative gels were then aligned and matched to the experimental gels using PDQuest. The protein spots were then

excised from the preparative gels with an automated spot cutter equipped with a 1.5 mm cutting head (ExQuest from Bio-Rad). The excised gels corresponding to the same protein spot from different preparative gels were pooled into the same tube for maximum protein yield. The excised gels were then subjected to in-gel tryptic digest as described in our previous study (Kumarathasan et al., 2005). Briefly, the gel spots were destained and then subjected to a 16 h digestion by trypsin (pH = 7) at 37 °C. All the digested samples were evaporated under a gentle stream of N_2(g) and were stored at −80 °C until further use.

IIa.2.7. Matrix-assisted laser desorption/ionization time-of-flight mass spectrometry (MALDI-TOF-TOF-MS)

Each sample was reconstituted in 5 to 20 μL of 30 % acetonitrile (ACN) in 0.1 % trifluoroacetic acid (TFA) depending on the spot volume and was spotted (1.5 μL) on an AnchorChip target plate (600/384F, Bruker Daltonics Ltd, Bremen, Germany) together with 1.5 μL of freshly prepared α-cyano-4-hydroxy-cinnamic acid (5 μg/μL in 50 % ACN in 0.1 % TFA). The spotted sample/matrix was dried under vacuum for at least 2 h. Each dried sample/matrix was washed with 2.5 μL of cold 0.1 % TFA and briefly dried under vacuum. Each sample was analyzed by MALDI-TOF-TOF-MS using an automated analysis option (Bruker Daltonics, Bremen, Germany). In brief, MS scan of each spot was done to obtain the peptide mass fingerprint (PMF). Six major analyte peaks from the PMF spectrum were subjected to tandem MS (MS/MS) analysis in the “voltage lift mode”. The mass spectral information was matched against the SwissProt and RefSeq data bases using the Mascot search engine (Matrix Sciences) for protein identification. In the case that > 1 protein was identified per spot, we attributed the protein with the highest score to such spot.

IIa.2.8. Statistics and bioinformatics

Two-way analysis of variance (ANOVA) was performed on 2D-GE and cytotoxicity (LDH, BrdU, ATP and CTB) data with treatment and dose as factors. When the assumption of equal variance and normal distribution were not met, the data were rank-transformed. Holm-Sidak was the post-hoc method used for all pairwise comparison procedures. A data point is considered as significant if $p < 0.05$. If the *Treatment x Dose* interaction was significant for a protein spot, its change in expression for a given treatment and dose that was found significant by Holm-Sidak analysis was reported as it is, as seen in Table IIa – 2. The same applied for those proteins that were found to have significant *Treatment and Dose* main effects. If a protein was found to have significant *Treatment* main effect, fold changes were estimated using least mean square (Searle et al., 1980; Goodnight and Harvey, 1978). In the case where the *Dose* main effect was significant, the average fold change estimate was reported for each significant dose group. It should be noted that multiple protein spots with the same protein ID may have a p-value < 0.05, which suggests different isoforms of the same protein were significantly altered, and thus rigorous assessment may be required for proper interpretation of biological implication if the directions of change of these isoforms are different. However, our data showed that the direction of expression of all significant protein spots with the same ID aligned in the same direction, thus we chose the protein with the greatest fold-change (either increase or decrease) to conduct pathway analysis. Protein interaction network and pathway analyses were con-ducted by Ingenuity Pathway Analysis (www.ingenuity.com). Venn diagrams used to assess the similarities and/or differences in the protein profile following particle exposures were generated via VENNY (Oliveros, 2015).

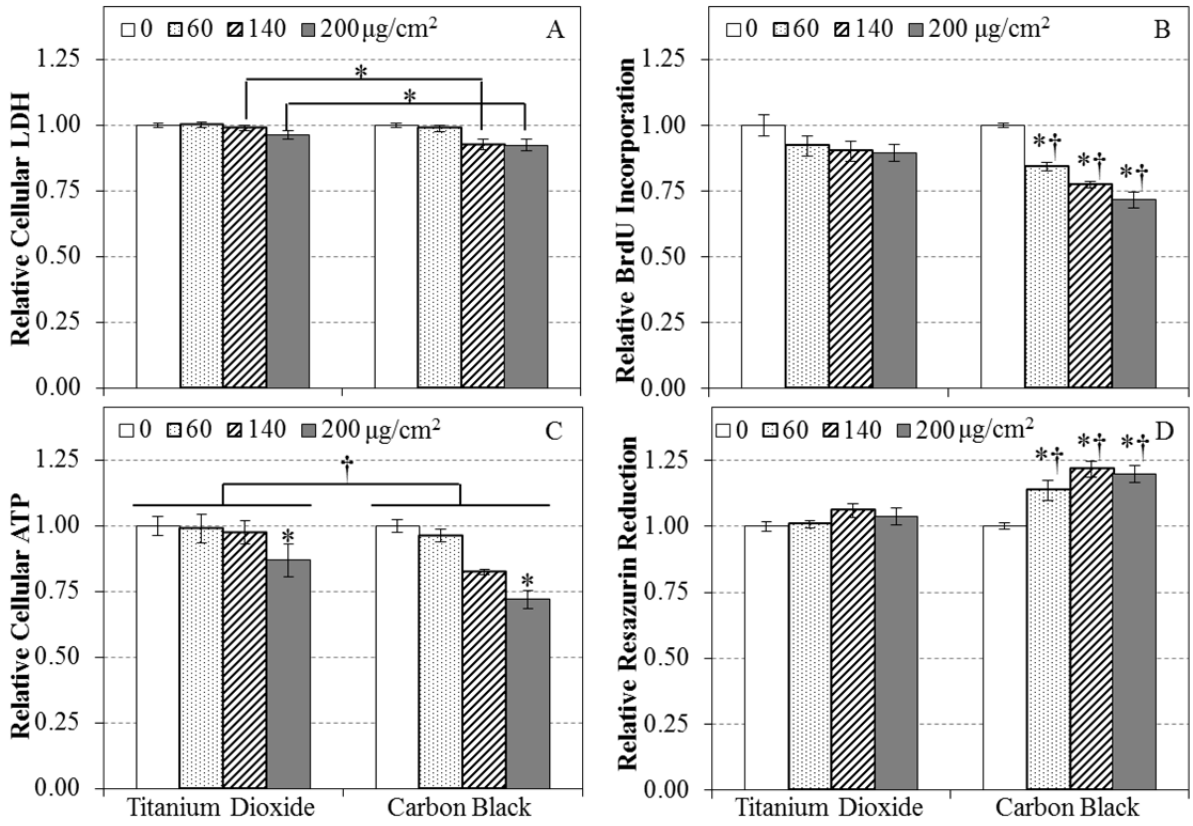

Figure IIa – 1. The cytotoxicity of titanium dioxide (TiO_2) and carbon black (CB).
A549 cells after 24 h of exposures to TiO_2 and CB were examined by cellular LDH (A), BrdU incorporation (B), cellular ATP (C) and resazurin reduction (D) assays. Data are expressed as mean fold effect ± standard error, relative to control (0 µg/cm^2), n = 4. Two-way ANOVA was used to determine significant effects of the particles, where Holm-Sidak was the post-hoc method used for all pairwise comparison procedures. * indicates a significant change ($p < 0.05$) compared to control (0 µg/cm^2) and † indicates significant differences between the two particles.

IIa.3. Results

IIa.3.1. Cytotoxicity assays

Cellular LDH levels (Figure IIa – 1A) were found to decrease with particle dose (Two-way ANOVA: *Dose* main effect, $p < 0.05$; Holm-Sidak: 140, 200 vs 0 μg/cm^2, $p < 0.05$). Reduction in cytoplasmic LDH was more pronounced after exposure to CB than with TiO_2, but this difference did not reach statistical significance. Cellular proliferation measured by BrdU incorporation (Figure IIa – 1B) was decreased by exposure to CB, but not with TiO_2 (Figure IIa – 1B; Two-way ANOVA, *Treatment* × *Dose* interaction, $p < 0.05$; Holm-Sidak: 60, 140, 200 vs 0 μg CB/cm^2, $p < 0.05$). Decrease of cellular ATP (Figure IIa – 1C) was statistically significant for treatment (Two-way ANOVA, *Treatment* main effect, $p < 0.05$; Holm-Sidak: CB vs TiO_2, $p < 0.05$) and dose (Two-way ANOVA, *Dose* main effect, $p < 0.05$; Holm-Sidak: 200 vs 0 μg/cm^2, $p < 0.05$). Resazurin reduction assay (Figure IIa – 1D) revealed a *Treatment* × *Dose* interaction (Two-way ANOVA: *Treatment* × *Dose*, $p < 0.05$; Holm-Sidak, 60, 140 & 200 vs 0 μg/cm^2, $p < 0.05$), where only CB, but not TiO_2, significantly increased the reduction of resazurin.

IIa.3.2. Two-dimensional gel electrophoresis (2D-GE)

It was experimentally determined that approximately 200 μg of protein can be extracted from 1 × 10^6 A549 cells. The protein profile of the A549 cells was initially evaluated with two pH ranges (pH 3–10 and pH 5–8) in the first dimension, while keeping the second dimension constant (12 % SDS-PAGE). The 2D gel image in Figure IIa – 2A showed that the pH 3–10 range encompassed most of the proteins detected by Coomassie blue. The pH 5–8 range gel detected approximately 85 % of the proteins that were found in

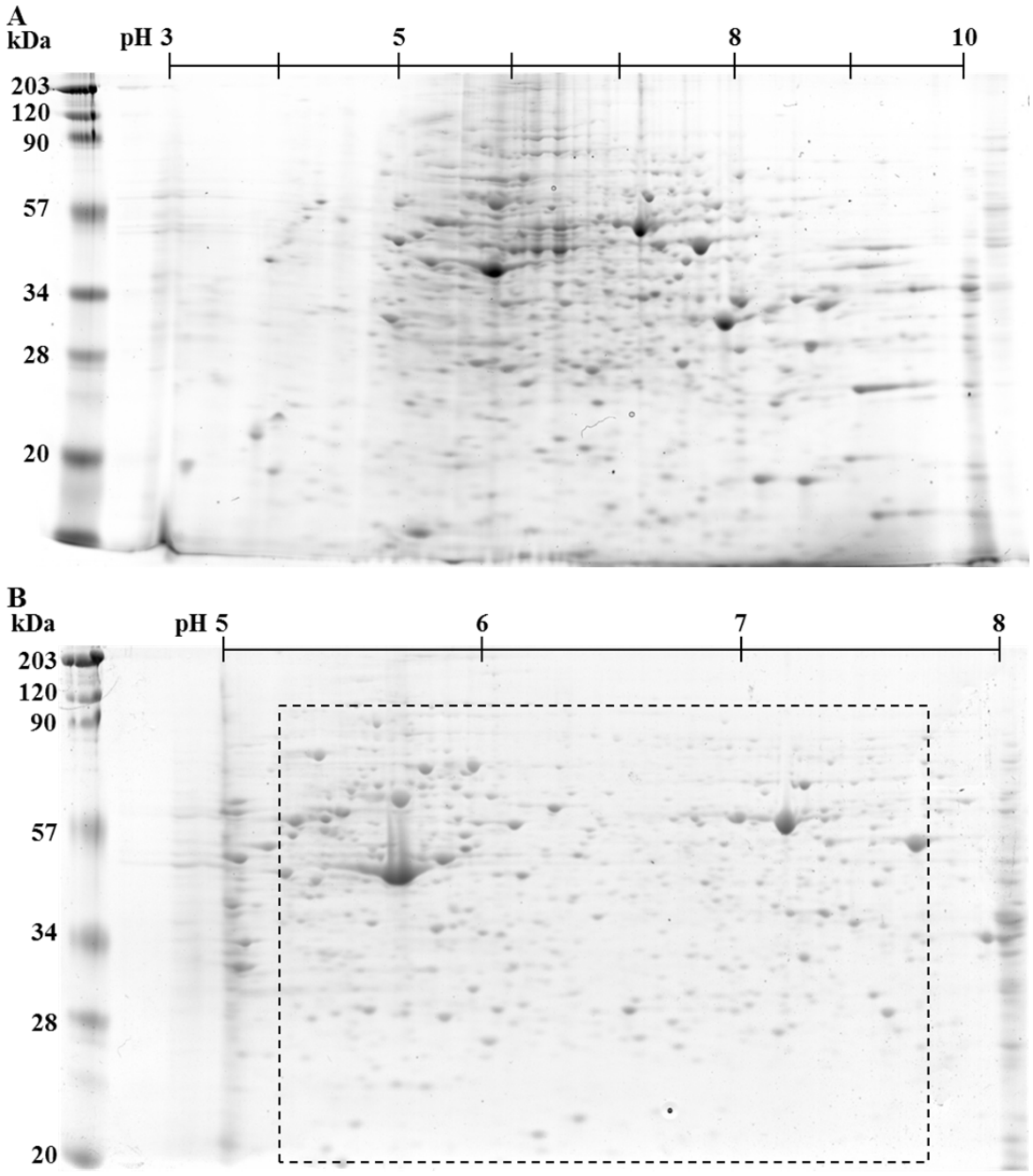

Figure IIa – 2. Selection of the information-rich region in the two-dimensional gel electrophoresis (2D-GE) map of A549 proteins to investigate particle exposure-related changes.

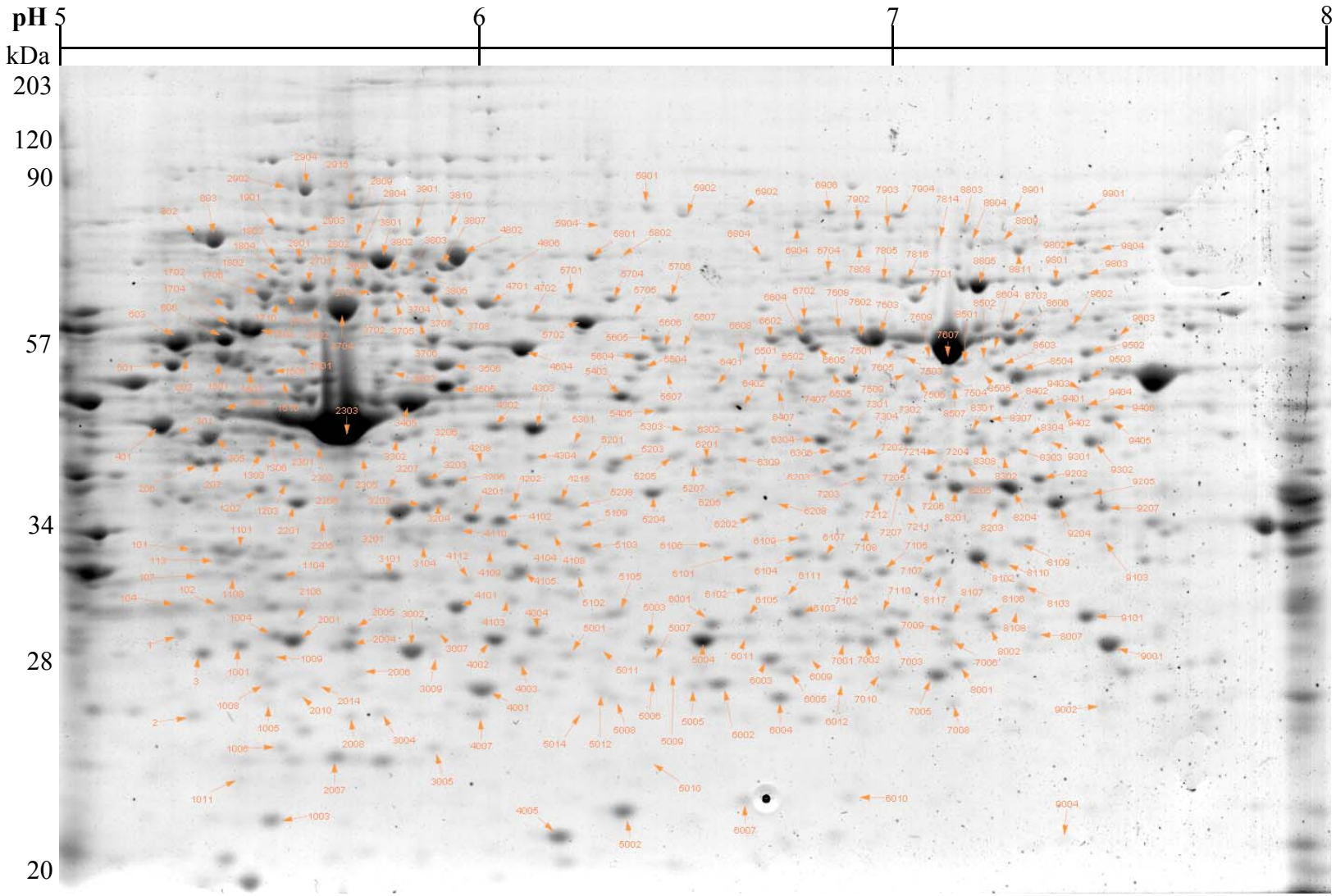

Figure IIa – 3. 2D-GE map of proteins in A549 cells used for further protein identification by mass spectrometry.
The numbers in the map correspond to the identified protein spots listed in Table IIb – 2 of the "Data in Brief" article (Vuong et al., 2016b) submitted along with this manuscript.

the pH 3–10 range (Figure IIa – 2B). The protein spots in the pH 5–8 range were notably better resolved than that of pH 3–10. For this reason, the pH 5–8 range and 12 % SDS-PAGE were selected to examine changes in the proteome of A549 cells following particle exposure. It was determined that when using 11 cm, pH 5–8 IPG strips, the optimal protein loading to visualize Coomassie Blue stained protein spots was between 100 and 175 μg (data not shown), as lower protein amounts resulted in missing spots, and higher protein loading led to poor resolution between spots due to the limited separation capacity of the 11 cm IPG strip. Coomassie blue stain was chosen since it is economical for the purpose of large toxicity screening studies and it is also compatible with MALDI-TOF-TOF-MS.

To assess the A549 proteome differences due to particle exposures, a common area that clearly displayed the majority of protein spots was employed across all experimental gels (Figure IIa – 2B). This area (between pH 5.1–7.8 and 20–100 kDa) was chosen to overcome the typical warping, distortion and variation that were commonly encountered with 2D gels, particularly near the extremities of the molecular weight and pH range. Of the 543 protein spots detected in the common area of the gels, 333 spots were identified with MALDI-TOF-TOF-MS/MS (Figure IIa – 3 and Supplementary Table IIb – 2 in the related "Data in Brief" article (Vuong et al., 2016b)). In many cases, the same protein was detected in multiple spots; these multiple IDs (likely representing post-translational modifications, isoforms or degradation products) are summarized in Supplementary Table IIb – 2 in the related "Data in Brief" article. In total, the 2D-GE map resulted in the identification of 180 unique proteins.

Table IIa – 1. Two-way ANOVA results for the A549 protein spot changes due to particle exposures (n = 3).
The number below *Treatment* main effect (Trt), *Dose* main effect (Dose) or interaction (*T* × *D*) corresponds to the p-value, where the bold number is <0.05. The number below the particles corresponds to the adjusted fold change (versus control) of the protein. Only the protein spots identified by MALDI-TOF-TOF-MS are provided here.

		Two-Way ANOVA			TiO_2 (µg/cm^2)			CB (µg/cm^2)		
SSP	**Protein**	**Trt**	**Dose**	**T x D**	**60**	**140**	**200**	**60**	**140**	**200**
3202	CAPZA1	**0.004**	**0.016**	**0.031**						1.15
9804	FUBP1	**0.039**	0.947	**0.044**			1.29			-1.41
7701	CCT6A	0.507	**0.031**	**0.034**						1.51
8501	EEF2	0.571	**0.004**	**0.020**		3.00				-2.63
6501	PA2G4	0.165	**0.023**	**0.047**						1.40
7501	PA2G4	0.953	**0.009**	**0.037**						1.49
1602	TUBA1C	0.793	**0.015**	**0.049**						2.43
2902	VCP	0.457	**0.002**	**0.024**						1.63
7603	ALDH1A1	0.096	0.131	**0.034**			-1.61			
6604	CCT2	0.792	0.237	**0.023**			-1.24			1.53
4702	PDIA3	0.368	0.220	**0.021**					1.45	
3207	TRIM28	0.192	0.096	**0.035**			1.49			-1.44
4102	VCP	0.554	0.083	**0.036**						-1.35
2006	CRK	**<0.001**	**<0.001**	0.085	1.29	1.77	1.44	4.28	6.20	5.93
8205	AKR1A1	**0.041**	0.431	0.395				1.33	1.33	1.33
102	HSPA5	**0.017**	**0.134**	0.441				1.51	1.51	1.51
8809	LMNA	**0.028**	0.311	0.303	-1.10	-1.10	-1.10	1.19	1.19	1.19
2301	TMOD3	**0.005**	0.201	0.139	-1.19	-1.19	-1.19	1.28	1.28	1.28
6502	ANXA7	0.124	**0.037**	0.502		1.32	-1.68		1.32	-1.68
8108	ARMCX1	0.472	**0.017**	0.379		1.88			1.88	
9502	DIS3L	0.298	**0.000**	0.504			-1.52			-1.52
8107	EEF2	0.580	**0.031**	0.719		1.52	-1.30		1.52	-1.30
7205	ENO1	0.723	**0.021**	0.416		1.59	-1.18		1.59	-1.18
8503	ENO1	0.413	**0.035**	0.561		1.32	-1.29		1.32	-1.29
9405	ENO1	0.876	**0.043**	0.593		1.57	-1.26		1.57	-1.26
5607	HNRNPH1	0.852	**0.022**	0.458		-1.33	1.35		-1.33	1.35
2701	HNRNPK	0.913	**0.020**	0.146		-1.77			-1.77	
3104	HSP90AB3P	0.568	**0.026**	0.615		1.56	-1.15		1.56	-1.15
8106	HSPA8	0.622	**0.035**	0.533		1.51	-1.07		1.51	-1.07
8117	IDH1	0.899	**0.014**	0.443		1.58	-1.37		1.58	-1.37
5902	IMMT	0.510	**0.019**	0.761	1.35	-1.38		1.35	-1.38	
3705	INA	0.967	**0.002**	0.084		2.16	1.72		2.16	1.72
8103	NIT2	0.410	**0.017**	0.797		1.26	-1.11		1.26	-1.11
8110	PDIA3	0.270	**0.029**	0.580		1.53	-2.30		1.53	-2.30
6306	PGK1	0.363	**0.034**	0.282		1.27	-1.43		1.27	-1.43
7204	PKM	0.431	**0.003**	0.922			-1.86			-1.86
8606	PKM	0.942	**0.026**	0.889			-1.68			-1.68
5105	PSMB7	0.367	**0.019**	0.466			1.38			1.38
8301	RBM4	0.676	**0.038**	0.402	1.65			1.65		
8308	RBM4	0.708	**0.025**	0.634		-1.27			-1.27	
2904	VCP	0.745	**0.004**	0.141		-2.23			-2.23	
5301	XXYLT1	0.131	**0.008**	0.499	1.24	1.19	1.26	1.24	1.19	1.26

IIa.3.3. PM-induced changes in the proteome of A549 cells

Analysis of proteomic changes due to particle exposures revealed that the expressions of 60 protein spots were affected by both TiO_2 and CB, of which 42 protein spots were identified by MALDI-TOF-TOF-MS (Table IIa – 1). For proteins represented by multiple spots, the spot with the greatest fold change was selected for pathway analysis as mentioned in the Materials and Methods. Particle dose-related changes were noticed in 24 protein spots (Two-way ANOVA: *Dose* main effect, $p < 0.05$), 20 of which are unique proteins. Particle type-specific changes were noticed in 5 protein spots (Two-way ANOVA: *Treatment* main effect, $p < 0.05$), all of which are unique proteins; while 13 protein spots exhibited *Treatment* × *Dose* interaction (Two-way ANOVA: *Treatment* × *Dose* main effect, $p < 0.05$), 12 of these are unique proteins. Figure IIa – 4A illustrates the effect of TiO_2 and CB exposures on A549 cellular proteome, where the particles up- and down-regulated the expression of proteins. The proteins that were affected commonly by both particle exposures and particle-specific alteration are shown in Figure IIa – 4B and C. Protein interaction network and pathway analyses revealed that all the proteins (common and unique) affected by the two particles were known to be associated with cell death (necrosis and/or apoptosis), proliferation, migration, protein metabolism, inflammation and survival/viability pathways (Table IIa – 2). To determine the toxicoproteomic differences between TiO_2 and CB, the proteins that were differentially affected by the two particles were interrogated; these proteins were highlighted in Table IIa – 1 that two-way ANOVA identified as significant for interaction and treatment main effects. The results in Table IIa – 3 show that the differential toxicoproteomic effect between TiO_2 and CB lies mainly in those proteins that regulate proliferation, viability, apoptosis and necrosis in cells. Figure IIa – 5 shows that there were

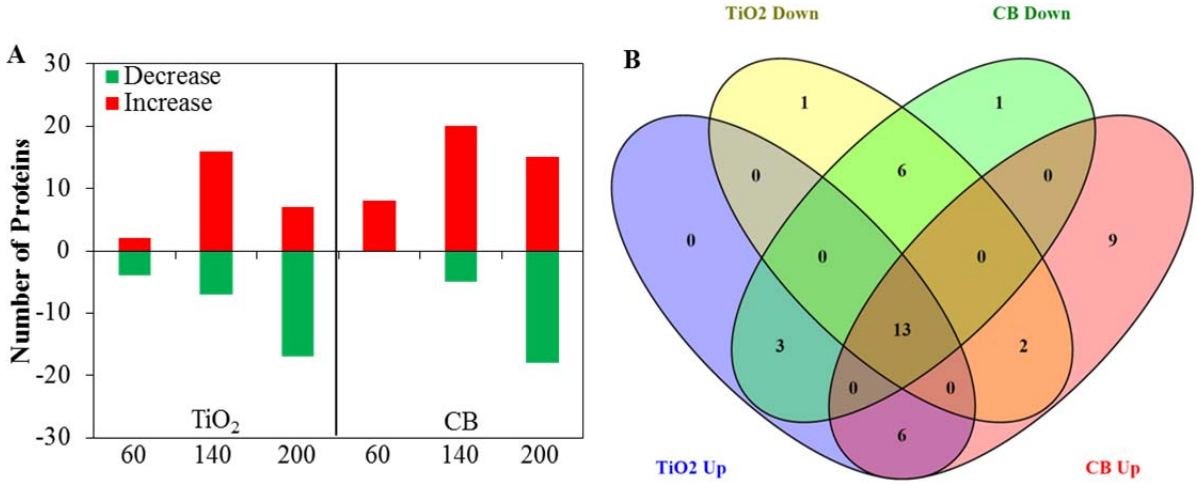

C

Only CB↑: 9		Only CB↓: 1		Only TiO_2↓: 1		CB↑ TiO_2↓: 2		CB↓ TiO_2↑: 3		CB↓ TiO_2↓: 6		CB↑ TiO_2↑: 6		CB↑ CB↓ TiO2↑ TiO_2↓: 13	
No.	Protein	No.	Protein	No.	Protein	No.	Protein	No.	Protein	No.	Protein	No.	Protein	No.	Protein
4	HSPA5	103	VCP	218	ALDH1A1	48	TMOD3	76	TRIM28	53	HNRNPK	334	ARMCX1	181	ANXA7
32	TUBA1C					296	LMNA	244	EEF2	63	VCP	43	CRK	231	EEF2
61	VCP					184	CCT2	279	FUBP1	202	PKM	85	INA	203	ENO1
71	CAPZA1									242	RBM4	132	PSMB7	246	ENO1
116	PDIA3									251	PKM	238	RBM4	269	ENO1
180	PA2G4									271	DIS3L	289	XXYLT1	145	HNRNPH1
212	PA2G4													311	HSP90AB3P
223	CCT6A													230	HSPA8
237	AKR1A1													234	IDH1
														153	IMMT
														229	NIT2
														233	PDIA3
														177	PGK1

Figure IIa – 4. Two-way ANOVA results of differentially expressed proteins (p-value < 0.05) in A549 cells following exposures to carbon black (CB) or titanium dioxide (TiO_2). (A) The bar graph shows the number of proteins which increased or decreased in expression following particle treatments at doses 60, 140 and 200 μg/cm^2. (B) The Venn diagram shows the number of proteins that exhibited specific and non-specific changes due to particle exposures. (C) Tabulation of unique and common proteins associated with CB and TiO2 exposures. Only the proteins that were identified by MALDI-TOF-TOF-MS/MS are shown. ↑ indicates increased expression and ↓ specifies decreased expression.

Table IIa – 2. All A549 proteins that exhibited altered expressions (fold change compared to control) due to particle exposures and relevant cellular functions using Ingenuity Pathway Analysis.

Cellular Function	TiO_2 (μg/cm^2)			CB (μg/cm^2)		
	60	140	200	60	140	200
Cell Death (Apoptosis & Necrosis)						
ALDH1A1			-1.61			
ANXA7		1.32	-1.68		1.32	-1.68
ENO1*		1.57	-1.26		1.57	-1.26
FUBP1			1.29			-1.41
CRK	1.29	1.77	1.44	4.28	6.20	5.93
HNRNPH1		-1.33	1.35		-1.33	1.35
HNRNPK		-1.77			-1.77	
HSPA5				1.51	1.51	1.51
HSPA8		1.51	-1.07		1.51	-1.07
IMMT	1.35	-1.38		1.35	-1.38	
LMNA	-1.10	-1.10	-1.10	1.19	1.19	1.19
PA2G4*						1.49
PDIA3*		1.53	-2.30		1.53	-2.30
PKM*			-1.86			-1.86
TMOD3	-1.19	-1.19	-1.19	1.28	1.28	1.28
TRIM28			1.49			-1.44
VCP*		-2.23			-2.23	1.63
CCT6A						1.51
CCT2			-1.24			1.53
Inflammation						
AKR1A1				1.33	1.33	1.33
ANXA7		1.32	-1.68		1.32	-1.68
EEF2*		3.00	-1.30		1.52	-2.63
ENO1*		1.57	-1.26		1.57	-1.26
FUBP1			1.29			-1.41
HSPA5				1.51	1.51	1.51
HSPA8		1.51	-1.07		1.51	-1.07
PDIA3*		1.53	-2.30		1.53	-2.30
PGK1		1.27	-1.43		1.27	-1.43
PKM*			-1.86			-1.86
TRIM28			1.49			-1.44
TUBA1C						2.43
VCP*		-2.23			-2.23	1.63
Protein Metabolism						
CRK	1.29	1.77	1.44	4.28	6.20	5.93
EEF2*		3.00	-1.30		1.52	-2.63
HNRNPK		-1.77			-1.77	
HSPA5				1.51	1.51	1.51
PDIA3*		1.53	-2.30		1.53	-2.30
RBM4*	1.65	-1.27		1.65	-1.27	
VCP*		-2.23			-2.23	1.63

* indicates protein represented by multiple spots. The spot with the highest fold change was used as mentioned in material and method.

Table IIa – 2 (Continued…)

Cellular Function	TiO_2 (µg/cm^2) 60	140	200	CB (µg/cm^2) 60	140	200
Cell Survival & Viability						
EEF2*		3.00	-1.30		1.52	-2.63
IDH1		1.58	-1.37		1.58	-1.37
LMNA	-1.10	-1.10	-1.10	1.19	1.19	1.19
PDIA3*		1.53	-2.30		1.53	-2.30
PKM*			-1.86			-1.86
TRIM28			1.49			-1.44
HSPA5				1.51	1.51	1.51
VCP*		-2.23			-2.23	1.63
Cell Proliferation						
ANXA7		1.32	-1.68		1.32	-1.68
ENO1*		1.57	-1.26		1.57	-1.26
CRK	1.29	1.77	1.44	4.28	6.20	5.93
HNRNPK		-1.77			-1.77	
HSPA8		1.51	-1.07		1.51	-1.07
IDH1		1.58	-1.37		1.58	-1.37
IMMT	1.35	-1.38		1.35	-1.38	
LMNA	-1.10	-1.10	-1.10	1.19	1.19	1.19
PDIA3*		1.53	-2.30		1.53	-2.30
PGK1		1.27	-1.43		1.27	-1.43
VCP*		-2.23			-2.23	1.63
ALDH1A1			-1.61			
CCT2			-1.24			1.53
DIS3L			-1.52			-1.52
PKM*			-1.86			-1.86
TRIM28			1.49			-1.44
HSPA5				1.51	1.51	1.51
CAPZA1						1.15
PA2G4*						1.49
Cell Migration						
CRK	1.29	1.77	1.44	4.28	6.20	5.93
ENO1*		1.57	-1.26		1.57	-1.26
HNRNPK		-1.77			-1.77	
HSPA5				1.51	1.51	1.51
IDH1		1.58	-1.37		1.58	-1.37
LMNA	-1.10	-1.10	-1.10	1.19	1.19	1.19
PA2G4*						1.49
PDIA3*		1.53	-2.30		1.53	-2.30
PKM*			-1.86			-1.86
TMOD3	-1.19	-1.19	-1.19	1.28	1.28	1.28
TUBA1C						2.43
VCP*		-2.23			-2.23	1.63

* indicates protein represented by multiple spots. The spot with the highest fold change was used as mentioned in material and method.

distinctive patterns of protein expression in A549 cells in response to the two particles as demonstrated in the networks of cell death (apoptosis and necrosis) and cell proliferation pathways.

IIa.4. Discussion

In this work, we utilized a well-established human lung epithelial cell line (A549) to assess the effects of CB and TiO_2, two respirable particles with distinct chemical and physical properties. Decrease of the cytoplasmic LDH content is suggestive of alteration of cell membrane integrity. BrdU incorporation, which assesses DNA synthesis during cell proliferation, was reduced with increasing doses of CB but not TiO_2. Cellular energy metabolism investigated by the ATP assay demonstrated that both particles reduced the level of ATP in A549 cells, with CB being more potent than TiO_2. In the resazurin reduction assay, CB but not TiO_2 increased the rate of reduction. In short, the results from the cytotoxicity assays indicate that A549 cells were reactive to the particles, with CB being more potent than TiO_2 in eliciting cellular responses, but both particles were mildly cytotoxic under the experimental conditions with a cellular viability greater than 75 % at the highest exposure level tested.

Cellular proteomic changes were analyzed by 2D-GE followed by protein identification using mass spectrometry. We chose to examine the A549 proteome in the window of pH 5.2–pH 7.8 and 100–20 kDa because this area contained most of the protein spots (543) that were well-resolved across all experimental gels (Figure IIa – 2B). Of the 543 protein spots, we have determined the identities of 333 protein spots via MALDI-TOF-TOF-MS/MS, and to our knowledge this is the largest repository of A549 cellular proteome identified by 2D-GE thus far. It should be noted that the same protein was detected in

Table IIa – 3. A549 proteins that are differentially affected by TiO_2 and CB and associated cellular functions.
The proteins in this table were identified by two-way ANOVA as *Treatment* main effect and *Treatment* × *Dose* interaction, which were highlighted in Table IIa – 1.

Cellular	**TiO_2 (μg/cm^2)**			**CB (μg/cm^2)**		
Function	**60**	**140**	**200**	**60**	**140**	**200**
Cell Death (Apoptosis & Necrosis)						
ALDH1A1			-1.61			
CCT2			-1.24			1.53
CCT6A						1.51
FUBP1			1.29			-1.41
CRK	1.29	1.77	1.44	4.28	6.20	5.93
HSPA5				1.51	1.51	1.51
LMNA	-1.10	-1.10	-1.10	1.19	1.19	1.19
PA2G4*						1.49
TMOD3	-1.19	-1.19	-1.19	1.28	1.28	1.28
TRIM28			1.49			-1.44
VCP*		-2.23			-2.23	1.63
Cell Viability						
EEF2		3.00	-1.30		1.52	-2.63
HSPA5				1.51	1.51	1.51
LMNA	-1.10	-1.10	-1.10	1.19	1.19	1.19
TRIM28			1.49			-1.44
VCP*		-2.23			-2.23	1.63
Cell Proliferation						
ALDH1A1			-1.61			
CAPZA1						1.15
CCT2			-1.24			1.53
CRK	1.29	1.77	1.44	4.28	6.20	5.93
HSPA5				1.51	1.51	1.51
LMNA	-1.10	-1.10	-1.10	1.19	1.19	1.19
PA2G4*						1.49
TRIM28			1.49			-1.44
VCP*		-2.23			-2.23	1.63

* indicates protein represented by multiple spots. The spot with the highest fold change was used as mentioned in material and method.

multiple spots in many cases (Table IIb – 2 in the related "Data in Brief" article (Vuong et al., 2016b)), where these multiple IDs are likely representing post-translational modifications, isoforms or degradation products of the same protein.

Two-way ANOVA revealed that 60 of the protein spots showed significant changes ($p < 0.05$) as *Treatment* or *Dose* main effects, and with *Treatment* × *Dose* interaction following exposure of cells to TiO_2 and CB (Table IIa – 1). Figure IIa – 4A illustrates the effect of TiO_2 and CB exposures on A549 cellular proteome, where the particles up- and down-regulated the expression of proteins. This figure showed that 140 μg/cm^2 doses led to increased expression of more proteins relative to both 60 and 200 μg/cm^2 doses. These findings can potentially be attributed to non-monotonous toxicity effects. It is possible that the medium dose (140 μg/cm^2) enhanced protein synthesis as a response to increased toxicity compared to the low dose, whereas at the highest toxic dose (200 μg/cm^2), reduced protein synthesis and enhance protein degradation can occur as a result of cellular apoptosis.

It should be noted that the significant cut-off *p*-value was set at 0.05, it is possible that 27 significant spots (5 % of 543 protein spots examined) could be false positive by random chance. However, proteins do not act on their own in a cell, they normally interact with one another in a network or pathway to carry out a particular function. Thus, when a group of proteins in a particular pathway were identified as significantly altered with unadjusted *p*-value < 0.05, we posit that changes in a group of proteins are not likely to occur by random chance. Therefore, we decided to retain the 60 significant protein spots with *p*-value < 0.05 (not adjusted for false discovery), and the identities of 42 of these spots have been determined via MALDI-TOF-TOF-MS (Figure IIa – 4 and Table IIa – 1). In pathway analysis, only those pathways that were influenced by >5 significant proteins in any treatment were flagged as possible pathways that were affected by exposure treatments.

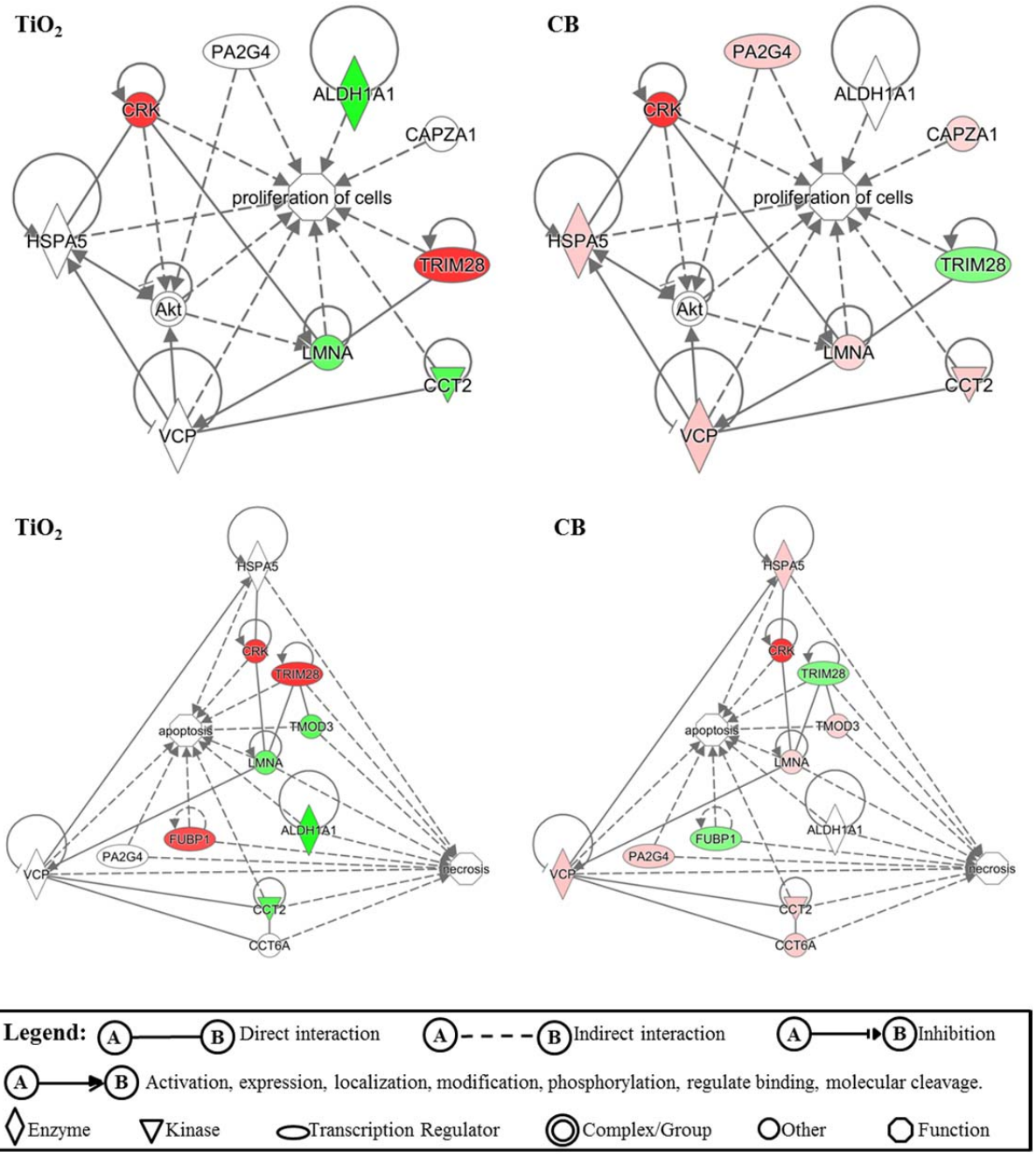

Figure IIa – 5. The networks of cell death (apoptosis and necrosis) and cell proliferation pathways that emphasize the toxicoproteomic differences between TiO_2 and CB at the dose 200 μg/cm^2 (Table IIa – 3). Red is for increased expression and green is for decreased expression.

Ingenuity pathway analysis revealed that TiO_2 and CB can significantly alter the expression of proteins that are known to be involved in inflammation, protein metabolism, cell migration, proliferation, death and survival (Table IIa – 2). Although the use of all significant proteins for pathway analysis gave an overall idea of the cellular functions that can be affected by both particles, in order to dissect the toxicoproteomic differences between TiO_2 and CB, we selected the proteins that were unique to TiO_2 and CB exposures for pathway analysis (Table IIa – 3). The results in Table IIa – 3 demonstrated that the proteins that regulate cell proliferation, viability, apoptosis and necrosis were affected by TiO_2 and CB differently. Nevertheless, the number of proteins that are unique to these pathways was found to be low. For instance, CCT6A, EEF2 and CAPZA1 were unique to cell death, cell viability and cell proliferation respectively, while the others were common to all three pathways. Even though it is possible that there can be network ambiguity through IPA analyses, the significant proteins that were affected by both particles in Table IIa – 2 showed more unique proteins specific to cell death (e.g., CCT6A, FUBP1, HNRNPH1 and TMOD3) and cell proliferation (e.g., CAPZA1, DIS3L and PGK1) pathways. In addition, the cytotoxicity assay results are indicative of induced cell death (decreased cellular LDH and ATP levels) and decreased cell proliferation (decreased BrdU incorporation) pathways upon particle exposures. Together, these observations suggest that these particle exposures affected cell death, cell viability and cell proliferation pathways in the A549 cells.

The networks of protein-protein interaction in Figure IIa – 5 showed how the two particles distinctively affected those proteins involved in cell death and proliferation pathway. In the network of cell proliferation, TiO_2 specifically increased the expression of TRIM28 and decreased the expression of ALDH1A1, CCT2 and LMNA, while CB specifically decreased the expression of TRIM28 and increased the expression of CAPZA1,

CCT2, HSPA5, LMNA, PA2G4 and VCP. The serine/threonine kinase Akt is a well-recognized signaling hub that orchestrates various cellular functions (including cell growth and survival) and this protein interacts directly and indirectly with the majority of the proteins that were up-regulated only by CB treatments (Figure IIa – 5). It would be interesting to examine the time-related functional interactions between Akt and these proteins. For example, the level of LMNA is reportedly regulated by the serine/threonine kinase Akt in C2C12 mouse myoblasts and HEK293 human embryonic kidney epithelial cells (Bertacchini et al., 2013), where Akt can phosphorylate LMNA and targets it for degradation through a lysosomal mechanism (Bertacchini et al., 2013), and Akt can also regulate the transcription of LMNA (Bertacchini et al., 2013). Since LMNA is an intermediate filament protein in the nuclear lamina that must be degraded for DNA synthesis and mitosis to occur, an increase in LMNA expression in A549 cells exposed to CB can be a marker of DNA synthesis, which was supported by BrdU incorporation assay (Figure IIa – 1B). Another protein that interacts with Akt and affects the proliferation of cells is PA2G4 that can bind to the androgen receptor (Zhang et al., 2002) and transcriptionally repress genes regulated by the receptor (Zhang et al., 2005). Overexpression of PA2G4 has been reported to inhibit growth in LNCaP human prostate adenocarcinoma cells (Zhang et al., 2005), NIH3T3 human fibroblasts (Squatrito et al., 2004) and rat pheochromocytoma PC-12 cells (Liu et al., 2006). Thus, the observed increased expression of PA2G4 in A549 mediated by CB exposure can be another marker that suppresses cell proliferation. In essence A549 cellular proteomic changes relevant to CB exposure involved in reduction in cell proliferation are consistent with the level of BrdU incorporation.

Toxicoproteomics also revealed particle-specific changes in the level and/or direction of a unique set of proteins that are known to regulate cell death (apoptosis and necrosis)

(Table IIa – 3). In the protein-protein interaction network of the cell death pathway in Figure IIa – 5, about a dozen of A549 proteins showed a stark difference between TiO_2 and CB exposures. For example, TiO_2 specifically increased the expression of TRIM28 and FUBP1 but decreased the expression of ALDH1A1, CCT2, LMNA and TMOD3. On the other hand, CB specifically decreased the expression of TRIM28 and FUBP1 but increased the expression of CAPZA1, CCT2, CCT6A, HSPA5, LMNA, PA2G4 and VCP. A number of these proteins can also be found in the cell proliferation network as these proteins have anti-proliferative effect as discussed above. Interestingly, CB appears to cause more cell death in A549 cells than TiO_2 based on the LDH assay (Figure IIa – 1A), but the variance in this assay did not allow statistical analysis to differentiate the toxic potencies between the two particles. Thus, toxicoproteomics is more sensitive in distinguishing the subtle effect of the particles on the cell death pathways. In addition, the VCP ATPase (Song et al., 2003) and HSPA5 heat shock protein (Wisniewska et al., 2010) in the endoplasmic reticulum are associated with ATPase activity, and thus CB-induced increases in VCP and HSPA5 can lower the level of cellular ATP by enhancing ATPase activity in A549 cells. These findings were supported by ATP assay (Figure IIa – 1C). In essence, the results of our study demonstrated that toxicoproteomics is a sensitive and informative method to differentiate the toxic effects of particulate matter.

IIa.5. Conclusion

In vitro toxicoproteomics has the capacity to distinguish cellular responses to two particles with distinct chemical and physical properties as illustrated by TiO_2 and CB exposures of A549 cells. The particles caused common and distinct A549 cellular responses

that were detectable via cytotoxicity assays and high-content proteomic analysis, which can be useful to investigate the molecular mechanisms of particle toxicity. This toxicoproteomic approach can be valuable in future particle toxicity evaluation studies.

Acknowledgements

We would like to thank Drs. Errol Thomson and Bhaja Krushna Padhi for their helpful comments. This work was supported by the Clean Air Regulatory Agenda at Health Canada (HC4340565) and, Ontario Gradu-ate Scholarship in Science and Technology (Student #1519592) and Ontario Graduate Scholarship (Student #1519592) (funding for Ngoc Vuong). We also acknowledge Christine MacKinnon-Roy and Alexandra Star for their valuable technical assistance.

References

Bell,M.L. (2012). Assessment of the health impacts of particulate matter characteristics. Res. Rep. Health Eff. Inst. 5-38.

Bertacchini,J., Beretti,F., Cenni,V., Guida,M., Gibellini,F., Mediani,L., Marin,O., Maraldi,N.M., de,P.A., Lattanzi,G., Cocco,L., and Marmiroli,S. (2013). The protein kinase Akt/PKB regulates both prelamin A degradation and Lmna gene expression. FASEB J. 27, 2145-2155.

Canova,C., Dunster,C., Kelly,F.J., Minelli,C., Shah,P.L., Caneja,C., Tumilty,M.K., and Burney,P. (2012). PM10-induced hospital admissions for asthma and chronic obstructive pulmonary disease: the modifying effect of individual characteristics. Epidemiology 23, 607-615.

Farhat,S.C., Almeida,M.B., Silva-Filho,L.V., Farhat,J., Rodrigues,J.C., and Braga,A.L. (2013). Ozone is associated with an increased risk of respiratory exacerbations in patients with cystic fibrosis. Chest 144, 1186-1192.

Ge,Y., Bruno,M., Wallace,K., Leavitt,S., Andrews,D., Spassova,M.A., Xi,M., Roy,A., Haykal-Coates,N., Lefew,W., Swank,A., Winnik,W.M., Chen,C., Woodard,J., Farraj,A., Teichman,K.Y., and Ross,J.A. (2015). Systematic proteomic approach to characterize the impacts of chemical interactions on protein and cytotoxicity responses to metal mixture exposures. J. Proteome. Res. 14, 183-192.

Ge,Y., Bruno,M., Wallace,K., Winnik,W., and Prasad,R.Y. (2011). Proteome profiling reveals potential toxicity and detoxification pathways following exposure of BEAS-2B cells to engineered nanoparticle titanium dioxide. Proteomics. 11, 2406-2422.

Goeminne,P.C., Kicinski,M., Vermeulen,F., Fierens,F., De,B.K., Nemery,B., Nawrot,T.S., and Dupont,L.J. (2013). Impact of air pollution on cystic fibrosis pulmonary exacerbations: a case-crossover analysis. Chest 143, 946-954.

Goodnight JH and Harvey WR. Least-Squares Means in the Fixed-Effects General Linear Models. SAS Technical Report R-103. 1978. SAS Institute Inc., SAS Technical Report. SAS Technical Report R-103.

Hosp,F., Scheltema,R.A., Eberl,C., Kulak,N.A., Keilhauer,E.C., Mayr,K., and Mann,M. (2015). A double-barrel LC-MS/MS system to quantify 96 interactomes per day. Mol. Cell Proteomics.

Johnston,H.J., Hutchison,G.R., Christensen,F.M., Peters,S., Hankin,S., and Stone,V. (2009). Identification of the mechanisms that drive the toxicity of TiO(2)particulates: the contribution of physicochemical characteristics. Part Fibre. Toxicol. 6, 33.

Kachuri,L., Villeneuve,P.J., Parent,M.E., Johnson,K.C., and Harris,S.A. (2013). Occupational exposure to crystalline silica and the risk of lung cancer in Canadian men. Int. J. Cancer.

Kumarathasan P, Das D, Salam MA, Mohottalage S, DeSilva N, Simard B, and Vincent R (2012). Mass spectrometry-based proteomic assessment of the in vitro toxicity of carbon nanotubes. Current Topics in Biochemica Research 14, 15-27.

Kumarathasan,P., Breznan,D., Das,D., Salam,M.A., Siddiqui,Y., Mackinnon-Roy,C., Guan,J., de,S.N., Simard,B., and Vincent,R. (2014). Cytotoxicity of carbon nanotube variants: A comparative in vitro exposure study with A549 epithelial and J774 macrophage cells. Nanotoxicology 9, 148-61.

Kumarathasan,P., Mohottalage,S., Goegan,P., and Vincent,R. (2005). An optimized protein in-gel digest method for reliable proteome characterization by MALDI-TOF-MS analysis. Anal. Biochem. 346, 85-89.

Lee,J.G., Noh,W.J., Kim,H., and Lee,M.Y. (2011). Generation of reactive oxygen species contributes to the development of carbon black cytotoxicity to vascular cells. Toxicol. Res. 27, 161-166.

Levy,J.I., Diez,D., Dou,Y., Barr,C.D., and Dominici,F. (2012). A meta-analysis and multisite time-series analysis of the differential toxicity of major fine particulate matter constituents. Am. J. Epidemiol. 175, 1091-1099.

Liu,L., Yu,L.Y., Mu,H.J., Xing,L.Y., Li,Y.X., and Pan,G.W. (2014). Shape of concentration-response curves between long-term particulate matter exposure and morbidities of chronic bronchitis: a review of epidemiological evidence. J. Thorac. Dis. 6, S720-S727.

Liu,Z., Ahn,J.Y., Liu,X., and Ye,K. (2006). Ebp1 isoforms distinctively regulate cell survival and differentiation. Proc. Natl. Acad. Sci. U. S. A 103, 10917-10922.

Long,C.M., Nascarella,M.A., and Valberg,P.A. (2013). Carbon black vs. black carbon and other airborne materials containing elemental carbon: physical and chemical distinctions. Environ. Pollut. 181, 271-286.

MacIntyre,E.A., Brauer,M., Melen,E., Bauer,C.P., Bauer,M., Berdel,D., Bergstrom,A., Brunekreef,B., Chan-Yeung,M., Klumper,C., Fuertes,E., Gehring,U., Gref,A., Heinrich,J., Herbarth,O., Kerkhof,M., Koppelman,G.H., Kozyrskyj,A.L., Pershagen,G., Postma,D.S., Thiering,E., Tiesler,C.M., and Carlsten,C. (2014). GSTP1 and TNF Gene variants and associations between air pollution and incident childhood asthma: the traffic, asthma and genetics (TAG) study. Environ. Health Perspect. 122, 418-424.

Malard,V., Prat,O., Darrouzet,E., Berenguer,F., Sage,N., and Quemeneur,E. (2005). Proteomic analysis of the response of human lung cells to uranium. Proteomics. 5, 4568-4580.

Merlo,F., Costantini,M., Reggiardo,G., Ceppi,M., and Puntoni,R. (1991). Lung cancer risk among refractory brick workers exposed to crystalline silica: a retrospective cohort study. Epidemiology 2, 299-305.

Morbt,N., Tomm,J., Feltens,R., Mogel,I., Kalkhof,S., Murugesan,K., Wirth,H., Vogt,C., Binder,H., Lehmann,I., and von,B.M. (2011). Chlorinated benzenes cause concomitantly oxidative stress and induction of apoptotic markers in lung epithelial cells (A549) at nonacute toxic concentrations. J. Proteome. Res. 10, 363-378.

Mroz,R.M., Schins,R.P., Li,H., Drost,E.M., Macnee,W., and Donaldson,K. (2007). Nanoparticle carbon black driven DNA damage induces growth arrest and AP-1 and NFkappaB DNA binding in lung epithelial A549 cell line. J. Physiol Pharmacol. 58 Suppl 5, 461-470.

Nadeau,D., Vincent,R., Kumarathasan,P., Brook,J., and Dufresne,A. (1996). Cytotoxicity of ambient air particles to rat lung macrophages: Comparison of cellular and functional assays. Toxicol. In Vitro 10, 161-172.

Oliveros, J. C. VENNY. An interactive tool for comparing lists with Venn's Diagrams. 2015. http://bioinfogp.cnb.csic.es/tools/venny/index.html.

Peng,Y., Gregorich,Z.R., Valeja,S.G., Zhang,H., Cai,W., Chen,Y.C., Guner,H., Chen,A.J., Schwahn,D.J., Hacker,T.A., Liu,X., and Ge,Y. (2014). Top-down proteomics reveals concerted reductions in myofilament and Z-disc protein phosphorylation after acute myocardial infarction. Mol. Cell Proteomics. 13, 2752-2764.

Pope,C.A., III, Burnett,R.T., Turner,M.C., Cohen,A., Krewski,D., Jerrett,M., Gapstur,S.M., and Thun,M.J. (2011). Lung cancer and cardiovascular disease mortality associated with ambient air pollution and cigarette smoke: shape of the exposure-response relationships. Environ. Health Perspect. 119, 1616-1621.

Sahu,D., Kannan,G.M., and Vijayaraghavan,R. (2014). Carbon black particle exhibits size dependent toxicity in human monocytes. Int. J. Inflam. 2014, 827019.

Saputra,D., Yoon,J.H., Park,H., Heo,Y., Yang,H., Lee,E.J., Lee,S., Song,C.W., and Lee,K. (2014). Inhalation of carbon black nanoparticles aggravates pulmonary inflammation in mice. Toxicol. Res. 30, 83-90.

Schneider,A., Hampel,R., Ibald-Mulli,A., Zareba,W., Schmidt,G., Schneider,R., Ruckerl,R., Couderc,J.P., Mykins,B., Oberdorster,G., Wolke,G., Pitz,M., Wichmann,H.E., and Peters,A. (2010). Changes in deceleration capacity of heart rate and heart rate variability induced by ambient air pollution in individuals with coronary artery disease. Part Fibre. Toxicol. 7, 29.

Scott,J.A. (1953). Fog and deaths in London, December 1952. Public Health Rep. 68, 474-479.

Searle SR, Speed FM, and Miliken GA (1980). The population marginal means in the linear model: An alternative to least squares means. The American Statistician 34, 216-221.

Siemiatycki,J., Dewar,R., Lakhani,R., Nadon,L., Richardson,L., and Gerin,M. (1989). Cancer risks associated with 10 inorganic dusts: results from a case-control study in Montreal. Am. J. Ind. Med. 16, 547-567.

Song,C., Wang,Q., and Li,C.C. (2003). ATPase activity of p97-valosin-containing protein (VCP). D2 mediates the major enzyme activity, and D1 contributes to the heat-induced activity. J. Biol. Chem. 278, 3648-3655.

Squatrito,M., Mancino,M., Donzelli,M., Areces,L.B., and Draetta,G.F. (2004). EBP1 is a nucleolar growth-regulating protein that is part of pre-ribosomal ribonucleoprotein complexes. Oncogene 23, 4454-4465.

Stocks,P. (1959). Cancer and bronchitis mortality in relation to atmospheric deposit and smoke. Br. Med. J. 1, 74-79.

Su,M.W., Tsai,C.H., Tung,K.Y., Hwang,B.F., Liang,P.H., Chiang,B.L., Yang,Y.H., and Lee,Y.L. (2013). GSTP1 is a hub gene for gene-air pollution interactions on childhood asthma. Allergy 68, 1614-1617.

Vincent,R., Goegan,P., Johnson,G., Brook,J.R., Kumarathasan,P., Bouthillier,L., and Burnett,R.T. (1997). Regulation of promoter-CAT stress genes in HepG2 cells by suspensions of particles from ambient air. Fundam. Appl. Toxicol. 39, 18-32.

Vuong,N.Q., Goegan,P., Mohottalage,S., Breznan,D., Ariganello,M., Williams,A., Elisma,F., Karthikeyan,S., Vincent,R., and Kumarathasan,P. (2016). Human lung epithelial cell A549 proteome data after treatment with titanium dioxide and carbon black. Data in Brief 8, 687-691.

Wagner,J.G., Kamal,A.S., Morishita,M., Dvonch,J.T., Harkema,J.R., and Rohr,A.C. (2014). PM2.5-induced cardiovascular dysregulation in rats is associated with elemental carbon and temperature-resolved carbon subfractions. Part Fibre. Toxicol. 11, 25.

Wang MJ, Gray CA, Reznek SA, Mahmud K, and Kutsovsky Y. Carbon Black. 4, 761-803. 2003. Kirk-Othmer Encyclopedia of Chemical Technology.

Watson,A.Y. and Valberg,P.A. (2001). Carbon black and soot: two different substances. AIHAJ. 62, 218-228.

Wisniewska,M., Karlberg,T., Lehtio,L., Johansson,I., Kotenyova,T., Moche,M., and Schuler,H. (2010). Crystal structures of the ATPase domains of four human Hsp70 isoforms: HSPA1L/Hsp70-hom, HSPA2/Hsp70-2, HSPA6/Hsp70B', and HSPA5/BiP/GRP78. PLoS. One. 5, e8625.

Yamawaki,H. and Iwai,N. (2006). Mechanisms underlying nano-sized air-pollution-mediated progression of atherosclerosis: carbon black causes cytotoxic injury/inflammation and inhibits cell growth in vascular endothelial cells. Circ. J. 70, 129-140.

Yang,X., Liu,J., He,H., Zhou,L., Gong,C., Wang,X., Yang,L., Yuan,J., Huang,H., He,L., Zhang,B., and Zhuang,Z. (2010). SiO2 nanoparticles induce cytotoxicity and protein expression alteration in HaCaT cells. Part Fibre. Toxicol. 7, 1.

Zhang,R., Dai,Y., Zhang,X., Niu,Y., Meng,T., Li,Y., Duan,H., Bin,P., Ye,M., Jia,X., Shen,M., Yu,S., Yang,X., Gao,W., and Zheng,Y. (2014). Reduced pulmonary function and increased pro-inflammatory cytokines in nanoscale carbon black-exposed workers. Part Fibre. Toxicol. 11, 73.

Zhang,Y., Fondell,J.D., Wang,Q., Xia,X., Cheng,A., Lu,M.L., and Hamburger,A.W. (2002). Repression of androgen receptor mediated transcription by the ErbB-3 binding protein, Ebp1. Oncogene 21, 5609-5618.

Zhang,Y., Wang,X.W., Jelovac,D., Nakanishi,T., Yu,M.H., Akinmade,D., Goloubeva,O., Ross,D.D., Brodie,A., and Hamburger,A.W. (2005). The ErbB3-binding protein Ebp1 suppresses androgen receptor-mediated gene transcription and tumorigenesis of prostate cancer cells. Proc. Natl. Acad. Sci. U. S. A 102, 9890-9895.

Chapter IIb. Human lung epithelial cell A549 proteome data after treatment with titanium dioxide and carbon black.

This manuscript was published in Data in Brief.

Vuong NQ, Goegan P, Mohattalage S, Breznan D, Ariganello M, Williams A, Elisma F, Karthikeyan S, Vincent R and Kumarathasan P. Human lung epithelial cell A549 proteome data after treatment with titanium dioxide and carbon black. Data in Brief. 2016 Jun 21;8:687-91.

Received: 6 April 2016
Received in revised form: 26 May 2016
Accepted: 14 June 2016
Available online: 21 June 2016

Ngoc Vuong wrote the entire manuscript, analyzed all the results (including cytotoxicity assays, 2D-GE, MALDI-TOF-MS, bioinformatics and pathway analyses), and performed all the experimental work (2D-GE and MALDI-TOF-MS) to determine the identities of all the protein spots in 2D gels.

Abstract

Here, we have described the dataset relevant to the A549 cellular proteome changes after exposure to either titanium dioxide or carbon black particles as compared to the non-exposed controls, "Proteomic changes in human lung epithelial cells (A549) in response to carbon black and titanium dioxide exposures" (Vuong et al., 2016). Detailed methodologies on the separation of cellular proteins by 2D-GE and the subsequent mass spectrometry analyses using MALDI-TOF-TOF-MS are documented. Particle exposure-specific protein expression changes were measured via 2D-GE spot volume analysis. Protein identification was done by querying mass spectrometry data against SwissProt and RefSeq protein databases using Mascot search engine. Two-way ANOVA analysis data provided information on statistically significant A549 protein expression changes associated with particle exposures.

Specifications table

Subject area	Biochemistry and in vitro toxicology
More specific subject area	Toxicology of particulate matter
Type of data	Tables
How data was acquired	2D-GE was carried out using a PROTEAN IEF cell to separate proteins based on isoelectric point in the first dimension, and proteins were separated based on molecular weight by SDS-PAGE using a *Criterion*^{TM}*Dodeca*^{TM} Cell. Analysis of 2D gels was conducted by *PDQuest*^{TM} Advance V8.0.1. Protein spots were excised from 2D gels using ExQuest, an automated robotic instrument. MALDI-TOF-TOF-MS analysis of tryptic-digested peptides from 2D-GE gel spots for protein identification was done using a Bruker Autoflex III Smartbeam instrument. The mass spectral data were queried using Mascot against *SwissProt* and *RefSeq*.
Data format	Raw, filtered and analyzed.
Experimental factors	A549 human lung epithelial cell line was exposed to TiO_2 and CB at 4 different doses of 0, 60, 140 and 200 μg/cm^2. Protein expression changes were based on Coomassie blue staining of 2D gels.
Experimental features	A549 cells were exposed to TiO_2 and CB for 24 h. The molecular mechanisms underpinning particles' toxicity were examined using 2D-GE- and mass spectrometry-based proteomic analysis.
Data source location	Environmental Health Centre, 50 Colombine Driveway, Ottawa, Ontario, K1S- 0K9, Canada
Data accessibility	Data are within this article

Value of the data

- The 2D-GE map data set the basis for particle induced-changes in A549 proteome.
- Identification of A549 proteins permits the analysis of A549 proteome.
- Particle-induced A549 protein expression changes along with protein identification help to characterize toxicity mechanisms and related altered cellular functions.
- These data and the toxicoproteomic approach are promising in the study of toxicity of environmental particles and engineered nano-materials.

IIb.1. Data

There are three datasets in this article. The first is the 2D-GE protein expression dataset associated with A549 cells exposed to TiO2 and CB particles (Supplementary Table IIb – 1). The second dataset describes the corresponding protein identification results based on MALDI-TOF-TOF-MS analyses (Supplementary Table IIb – 2). The third dataset reveals the 2D-GE protein spots that significantly changed due to particle exposures (Supplementary Table IIb – 3).

IIb.2. Experimental design, materials and methods

IIb.2.1. Experimental design

Culture flasks (T-25 and T-75), 96-well plate and plastic cell scraper were obtained from Corning Inc. (Corning, NY). Dulbecco's Modified Eagle's Medium (DMEM) and fetal bovine serum (FBS) were purchased from HyClone (Logan, UT). Gentamicin, trifluoroacetic acid, α-cyano-4-hydroxy-cinnamic acid, Tris–HCl, NaCl, Tween-20 and Tween-80 were obtained from Sigma-Aldrich (Oakville, ON). Iodoacetamide, bis-acrylamide, ammonium persulfate, glycerol, immobilized pH gradient strips, Criterion Cassette (13.3 x 8.7 cm W x L), Tris/Glycine/SDS buffer, and BioSafe Coomassie Blue were purchased from Bio-Rad (Mississauga, ON). Trypsin, resazurin reduction (CellTiterBlue®) and lactate dehydrogenase (LDH) (CytoTox-96®) cytotoxicity assay kits were from Promega Corporation (Madi-son, WI), ATP assay kits (ViaLight^{TM} Plus) were purchased from Lonza Corporation (Rockland, ME), and 5-bromo-20-deoxyuridine (BrdU) cell proliferation ELISA (chemiluminescent) assay kits were obtained from Roche Diagnostics (Laval, QC). All water used was deionized/demineralized (416 MΩ resistivity).

IIb.2.2. Particles preparation

TiO_2 (SRM-154b) obtained from the National Institute of Standards and Technology (Gaithersberg, MD) was subjected to three successive washes with methanol and then phosphate buffered saline (PBS) to remove possible soluble metals and organic contaminants before use in the experiments (Vincent et al., 1997). Carbon black (Cas#1333-86-4) obtained from Cabot Corporation (Boston, MA) was used as received. Particles were resuspended at 10 mg/mL in particle buffer (0.19 % NaCl and 25 μg/mL Tween-80) (Nadeau et al., 1996), vortexed (30 sec), sonicated (20 min on ice), homogenized with a Dounce Homogenizer (25 strokes), and then heated (56 ºC, 1 hour). The particles were stored at – 40 ºC until use.

IIb.2.3. Cell culture and particle exposure

The A549 cell line (American Type Culture Collection - CCL-185; human, epithelial, lung carcinoma) was subcultured in DMEM supplemented with 50 μg/mL gentamycin and 10 % FBS. The cells were maintained in T-75 flasks in a humidified atmosphere at 37 ºC containing 5 % CO_2 and 95 % air. For experiments, the cells were seeded at $1.5x10^6$ cells (T-25), $3.75x10^6$ cells (T-75) or $2.0x10^4$ cells/well (96-well plate for cytotoxicity assays) and incubated for 24 hours, resulting in approximately 75 % confluence prior to dosing with particles. The final volume of culture medium was 5 mL (T-25), 15 mL (T-75) or 200 μL/well (96-well plate). Solutions of particles were prepared by thawing the frozen stocks, sonicating on ice (20 min) then diluting in the culture medium to make up dosing concentrations of 0, 60, 140 and 200 $\mu g/cm^2$. The cells were exposed to the particles by replacing the existing culture medium with the particle-containing medium, and the flasks/plates were returned to the incubator for a 24 hour exposure to particles. To harvest the exposed cells, the medium in each flask was removed and the cells were detached from

the flasks using a plastic scraper. The cell suspension was collected in cell culture medium and centrifuged at 350 x g for 5 min, and the supernatant was discarded. The cell pellet was then washed twice with PBS. The final cell pellet was aspirated dry and stored frozen at – 80 ºC until further use. The integrated cytotoxicity bioassay which combined endpoints of cell viability (resazurin reduction assay), cellular membrane integrity (intracellular LDH release), and energy metabolism (ATP assay) was conducted in a 96-well plate as described in our previous study (Kumarathasan et al., 2014). The cell proliferation (BrdU incorporation) assay was performed in a separate 96-well plate.

IIb.2.4. Protein extraction

The cell pellets were solubilized in a protein extraction/rehydration buffer from Bio-Rad (8 M urea, 2 % CHAPS, 50 mM dithiothreitol, 0.2 % Biolyte 3/10), where the volume depends on the number of cells in the pellet to achieve 1 – 2 µg/µL, and $1x10^6$ A549 cells was experimentally estimated to yield about 200 µg of protein. The samples were vortexed (30 sec), sonicated (10 min), vortexed (30 sec) and centrifuged (15000 x g, 10 min). The extracted protein in the supernatant was collected, and the concentration of protein in each extract was determined immediately using the Coomassie Plus Protein assay kit (Thermo Scientific). The extracted protein samples were stored in –80 ºC until use.

IIb.2.5. Two-dimensional gel electrophoresis (2D-GE)

2D-GE was conducted as described in our previous study (Kumarathasan et al., 2005). Briefly, an appropriate quantity of protein was suspended in a total volume of 200 mL of extraction buffer, and applied to an immobilized pH gradient (IPG) strips (11 cm, pH3 – 10 or pH5 – 8) in a clean disposable rehydration tray and allowed to incubate for 1 h at room temperature. The IPG strip was then overlaid with mineral oil and allowed to continue

incubating overnight (16 – 20 h). The IPG strip was then moved to an isoelectric focussing tray, overlaid with mineral oil and subjected to isoelectric focussing using a PROTEAN IEF cell (BioRad). The focussing conditions were as follows: stage 1: linear ramp to 250 V for 20 min; stage 2: linear ramp to 8,000 V for 2.5 h; stage 3: rapid ramp for 20,000 V h. The strip was then stored at – 80 °C until use. The focused IPG strip was thawed and gently agitated for 10 min in equilibration buffer 1 (6 M urea, 2 % SDS, 375 mM Tris–HCl, 20 % glycerol, 130 mM dithiothreitol, 0.001 % bromo-phenol blue). Then each strip was gently agitated for another 10 min in equilibration buffer 2 (6 M urea, 2 % SDS, 375 mM Tris–HCl, 20 % glycerol, 135 mM iodoacetamide, 0.001 % bromophenol blue). The strip was then placed on a 12 % SDS-PAGE gel casted in a 1.0 mm thick Criterion Cassette (13.3 x 8.7 cm W x L) and subjected to electrophoresis at 200 V for 65 min. Following electrophoresis, the gel was removed from the Criterion Cassette, washed for 30 min in water, stained in BioSafe Coomassie Blue (Bio-Rad) overnight (16 – 20 h), destained twice in water, and then imaged with a standard scanner.

To overcome the typical warping and distortion issues from gel to gel near the extremities of the pH and the molecular weight range, a common area (Figure IIa – 2; pH5.1 – 7.8 and 20 – 100 kDa) that clearly shows the protein spots across all experimental gels was selected to assess the proteome differences among the treatments. The protein spots within the gels were matched and quantified with PDQuest™ Advance V8.0.1 (Bio-Rad), where spot volume was quantified using the available "Local regression model (LOESS)" algorithm in PDQuest. The reported spot volume for each protein was used to compare its level of expression across the treatments. Three gels representing three biological repeats were generated for each group in this experiment to assess the particle-induced changes in the proteome of A549 cells.

IIb.2.6. In-gel digest, preparing protein spots for identification

To identify the protein in each spot of interest, a large set of preparative gels (10 – 12 gels) were prepared with 175 mg of protein/gel as described above. The gels were then stained with Biosafe Coomassie blue and imaged. The spots in preparative gels were then aligned and matched to the experimental gels using PDQuest. The protein spots were then excised from the preparative gels with an automated spot cutter equipped with a 1.5 mm cutting head (ExQuest from Bio-Rad). The excised gels corresponding to the same protein spot from different preparative gels were pooled into the same tube for maximum protein yield. The excised gels were then subjected to in-gel tryptic digest as described in our previous study (Kumarathasan et al., 2005). Briefly, the gel spots were destained and then subjected to a 16 h digestion by trypsin (pH = 7) at 37 °C. All the digested samples were evaporated under a gentle stream of N_2 and were stored at – 80 °C until further use.

IIb.2.7. Matrix-assisted laser desorption/ionization time-of-flight mass spectrometry (MALDI-TOF-TOF-MS/MS)

Each sample was reconstituted in 5 to 20 µL of 30 % acetonitrile (ACN) in 0.1 % trifluoroacetic acid (TFA) depending on the spot volume and was spotted (1.5 µL) on an AnchorChip target plate (600/384, Bruker Daltonics Ltd, Bremen, Germany) together with 1.5 µL of freshly prepared α-cyano- 4-hydroxy-cinnamic acid (5 µg/µL in 50 % ACN in 0.1 % TFA). The spotted sample/matrix was dried under vacuum for at least 2 h. Each dried sample/matrix was washed with 2.5 µL of cold 0.1 % TFA and briefly dried under vacuum. Each sample was analyzed by MALDI-TOF-TOF-MS using an automated analysis option (Bruker Daltonics, Bremen, Germany). In brief, MS scan of each spot was done to obtain the peptide mass fingerprint (PMF). Six major analyte peaks from the PMF spectrum were

subjected to tandem MS (MS/MS) analysis in the "voltage lift mode". The mass spectral information was matched against the Swiss-Prot and RefSeq databases using the Mascot search engine (Matrix Sciences) for protein identification. In the case that more than 1 protein was identified per spot, we attributed the protein with the highest score to such spot.

IIb.2.8. Statistical analysis

Two-way analysis of variance (ANOVA) was performed on 2D-GE data with treatment and dose as factors. When the assumption of equal variance and normal distribution were not met, the data were rank transformed. A protein spot is considered as significant if $p < 0.05$. Particle treatment-related protein expression changes were normalized to the corresponding controls to obtain unadjusted fold-change values.

Acknowledgments

This work was supported by the Clean Air Regulatory Agenda at Health Canada (HC4340565) and, Ontario Graduate Scholarship in Science and Technology and Ontario Graduate Scholarship (funding for Ngoc Vuong, 1519592). We also acknowledge Christine MacKinnon-Roy and Alexandra Star for their valuable technical assistance

Conflict of Interest

The authors declare no conflict of interest.

Supplementary Table IIb – 1. 2D-GE protein expression (spot volume) profiles for A549 cells exposed to TiO_2 and CB.
The SSP number in the header of each column corresponds to the identifier number that PDQuest used to identify the spot based on its coordinates in the gel (Vuong et al., 2016).

This table is too large to fit within the margin of this page. It can be found online at: http://dx.doi.org/10.1016/j.dib.2016.06.013.

Supplementary Table IIb – 2. Identities of the protein spots in the 2D-GE map of the A549 cell line determined by MALDI-TOF-TOF-MS (Vuong et al., 2016).

This table is too large to fit within the margin of this page. It can be found online at: http://dx.doi.org/10.1016/j.dib.2016.06.013.

Footnotes:
[a]Denotes that this protein spot has also been identified the same by Malard et al., 2005.
[b]Denotes that this protein spot has also been identified the same by Morbt et al., 2009.
*SSP number corresponds to the identifier number assigned by PDQuest based on the coordinates of the spot in the gel (Vuong et al., 2016a).

Supplementary Table IIb – 3. Unadjusted fold-changes (vs controls) and two-way ANOVA results for the A549 protein expression changes due to particle exposures (n = 3).
The SSP number corresponds to the identifier number that PDQuest used to identify the spot based on its coordinates in the gel (Vuong et al., 2016a).

		TiO_2 (μg/cm^2)			CB (μg/cm^2)			Two-Way ANOVA (p-value)		
SSP	Protein	60	140	200	60	140	200	Trt (T)	Dose (D)	T x D
3202	CAPZA1	-1.10	-1.07	-1.07	-1.07	-1.07	1.15	**0.004**	**0.016**	**0.031**
9804	FUBP1	1.15	1.11	1.29	-1.08	1.04	-1.41	**0.039**	0.947	**0.044**
7701	CCT6A	1.31	-1.39	1.00	1.05	-1.29	1.51	0.507	**0.031**	**0.034**
8501	EEF2	2.06	3.00	1.73	1.62	2.47	-2.63	0.571	**0.004**	**0.020**
6501	PA2G4	-1.05	-1.23	-1.02	1.07	-1.11	1.40	0.165	**0.023**	**0.047**
7501	PA2G4	1.03	-1.49	-1.00	-1.04	-1.40	1.49	0.953	**0.009**	**0.037**
1602	TUBA1C	-1.12	-2.78	-1.56	-1.18	-2.32	2.43	0.793	**0.015**	**0.049**
2902	VCP	1.73	-1.68	1.51	-1.01	1.03	1.63	0.457	**0.002**	**0.024**
7603	ALDH1A1	1.23	-1.16	-1.61	-1.49	-1.77	1.08	0.096	0.131	**0.034**
6604	CCT2	1.21	-1.15	-1.24	-1.52	-1.23	1.53	0.792	0.237	**0.023**
4702	PDIA3	1.02	-1.09	-1.27	-1.07	1.45	1.15	0.368	0.220	**0.021**
3207	TRIM28	1.19	-1.47	1.49	1.08	-1.08	-1.44	0.192	0.096	**0.035**
4102	VCP	-1.05	1.19	1.07	-1.06	1.08	-1.35	0.554	0.083	**0.036**
2006	CRK	1.29	1.77	1.44	4.28	6.20	5.93	**<0.001**	**<0.001**	0.085
8205	AKR1A1	-1.07	1.17	-1.03	1.33	1.19	1.47	**0.041**	0.431	0.395
102	HSPA5	1.02	1.36	1.15	1.22	1.97	1.33	**0.017**	0.134	0.441
8809	LMNA	-1.09	-1.19	-1.03	1.41	1.02	1.13	**0.028**	0.311	0.303
2301	TMOD3	-1.39	-1.07	-1.10	1.22	1.11	1.50	**0.005**	0.201	0.139
6502	ANXA7	-1.12	1.08	-1.67	-1.10	1.57	-1.70	0.124	**0.037**	0.502
8108	ARMCX1	-1.24	1.93	1.15	1.16	1.84	-2.29	0.472	**0.017**	0.379
9502	DIS3L	-1.04	1.08	-1.30	-1.17	1.02	-1.73	0.298	**0.000**	0.504
8107	EEF2	-1.03	1.58	-1.26	1.21	1.45	-1.34	0.580	**0.031**	0.719
7205	ENO1	1.13	1.64	1.04	1.20	1.54	-1.39	0.723	**0.021**	0.416
8503	ENO1	-1.05	1.28	-1.14	1.11	1.37	-1.43	0.413	**0.035**	0.561
9405	ENO1	-1.04	1.61	-1.02	1.07	1.52	-1.51	0.876	**0.043**	0.593
5607	HNRNPH1	-1.00	-1.48	1.24	-1.23	-1.17	1.47	0.852	**0.022**	0.458
2701	HNRNPK	-1.13	-2.05	-1.23	-1.28	-1.49	-1.11	0.913	**0.020**	0.146
3104	HSP90AB3P	-1.08	1.56	1.01	1.23	1.55	-1.31	0.568	**0.026**	0.615
8106	HSPA8	1.09	1.56	-1.02	1.09	1.46	-1.12	0.622	**0.035**	0.533
8117	IDH1	1.01	1.63	-1.05	1.11	1.53	-1.69	0.899	**0.014**	0.443
5902	IMMT	1.40	-1.48	1.24	1.30	-1.28	1.34	0.510	**0.019**	0.761
3705	INA	1.14	2.94	1.85	1.27	1.39	1.60	0.967	**0.002**	0.084
8103	NIT2	-1.01	1.24	-1.08	1.14	1.28	-1.13	0.410	**0.017**	0.797
8110	PDIA3	1.03	1.42	-1.35	1.22	1.65	-3.25	0.270	**0.029**	0.580
6306	PGK1	-1.39	1.26	-1.20	1.01	1.27	-1.67	0.363	**0.034**	0.282
7204	PKM	-1.08	1.35	-2.08	1.09	1.34	-1.64	0.431	**0.003**	0.922
8606	PKM	-1.22	-1.09	-1.76	-1.16	-1.11	-1.60	0.942	**0.026**	0.889
5105	PSMB7	1.05	1.11	1.21	-1.11	1.17	1.54	0.367	**0.019**	0.466
8301	RBM4	1.60	1.74	1.41	1.69	1.41	1.72	0.676	**0.038**	0.402
8308	RBM4	-1.21	-1.34	-1.12	-1.12	-1.20	-1.39	0.708	**0.025**	0.634
2904	VCP	1.11	-2.75	-1.10	-1.16	-1.70	1.29	0.745	**0.004**	0.141
5301	XXYLT1	1.35	1.19	1.36	1.12	1.20	1.16	0.131	**0.008**	0.499

Transparency document. Supplementary material

Transparency data associated with this article can be found in the online version at http://dx.doi.org/10.1016/j.dib.2016.06.013.

Appendix A. Supplementary material

Supplementary data associated with this article can be found in the online version at http://dx.doi.org/10.1016/j.dib.2016.06.013.

References

Kumarathasan,P., Mohottalage,S., Goegan,P., and Vincent,R. (2005). An optimized protein in-gel digest method for reliable proteome characterization by MALDI-TOF-MS analysis. Anal. Biochem. 346: 85-89.

Kumarathasan,P., Breznan,D., Das,D., Salam,M.A., Siddiqui,Y., Mackinnon-Roy,C., Guan,J., de,S.N., Simard,B., and Vincent,R. (2014). Cytotoxicity of carbon nanotube variants: A comparative in vitro exposure study with A549 epithelial and J774 macrophage cells. Nanotoxicology 9(2):148-61.

Malard,V., Prat,O., Darrouzet,E., Berenguer,F., Sage,N., and Quemeneur,E. (2005). Proteomic analysis of the response of human lung cells to uranium. Proteomics. 5, 4568-4580.

Morbt,N., Mogel,I., Kalkhof,S., Feltens,R., Roder-Stolinski,C., Zheng,J., Vogt,C., Lehmann,I., and von,B.M. (2009). Proteome changes in human bronchoalveolar cells following styrene exposure indicate involvement of oxidative stress in the molecular-response mechanism. Proteomics. 9, 4920-4933.

Nadeau D, Vincent R, Kumarathasan P, Brook J, Dufresne A. 1996. Cytotoxicity of ambient air particles to rat lung macrophages: Comparison of cellular and functional assays. Toxicol. In Vitro 10: 161–172.

Vincent R, Goegan P, Johnson G, Brook JR, Kumarathasan P, Bouthillier L, Burnett RT. 1997. Regulation of promoter-CAT stress genes in HepG2 cells by suspensions of particles fromambient air. Fundam. Appl. Toxicol. 39: 18–32.

Vuong NQ, Goegan P, Mohottalage S, Breznan D, Ariganello M, Williams A, Elisma F, Karthikeyan K, Vincent R, Kumarathasan P. 2016a. Proteomic changes in human lung epithelial cells (A549) in response to carbon black and titanium dioxide exposures. J. Proteomics 149: 53–63.

Chapter III. Responses of A549 human lung epithelial cells to cristobalite and α-quartz exposures assessed by toxicoproteomics and gene expression analysis.

This manuscript was published in Journal of Applied Toxicology.

Vuong NQ, Goegan P, De Rose F, Breznan D, Thomson E, Williams A, Karthikeyan S, Kumarathasan P and Vincent R. Responses of A549 human lung epithelial cells to cristobalite and α-quartz exposures assessed by toxicoproteomics and gene expression analysis. J Appl Toxicol. 2017 Jun;37(6):721-731

Received: 17 August 2016
Received in revised form: 12 October 2016
Accepted: 26 October 2016
Available online: 5 December 2016

Ngoc Vuong wrote the entire manuscript, analyzed all the results (including cytotoxicity assays, RT-PCR, 2D-GE, MALDI-TOF-MS, bioinformatics and pathway analyses), and performed all the experimental work (2D-GE and MALDI-TOF-MS) to determine the identities of all the protein spots in 2D gels.

Abstract

In this study, we used cytotoxicity assays, proteomic and gene expression analyses to examine the difference in response of A549 cells to two silica particles that differ in physical properties, namely cristobalite (CR) and α-quartz (Min-U-Sil 5, MI). Cytotoxicity assays such as lactate dehydrogenase release, 5-bromo-2′-deoxyuridine incorporation and cellular ATP showed that both silica particles could cause cell death, decreased cell proliferation and metabolism in the A549 human lung epithelial cells. While cytotoxicity assays revealed little difference between CR and MI exposures, proteomic and gene expression analyses unveiled both similar and unique molecular changes in A549 cells. For instance, two-dimensional gel electrophoresis data indicated that the expression of proteins in the cell death (e.g., ALDH1A1, HTRA2 and PRDX6) and cell proliferation (e.g., FSCN1, HNRNPAB and PGK1) pathways were significantly different between the two silica particles. Reverse transcription–polymerase chain reaction data provided additional evidence supporting the proteomic findings. Preliminary assessment of the physical differences between CR and MI suggested that the extent of surface interaction between particles and cells could explain some of the observed biological effects. However, the differential dose–response curves for some other genes and proteins suggest that other physical attributes of particulate matter can also contribute to particulate matter-related cellular toxicity. Our results demonstrated that toxicoproteomic and gene expression analyses are sensitive in distinguishing subtle toxicity differences associated with silica particles of varying physical properties compared to traditional cytotoxicity endpoints.

III.1. Introduction

Inhalation of silica has been reported to cause pulmonary fibrosis or silicosis, a condition where scar tissue is formed in the lung (AGN, 1930; Belt, 1930; Cassel et al., 2008). It is known that exposure to silica can cause inflammatory response (Cassel et al., 2008; Dostert et al., 2008; Hornung et al., 2008; Peeters et al., 2013) and cell death (Cassel et al., 2008; Chao et al., 2001; Iyer et al., 1996; Joshi & Knecht, 2013) in the cells of the respiratory tract. Recent studies demonstrated the NALP3 inflammasome is a protein complex (composed of NLRP3, ASC and caspase-1) that is essential for the inflammatory response (Cassel et al., 2008; Dostert et al., 2008; Hornung et al., 2008; Peeters et al., 2013) and the development of silicosis (Cassel et al., 2008) from silica exposure. However, there are discrepancies in the molecular mechanisms reported for the effect of silica on the cells. For example, data from Cassel et al. (2008) and Dostert et al. (2008) demonstrated that the inflammatory response depends on the production of reactive oxygen species (ROS), whereas data from Hornung et al. (2008) suggested that the production of ROS is not necessary. These discrepancies may arise from the difference in materials and/or the methods used in these studies. The silica particles used in these three studies were 1.5 μm amorphous silicon dioxide (Dostert et al., 2008), Min-U-Sil 5 (MI; quartz, 5 μm top size) (Cassel et al., 2008) and Min-USil 15 (quartz, 15 μm top size) (Hornung et al., 2008).

Given that silica or silicon dioxide can form various physical structures such as amorphous (non-crystalline) and crystalline (e.g., quartz, cristobalite [CR] and tridymite), it is possible that exposure to different forms of silica may lead to different health impacts. To date, most toxicological studies as mentioned above have focused on quartz, and very limited data have been reported on the toxicity of other forms of silica. There is a wide range of current industrial products/applications for different forms of silica, which include clay,

ceramics, road building, sand blasting, pet litter, electronic devices and cosmetic products (IARC, 1997, 2012). Thus, there is a need to distinguish the difference in toxicity of different forms of silica, if there is any, to inform the workers or consumers about the hazard of the relevantmaterials. Thereby, it is fundamental to assess whether different forms of silica can trigger differential responses at the cellular level. Recently, we demonstrated that toxicoproteomics is a useful approach to identify and differentiate the mechanisms of particle toxicity of two respirable particles that are physically and chemically different such as titanium dioxide and carbon black (Vuong et al., 2016a). In this study, we questioned whether *in vitro* toxicoproteomics in conjunction with gene expression analysis were sensitive enough to differentiate the effect of two particles that are identical in chemical formula (silicon dioxide) but differed only in their physical properties. The results of this study demonstrated that subtle differences in cytotoxic effects of CR and MI on A549 human lung epithelial cells could be addressed through *in vitro* toxicoproteomic and gene expression analyses.

III.2. Materials and methods

III.2.1. Materials.

Culture flasks (T-25 and T-75), 96-well plates and plastic cell scrapers were obtained from Corning Inc. (Corning, NY, USA). Dulbecco's modified Eagle's medium and fetal bovine serum were purchased from Hyclone (Logan, UT, USA). Gentamicin, trifluoroacetic acid, α-cyano-4-hydroxy-cinnamic acid, Tris-HCl, NaCl, Tween-20 and Tween-80 were obtained from Sigma-Aldrich (Oakville, ON, Canada). Iodoacetamide, bis-acrylamide, ammonium persulfate, glycerol, immobilized pH gradient (IPG) strips, Criterion Cassette

(13.3cm× 8.7cmW× L), Tris/glycine/sodium dodecyl sulfate buffer and BioSafeCoomassie Blue were purchased from Bio-Rad (Mississauga, ON, Canada). Trypsin, resazurin reduction (CellTiter-Blue®) and lactate dehydrogenase (LDH) cytotoxicity assay kits (CytoTox-96®) were from Promega Corporation (Madison, WI, USA), ATP assay kit (ViaLight™ Plus) was from Lonza Corporation (Rockland, ME, USA) and 5-bromo-2′-deoxyuridine (BrdU) cell proliferation enzyme-linked immunosorbent assay (chemiluminescent) assay kit was obtained from Roche Diagnostics (Laval, QC, Canada). All water used was deionized/demineralised (>16MΩ resistivity).

III.2.2. Particle preparation

CR (SRM-1879a) was obtained from NIST (Gaithersburg, MD, USA) and MI was a generous gift fromthe US Silica Co. (Berkeley Springs, WV, USA). Both silica particles were subjected to three successive washes with methanol followed by 1× phosphate-buffered saline to remove possible soluble metals and organic contaminants before use in the experiments (Vincent et al., 1997). Particles were resuspended at 10mg/ml in particle buffer (0.19% NaCl and 25 μg/ml Tween-80) (Nadeau et al., 1996), vortexed (30 s), sonicated (20min on ice), homogenized with a Dounce homogenizer (25 strokes) and then heated (56 °C, 1 h). The particles were stored at – 40 °C until use.

III.2.3. Scanning electron microscopy

The size and morphology of CR and MI samples were characterized by scanning electron microscopy (SEM). Images were collected on a JSM-7500F FESEM (JEOL, Peabody, MA, USA) instrument equipped with a field emission gun under the following parameters: beam acceleration voltage, 2 kV; working distance, between 7 and 9 mm; imaging mode, lower secondary electron image. Magnification and sizing bar are as

indicated in the figure captions for each individual image. Samples were prepared by dropping a small amount of powder on to an aluminum stage painted with carbon paint (electron microscope sciences). The paint was allowed to dry for 20 min, and the excess powder was then removed by blowing the surface with compressed, dry air. Particle size distributions were calculated from SEM images using the software program ImageJ. The measurements reported are the average of at least 100 random particles. For all particles that were not spherical, the longest axis was measured and reported.

III.2.4. Cell culture and particle exposure

The A549 cell line (American Type Culture Collection, Manassas, VA, USA; CCL-185; human, epithelial, lung carcinoma) was subcultured in Dulbecco's modified Eagle's medium supplemented with 50 μg/ml gentamicin and 10 % fetal bovine serum. The cells were maintained in T-75 flasks in a humidified atmosphere containing 5 % CO_2 and 95 % air at 37 °C. For experiments, the cells were seeded at 1.5×10^6 cells/T-25 flask (for gene expression analysis and proteomics) or 2.0×10^4 cells per well (96-well plate for cytotoxicity assays) and incubated for 24 h, resulting in approximately 75% confluence before dosing with particles. The final volume of culture medium was 5 ml (T-25), 15 ml (T-75) or 200 μl per well (96-well plate). Solutions of particles were prepared by thawing the frozen stocks, sonicating on ice (20 min) then diluting in the culture medium to generate dosing concentrations of 0, 60, 140 and 200 μg/cm^2. The cells were exposed to the particles by replacing the existing culture medium with the particle-containing medium, and the flasks/plates were returned to the incubator for a 24 h exposure to particles. To harvest the exposed cells, the medium in each flask was removed and the cells were detached from the flasks using a plastic scraper. The cell suspension was collected in cell culture medium and

centrifuged at 350 g for 5 min, and the supernatant was discarded. The cell pellet was then washed twice with phosphate-buffered saline. The final cell pellet was aspirated dry and stored frozen at – 80 °C until further use. The integrated cytotoxicity bioassay, which combined endpoints of cell viability (resazurin reduction assay), cellular membrane integrity (intracellular LDH release) and energy metabolism (ATP assay), was conducted in a 96-well plate as described previously (Kumarathasan et al., 2015). The cell proliferation (BrdU incorporation) assay was performed in a separate 96-well plate.

III.2.5. Protein extraction and two-dimensional gel electrophoresis

Total protein from the A549 cells (control and particle-exposed) was extracted and examined by two-dimensional gel electrophoresis (2D-GE) as previously described (Vuong et al., 2016a,b). Following electrophoresis, the gel was washed for 30min in water, stained in BioSafe Coomassie Blue (Bio-Rad) overnight (16–20 h), destained twice in water (20 min) and then imaged with a standard scanner. To overcome the typical warping and distortion issues from gel to gel particularly near the extremities of the pH range and the molecular weight, a common area across all experimental gels that clearly shows the protein spots was selected to assess the proteome differences among the treatments, where proteins in the window of pH5.1–7.8 and 100–20 kDa were analyzed (Vuong et al., 2016a,b). A total of 543 well-resolved protein spots in this common area were compared across all experimental gels, and the identities of 333 of these protein spots were determined via matrix-assisted laser desorption/ionization time-of-flight/time-of-flight mass spectrometry (MALDI-TOF-TOF-MS; Vuong et al., 2016a,b). The protein spots within the gels were matched and quantified with PDQuestTM Advance V8.0.1 (Bio-Rad), where spot volume was quantified using the

available “Local regression model (LOESS)” algorithm in PDQuest. The reported spot volume for each protein was used to compare its level of expression across the treatments.

III.2.6. Gene expression analysis

Total RNA from cell pellets of different treatments was extracted, quantified and prepared for gene expression analysis by reverse transcription–polymerase chain reaction (RT-PCR) as described elsewhere (Thomson et al., 2015). Four house-keeping genes (RPL32, ACTB, HPRT1 and YWHAZ) were assessed as potential reference genes for normalization purposes according to stability across treatments (Chen et al., 2011), and RPL32 was found as the least affected gene across all treatments (data not shown).

III.2.7. Statistical analyses

Two-way analysis of variance (ANOVA) was performed on 2D-GE (n = 3), RT-PCR (n = 3) and cytotoxicity (LDH, BrdU, ATP and CTB; n = 4) data with treatment and dose as factors, using R (R Core Team, 2013). When the assumptions of equal variance and normal distribution were not met, the data were rank-transformed. Holm–Sidak was the post-hoc method used for all pairwise comparisons. A data point was considered as having a significant effect if $p < 0.05$. If the *Treatment* × *Dose* interaction was significant for a protein spot or gene, its change in expression for a given treatment and dose that was found significant by Holm–Sidak analysis was reported as it is (as seen in Supporting information Tables S1 and S3). The same applied for those proteins or genes that were found to have significant *Treatment and Dose* main effects. If a protein was found to have a significant *Treatment* main effect, fold-changes (FCs) were estimated using least square mean (Goodnight & Harvey, 1978; Searle et al., 1980). In the case where the *Dose* main effect was significant, the average FC estimate was reported for each significant dose group.

Pearson correlation analysis was conducted on 2D-GE (n=3), RT-PCR (n = 3) and cytotoxicity (LDH, BrdU, ATP and CTB; n=4) data using R (R Core Team, 2013). The FC in all data sets was transformed to Log_2(FC) to ensure that all data are linear and continuous. Correlation between the responses of A549 cells to the doses of silica particles was conducted on two dosemetrics, namely mass (e.g., of 0, 60, 140 and 200 μg/cm^2 for both CR andMI) and surface area (SA; e.g., 0, 32, 74 and 106 mm^2/cm^2 for CR and 0, 54, 127 and 181 mm^2/cm^2 for MI) (Table 1). Correlations were calculated based on pooled data from both CR andMI for each protein spot, gene or assay. Venn diagrams used to assess the similarities and/or differences in responses in A549 cells following particle exposures were generated via VENNY (Oliveros, 2015).

III.2.8. Bioinformatic analysis (pathway analysis).

2D-GE data showed that multiple protein spots with the same protein ID may have $p< 0.05$, which suggests different isoforms of the same protein were significantly altered, and thus rigorous assessment may be required for proper interpretation of biological implication if the directions of change of these isoforms are different. However, our data showed that the expression of all significant protein spots with the same ID aligned in the same direction. Therefore, we simply chose the protein with the greatest FC (either increase or decrease) to conduct pathway analysis. Furthermore, protein spots that were deemed as small peptides/fragments (based on molecular weight and unique peptide sequences) of their native proteins were excluded from pathway analysis, unless functional data can be found for such peptides based on PubMed (http://www.ncbi.nlm.nih.gov/pubmed) and UniProt (www.uniprot.org) searches. For pathway analysis, an FC cut-off of ± 1.10 and ± 1.50 were applied on top of the significantly changed ($p < 0.05$) protein spots and genes, respectively,

Table III – 1. Physical characteristics (density and diameter) of the silica particles, and the doses expressed in mass or SA in which the A549 cells were exposed.

	Cristobalite				**Min-U-Sil 5**			
Density	2.27 g/cm^3				2.65 g/cm^3			
Median diameter	5.0 μm				2.5 μm			
Calculated SA	0.53 mm^2/μg				0.91 mm^2/μg			
Mass dose (μg/cm^2)	0	60	140	200	0	60	140	200
SA dose (mm^2/cm^2)*	0	32	74	106	0	54	127	181

*Values were calculated based on the assumption that the individual particles have a spherical shape.

to filter out nuanced changes in expressions that may not contribute to any biological impact. Pathway analysis was conducted using Ingenuity Pathway Analysis (www.ingenuity.com). When conducting pathway analysis, only the pathways that were influenced by more than five significant proteins or genes in any particle treatment group were flagged. This arbitrary cut-off was set to identify the more probable cellular pathways that could be affected in A549 cells following particle exposure.

III.3. Results

III.3.1. Physical properties of the silica particles

The SEM image in Figure III – 1B showed that MI particles cover a broad range of sizes. The particles are irregularly shaped, possessing both sharp edges and flat, stepped terraces, consistent with a crystalline sample. There is a lack of porosity observed on the surface of the particles, which is consistent with a highly crystalline solid sample that has been ground from a larger, non-porous sample. CR particles have a similar appearance to that of MI, but the CR particles are more uniform in size (Figure III – 1A). CR particles were distributed over a size range of 1.5 to >8 μm and MI were distributed over a broader size range of <0.5 to >8 μm (Figure III – 1C). There is an overlap in particle size distribution between CR and MI from 1.5 to >8 μm, and MI has more particles in smaller sizes. The median particle sizes for CR and MI are 5.0 and 2.5 μm, respectively. The A549 cell monolayers were exposed to CR andMI at particle mass doses of 0, 60, 140 and 200 $\mu g/cm^2$, and the corresponding particle SA doses for CR were 0, 32, 74 and 106 mm^2/cm^2, and for MI were 0, 54, 127 and 181 mm^2/cm^2 (Table III – 1).

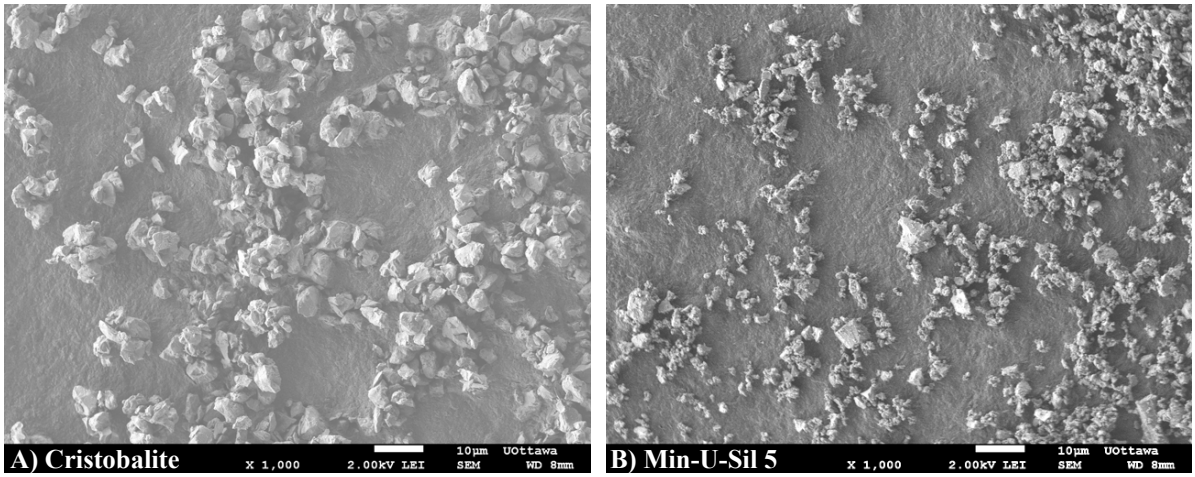

Figure III – 1. Size and shape of the particles in cristobalite (A) and Min-U-Sil 5 (B) samples observed by scanning electron microscopy.
(C) Distribution of the particle size in the silica samples, where the median particle size for cristobalite is about 5.0 µm and Min-U-Sil 5 is about 2.5 µm.

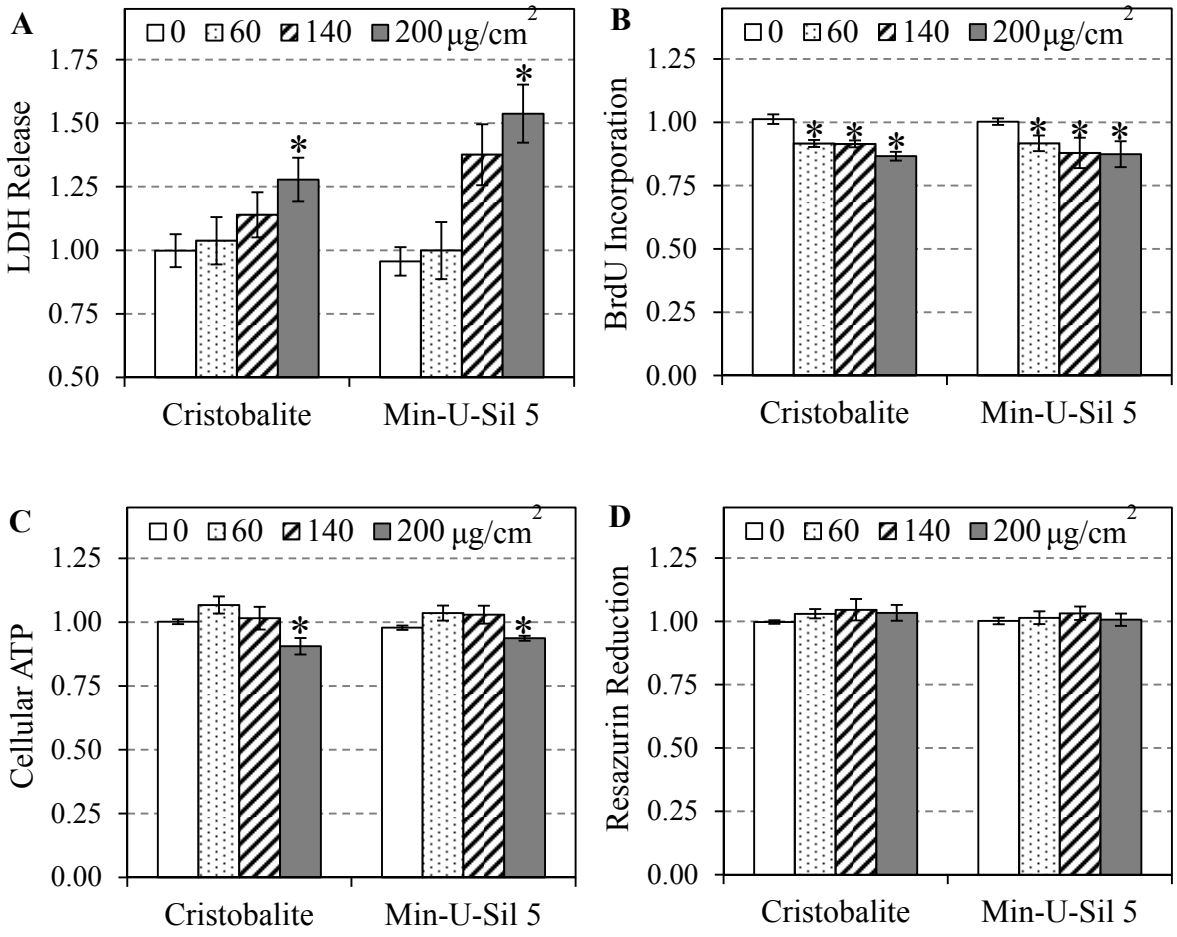

Figure III – 2. Cytotoxicities of cristobalite and Min-U-Sil 5 in A549 cells after 24 h of exposure were assessed by LDH release (A), BrdU incorporation (B), cellular ATP (C) and resazurin reduction (D) assays.
Data are expressed as mean fold effect standard error, relative to control (0 µg/cm^2), n = 4. Two-way ANOVA was used to determine significant effects of the particles, where Holm-Sidak was the post-hoc method used for all pairwise comparison procedures. *Significant change ($p < 0.05$) compared to control (0 µg/cm^2). BrdU, 5-bromo-2′-deoxyuridine; LDH, lactate dehydrogenase.

III.3.2. Cytotoxicity assays

The LDH assay in Figure III – 2A, which assessed the integrity of the cell membrane, showed that both silica particles can cause a significant leakage of LDH from A549 cells at the highest dose, but there was no significant difference in cytotoxicity caused by CR and MI (two-way ANOVA: *Dose* main effect, $p < 0.05$; Holm–Sidak: 200 vs 0 μg/cm^2, $p < 0.05$). Cellular proliferation measured by BrdU incorporation (Figure III – 2B) revealed that both silica particles decreased the mitotic activity of A549 cells to similar levels at all doses (two-way ANOVA: *Dose* main effect, $p < 0.05$; Holm–Sidak: 60, 140 and 200 vs 0 μg/cm^2, $p < 0.05$). Both particles also significantly decreased cellular ATP at the highest dose to a similar level (Figure III – 2C) (two-way ANOVA: *Dose* main effect, $p < 0.05$; Holm–Sidak: 200 vs 0 μg/cm^2, $p < 0.05$). There was no significant change in resazurin reduction in A549 cells exposed to any dose of CR and MI (Figure III – 2D).

III.3.3. Particulate matter-induced changes in the proteome of A549 cells examined by two-dimensional gel electrophoresis

Changes in the proteome of A549 cells after 24 h of exposure to CR and MI particles were assessed via 2D-GE as described previously (Vuong et al., 2016a,b). The results presented in Supporting information Table III – S1 revealed that the expressions of 49 protein spots were significantly affected by both CR and MI (two-way ANOVA: *Treatment* × *Dose* interaction, *Treatment* or *Dose* main effects, $p < 0.05$). Of the significant 49 protein spots, 30 of them passed the Holm–Sidak post-hoc test and their identities have also been determined by MALDI-TOF-TOF-MS. 2D-GE data showed that particle dose-related changes were observed in half (15) of the protein spots (two-way ANOVA: *Dose* main effect, $p < 0.05$), 14 of which are unique proteins. Particle-specific changes were observed in

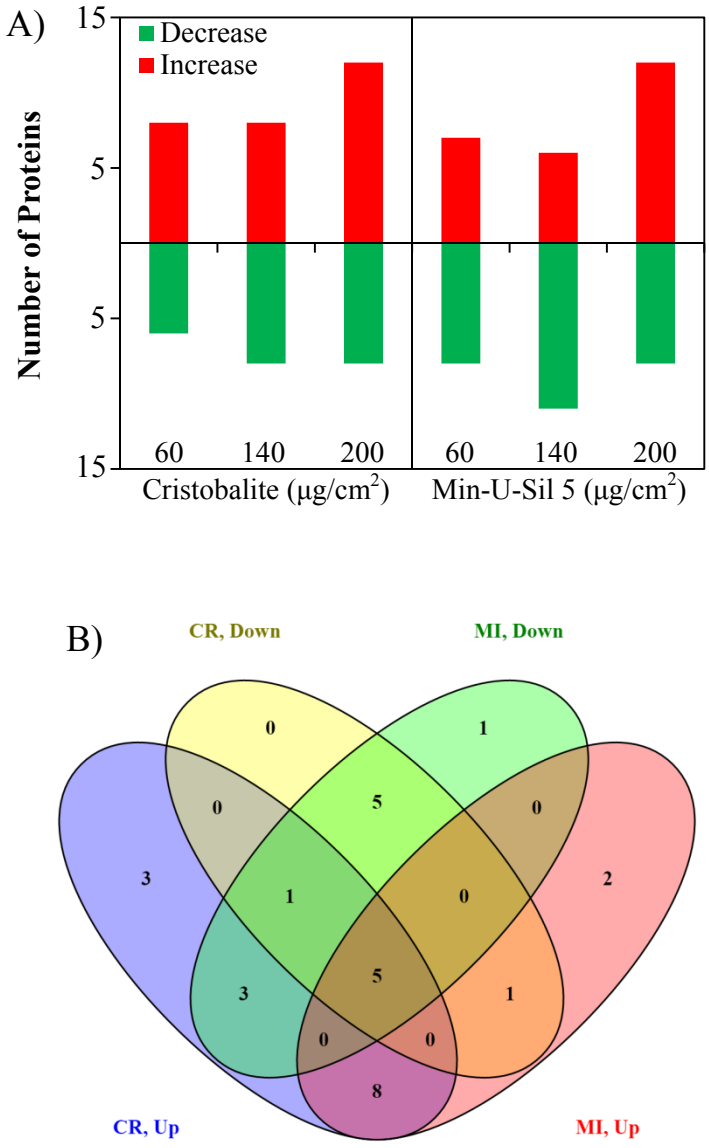

Figure III – 3. Changes in two-dimensional gel electrophoresis protein spots ($p < 0.05$; two-way ANOVA) associated with *in vitro* exposure of A549 cells to silica particles.
(A) Bar graph shows the number of proteins that increased or decreased in expression following particle treatments at doses 60, 140 and 200 µg/cm^2. (B) Venn diagram shows the number of protein spots that exhibited particle-specific and non-specific changes. CR, cristobalite; MI, Min-U-Sil 5.

nine protein spots (two-way ANOVA: *Treatment* main effect, $p < 0.05$), all of which were unique proteins, while six protein spots exhibited *Treatment* × *Dose* interaction (two-way ANOVA: *Treatment* × *Dose* interaction, $p < 0.05$), all six of these being unique proteins. It was noticed that greater change in the number of protein spots were observed for both particles at the higher doses (Figure III – 3A). The Venn diagram in Figure III – 3B provides an overview of the unique and similar changes in the proteome of A549 cells following CR and MI exposures. For pathway analysis, FC cut-off was set at ±1.10.

Pathway analysis revealed that all the proteins affected by the two silica particles were known to be associated with cell death (necrosis and/or apoptosis), proliferation, inflammation, homeostasis and cell movement pathways (Table III – 2). It was noticeable that CR and MI induced distinct patterns of protein expression in these pathways. For example, the spider charts in Figure III – 4 demonstrated that CR and MI induced distinguishable characteristic changes in those proteins involved in the cell death and cell proliferation pathways in A549 cells.

III.3.4. Gene expression changes in A549 cells exposed to silica particles

To understand better the reactivity of A549 cells to the silica particles, RT-PCR was chosen as a gene expression analysis method to assess how CR and MI affected the expression of genes in the exposed cells. For this purpose, a panel of 89 genes was selectedfor gene expression analysis (Supporting information Table III – S2). Some of these selected genes were known to be affected by silica particles in the literature (Sellamuthu et al., 2011), some were genes upstream and/or downstream of those proteins in the identified pathways based on the proteomic changes in the present study, and some were selected from unrelated pathways. Of the genes selected, 37 were found to exhibit altered expression

Table III – 2. Biological functions that were estimated to be affected by the particles based on the proteins that were significantly affected using ingenuity pathway analysis.
Values in the table indicate the number of significant proteins affected by the treatment. Only the pathways that were influenced by more than five proteins in any particle treatment group were shown.

	Cristobalite (μg/cm^2)			**Min-U-Sil 5 (μg/cm^2)**		
Biological Function	**60**	**140**	**200**	**60**	**140**	**200**
Mitotic Activity (Proliferation or Cell Cycle)		8	5		8	5
Cell Death (Apoptosis or Necrosis)	6	6	8	7	7	8
Inflammatory Response		5			6	
Cell Movement		5		6	5	
Protein Metabolism			6			5
Cellular Homeostasis			6			6

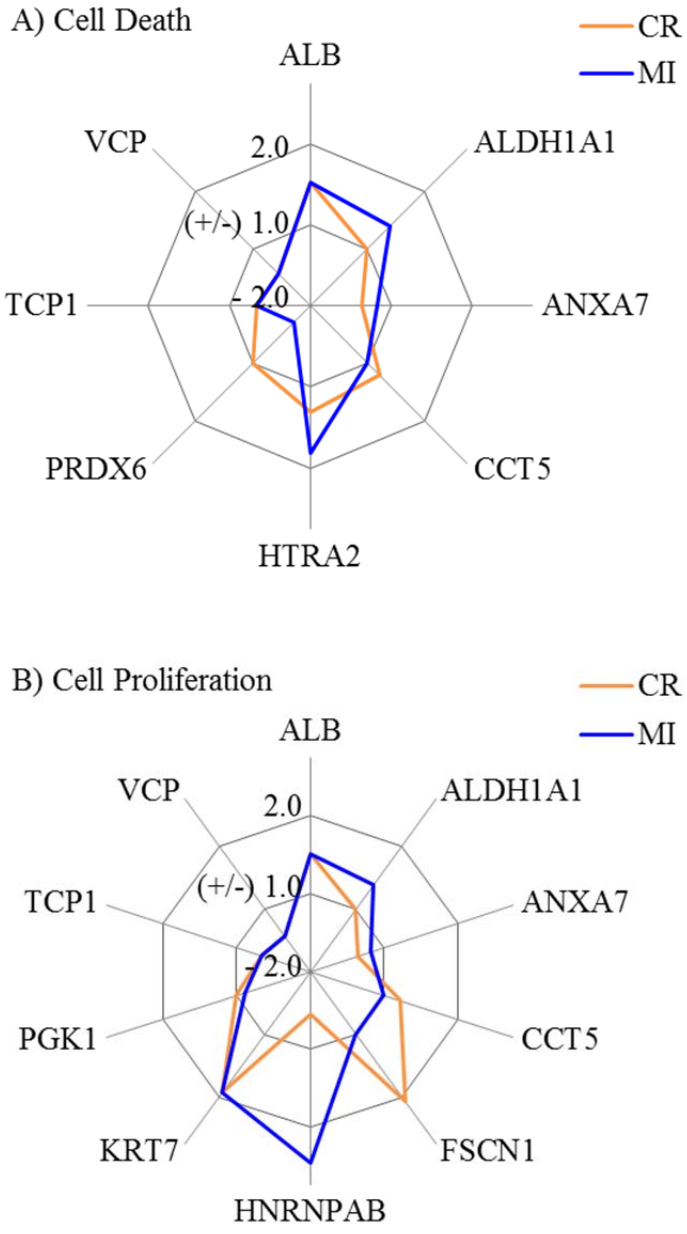

Figure III – 4. Characteristic changes in the expression of proteins involved in the cell death (A) and cell proliferation (B) pathways in A549 cells induced by CR and MI exposures at 140 μg/cm^2.
Y-axis shows the fold-change in expression relative to the control (0 μg/cm^2). CR, cristobalite; MI, Min-U-Sil 5.

following particle exposures (Supporting information Table III – S3). Only two genes (CDKN1A and TNFSF10) were commonly affected by both CR and MI (two-way ANOVA: *Dose* main effect, $p < 0.05$). The remaining genes were differentially affected by the two particles, where 12 showed *Treatment* × *Dose* interaction (two-way ANOVA: *Treatment* × *Dose* interaction, $p < 0.05$) and 23 exhibited Treatment main effect (two-way ANOVA: *Treatment* main effect, $p < 0.05$). Interestingly, the lowest dose of MI (mass: 60 μg/cm^2) was capable of influencing a greater change in the expressions of most genes than the highest dose of CR (mass: 200 μg/cm^2) (Supporting information Table III – S3). Only those genes with FC greater than ±1.50 in any treatment were used for pathway analysis. Ingenuity pathway analysis based on all the genes that were identified as significantly altered based on two-way ANOVA (Supporting information Table III – S3) revealed that most of the affected genes are involved in the cell death, mitosis, homeostasis, ROS metabolism and inflammatory response pathways (Table III – 3). For example, the signature effects of CR and MI on those genes involved in the ROS metabolism and inflammatory response pathways in A549 cells can be clearly differentiated in the spider charts in Figure III – 5.

III.3.5. Pearson correlation

It was mentioned earlier that the median particle size of CR (~5.0 μm) is larger than MI particles (~2.5 μm). Thus, a potential relationship between particle size and their differential response profiles in A549 cells was examined using Pearson correlation analysis. Pearson correlation analysis conducted on cytotoxicity assays (Supporting information Table III – S4) indicated that the level of cellular ATP in A549 cells correlated well with mass, whereas LDH leakage associated better with SA, while similar correlation coefficients were found for both mass and SA for BrdU incorporation. No correlation was found for either

Table III – 3. Biological functions indicated by ingenuity pathway analysis that were likely impacted by the particles based on the genes that were significantly affected.
Values in the table indicate the number of genes that were significantly affected by the treatment. Only the pathways that were influenced by more than five genes in any particle treatment group were shown.

	CR (μg/cm^2)			MI (μg/cm^2)		
Biological Function	**60**	**140**	**200**	**60**	**140**	**200**
Mitotic Activity			7	10	16	16
Cell Death (Apoptosis & Necrosis)			7	9	16	16
Inflammatory Response			7	10	12	12
Cell Movement			6	5	12	10
Protein Metabolism			5			7
Lipid Metabolism			6	7	12	12
Carbohydrate Metabolism			6	6	12	12
ROS Metabolism				7	11	11
Fibrosis				5	7	
Cell Differentiation					14	9
Molecular Transport					11	12
Filopodia Formation						5
Hormone Metabolism						5

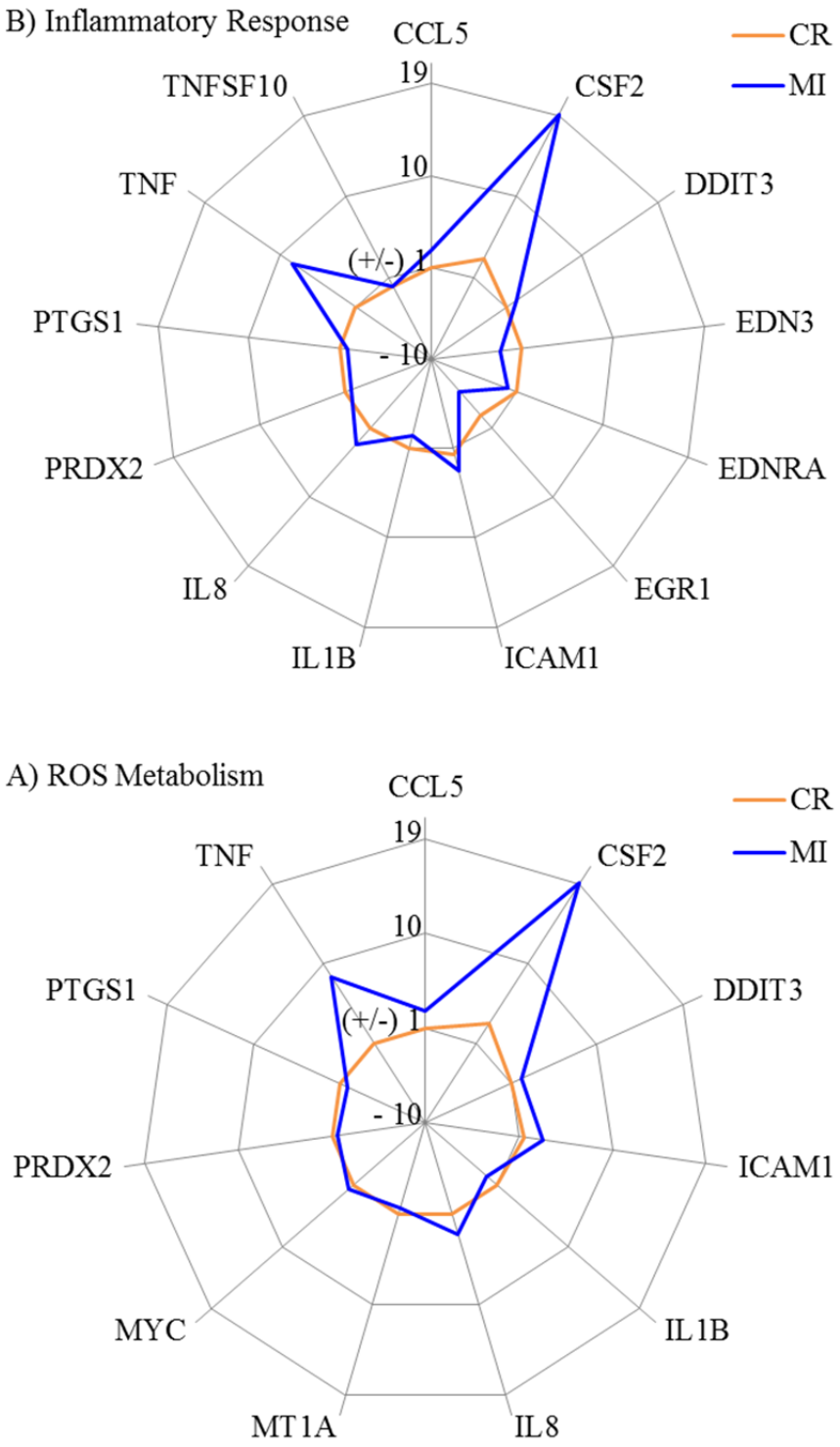

Figure III – 5. Signature changes in the expression of genes involved in the ROS metabolism (A) and inflammatory response (B) pathways in A549 cells induced by CR and MI exposures at 140 μg/cm^2.
Y-axis shows the fold-change in expression relative to the control (0 μg/cm^2). CR, cristobalite; MI, Min-U-Sil 5; ROS, reactive oxygen species.

mass or SA with the pattern of cellular resazurin reduction. The dose–response plots in Figure III – 6 are representative visual demonstrations of two cytotoxicity assays, namely LDH leakage and cellular ATP, which showed the dose–response curves of CR and MI exposures are similar. Pearson correlation conducted on 2D-GE data identified 96 protein spots correlated significantly with either mass or SA (Supporting information Table III – S5), but stronger correlation was found with SA (81 protein spots, $p < 0.05$) than mass (46 protein spots, $p < 0.05$). Interestingly, the dose–response curves for a number of protein spots were different for the CR andMI treatments regardless if the protein spot is significantly correlated (e.g., NDUFV2 or ssp5006 in Figure III – 7) or not correlated (e.g., PRDX6 or ssp7002 in Figure III – 7). Similarly, Pearson correlation on gene expression in A549 cells following particle exposures showed that the dose–responses of 52 from the 88 genes examined were significantly correlated with SA and mass (Supporting information Table III – S6). Similar to the proteomic result, the expression of most genes associated stronger with SA than mass, and the dose–response curves of CR and MI were different for the majority of the correlated genes (Figure III – 8).

Discussion

Silica or silicon dioxide can adopt various physical structures such as amorphous (non-crystalline) or crystalline (e.g., quartz, CR and tridymite). However, most toxicological studies thus far have focused mainly on one form of silica, which is α-quartz, and very limited data have been reported on the toxicity of other forms of silica. The exposure regulatory limits for all forms of silica have been based on quartz. Yet, physical properties of

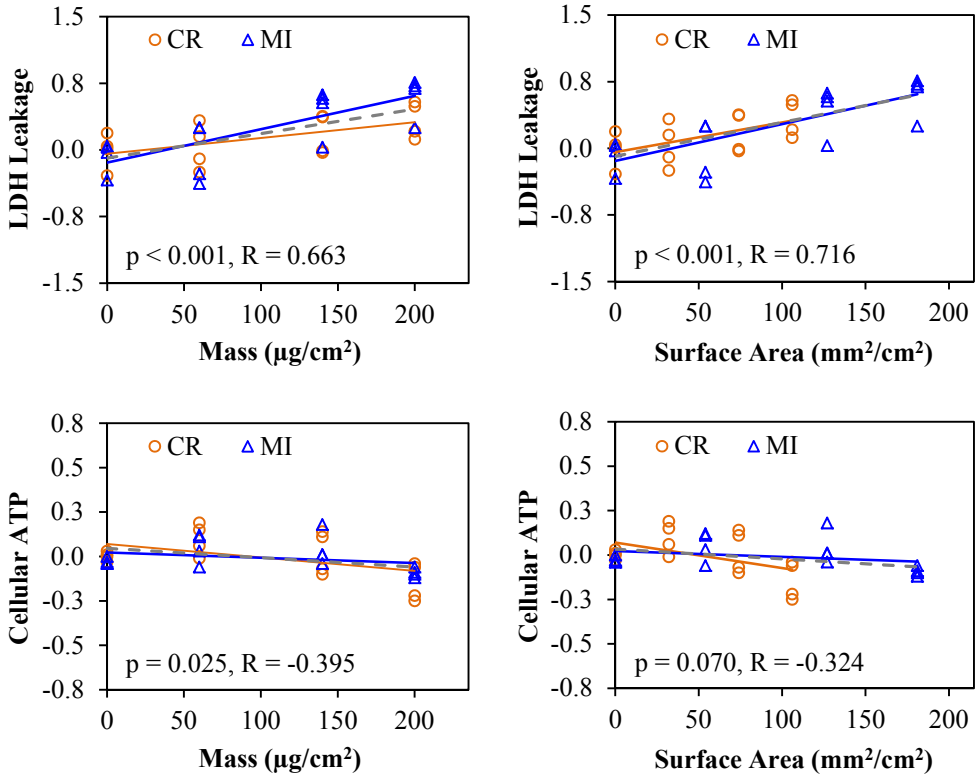

Figure III – 6. Cytotoxicity endpoints associated with mass or surface area dose metrics. Pearson correlation was conducted to assess the linear association between the responses (in Log_2(fold-effect)) and the doses (in mass or surface area), where R corresponds to the correlation coefficient and $p < 0.05$ indicates a significant correlation. Orange and blue lines correspond to the dose–response curves for CR and MI exposures, respectively, whereas the grey-dashed line indicates the dose–response curve, when both particles are considered together. CR, cristobalite; LDH, lactate dehydrogenase; MI, Min-U-Sil 5.

particles can modify their toxicity characteristics. In this study, we used *in vitro* toxicoproteomic and gene expression analysis approaches to assess the difference between two silica particles, namely CR and α- quartz (MI). The main physical differences between these two silica particles are their crystalline structures, densities and sizes (Table III – 1).

In this work, the A549 cells were exposed to CR and MI at relatively low toxic levels (Figures III – 2 and 3). Only the highest dose (200 μg/cm^2) of CR and MI appeared to affect the cellular membrane integrity and a loss of energy content in A549 cells, potentially leading to cell death. These silica particles also decreased the mitotic activity of the cells, at all doses (Figure III – 2B). These cytotoxicity assays were not able to distinguish the toxicity differences due to CR and MI exposures, except for the LDH release assay in Figure III – 2A that suggested a possible difference in potencies (MI>CR). However, this difference did not reach statistical significance.

Toxicity changes due to these particulate matter (PM) exposures were also analyzed using toxicoproteomic and gene expression analysis strategies. The goal of this study was not to obtain exhaustive proteomic information, but rather to obtain some information on PM exposure-related changes at the molecular level that can be amenable to traditional toxicity testing methods. This is a proof-of-principle study to test the influence of PM's physical characteristics on their toxicity properties.

Proteomic analysis was thus conducted using less costly 2D-GE separation of proteins, with analysis for PM exposure-related changes captured for proteins in the pH range 5.1–7.8, stained only by Coomassie Blue. Nevertheless, we observed statistically significant PM exposure-related changes, following this protocol. For instance, CR and MI exposures led to significant ($p < 0.05$) changes in 49 protein spots based on two-way ANOVA, where the identities of 30 of these protein spots were achieved using MALDI-

TOF-TOF-MS (Supporting information Table III – S1). Such mild changes in the cell proteome were not surprising because the exposure conditions were only moderately cytotoxic to A549 cells as seen by the cytotoxicity assay results.

In this study, we only considered the proteomic and gene expression changes that were significantly different based on the two-way ANOVA results as differential effects associated with particle toxicity. For example, the results shown in Supporting information Table III – S1 indicated that there was a significant Treatment main effect in the expression of AUH (SSP5205) due to particle exposures. This means on average, CR treatments decreased its expression by –1.22 and MI treatments increased its expression by 1.14. It is important to understand that such FCs were relative to the control (0 $\mu g/cm^2$). More importantly, it must also be understood that the net difference in the expression of AUH was 36 % (from – 1.22 to 1.14) between CR andMI exposures. Thus, such difference cannot be ignored, particularly when the P value is reasonably small (two-way ANOVA: *Treatment* main effect, $p = 0.027$), and the goal of this study is to identify differential responses of A549 cells to CR and MI. When choosing an appropriate FC cut-off value for pathway analysis, we considered that if a cut-off were set at ± 1.50, it would remove differential effects ranging from 50 to 98 % (e.g., FC from 1.49 to – 1.01 and FC from 1.49 to – 1.49). A cut-off at ± 1.25 will filter out differential effects ranging from 25 to 48 % (e.g., FC from 1.24 to – 1.01 and FC from 1.24 to – 1.24). A cut-off at ± 1.10 can remove all differential effects below 10 % (e.g., FC from 1.09 to – 1.01) and up to 18 % (e.g., FC from 1.09 to – 1.09). We believe that ± 1.10 FC cut-off for the significant protein spots ($p < 0.05$) and ± 1.50 FC cut-off for significant genes ($p < 0.05$) were sufficient to remove nuanced changes in expression that may not contribute to any biological impact (see Supporting information Tables III – S1 and S3).

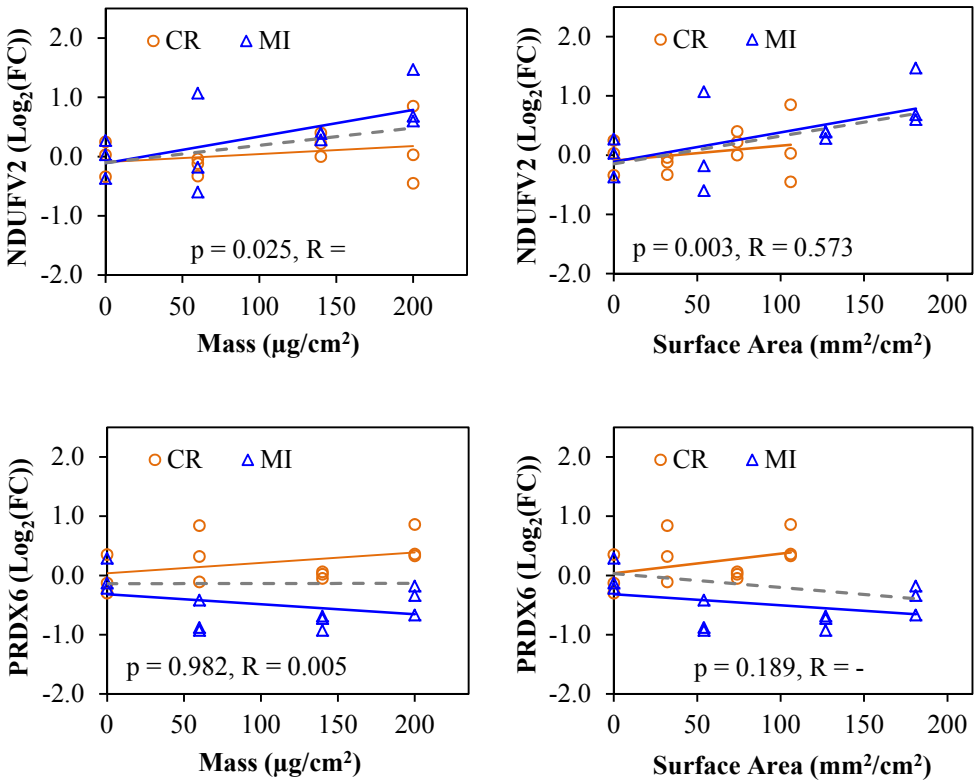

Figure III – 7. Dose–response curves for proteins based on mass or surface area.
R corresponds to the correlation coefficient and $p < 0.05$ indicates a significant correlation based on Pearson correlation analyses. Orange and blue lines correspond to the dose–response curves for CR and MI exposures, respectively, whereas the grey-dashed line indicates the dose–response curve, when both particles are visualized together. CR, cristobalite; FC, fold-change; MI, Min-U-Sil 5.

When conducting pathway analysis, we chose to evaluate the effects of the particles at a subtoxic level (i.e., 140 μg/cm^2) and yielded maximum responses from mostly "living" cells. Our results revealed that both silica particles could significantly alter the expressions of proteins that are known to be involved in cell death (necrosis and/or apoptosis), proliferation, inflammation, homeostasis, cell cycle and cell movement pathways (Table III – 2). Meanwhile, the cytotoxicity assay results (Figure III – 2) indicated that CR and MI can cause damage to the cell membrane (an indicator of cell death), decreased BrdU incorporation (an indicator of decreased cell proliferation) and lowered cellular ATP level (an indicator of energy content) in A549 cells, which were consistent with the observed proteomic results. In addition, these findings were supported by a large body of evidence in the literature that silica particles (mostly α-quartz in the form of Min-U-Sil) can induce cell death (Cassel et al., 2008; Chao et al., 2001; Iyer et al., 1996; Joshi & Knecht, 2013) and inflammatory response (Cassel et al., 2008; Dostert et al., 2008; Hornung et al., 2008; Peeters et al., 2013). These cellular responses were reported in respiratory tract macrophages and epithelial cells.

The spider chart in Figure – 4A demonstrates that more than half of the proteins (e.g., ALDH1A1, ANXA7, CCT5, HTRA2 and PRDX6) involved in the cell death pathway in A549 cells are differently altered in A549 cells due to CR and MI exposures. The GTPase calcium-dependent phospholipid-binding protein ANXA7 can act as an anti-apoptotic protein (Huang et al., 2014, 2015; Liu et al., 2016; Torosyan et al., 2009), whereas HTRA2 (or OMI) is a pro-apoptotic serine peptidase that is known to cleave inhibitors of apoptosis to facilitate the activation caspase 3 (Cory & Adams, 2002; Sutton et al., 2003; Wang et al., 2013). Increased expression of the pro-apoptotic protein HTRA2 and decreased expression of the anti-apoptotic protein ANXA7 following particle exposures suggested that both silica particles could stimulate apoptotic cell death, which were consistent with the LDH release

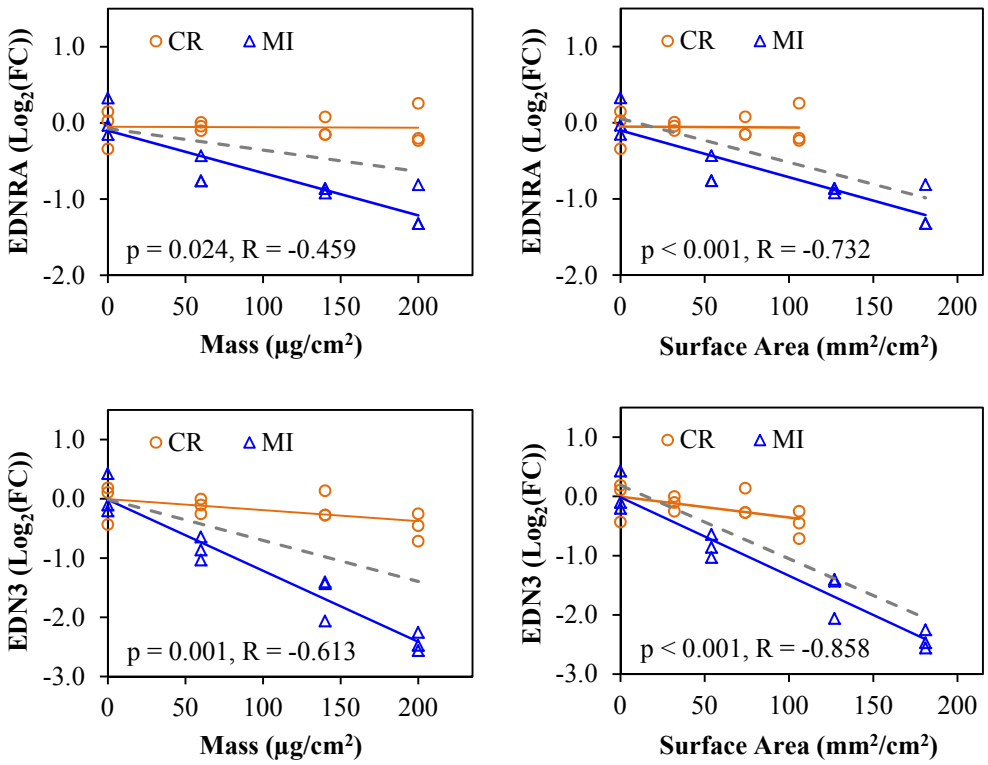

Figure III – 8. Dose–response curves for EDNRA and EDN3 genes based on mass or surface area.

R corresponds to the correlation coefficient and $P < 0.05$ indicates significant correlation based on Pearson correlation. Orange and blue lines correspond to the dose–response curves for CR and MI exposures, respectively, whereas the grey-dashed line indicates the dose–response curve, when both particles are considered together. CR, cristobalite; FC, fold-change; MI, Min-U-Sil 5.

assay (Figure III – 2A). The main difference between the two particles is that MI increased the expression of the pro-apoptotic protein HTRA2 more than its counterpart did, while CR suppressed the expression of the anti-apoptotic protein ANXA7 more than MI. Furthermore, only MI affected the expression of antioxidant proteins such as aldehyde dehydrogenase (ALDH1A1) and peroxiredoxin-6 (PRDX6), which are known to protect cells from apoptotic cell death (Luo et al., 2012; Zha et al., 2015). These results suggested that the MI exposures might be triggering oxidative stress pathways as MI has been reported to cause oxidative stress and apoptosis in human bronchial epithelial cells (Antognelli et al., 2015).

Similarly, the signature effects of CR andMI on those proteins involved in the cell proliferation pathway in A549 cells can be readily identified based on the spider chart in Figure III – 4B. The expression of ANXA7 was inhibited by both silica particles, but a stronger inhibition was noticed with CR exposure compared to MI exposure. As ANXA7 acts as an anti-apoptotic protein (discussed above), down-regulation of this protein by both silica particles can decrease the proliferation of cells. Interestingly, all ALDH1A1 (Moreb et al., 2008), actin-bundling protein FSCN1 (Kano et al., 2010), heterogeneous nuclear ribonucleoprotein HNRNPAB (He et al., 2005) and ATP-generating glycolytic enzyme phosphoglycerate kinase-1 PGK1 (Wang et al., 2010) have been reported to promote mitotic activity in cells. Yet, the expression of these proteins can be stimulated (increase in cell growth) or suppressed (decrease in cell growth) depending on the particle type in the exposure. Suppressing the expression of proliferative proteins can be a mechanism of particle toxicity in A549 cells, while increased expression of proliferative proteins is likely a survival mechanism of the exposed cells. The limited proteomic analysis conducted in this study was able to distinguish particles with different physical characteristics and provided some insights into potential pathways that maybe perturbed. Exhaustive proteomic analysis

through future works can provide more detailed information on mechanistic changes associated with these particle exposures.

To understand further the particle toxicity-related molecular mechanisms, we conducted gene expression analysis via RT-PCR to assess how the A549 cells responded to the silica particles at the transcriptional level. Gene expression analysis indicated that the two silica particles can perturb similar transcriptional mechanisms in A549 cells following 24 h of exposure (Supporting information Table III – S3), but the majority of the genes altered by CR and MI were particle-specific (two-way ANOVA: *Treatment* main effect and *Treatment* × *Dose* interaction, $p < 0.05$). For example, the lowest dose of MI (60 μg/cm^2) was capable of influencing a greater change in the expression of most genes than the highest dose of CR (200 μg/cm^2), clearly indicating that MI is more potent than CR (Supporting information Table III – S3). Furthermore, the response of a number of genes to CR and MI exposures resulted in two different curves (representative examples can be found in Figure III – 8). Thus, CR and MI caused distinguishable cytotoxic effects in A549 cells at the transcriptional level.

Pathway analysis showed that the majority of the affected genes are involved pathways such as cell death (apoptosis or necrosis), cell proliferation, inflammatory response and metabolism of ROS, lipid, protein and carbohydrate (Table III – 3). These results were in line with our proteomic and cytotoxicity assay results. In agreement, a recent genomic study (using microarray) on the toxicity of MI reported that the particle perturbed the expression of genes in A549 cells that govern cellular growth and proliferation, cell death, inflammatory response and cell cycle (Sellamuthu et al., 2011). More importantly, our gene expression analysis revealed a characteristic difference between CR and MI exposures. For example, the spider charts in Figure III – 5 demonstrated that the effects of CR and MI exposure were

unequivocally distinct in A549 cells. The chart showed that MI induced a significantly greater level of changes than CR in the expressions of genes involved in the ROS metabolism and inflammatory response pathways; where the effect of CR in these pathways were likely non-significant.

A physical difference between the two silica particles that may provoke differential responses in A549 cells is the grain size of the particles, where the median size of CR (~5.0 μm) particles is two times larger than MI (~2.5 μm) (Table III – 1). As A549 cells were exposed to equal mass dose, MI has twice the SA available to interact with the cells as compared to CR. Hence, it is possible that the responses of A549 cells to the two silica particles could be a function of SA. Thus, all the RT-PCR, proteomic and cytotoxicity assay data were examined by linear Pearson correlation analysis to assess whether mass or SA was a better physical attribute for these biological changes. Pearson correlation for different cytotoxicity assays indicated that certain cellular responses were better associated to mass, while others were better associated to SA (Supporting information Table III – S4; Figure III – 6). For example, LDH leakage levels are better associated with SA than with mass, which suggested that the cell surface–PM interaction could be an important mechanism in causing cell membrane damage. On the other hand, cellular ATP levels are correlated better with mass than with SA. Pearson correlation results in Supporting information Table III – S5 indicated that some of the proteomic responses in A549 cells were better associated with SA (81 protein spots, $p < 0.05$) than mass (46 protein spots, $p < 0.05$). Intriguingly, the dose–response relationships for a number of other proteins were not correlated with mass or SA suggesting that these protein changes may be better described by other particle physical characteristics such as crystallinity (Table III – 1). Similarly, RT-PCR data also showed that the expressions of the majority of the genes examined were significantly correlated with SA

and mass, but SA generally showed a stronger correlation than mass (Supporting information Table III – S6). As with protein changes, there were some gene expression changes that correlated less with SA or mass and these can also perhaps be explained by other physicochemical properties of PM.

Association between physical properties of these particles and the observed proteomic and gene expression responses will need to be explored further through additional studies. In summary, this study demonstrated that toxicoproteomics and gene expression analysis are sensitive strategies to dissect cellular changes relevant to the PM's physical characteristics related to the toxicity changes that are not clearly apparent by use of traditional cytotoxicity assays. This approach can be useful in understanding toxicity mechanisms mediated by environmental air PM and engineered nanomaterials.

Conclusion

In conclusion, *in vitro* toxicoproteomics in conjunction with gene array can provide insight into the effects of physical properties of respirable PM on biological responses of A549 human lung epithelial cells. Such high-content *in vitro* cellular toxicity data at the molecular level can be useful in discriminating toxicity mechanisms affected by the physical nature of particles.

Acknowledgments

We would like to thank Drs. Ella Atlas and Azam Tayabali for their helpful comments. This work was supported by the Clean Air Regulatory Agenda at Health Canada (

grant no. 4340565) and, Ontario Graduate Scholarship in Science and Technology and Ontario Graduate Scholarship (funding for Ngoc Vuong, Student ID: 1519592).

Conflict of interest

The authors did not report any conflict of interest.

References

AGN. 1930. Silicosis. Can. Med. Assoc. J. 23: 827–829.

Antognelli C, Gambelunghe A, Muzi G, Talesa VN. 2015. Peroxynitrite-mediated glyoxalase I epigenetic inhibition drives apoptosis in airway epithelial cells exposed to crystalline silica via a novel mechanism involving argpyrimidine-modified Hsp70, JNK, and NF-KappaB. Free Radic. Biol. Med. 84: 128–141.

Belt TH. 1930. Silicosis. Can. Med. Assoc. J. 23: 802–804.

Cassel SL, Eisenbarth SC, Iyer SS, Sadler JJ, Colegio OR, Tephly LA, Carter AB, Rothman PB, Flavell RA, Sutterwala FS. 2008. The Nalp3 inflammasome is essential for the development of silicosis. Proc. Natl. Acad. Sci. U. S. A. 105: 9035–9040.

Chao SK, Hamilton RF, Pfau JC, Holian A. 2001. Cell surface regulation of silica-induced apoptosis by the SR-A scavenger receptor in a murine lung macrophage cell line (MH-S). Toxicol. Appl. Pharmacol. 174: 10–16.

Chen D, Pan X, Xiao P, Farwell MA, Zhang B. 2011. Evaluation and identification of reliable reference genes for pharmacogenomics, toxicogenomics, and small RNA expression analysis. J. Cell. Physiol. 226: 2469–2477.

Cory S, Adams JM. 2002. The Bcl2 family: Regulators of the cellular life or death switch. Nat. Rev. Cancer 2: 647–656.

Dostert C, Petrilli V, Van BR, Steele C, Mossman BT, Tschopp J. 2008. Innate immune activation through Nalp3 inflammasome sensing of asbestos and silica. Science 320: 674–677.

Goodnight JH, Harvey WR. 1978. Least-Squares Means in the Fixed-Effects General Linear Models. SAS Technical Report R-103. SAS Institute Inc., SAS Technical Report. SAS Technical Report R-103.

He Y, BrownMA, Rothnagel JA, Saunders NA, Smith R. 2005. Roles of heterogeneous nuclear ribonucleoproteins A and B in cell proliferation. J. Cell Sci. 118: 3173–3183.

Hornung V, Bauernfeind F, Halle A, Samstad EO, Kono H, Rock KL, Fitzgerald KA, Latz E. 2008. Silica crystals and aluminum salts activate the NALP3 inflammasome through phagosomal destabilization. Nat. Immunol. 9: 847–856.

Huang Y,Wang Q, Du Y, Bai L, Jin F, Zhang J, Fan S, Wang H, Song L, Gao Y, Wang X, Tang J. 2014. Inhibition of annexin A7 gene and protein induces the apotosis and decreases the invasion, migration of the hepatocarcinoma cell line. Biomed. Pharmacother. 68: 819–824.

Huang Y, Du Y, Zhang X, Bai L,MibrahimM, Zhang J,Wei Y, Li C, Fan S,Wang H, Zhao Z, Tang J. 2015. Down-regulated expression of annexin A7 induces apoptosis in mouse hepatocarcinoma cell line by the intrinsic mitochondrial pathway. Biomed. Pharmacother. 70: 146–150.

IARC. 1997. IARCWorking Group on the Evaluation of Carcinogenic Risks to Humans: Silica, Some Silicates, Coal Dust and Para-Aramid Fibrils. Lyon, 15–22 October 1996. IARC Monogr. Eval. Carcinog. Risks Hum. 68: 1–475.

IARC. 2012. Silica dust, crystalline, in the form of quartz or cristobalite. IARC Monogr. 100: 355–405.

Iyer R, Hamilton RF, Li L, Holian A. 1996. Silica-induced apoptosis mediated via scavenger receptor in human alveolar macrophages. Toxicol. Appl. Pharmacol. 141: 84–92.

Joshi GN, Knecht DA. 2013. Silica phagocytosis causes apoptosis and necrosis by different temporal and molecular pathways in alveolar macrophages. Apoptosis 18: 271–285.

Kano M, Seki N, Kikkawa N, Fujimura L, Hoshino I, Akutsu Y, Chiyomaru T, Enokida H, Nakagawa M, Matsubara H. 2010. MiR-145, MiR-133a and MiR-133b: Tumor-suppressive MiRNAs target FSCN1 in esophageal squamous cell carcinoma. Int. J. Cancer 127: 2804–2814.

Kumarathasan P, Breznan D, Das D, SalamMA, Siddiqui Y, Mackinnon-Roy C, Guan J, de Silva N, Simard B, Vincent R. 2015. Cytotoxicity of carbon nanotube variants: a comparative in vitro exposure study with A549 epithelial and J774 macrophage cells. Nanotoxicology 9(2): 148–161.

Liu S, Ge D, Chen L, Zhao J, Su L, Zhang S, Miao J, Zhao B. 2016. A small molecule induces integrin Beta4 nuclear translocation and apoptosis selectively in cancer cells with high expression of integrin Beta4. Oncotarget 7(13): 16282–16296.

Luo Y, Dallaglio K, Chen Y, Robinson WA, Robinson SE, McCarter MD, Wang J, Gonzalez R, Thompson DC, Norris DA, Roop DR, Vasiliou V, Fujita M. 2012. ALDH1A Isozymes are markers of human melanoma stem cells and potential therapeutic targets. Stem Cells 30: 2100–2113.

Moreb JS, Baker HV, Chang LJ, Amaya M, Lopez MC, Ostmark B, Chou W. 2008. ALDH isozymes downregulation affects cell growth, cell motility and gene expression in lung cancer cells. Mol. Cancer 7: 87.

Nadeau D, Vincent R, Kumarathasan P, Brook J, Dufresne A. 1996. Cytotoxicity of ambient air particles to rat lung macrophages: Comparison of cellular and functional assays. Toxicol. In Vitro 10: 161–172.

Oliveros JC. 2015. VENNY. An interactive tool for comparing lists with Venn's Diagrams. http://bioinfogp.cnb.csic.es/tools/venny/index.html accessed: 21 March 2016.

Peeters PM, Perkins TN, Wouters EF, Mossman BT, Reynaert NL. 2013. Silica induces NLRP3 inflammasome activation in human lung epithelial cells. Part. Fibre Toxicol. 10: 3.

R Core Team. 2013. R: A language and environment for statistical computing. http://www.R-project.org/ accessed: 26 October 2016.

Searle SR, Speed FM, Miliken GA. 1980. The population marginal means in the linear model: An alternative to least squares means. Am. Stat. 34:216–221.

Sellamuthu R, Umbright C, Li S, Kashon M, Joseph P. 2011. Mechanisms of crystalline silica-induced pulmonary toxicity revealed by global gene expression profiling. Inhal. Toxicol. 23: 927–937.

Sutton VR, Wowk ME, Cancilla M, Trapani JA. 2003. Caspase activation by granzyme B is indirect, and caspase autoprocessing requires the release of proapoptotic mitochondrial factors. Immunity 18: 319–329.

Thomson EM, Breznan D, Karthikeyan S, Mackinnon-Roy C, Charland JP, Dabek-Zlotorzynska E, Celo V, Kumarathasan P, Brook JR, Vincent R. 2015. Cytotoxic and inflammatory potential of size-fractionated particulate matter collected repeatedly within a small urban area. Part. Fibre Toxicol. 12: 24.

Torosyan Y, Simakova O, Naga S,Mezhevaya K, Leighton X, Diaz J, HuangW, Pollard H, SrivastavaM. 2009. Annexin-A7 protects normal prostate cells and induces distinct patterns of RB-associated cytotoxicity in androgensensitive and -resistant prostate cancer cells. Int. J. Cancer 125: 2528–2539.

Vincent R, Goegan P, Johnson G, Brook JR, Kumarathasan P, Bouthillier L, Burnett RT. 1997. Regulation of promoter-CAT stress genes in HepG2 cells by suspensions of particles fromambient air. Fundam. Appl. Toxicol. 39: 18–32.

Vuong NQ, Goegan P, Mohottalage S, Breznan D, Ariganello M, Williams A, Elisma F, Karthikeyan K, Vincent R, Kumarathasan P. 2016a. Proteomic changes in human lung epithelial cells (A549) in response to carbon black and titanium dioxide exposures. J. Proteomics 149: 53–63.

Vuong NQ, Goegan P, Mohottalage S, Breznan D, Ariganello M, Williams A, Elisma F, Karthikeyan S, Vincent R, Kumarathasan P. 2016b. Human lung epithelial cell A549 proteome data after treatment with titanium dioxide and carbon black. Data Brief 8: 687–691.

Wang J, Ying G, Wang J, Jung Y, Lu J, Zhu J, Pienta KJ, Taichman RS. 2010. Characterization of phosphoglycerate kinase-1 expression of stromal cells derived fromtumormicroenvironment in prostate cancer progression. Cancer Res. 70: 471–480.

Wang K, Zhang J, Liu J, Tian J, Wu Y, Wang X, Quan L, Xu H, Wang W, Liu H.

2013. Variations in the protein level of Omi/HtrA2 in the heart of aged rats may contribute to the increased susceptibility of cardiomyocytes to ischemia/reperfusion injury and cell death: Omi/HtrA2 and aged heart injury. Age (Dordr.) 35: 733–746.

Zha X,Wu G, Zhao X, Zhou L, Zhang H, Li J, Ma L, Zhang Y. 2015. PRDX6 protects ARPE-19 cells from oxidative damage via PI3K/AKT signaling. Cell. Physiol. Biochem. 36: 2217–2218.

Table III – S1. Two-way ANOVA results for the A549 protein spots changed due to particle exposures (n = 3).
The SSP number corresponds to the identifier number that PDQuest used to identify the spot based on its coordinate in the gel. The number below *Treatment* main effect (Trt), *Dose* main effect (Dose) or interaction between *Treatment and Dose* (T x D) corresponds to the *p*-value, where the bolded number emphasized *p*-value<0.05. Only the protein spots identified by MALDI-TOF-TOF-MS/MS are provided here (Vuong et al., 2016a;Vuong et al., 2016b). The proteins indicated in red (likely degradation product of the native protein) and fold-change indicated in blue (cut-off at ±1.10) were excluded from pathway analysis (see Materials and Methods).

		§Cristobalite (μg/cm²)			§Min-U-Sil 5 (μg/cm²)			Two-way ANOVA			†Cristobalite (μg/cm²)			†Min-U-Sil 5 (μg/cm²)		
SSP	**ID**	**60**	**140**	**200**	**60**	**140**	**200**	**Trt**	**Dose**	**T x D**	**60**	**140**	**200**	**60**	**140**	**200**
1005	PNMA6C	-1.03	-1.13	1.01	7.23	8.06	7.24	**0.042**	0.086	**0.043**				7.23	8.06	7.24
7002	PRDX6	1.32	1.01	1.45	-1.65	-1.72	-1.30	**0.041**	0.067	**0.019**				-1.65	-1.72	
2010	ARMCX1	-1.56	1.23	-1.32	1.23	-1.61	-3.19	0.156	0.127	**0.037**		1.23			-1.61	
9603	FSCN1	2.20	2.07	1.31	-1.26	-1.32	1.43	0.110	0.500	**0.025**	2.20	2.07	1.31	-1.26		1.43
7301	HNRNPAB	-1.09	-1.46	-1.14	1.81	2.46	1.79	0.375	0.562	**0.047**		-1.46			2.46	
8007	TPI1	2.32	1.23	-1.14	-1.45	-1.02	1.25	0.426	0.242	**0.002**	2.32			-1.45		
6208	HTRA2	1.33	1.01	1.59	1.95	1.56	1.96	**0.026**	**0.040**	0.764	1.31	1.31	1.31	1.83	1.83	1.83
1009	JARID2	-1.29	-1.10	-1.38	-1.69	-1.41	-1.26	**0.000**	**0.045**	0.534	-1.26	-1.26	-1.26	-1.45	-1.45	-1.45
7504	ALDH1A1	-1.13	1.07	1.03	1.14	1.46	1.57	**0.023**	0.535	0.855	-1.01	-1.01	-1.01	1.39	1.39	1.39
6502	ANXA7	-1.63	-1.02	-1.42	-1.00	1.11	-1.63	**0.042**	0.206	0.621	-1.36	-1.36	-1.36	-1.17	-1.17	-1.17
5205	AUH	-1.23	-1.14	-1.28	1.32	1.14	-1.04	**0.027**	0.832	0.677	-1.22	-1.22	-1.22	1.14	1.14	1.14
4701	CCT5	1.16	1.20	1.28	1.07	1.14	1.04	**0.013**	0.414	0.794	1.21	1.21	1.21	1.08	1.08	1.08
1008	GLRX3	-1.22	-1.39	-1.20	-1.61	-1.68	-1.63	**0.016**	0.189	0.948	-1.27	-1.27	-1.27	-1.64	-1.64	-1.64
301	HSPA2	-2.10	-1.56	-1.33	-1.14	-1.13	-1.61	**0.022**	0.178	0.305	-1.66	-1.66	-1.66	-1.29	-1.29	-1.29
6306	PGK1	-1.10	1.10	1.08	-1.18	1.19	-1.35	**0.025**	0.672	0.834	1.03	1.03	1.03	-1.11	-1.11	-1.11
8901	ALB	1.54	1.35	1.42	1.38	1.69	1.28	0.777	**0.024**	0.410	1.46	1.52		1.46	1.52	
7503	CSTF1	1.19	1.05	1.44	1.42	1.40	1.73	0.510	**0.033**	0.822			1.59			1.59
3704	HNRNPK	1.10	-1.08	-1.01	1.80	1.29	1.53	0.116	**0.008**	0.070	1.45			1.45		
3702	HSPD1	1.23	1.06	1.42	2.45	2.66	3.30	0.687	**0.003**	0.123			2.36			2.36
5403	KRT18	-1.16	-1.27	-2.05	-1.70	-1.02	-1.43	0.439	**0.032**	0.239			-1.74			-1.74
2601	KRT7	1.55	2.17	2.08	1.61	1.69	1.43	0.930	**0.018**	0.589		1.93			1.93	
3204	PDHB	1.16	1.18	1.51	1.26	1.29	1.38	0.439	**0.008**	0.649			1.44			1.44
7204	PKM	1.10	1.35	-1.37	-1.38	1.04	-1.62	0.257	**0.044**	0.662		1.20	-1.49		1.20	-1.49
8301	RBM4	1.77	1.44	1.91	1.23	1.44	1.73	0.053	**0.002**	0.413			1.82			1.82
1203	SEC13	-1.28	-1.04	1.32	1.02	1.27	1.16	0.080	**0.040**	0.140	-1.13		1.24	-1.13		1.24
5706	TCP1	1.46	-1.10	1.60	-1.15	-1.60	1.01	0.134	**0.034**	0.375		-1.35	1.30		-1.35	1.30
1602	TUBA1C	1.27	-1.72	2.46	-1.32	-2.51	-1.29	0.296	**0.019**	0.117		-2.11	1.59		-2.11	1.59
2902	*VCP	1.17	-1.13	1.44	1.06	-1.17	1.58	0.091	**0.005**	0.730			1.51			1.51
2904	*VCP	1.22	-1.35	1.17	-1.21	-1.53	1.20	0.083	**0.049**	0.491		-1.44	1.19		-1.44	1.19
107	YWHAE	1.64	1.12	-1.36	1.14	1.08	-1.38	0.206	**0.039**	0.728	1.39		-1.37	1.39		-1.37

§ Spot volume intensity normalized to the control (n = 3).
† Significant change in protein expression identified by multiple comparison based on Holm-Sidak method (see Materials and Methods), which was used for pathway analysis, and the blank entries imply non-significant changes as compared to the control (i.e., fold-change = 1.0). Those protein spots with *p*-value < 0.05 (two-way ANOVA) but did not pass Holm-Sidak test were excluded.
* Protein represented by multiple spots. The spot with the highest fold-change was used for bioinformatics.

Table III – S2. Primers used in RT-PCR to detect expression of genes in A549 cells.

Gene	Forward Primer	Reverse Primer	% Efficiency
ALDH1A1	TGTTAGCTGATGCCGACTTG	CTGGATGCGGCTATACAACA	98.32
ANXA5	CAAGTTGAACAAGATGCTCAGG	TCTTCATCTGTCCCCCATTT	95.57
ANXA7	ACAGATGCCTTCTCAGTATC	GCTGACTAGGGTAAGTAGGTT	97.84
ATM	CTATGGAAATTAAGGTGGAC	AATTTACACCTCCTGCTAAG	98.18
ACTB	GCACCCAGCACAATGAAGA	CGATCCACACGGAGTACTTG	93.19
BAX	AGCTCTGAGCAGATCATGAAGA	GATCCTGGATGAAACCCTGA	96.67
CASP1	GGGGTACAGCGTAGATGTGAA	TGCTGTCAGAGGTCTTGTGC	99.08
CASP3	GCTATTGTGAGGCGGTTGTAG	CAGGGCTCGCTAACTCCTC	95.70
CASP8	TCCAAATGCAAACTGGATGA	TCTCCCAGGATGACCCTCTT	96.83
CAT	GCCATTGCCACAGGAAAG	CCTTGTGAGGCCAAACCTT	97.09
CCL5	CCTCATTGCTACTGCCCTCT	GGTGTGGTGTCCGAGGAATA	98.67
CCNG1	GCACAGAAGTGTGTAGAGTTAACAGA	AGCTCTTGCCAGAAGGTCAG	92.12
CDKN1A	CCAGCTGAGGTGTGAGCA	TGACATGGCGCCTCCT	93.62
JUN	CCCCATCGACATGGAGTC	CTCTCCAGCTTCCTTTTTCG	97.81
CSF2	TCTCAGAAATGTTTGACCTCCA	GCCCTTGAGCTTGGTGAG	108.88
CSTF1	CGGTAGATTGGGCAGGATT	CTGGTCCGGTTCTCTTGGTA	106.13
CYP1A1	CCAGGCTCCAAGAGTCCAC	AAGCATGATCAGTGTAGGGATCT	106.29
CYP1B1	ACGTACCGGCCACTATCACT	CTCGAGTCTGCACATCAGGA	100.47
DDIT3	TGCTTTTCCAGACTGATCCA	GACAGTGTCCCGAAGGAGAA	95.15
DEK	CCGAGAAAGAACCCGAAAT	CCTTCCACGATGAGACTCTTTT	95.25
DNMT3A	GACCCTCCAAAGGTTTACCC	CCAAGTCCTTCAGCACCAG	96.94
DNMT3B	TCCTATCGAAAAGCCATGTACC	TGGTCCTCCAATGAGTCTCC	101.43
ECE1	ACAGATGCCTGCTCAACAACT	GCCCAGGTTGTTTTCTGTGT	92.13
EDNRA	GCGCTCTTAGTGTTGACAGGT	GAATCCCAATTCCCTGAACA	89.45
EGR1	GGCCCTCAATACCAGCTACC	AAGCGTAAGGGCGTTCGT	101.26
NOS3	CGGAGAATGGAGAGAGATGG	CTCACGTCTATAATCGCAGCA	97.79
EPHX1	ACTGGCGGAATGAATTTGAC	CACGTGGATGAAGTGGATGT	100.95
ERCC1	GAAACCAGCGGACCTCCT	CACGGTGGTCAGACATTCAG	97.53
ERCC3	TGTCCTCATTCAGATCTCATCC	TTGTACTCTTCTGCAACCATCC	92.11
EDN1	GCTCGTCCCTGATGGATAAA	CTCTTGGACCTAGGGCTTCC	92.14
EDN2	GTGCCACCTTCTGCCTTC	CACGTCTGCAGGGGACTT	91.43
EDN3	CAAAGAAGAGGAAGGGAAGGTT	GGGGGCAGGTAGATGGAG	100.98
FMO5	ATTAGCCAAACAGCCAAGCA	ACACGATTCAGGATCCAAGC	99.44
FSCN1	GCCAACGAGAGGAACGTG	GGCACACTTTTTGGTGTCG	98.14
GADD45A	GGAGAGCAGAAGACCGAAAG	AGTGATCGTGCGCTGACTC	100.08
GAPDH	AGCCACATCGCTCAGACAC	GCCCAATACGACCAAATCC	99.02
GPX1	CAACCAGTTTGGGCATCAG	GTTCACCTCGCACTTCTCG	98.77
GRSF1	TGGATGATGTCTTTCTCATTCG	CTCACCGTTGCGGATTCT	95.40
GSR	TGCCAGCTTAGGAATAACCAG	CCTGCACCAACAATGACG	96.34
GSTP1	CCCTCATCTACACCAACTAT	AGCGAAGGAGATCTGG	96.43
HMOX	AGGGTGATAGAAGAGGCCAAG	CTGGTCCTTGGTGTCATGG	99.19
HNRNPAB	CTACGACTACTCGCCCTAT	TACTACCCTGACTGTAGTCGT	96.61
HPRT1	AAGATGGTCAAGGTCGCAAG	CCAACAAAGTCTGGCTTATATCC	92.99
HSP90AB1	GCTTGGAATCCACGAAGACT	TCTCCAGACTGGGAGGTATGA	91.48
HSPA1A	CCGGCCTACTTCAACGACT	GATGATCCGCAGCACGTT	94.02
HSPA2	AGGTGATCAACTGGCTCGAC	CGAGCTCTTTCTGCTTGTGTT	99.42
HSPA5	GATATTGGAGGTGGGCAAAC	TAACAACTGCATGGGTAACCTTC	97.38
HSPA6	CCGCCTATTTCAATGACTCG	ATTGATGATCCGCAACACG	100.36
HSPA9	AGGTGGGGAAGACTTTGACC	TCCTTCACAATGTGCCGTAG	97.54
HSPB1	TCCCTGGATGTCAACCACTT	GATGTAGCCATGCTCGTCCT	96.02
HSPD1	CCTGCACTCTGTCCCTCACT	GGTAACCGAAGCATTTCTGC	94.88
HSPE1	ACAGTAGTCGCTGTTGGATCG	AGAACTACTTTGGTGCCTCCAT	95.81
HSPH1	AGCCATGTTGTTGACTAAGCTG	TCTGTAAAGAAGGAGGGGACTG	94.64
HTRA2	ATTGGGGTGATGATGCTGAC	AGCTTGGTTCTCGAAGCTGT	99.10

ICAM1	GTGCAATCATGGTTCACTGC	GGTGTGGTGTTGTGAGCCTA	96.20
IL1B	CAGCCAATCTTCATTGCTCA	AGTCATCCTCATTGCCACTGT	97.16
IL8	GAGCACTCCATAAGGCACAAA	ATGGTTCCTTCCGGTGGT	104.62
INA	GCGAGGAGACACGTTTTAGC	GTGGGAGCAGGTAACTTGGA	98.05
NOS2	CCAGTACGTTTGGCAATGG	CCAAACACAGCGTACCTGAA	98.79
KDM6B	GGCACCAACATCGACTTGT	GTGGATGTTACCCGCATGA	94.88
LTA	AACCTGCTGCTCACCTCATT	TGCTCAAGGAGAAACCATCC	93.31
MT1A	GGTTCCTGCAAGTGCAAAG	CCTGGGCACACTTGCTACA	97.83
MT2A	TGCACCTCCTGCAAGAAA	CAGCAGCTGCACTTGTCC	97.43
MYC	AATGTCAAGAGGCGAACACA	TCCGTTTTAGCTCGTTCCTC	95.19
NFAT5	GGCACAATGAACCAACTGC	GCTGGTCCAGAGGTTAAAAGC	92.84
NFKB1	ATGCTCAGGAGCAGAAGTCC	GTCCACATGGGCATCACC	99.29
OGG1	CTCCACTCCTGCCCTGTG	CAGTGTGCAGGACTTTGCTC	98.36
PDHB	CAGGTGACAGTTCGTGATGC	TCCAAGCAGAAATACCTTCTCAT	95.99
POR	ACAACCTGGATGAGGAGT	TGGTGATGTCCAGGTAGT	97.74
POU4F1	CTCCCTGAGCACAAGTACCC	GGCGAAGAGGTTGCTCTG	98.25
PRDX1	GGTTGAACCCCAAGCTGATA	CAGCTGTGGCTTTGAAGTTG	99.52
PRDX2	GCCTTCCAGTACACAGACGAG	GTTGGGCTTAATCGTGTCACT	95.79
PRDX6	CCCAACTTTGAGGCCAATAC	GTCTCCCAGAAAGTCGTGGA	96.15
PTGS1	TGCGCCTGGTACTCACAGT	CGAGTGTAATAGCTCACGTTGG	95.94
RPL32	GAAGTTCCTGGTCCACAACG	AGCGATCTCGGCACAGTAAG	96.49
SEC13	CATTATCTGGAGAGAGGAAAACG	AGCACACCGAGTTCACTGAG	94.07
SEMG1	AAATGACAAGGTCGGCTCAG	GATCCACCTTTTTGTCCCATC	94.49
SOD2	AATCAGGATCCACTGCAAGG	TAAGCGTGCTCCCACACAT	96.84
TCP1	TTTTGAAGCTGCAATGTTGG	TGCAGACGTACGAGCCTTAG	94.24
TIMP1	GCTTCTGGCATCCTGTTGTT	ACTTGGCCCTGATGACGA	91.78
TNFa	CAGTCAGATCATCTTCTCG	GCTTGAGGGTTTGCTAC	100.23
TNFSF10	TTCACAGTGCTCCTGCAGTC	GCCACTTTTGGAGTACTTGTCC	98.45
TP53	AGGCCTTGGAACTCAAGGAT	GGTAGACTGACCCTTTTTGGAC	100.66
TUBB4B	CTGCTGCTGTTTGTCTACTTCC	CTGCAAGTGCACGATTTCC	95.18
VHL	CATCCACAGCTACCGAGGTC	CCGTCAACATTGAGAGATGG	95.17
VIM	CAAAGACAGGCTTTAGCGAGTT	GACAAGAGCGCCCCTAAGTT	106.62
XRCC1	AAAGAAGACCCCCAGCAAAC	TGGAGCTGGCAATTTAGGTC	98.79
XRCC2	ACCCATCTCTCTGCCTTTTG	ATTGACGCGGTCTATCCAGT	95.92
YWHAZ	AGACAGCACGCTAATAATGCAA	AATGAGGCAGACAAAAGTTGG	99.49

Table III – S3. Two-way ANOVA results showing significant alteration of genes in A549 cells due to particle exposures (n = 3).
The number below Treatment main effect (Trt), Dose main effect (Dose) or interaction between Treatment and Dose (T x D) corresponds to the *p*-value, where the bolded number emphasized *p*-value < 0.05. The fold-change of gene indicated in blue (cut-off at ±1.10) was excluded from pathway analysis. CR = Cristobalite; MI = Min-U-Sil 5.

	§CR (μg/cm²)			§MI (μg/cm²)			Two-way ANOVA			†CR (μg/cm²)			†MI (μg/cm²)		
Gene	**60**	**140**	**200**	**60**	**140**	**200**	**Trt**	**Dose**	**T x D**	**60**	**140**	**200**	**60**	**140**	**200**
DDIT3	1.10	1.19	1.44	1.86	2.12	2.28	**0.000**	**0.000**	**0.014**				1.86	2.12	2.28
EDNRA	-1.00	-1.02	-1.00	-1.64	-1.93	-2.29	**0.000**	**0.004**	**0.005**				-1.64	-1.93	-2.29
EPHX1	1.18	-1.01	-1.08	-1.41	-1.84	-2.04	**0.000**	**0.010**	**0.035**	1.18			-1.41	-1.84	-2.04
EDN3	-1.07	-1.07	-1.36	-1.87	-3.20	-5.64	**0.000**	**0.000**	**0.005**				-1.87	-3.20	-5.64
FMO5	-1.20	-1.71	-1.95	-2.78	-5.36	-7.01	**0.000**	**0.000**	**0.003**		-1.71	-1.95	-2.78	-5.36	-7.01
ICAM1	1.11	1.54	2.58	2.32	3.26	6.50	**0.005**	**0.000**	**0.034**	1.11	1.54	2.58	2.32	3.26	6.50
IL1B	1.26	-1.34	-1.71	-1.41	-2.24	-1.26	**0.048**	**0.006**	**0.030**	1.26	-1.34	-1.71	-1.41	-2.24	
MT1A	1.11	-1.04	-1.09	-1.29	-1.60	-1.54	**0.000**	**0.005**	**0.046**	1.11			-1.29	-1.60	-1.54
MYC	1.11	1.30	1.26	1.47	1.60	1.64	**0.000**	**0.000**	**0.022**		1.30	1.26	1.47	1.60	1.64
TNF	-1.24	3.06	-1.60	4.80	8.55	15.40	**0.000**	**0.010**	**0.024**	-1.24		-1.60	4.80	8.55	15.40
HSPA2	1.02	1.05	1.05	-1.08	-1.13	-1.27	**0.001**	0.160	**0.016**		1.05			-1.13	-1.27
NFAT5	1.04	1.26	1.17	1.29	1.09	1.10	0.893	0.076	**0.040**				1.29		
ALDH1A1	-1.05	-1.11	-1.23	-1.38	-1.56	-1.90	**0.000**	**0.000**	0.098				-1.38	-1.56	-1.90
CAT	-1.05	-1.09	-1.15	-1.24	-1.42	-1.48	**0.004**	**0.003**	0.178					-1.42	-1.48
DNMT3B	1.01	1.00	-1.06	-1.10	-1.31	-1.41	**0.004**	**0.015**	0.106				-1.10	-1.31	-1.41
EGR1	-1.65	-2.70	-4.48	-2.71	-5.82	-8.46	**0.036**	**0.000**	0.257	-1.65	-2.70	-4.48	-2.71	-5.82	-8.46
HSPA6	1.45	1.76	2.32	1.86	2.74	4.51	**0.021**	**0.007**	0.260	1.45	1.76	2.32	1.86	2.74	4.51
IL8/CXCL8	1.24	1.46	2.30	2.23	3.09	4.96	**0.001**	**0.000**	0.062	1.24	1.46	2.30	2.23	3.09	4.96
PDHB	1.03	-1.03	-1.08	-1.19	-1.34	-1.50	**0.000**	**0.003**	0.061					-1.34	-1.50
PRDX2	-1.10	-1.21	-1.26	-1.39	-1.59	-1.60	**0.002**	**0.005**	0.582		-1.21	-1.26		-1.59	-1.60
SEMG1	1.43	1.62	2.96	2.00	2.91	8.05	**0.016**	**0.003**	0.766		1.62	2.96		2.91	8.05
TP53	1.18	1.00	-1.21	-1.39	-1.75	-1.90	**0.008**	**0.028**	0.161						-1.90
CCL5	-1.19	-1.04	1.27	2.00	2.83	3.20	**0.010**	0.068	0.187	1.01	1.01	1.01	2.68	2.68	2.68
CSF2	2.11	4.80	2.66	11.57	10.71	35.02	**0.049**	0.233	0.262	3.19	3.19	3.19	19.10	19.10	19.10
CYP1A1	1.08	1.02	1.13	-1.22	1.10	-1.19	**0.028**	0.734	0.204	1.08	1.08	1.08	-1.10	-1.10	-1.10
DNMT3A	-1.02	1.03	-1.10	-1.13	-1.29	-1.36	**0.040**	0.177	0.416	-1.03	-1.03	-1.03	-1.26	-1.26	-1.26
ECE1	-1.02	1.08	1.04	-1.17	-1.25	-1.34	**0.008**	0.571	0.208				-1.25	-1.25	-1.25
ERCC3	-1.06	1.01	-1.13	-1.13	-1.29	-1.25	**0.015**	0.090	0.246				-1.22	-1.22	-1.22
EDN1	1.04	1.06	-1.00	-1.07	-1.24	-1.25	**0.028**	0.352	0.237				-1.19	-1.19	-1.19
GADD45A	1.20	1.12	1.06	1.17	1.28	1.39	**0.021**	0.141	0.272				1.28	1.28	1.28
GSR	1.02	-1.01	-1.10	-1.09	-1.20	-1.34	**0.047**	0.052	0.494				-1.21	-1.21	-1.21
HSPA1A	1.17	1.29	1.16	1.50	1.42	1.53	**0.015**	0.107	0.586	1.21	1.21	1.21	1.48	1.48	1.48
OGG1	1.02	1.04	1.00	-1.07	-1.17	-1.23	**0.018**	0.375	0.290				-1.16	-1.16	-1.16
PRDX1	1.01	1.07	1.01	1.13	1.17	1.17	**0.028**	0.071	0.338				1.16	1.16	1.16
PTGS1	-1.22	-1.18	-1.16	-1.55	-1.80	-2.06	**0.030**	0.058	0.456				-1.80	-1.80	-1.80
CDKN1A	-1.26	-1.21	-1.35	-1.20	-1.33	-1.27	0.223	**0.026**	0.827			-1.31			-1.31
TNFSF10	-1.46	-2.00	-2.12	-1.39	-1.91	-2.02	0.850	**0.000**	0.990	-1.43	-1.96	-2.07	-1.43	-1.96	-2.07

§ Average fold-change of gene compared to the control (n = 3).
† Significant change in gene expression identified by Holm-Sidak multiple comparisons, which was used for pathway analysis. Those genes with *p*-value < 0.05 (based on Two-way ANOVA) but did not pass Holm-Sidak test were excluded.

Table III – S4. Pearson Correlations indicating the cytotoxic effects that significantly associated ($p < 0.05$) with the dose of exposure in A549 cells.
Correlation was conducted by correlating Log_2(fold-effect) from each cytotoxicity assay against the doses expressed in mass and surface area (SA) metrics, where R corresponds to the correlation coefficient and *p*-value < 0.05 indicates a significant correlation. Two-way ANOVA results were also included in this table to show the significant cytotoxicity caused by CR and MI exposures. The highlighted numbers in blue and red pointed out *p*-value less than 0.05 based on Pearson correlation and two-way ANOVA analyses.

				Pearson Correlation			
	Two-Way ANOVA (*p*-value)			**Mass (μg/cm^2)**		**SA (mm^2/cm^2)**	
Cytotoxicity Assay	**Trt**	**Dose**	**TxD**	**R**	***p*-value**	**R**	***p*-value**
LDH Release	0.138	**0.000**	0.236	0.663	**0.000**	0.716	**0.000**
BrdU Incorporation	0.683	**0.002**	0.915	-0.605	**0.000**	-0.584	**0.000**
Cellular ATP	0.906	**0.000**	0.652	-0.395	**0.025**	-0.324	0.070
Resazurin Reduction	0.472	0.506	0.944	0.170	0.352	0.089	0.626

Table III – S5. The protein spots that were significantly correlated between their expressions and exposure doses based on Pearson correlation.
Correlation was done by correlating Log_2(fold-change) of each protein spot against the doses expressed in mass and surface area (SA) metrics as shown in Table III – 1, where R corresponds to the correlation coefficient and *p*-value < 0.05 indicates a significant correlation. The SSP number corresponds to the identifier number that PDQuest used to identify the spot based on its coordinate in the gel. #N/A indicates the protein spots whose identity is not available. Two-way ANOVA result was also included in this table to show the protein spots that were differentially expressed in A549 cells due to CR and MI exposures. The highlighted numbers in blue and red pointed out *p*-value less than 0.05 based on Pearson correlation and two-way ANOVA analyses.

					Pearson Correlation			
		Two-Way ANOVA			Mass (µg/cm^2)		SA (mm^2/cm^2)	
SSP	**Protein**	**Trt**	**Dose**	**TxD**	**R**	***p*-value**	**R**	***p*-value**
3702	HSPD1	0.687	**0.003**	0.123	0.511	**0.011**	0.725	**0.000**
4002	HSPB1	0.629	0.055	0.493	-0.537	**0.007**	-0.616	**0.001**
6009	NT5C	0.059	0.118	0.138	-0.362	0.082	-0.613	**0.001**
1005	PNMA6A	**0.042**	0.086	**0.043**	0.314	0.135	0.603	**0.002**
3204	PDHB	0.439	**0.008**	0.649	0.654	**0.001**	0.597	**0.002**
7503	CSTF1	0.510	**0.033**	0.822	0.504	**0.012**	0.583	**0.003**
2805	HSPA9	0.360	0.158	0.313	0.361	0.083	0.574	**0.003**
5006	NDUFV2	0.528	0.142	0.510	0.456	**0.025**	0.573	**0.003**
1401	ACTB	0.642	0.100	0.830	0.510	**0.011**	0.573	**0.003**
2603	#N/A	0.709	0.247	0.302	0.443	**0.030**	0.561	**0.004**
9403	METTL18	0.568	0.106	0.394	0.424	**0.039**	0.559	**0.005**
802	HSPA5	0.986	0.246	0.324	0.371	0.075	0.556	**0.005**
1711	HSPA9	0.470	0.077	0.256	0.505	**0.012**	0.555	**0.005**
8301	RBM4	0.053	**0.002**	0.413	0.658	**0.000**	0.552	**0.005**
1502	#N/A	0.410	0.186	0.828	0.469	**0.021**	0.551	**0.005**
4101	PHB	0.829	0.238	0.080	0.275	0.194	0.547	**0.006**
1108	C1QTNF9B	0.225	0.066	0.540	0.405	**0.050**	0.544	**0.006**
1004	KRT81	0.446	0.228	0.414	0.346	0.097	0.543	**0.006**
6307	#N/A	0.303	0.219	0.564	0.406	**0.049**	0.536	**0.007**
3709	#N/A	0.634	0.095	0.870	0.450	**0.028**	0.536	**0.007**
1306	ACTB	0.787	0.204	0.693	0.362	0.082	0.534	**0.007**
5102	PSME3	0.102	0.052	0.602	-0.535	**0.007**	-0.532	**0.007**
3007	PHB	0.383	0.104	0.917	0.480	**0.017**	0.531	**0.008**
7202	MRPS22	0.444	0.181	0.145	0.333	0.112	0.527	**0.008**
5301	XXYLT1	0.633	0.200	0.446	0.460	**0.024**	0.527	**0.008**
7508	#N/A	0.521	0.416	0.623	0.375	0.071	0.525	**0.008**
3816	#N/A	0.617	0.284	0.302	0.307	0.144	0.525	**0.008**
2010	ARMCX1	0.156	0.127	**0.037**	-0.387	0.062	-0.519	**0.009**
7206	BCO2	0.498	0.543	0.507	0.351	0.092	0.516	**0.010**
3705	INA	0.530	**0.041**	0.988	0.514	**0.010**	0.516	**0.010**
1508	PSMC3	0.737	0.171	0.579	0.441	**0.031**	0.511	**0.011**
8203	AKR1B1	0.947	0.304	0.607	-0.324	0.122	-0.509	**0.011**
6702	BRCC3	0.921	0.109	0.554	-0.370	0.075	-0.509	**0.011**
1003	EIF1AX	0.282	0.145	0.077	0.272	0.198	0.508	**0.011**
4802	HSPA9	0.078	**0.045**	0.198	0.420	**0.041**	0.506	**0.012**
4505	#N/A	0.692	0.136	0.683	0.358	0.086	0.502	**0.012**
1203	SEC13	0.080	**0.040**	0.140	0.477	**0.019**	0.501	**0.013**
2702	HSPD1	0.473	0.709	0.233	0.242	0.255	0.494	**0.014**
1006	RBM8A	0.249	0.088	0.990	0.532	**0.007**	0.494	**0.014**
6302	PSMC5	0.237	0.235	0.766	0.389	0.060	0.489	**0.015**
8602	#N/A	0.951	0.172	0.065	-0.235	0.269	-0.485	**0.016**

7504	ALDH1A1	**0.023**	0.535	0.855	0.347	0.096	0.484	**0.017**
6005	PSMB3	0.423	0.097	0.134	-0.274	0.195	-0.483	**0.017**
6605	PKM	0.079	0.208	0.154	-0.294	0.163	-0.480	**0.018**
3001	#N/A	0.136	0.458	0.705	0.348	0.096	0.479	**0.018**
4207	#N/A	0.342	0.818	0.115	0.188	0.380	0.474	**0.019**
804	#N/A	0.065	0.221	0.638	0.433	**0.035**	0.473	**0.019**
7607	ALDH1A1	0.057	**0.047**	0.163	-0.391	0.059	-0.468	**0.021**
3802	HSPA1A	0.391	0.274	0.758	0.374	0.072	0.465	**0.022**
4303	MSN	0.511	0.177	0.466	-0.327	0.119	-0.460	**0.024**
7805	ANKLE2	0.441	0.287	0.153	-0.239	0.262	-0.459	**0.024**
4004	PRDX4	0.835	0.569	0.449	0.243	0.253	0.458	**0.024**
9805	#N/A	0.872	0.230	0.207	0.343	0.100	0.456	**0.025**
2303	ACTB	0.383	0.578	0.568	0.346	0.098	0.456	**0.025**
4406	#N/A	0.883	0.063	0.976	-0.461	**0.023**	-0.455	**0.026**
8606	PKM	0.645	0.107	0.372	-0.422	**0.040**	-0.454	**0.026**
6704	CSTF2	0.606	0.437	0.608	0.342	0.102	0.449	**0.028**
5705	PDIA3	0.234	0.166	0.465	0.515	**0.010**	0.448	**0.028**
6504	#N/A	0.269	0.083	0.153	-0.250	0.240	-0.448	**0.028**
6208	HTRA2	**0.026**	**0.040**	0.764	0.398	0.054	0.446	**0.029**
6703	#N/A	0.693	0.205	0.338	0.489	**0.015**	0.445	**0.030**
9502	DIS3L	0.781	0.146	0.103	-0.386	0.062	-0.443	**0.030**
6203	PKM	0.164	0.120	0.833	-0.350	0.094	-0.441	**0.031**
3701	HNRNPK	0.387	0.290	0.398	-0.411	**0.046**	-0.439	**0.032**
1503	PSMC4	0.331	0.195	0.513	0.402	0.052	0.435	**0.033**
8501	EEF2	0.058	0.078	0.643	0.273	0.197	0.435	**0.034**
6402	ACTB	0.588	0.055	0.832	0.389	0.060	0.432	**0.035**
8307	FAH	0.220	0.185	0.339	0.219	0.303	0.429	**0.037**
2704	HSPD1	0.542	0.135	0.577	0.460	**0.024**	0.427	**0.037**
9202	HNRNPDL	0.733	0.483	0.577	0.259	0.221	0.426	**0.038**
5107	#N/A	0.840	0.098	0.111	0.414	**0.044**	0.424	**0.039**
1804	HSPA5	0.723	0.217	0.326	0.339	0.105	0.422	**0.040**
6604	CCT2	0.449	0.205	0.445	0.333	0.112	0.420	**0.041**
3506	KRT8	0.161	0.144	0.233	-0.358	0.086	-0.419	**0.041**
2915	HSP90AA1	0.460	0.233	0.775	-0.331	0.114	-0.418	**0.042**
4702	PDIA3	0.278	0.297	0.285	-0.260	0.219	-0.417	**0.042**
8105	#N/A	0.504	0.456	0.101	-0.273	0.196	-0.412	**0.045**
7808	LMNA	0.564	0.755	0.301	-0.194	0.362	-0.411	**0.046**
3707	HNRNPK	0.237	0.106	0.416	-0.337	0.107	-0.409	**0.047**
8901	ALB	0.777	**0.024**	0.410	0.430	**0.036**	0.407	**0.048**
2005	ANXA1	0.307	0.102	0.932	-0.404	0.050	-0.405	**0.049**
2601	KRT7	0.930	**0.018**	0.589	0.570	**0.004**	0.401	0.052
3101	OFD1	0.369	0.057	0.859	-0.518	**0.010**	-0.379	0.068
5105	PSMB7	0.874	0.125	0.546	0.513	**0.010**	0.400	0.053
8801	#N/A	**0.019**	**0.038**	0.195	0.510	**0.011**	0.351	0.093
7106	#N/A	0.085	0.122	0.613	0.467	**0.021**	0.215	0.313
5403	KRT18	0.439	**0.032**	0.239	-0.466	**0.022**	-0.366	0.079
6401	TUBB4B	0.768	**0.036**	0.478	-0.464	**0.022**	-0.397	0.055
2405	#N/A	0.429	0.181	0.556	-0.455	**0.025**	-0.402	0.052
104	IPO4	0.506	0.082	0.765	0.446	**0.029**	0.348	0.096
7203	RGS1	0.731	0.102	0.410	0.435	**0.034**	0.236	0.268
1507	#N/A	0.592	0.151	0.771	-0.430	**0.036**	-0.325	0.121
7609	GART	0.831	0.134	0.874	0.427	**0.037**	0.341	0.103
7010	BAG2	0.339	0.239	0.460	0.422	**0.040**	0.205	0.336
3109	#N/A	0.764	0.243	0.822	-0.418	**0.042**	-0.307	0.145
5602	#N/A	0.310	0.134	0.099	0.406	**0.049**	0.306	0.146

Table III – S6. Pearson correlation conducted to identify significant responses of genes in A549 cell to the exposure dose regardless of the type of silica particle.
Correlation was done by correlating Log_2(fold-change) of each gene against the doses expressed in mass and surface area (SA) as shown in Table III – 1, where R corresponds to the correlation co-efficient and *p*-value < 0.05 indicates a significant correlation. Two-way ANOVA result was also included in this table to show the genes that were differentially expressed in A549 cells due to CR and MI exposures. The highlighted numbers in blue and red pointed out *p*-value less than 0.05 based on Pearson correlation and two-way ANOVA analyses.

	Two-Way ANOVA			Pearson Correlation			
				Mass (μg/cm^2)		SA (mm^2/cm^2)	
Gene	**Trt**	**Dose**	**TxD**	**R**	***p*-value**	**R**	***p*-value**
EGR1	**0.036**	**0.000**	0.257	-0.907	**0.000**	-0.953	**0.000**
FMO5	**0.000**	**0.000**	**0.003**	-0.714	**0.000**	-0.910	**0.000**
IL8/CXCL8	**0.001**	**0.000**	0.062	0.782	**0.000**	0.901	**0.000**
ICAM1	**0.005**	**0.000**	0.073	0.778	**0.000**	0.896	**0.000**
HSPA6	**0.021**	**0.007**	0.260	0.743	**0.000**	0.861	**0.000**
EDN3	**0.000**	**0.000**	**0.005**	-0.613	**0.001**	-0.858	**0.000**
ALDH1A1	**0.000**	**0.000**	0.098	-0.640	**0.001**	-0.839	**0.000**
MYC	**0.000**	**0.000**	**0.022**	0.702	**0.000**	0.832	**0.000**
CAT	**0.004**	**0.003**	0.178	-0.621	**0.001**	-0.795	**0.000**
TNFSF10	0.850	**0.000**	0.990	-0.865	**0.000**	-0.794	**0.000**
SEMG1	0.064	**0.020**	0.235	0.652	**0.001**	0.789	**0.000**
DDIT3	**0.000**	**0.000**	**0.014**	0.592	**0.002**	0.787	**0.000**
PDHB	**0.000**	**0.003**	0.061	-0.561	**0.004**	-0.786	**0.000**
EPHX1	**0.000**	**0.010**	**0.035**	-0.520	**0.009**	-0.757	**0.000**
TP53	**0.008**	**0.028**	0.161	-0.565	**0.004**	-0.746	**0.000**
DNMT3B	**0.004**	**0.015**	0.106	-0.535	**0.007**	-0.741	**0.000**
CSF2	**0.049**	0.233	0.262	0.540	**0.006**	0.734	**0.000**
EDNRA	**0.000**	**0.004**	**0.005**	-0.459	**0.024**	-0.732	**0.000**
MT1A	**0.000**	**0.005**	**0.046**	-0.501	**0.013**	-0.717	**0.000**
PRDX2	**0.002**	**0.005**	0.582	-0.541	**0.006**	-0.708	**0.000**
CCL5	**0.010**	0.068	0.187	0.507	**0.011**	0.685	**0.000**
GSR	**0.047**	0.052	0.494	-0.536	**0.007**	-0.683	**0.000**
EDN2	0.088	0.067	0.496	0.571	**0.004**	0.652	**0.001**
PTGS1	**0.030**	0.058	0.456	-0.475	**0.019**	-0.635	**0.001**
INA	0.155	**0.033**	0.828	0.565	**0.004**	0.627	**0.001**
TNF	**0.015**	0.124	0.122	0.387	0.062	0.624	**0.001**
VHL	0.069	0.065	0.801	-0.525	**0.008**	-0.613	**0.001**
CCNG1	0.415	0.064	0.646	-0.551	**0.005**	-0.612	**0.001**
PRDX6	0.080	0.106	0.512	-0.494	**0.014**	-0.609	**0.002**
ERCC3	**0.015**	0.090	0.246	-0.444	**0.030**	-0.608	**0.002**
HSPA2	**0.001**	0.160	**0.016**	-0.328	0.118	-0.605	**0.002**
DNMT3A	**0.040**	0.177	0.416	-0.431	**0.036**	-0.599	**0.002**
YWHAZ	0.198	0.063	0.574	0.510	**0.011**	0.582	**0.003**
CDKN1A	0.223	**0.026**	0.827	-0.545	**0.006**	-0.581	**0.003**
PRDX1	**0.028**	0.071	0.338	0.412	**0.046**	0.575	**0.003**
GADD45A	**0.021**	0.141	0.272	0.376	0.070	0.567	**0.004**
OGG1	**0.018**	0.375	0.290	-0.349	0.094	-0.560	**0.004**
NOS3	0.230	0.238	0.765	0.488	**0.015**	0.558	**0.005**
JMJD	**0.001**	0.107	0.837	0.402	0.052	0.556	**0.005**
IL1B	0.050	**0.037**	0.100	-0.498	**0.013**	-0.551	**0.005**
EDN1	**0.028**	0.352	0.237	-0.351	0.093	-0.550	**0.005**
HSPA1A	**0.015**	0.107	0.586	0.378	0.068	0.532	**0.007**
SOD2	0.079	0.097	0.730	0.420	**0.041**	0.531	**0.008**
HSPA5	0.586	0.102	0.964	0.530	**0.008**	0.501	**0.013**
GAPDH	0.208	0.277	0.744	-0.412	**0.045**	-0.485	**0.016**
CYP1B1	0.083	0.498	0.199	-0.294	0.164	-0.471	**0.020**
ECE1	**0.008**	0.571	0.208	-0.212	0.319	-0.463	**0.023**
FSCN1	0.711	0.087	0.818	0.527	**0.008**	0.448	**0.028**
CASP1	0.707	**0.016**	0.202	-0.560	**0.004**	-0.446	**0.029**
XRCC2	0.406	0.336	0.750	0.404	0.050	0.434	**0.034**
NOS2	0.240	0.244	0.465	0.372	0.073	0.434	**0.034**
POR	0.805	0.184	0.868	0.458	**0.024**	0.431	**0.035**

Chapter IV. Examining the biological responses of A549 human lung epithelial cells to fractional components of urban air PM using *in vitro* toxicoproteomics.

This manuscript was published in Particle & Fibre Toxicology

Vuong NQ, Breznan D, Goegan P, O'Brien JS, Williams A, Karthikeyan S, Kumarathasan P and Renaud Vincent. Examining the biological responses of A549 human lung epithelial cells to fractional components of urban air PM using in vitro toxicoproteomics. Part Fibre Toxicol. 2017 Oct 2;14(1):39.

Received: 10 February 2017
Received in revised form: 19 June 2017
Accepted: 17 September 2017
Published: 02 October 2017

Ngoc Vuong wrote the entire manuscript, analyzed all the results (including cytotoxicity assays, 2D-GE, MALDI-TOF-MS, bioinformatics and pathway analyses), and performed all the experimental work (2D-GE and MALDI-TOF-MS) to determine the identities of all the protein spots in 2D gels.

Abstract

Background: Toxicity of airborne particulate matter (PM) is difficult to assess because PM composition is complex and variable due to source contribution and atmospheric transformation. In this study, we used an in vitro toxicoproteomic approach to identify the toxicity mechanisms associated with different subfractions of Ottawa urban dust (EHC-93).

Methods: A549 human lung epithelial cells were exposed to 0, 60, 140 and 200 μg/cm^2 doses of EHC-93 (total), its insoluble and soluble fractions for 24 hrs. Multiple cytotoxicity assays and proteomic analyses were used to assess particle toxicity in the exposed cells.

Results: The cytotoxicity data based on cellular ATP, BrdU incorporation and LDH leakage indicated that the insoluble, but not the soluble, fraction is responsible for the toxicity of EHC-93 in A549 cells. Two-dimensional gel electrophoresis results revealed that the expressions of 206 protein spots were significantly altered after particle exposures, where 154 were identified by MALDI-TOF-TOF-MS/MS. The results from cytotoxicity assays and proteomic analyses converged to a similar finding that the effects of the total and insoluble fraction may be alike, but their effects were distinguishable, and their effects were significantly different from the soluble fraction. Furthermore, the toxic potency of EHC-93 total is not equal to the sum of its insoluble and soluble fractions, implying inter-component interactions between insoluble and soluble materials resulting in synergistic or antagonistic cytotoxic effects. Pathway analysis based on the low toxicity dose (60 μg/cm^2) indicated that the two subfractions can alter the expression of those proteins involved in pathways including cell death, cell proliferation and inflammatory response in a distinguishable manner. For example, the insoluble and soluble fractions differentially affected the secretion of pro-inflammatory cytokines such as MCP-1 and IL-8 and distinctly altered the expression

of those proteins (e.g., TREM1, PDIA3 and ENO1) involved in an inflammatory response pathway in A549 cells.

Conclusion: This study demonstrated the impact of different fractions of urban air particles constituted of various chemical species on different mechanistic pathways and thus on cytotoxicity effects. *In vitro* toxicoproteomics can be a valuable tool in mapping these differences in air pollutant exposure-related toxicity mechanisms.

IV.1. Introduction

Airborne particulate matter (PM) is a complex mixture of particles with a wide range of sizes and physicochemical properties. Inhalation of airborne PM is linked to the development or exacerbation of respiratory illnesses such as bronchitis (Liu et al., 2014; Scott, 1953; Stocks, 1959), asthma (Canova et al., 2012; MacIntyre et al., 2014; Su et al., 2013) and lung cancer (Merlo et al., 1991; Pope, III et al., 2011; Siemiatycki et al., 1989); and it is also associated with decline in cognitive function (Ailshire and Crimmins, 2014; Jedrychowski et al., 2014; Julvez et al., 2007; Tonne et al., 2014) and increased risk of developing diabetes mellitus (Brook et al., 2013; Rao et al., 2015; Vora et al., 2014) and cardiovascular disease (Gan et al., 2013; Huang et al., 2012; Pope, III et al., 2009; Schneider et al., 2010; Vincent et al., 2001). A number of epidemiological studies have reported that there is an association between particle composition and health impacts of ambient air particles (Bell et al., 2014; Burnett et al., 2000; Peng et al., 2005; Zanobetti et al., 2009). However, composition of the respirable particles can vary in different geographical locations depending on the local sources of release (Burnett et al., 2000). Thus, identifying the drivers of toxic potency and determining their mechanism of effects in airborne PM should be important and useful in the development of regulatory measures to reduce the negative health effects of air pollution.

There are several approaches to the identification of toxic components of ambient air PM. Some studies examined or regressed the toxic effect of the total particles to its water-soluble and/or insoluble components (Huang et al., 2014; Snow et al., 2014; Verma et al., 2012; Yi et al., 2014), whereas others investigated the effects of particles with defined aerodynamic size range (e.g., <10 μm (PM10), <2.5 μm (PM2.5) and/or <0.1 μm ultrafine

particles) *in vitro* or *in vivo* (Amatullah et al., 2012; Guan et al., 2016; Thomson et al., 2015). The limitation to most studies assessing the toxicity of PM is the ability to collect sufficient materials for physical and chemical characterization of the particles, and for *in vitro* and *in vivo* toxicological investigations. Thus, it is rare to find a single report that could provide all the important details regarding the physicochemical properties, relative cytotoxicities and mechanisms of particle toxicity of the total PM and its constituent components or sub-fractions.

In 1993, a large quantity of ambient air particles from the Environmental Health Centre in Ottawa (EHC-93) was collected to serve the purpose of a reference outdoor urban dust sample to use in different toxicological studies (Vincent et al., 1997b; Vincent et al., 1997a). Since then, EHC-93 has been used extensively in numerous *in vivo* and *in vitro* studies. EHC-93 has been partially characterized for the presence of various particle components such as endotoxin, polycyclic aromatic hydrocarbons and metal contents in its total particles (Breznan et al., 2016; Vincent et al., 1997b). The potency of EHC-93 in causing oxidative/nitrative stress, inflammation and cardiovascular stress in animals has been well documented (Adamson et al., 1999; Bouthillier et al., 1998; Kumarathasan et al., 2015; Thomson et al., 2005; Vincent et al., 1997a; Vincent et al., 2001). EHC-93 was also reported to alter the expression of several genes and cytokines in animals and cells in the respiratory tract (Breznan et al., 2016; Chauhan et al., 2005; Fujii et al., 2001; Sakamoto et al., 2007; Thomson et al., 2005; Thomson et al., 2013). However, a detailed proteomic investigation to assess the molecular mechanisms delineating the toxic effects of EHC-93 as a whole (total) or separated fractions (i.e., insoluble and soluble) has not been conducted. In our recent studies, we demonstrated that *in vitro* toxicoproteomics is an approach that is capable of distinguishing the pathways associated with cytotoxic effects of respirable particles that are

different in physicochemical properties such as carbon black and titanium dioxide (Vuong et al., 2016c; Vuong et al., 2016b). Furthermore, we also showed that our *in vitro* toxicoproteomic approach was capable of differentiating the effects of particles that were identical in chemical formula (SiO_2) but differed in physical properties such as cristobalite and α-quartz (Vuong et al., 2016a). In this study, we used in vitro toxicoproteomics to dissect the effects of insoluble and soluble components of EHC-93 on A549 human lung epithelial cells. The results from this study showed that cytotoxicity assays, cytokine assays and proteomic analyses (based on two-dimensional gel electrophoresis and mass spectrometry) can differentiate the subtle differences in toxicity between EHC-93 total and its insoluble fraction as well as the drastic difference in toxicity between the soluble fraction and the total or insoluble fraction in A549 cells. To our knowledge, this is the first study that is able to provide extensive details on the physicochemical characteristics of an urban air PM and its sub-fractions, followed by comparing their cytotoxic potencies with multiple assays and comparing their associated cellular mechanisms of effects with proteomic analyses.

IV.2. Materials and methods

IV.2.1 Materials.

Culture flasks (T-25 and T-75), 96-well plates and plastic cell scraper were obtained from Corning Inc. (Corning, NY, USA). Dulbecco's Modified Eagle's Medium (DMEM) and fetal bovine serum (FBS) were purchased from Hyclone (Logan, UT, USA). Gentamicin, trifluoroacetic acid, α-cyano-4-hydroxy-cinnamic acid, Tris-HCl, NaCl, Tween-20 and Tween-80 were obtained from Sigma-Aldrich (Oakville, ON, Canada). Iodoacetamide, bis-acrylamide, ammonium persulfate, glycerol, immobilized pH gradient strips, Criterion

Cassette (13.3 x 8.7 cm W x L), Tris/Glycine/SDS buffer, and Bio-Safe Coomassie Blue were purchased from Bio-Rad (Mississauga, ON, Canada). Trypsin, resazurin reduction (CellTiter-Blue®) and lactate dehydrogenase (LDH) cytotoxicity assay kits (CytoTox-96®) were from Promega Corporation (Madison, WI, USA), ATP assay kit (ViaLight™ Plus) was from Lonza Corporation (Rockland, ME, USA), and 5-bromo-2′-deoxyuridine (BrdU) cell proliferation ELISA (chemiluminescent) assay kit was obtained from Roche Diagnostics (Laval, QC, Canada). All materials were analyzed for endotoxin using the chromogenic Limulus amebocyte lysate assay (Lonza, Walkersville, MD, USA). All water used was deionized/demineralized (>16 MOhms resistivity). Water bath Branson 1510 sonicator was from Bransonic (Danbury, CT, USA), which provides an output of 70 watts and 42 kHz was used for all particle preparations and protein extraction purposes.

IV.2.2. Particle preparation.

The urban dust EHC-93 was collected from baghouse air filters from the Environmental Health Centre in Ottawa, Ontario, Canada in 1993 and its preparation for toxicological studies have been described previously (Vincent et al., 1997b). The water-soluble and water-insoluble fractions of EHC-93 were prepared as follows; a sample of EHC-93 was removed from a – 80 ºC freezer and was warmed up to room temperature, 1 gram of EHC-93 was placed in a clean 15 mL Falcon tube, re-suspended in 5 mL of sterile water and sonicated in a pre-chilled water bath for 20 minutes. The tube was then centrifuged (500xg, 10 min), and the aqueous supernatant was collected into another clean 15 mL Falcon tube. The pellet (insoluble) was resuspended in 5 mL of water, and this process was carried out three times to collect a total volume of 15 mL of aqueous supernatant. The pooled supernatant was further centrifuged (900xg, 3.5 hr), the supernatant was collected and the

remaining pellet was pooled with the insoluble materials. The aqueous supernatant was then filtered through a 0.2 μm nylon syringe-tip filter into a clean 50 mL Falcon tube. This filter was then washed with 5 mL of methanol and pooled with the aqueous suspension. The pooled aqueous suspension and the pooled pellet were then lyophylized and stored frozen at – 80 ºC. The final mass percentage recoveries of the particle fractions were 17 % water-soluble (soluble) and 83 % water-insoluble (insoluble).

To prepare the particles for dosing, the dried particulate materials from the total, insoluble and soluble fractions each were resuspended in particle preparation buffer (NaCl: 1.9 mg/mL or 32.5 mM; Tween-80: 25.0 μg/mL or 19.1 μM) in a Dounce glass-glass microhomogenizer. The final concentrations of the total, insoluble and soluble fractions were prepared according to their mass percentages (i.e., 10.0, 8.3 and 1.7 mg/mL, respectively). In this manner, the cytotoxicities of the insoluble and soluble fractions in relative to the total can be directly assessed. The suspensions were sonicated on ice for 20 minutes and then dispersed as much as possible by 25 strokes of the homogenizer piston. Particle suspensions were then aliquotted into sterile, O-ring seal microcentrifuge tubes, heated to 56 ºC in a water bath for 30 minutes, and were subsequently frozen at – 80 ºC until use. All materials were analyzed for endotoxin using the chromogenic Limulus amebocyte lysate assay (Lonza, Walkersville, MD, USA).

IV.2.3. Scanning electron microscopy (SEM).

The size and morphology of EHC-93 was characterized by SEM. Images were collected on a JSM-7500F FESEM (JEOL) instrument equipped with a Field Emission Gun (FEG) under the following parameters: beam acceleration voltage, 2 KV; working distance, between 7 and 9 mm; imaging mode, Lower Secondary Electron Image (LEI). Magnification

and sizing bar are as indicated in the figure captions for each individual image. Samples were prepared by dropping a small amount of powder onto an aluminum stage painted with carbon paint (Electron Microscope Sciences, (EMS)). The paint was allowed to dry for 20 min, and the excess powder was then removed by blowing the surface with compressed, dry air.

IV.2.4. Energy dispersive X-ray spectroscopy (EDX).

EDX spectra were collected using a JSM-7500F FESEM (JEOL) instrument with the following parameters: beam acceleration voltage, 20 KV; acceleration current, 10 mA; working distance, between 8 and 9 mm. Since this instrument is attached to the SEM purchased from JSM, sample analysis was run concomitantly with SEM imaging, and thus, sample preparation for the collection of EDX spectra is identical to that for SEM. It should be noted that the carbon content in the sample cannot be determined because the stage is coated with carbon paint. The weight percent and atomic percent results were produced automatically from the instrument software analysis package.

IV.2.5. Inductively coupled plasma–mass spectrometry (ICP-MS).

Elemental analysis on EHC-93 total and its insoluble and soluble fraction were analyzed by ICP-MS in a previous report (Vincent et al., 2001). The results that are pertinent to this manuscript were summarized in Table IV – S1.

IV.2.6. Powder X-ray diffraction (pXRD).

The powder X-ray diffraction plot was obtained with a Rigaku Ultima IV instrument, equipped with a Cu tube. The powder sample was pressed by hand into a custom sample holder, such that a flat powder sample with a specified surface height would be presented to the X-ray beam. The pXRD plot was then collected in the 2 to 70 2theta degree range in

continuous-scan mode, with a sample width of 0.02 degrees, and a scan speed of 0.25 deg/min. Percent distribution was measured following identification and integration of the peak areas for each crystal phase observed in the spectrum.

IV.2.7. Cell culture and particle exposure.

The A549 cell line (American Type Culture Collection - CCL-185; human, epithelial, lung carcinoma) was subcultured in DMEM supplemented with 50 μg/mL gentamicin and 10 % FBS. It should be noted that final FBS concentration the cells are exposed to is 5 % after dosing with particles (particle preparations that were used to dose the cells were in serum-free media, then they were added to the 10 % FBS culture media that contained the cells). The cells were maintained and subcultured in T-75 flasks in a humidified atmosphere containing 5 % CO_2 and 95 % air at 37 ºC. For exposure experiments, the cells were seeded at $1.5x10^6$ cells/T-25 flask (for proteomics) or $2.0x10^4$ cells/well in 96-well plate (for cytotoxicity assays), incubated for 24 hours, resulting in approximately 75 % confluence prior to dosing with particles. The final volume of culture medium was 5 mL (T-25), 15 mL (T-75) or 200 μL/well (96-well plate). Solutions of particles were prepared from frozen stocks, which were thawed to room temperature, sonicated on ice (20 min), then diluted in the culture medium to generate dosing concentrations that are equivalent to 0, 60, 140 and 200 μg/cm^2 of the total (i.e., 0, 50, 116 and 166 μg/cm^2 for the insoluble fraction and 0, 10, 24 and 34 μg/cm^2 for the soluble fraction). The exposures were performed in this proportional manner so that the contributions of the insoluble and soluble components in EHC-93 total can be directly compared. However, the concentrations for both insoluble and soluble fractions were expressed in equivalent concentrations to the total in all the tables and figures in this study in order to assess the relative impacts of the two fractions. The cells

were exposed to the particles by replacing the existing culture medium with the particle-containing medium, and the flasks/plates were returned to the incubator for a 24 hour exposure to the particles. To harvest the exposed cells, the medium in each flask was removed and the cells were detached from the flasks using a plastic scraper. The cell suspension was collected in cell culture medium and centrifuged at 350 x g for 5 min, and the supernatant was discarded. The cell pellet was then washed twice with phosphate buffer saline (PBS). The final cell pellet was aspirated dry and stored at – 80 ºC until further use for proteomic analysis. This experiment was conducted in triplicate (n = 3) for all treatments.

IV.2.8. Integrated cytotoxicity assays.

The integrated cytotoxicity bioassays which combined endpoints of cell viability (resazurin reduction assay), cellular membrane integrity (intracellular LDH release), and energy metabolism (ATP assay) were conducted in a single 96-well plate as described in a previous study (Kumarathasan et al., 2014). The assays were carried out in the following sequence; after 24 hours of exposure to particles, 100 µL of cell culture supernatant was transferred in a clear 96-well plate and clarified at 300 x g for 5 min (room temperature); 25 µL was used for LDH assay, 75 µL was frozen for other assays such as cytokine assays. Then, 50 µL of resazurin reduction reagent, prepared in culture medium (40 % v/v), was added to the remaining 100 µL of culture medium and the cells were incubated (5 % CO_2, 37 ºC) for 2 hours. Aliquots (20 µL) were taken for measurement of resazurin reduction at 10 min and 120 min as described below. The cell culture supernatant was discarded by aspiration and the cells were lysed with 200 µL of lysis buffer (100 mM $MgCl_2$ and 0.025 % Triton X-100 in PBS) at room temperature, for 10 min. The lysate was recovered in clean plates and clarified by centrifugation as above; 25 µL of lysate was used for LDH

measurement, 50 µL was used for ATP measurement, and 100 µL was frozen for additional analyses. The cell proliferation (BrdU incorporation) assay was performed in a separate 96-well plate. For all assays, supernatants and cell lysates were clarified by centrifugation to prevent interference of particles in the assays. All cytotoxicity assays were conducted in quadruplicate (n = 4) for all treatments.

In the resazurin reduction assay, viable cells reduce a non-fluorescent redox dye resazurin (dark blue in color) to a fluorescent reaction product resorufin (pink in color), and nonviable cells lose metabolic capacity to convert the indicator dye. Mitochondrial, cytosolic and microsomal enzymes have been implicated in the reduction of resazurin (Gonzalez and Tarloff, 2001). For measurement of resazurin reduction, 20 µL of supernatant aliquots at 10 and 20 min were transferred into clean plates containing 80 µL of serum-free medium per well, shaken at 350 rpm for 30 sec on a circular plate shaker, and clarified by centrifugation at 300 x g for 5 min. Fluorescence of the diluted supernatants was measured by top reading at λ_{Ex} = 540 and λ_{Em} = 600 nm (Synergy 2, BioTek, Winooski, VT, USA). Resazurin reduction is calculated by fluorescence at 120 min minus fluorescence at 10 min.

The CytoTox 96® colorimetric assay quantitates the activity of cytosolic LDH released extracellularly during cell membrane damage (an indicator of cell death). The enzymatic activity released in the cell culture supernatants and recovered in the lysis buffer was measured with a coupled enzymatic reaction. LDH catalyzes the oxidation of lactate to pyruvate that is accompanied with the reduction of NAD+ to NADH, which in turn is consumed simultaneously in a diaphorase-catalysed reduction of tetrazolium salt, generating a soluble red formazan that can be detected by absorbance at 490 nm. For the assay of released LDH, 25 µL of the cell supernatants were combined with 25 µL of cell culture medium and 50 µL of LDH substrate from the assay kit. Absorbance at 490 nm (Synergy 2)

was measured after 20 and 40 min of incubation in the dark. For the assay of cellular LDH, 25 µL aliquots of the cell lysates was combined with 25 µL of lysis buffer and 50 µL of substrate from the LDH assay kit. Absorbance at 490 nm was measured immediately and after 10 min of incubation in dark. The relative cellular LDH was calculated as a fraction of total LDH, that is LDH activity in cell lysate was divided by total LDH activity recovered in supernatant and cell lysate.

The ViaLight Plus is a bioluminescent assay for measurement of cellular ATP. Cell injury leading to mitochondrial perturbation results in a decrease of cellular ATP. In the presence of ATP and oxygen, the luciferase enzyme oxidises luciferin to oxyluciferin that accompany with photons emission. Chemiluminescence in the assay is proportional to the concentration of ATP in the cell lysate. The ATP working reagent was prepared 15 min prior to conducting the assay by mixing ATP monitoring reagent and the assay buffer provided in the kit, where 50 µL of the cell lysate was added to 100 µL of freshly prepared ATP reagent in a white-walled 96 well plate. Luminescence was measured (Synergy 2, Biotek) following 2 min incubation in the dark.

The BrdU Cell Proliferation ELISA is an enzyme immunoassay based on the incorporation of the thymidine analog BrdU during DNA synthesis in proliferating cells. Cells were grown in black-walled 96-well plates and exposed to particles for 24 hours as described above. The BrdU labelling medium (10 µM BrdU) was added to each well, followed by a 4 hour incubation (5 % CO_2, 37 ºC). The medium was discarded and the plates were dried at 60 ºC for 1 hour, and stored at -40 ºC until use. The cell monolayers were fixed with 200 µL of the fixation-denaturation reagent for 30 min and then incubated with anti-BrdU antibody for 2 hours at room temperature. The wells were washed three times with 150 µL of PBS containing 0.01 % Tween-80, and the substrate provided in the BrdU ELISA kit

was added. The plates were covered with black tape and were shaken for 4 min. Chemiluminescence was measured (Synergy 2) with 1 sec integrated readings per well.

IV.2.9. ELISA-based secretory cytokine assays.

Levels of cytokines from the supernatant were measured by a Millipore MAP 8-plex human cytokine panel (EMD Millipore, Billerica, MA). The simultaneous quantification of cytokine levels was carried out using the Bio-Rad Bioplex 200 array reader (Bio-Rad Laboratories, Mississauga, ON), according to Millipore recommended procedure, where a panel of 11 cytokines were assessed (GM-CSF, IL-1β, IL-1RA, IL-6, IL-8, IL-9, IL-10, IL-12p70, MCP-1, TNFα and VEGF). Briefly, cell supernatants were thawed on ice and centrifuged at 956 x g for 5 min, at 4 °C. Next, 25 µl of samples were incubated with 25 µl of microbeads labeled with antibodies to the specific cytokines in a 96-well flat-bottom plate overnight at 4 °C. After the incubation the samples were washed twice using Bio-Rad Bioplex Pro II wash system, followed by incubation with the 25 µl of detection antibody cocktail for 1 hr at room temperature (RT). The beads were then incubated with 25 µl of streptavidin-phycoerythrin for 30 min at RT, washed twice, and suspended in 150 µl of sheath fluid. The data were analyzed using the Bio-Rad Bio-Plex ManagerTM version 6.0 software, with 5PL curve fit and background fluorescence subtraction. The analysis was conducted in pooled samples of 3 wells per sample within each experiment, in quadruplicate experiments (n = 4). Cytokine levels in cell supernatants were determined from cytokine standard curves included on each plate. Only those cytokines that were detected at a concentration >5 pg/ml in all data points would be used to filter out noises in the data. The final levels of cytokines for each treatment was adjusted to the viability of cells based on cellular LDH, BrdU incorporation and cellular ATP assays as previously described (Breznan

et al., 2016). Data were expressed as normalized fold-change (FC) in relative to the control (0 μg/cm^2).

IV.2.10. Protein extraction and two-dimensional gel electrophoresis (2D-GE).

Total protein from the A549 cells (control & particle-exposed) was extracted and subjected to 2D-GE as previously described (Vuong et al., 2016b; Vuong et al., 2016c). Following electrophoresis, the gel was washed for 30 min in water, stained in BioSafeCoomassie Blue (Bio-Rad) overnight (16 – 20 hours), destained twice in water (20 minutes), and then imaged with a standard scanner. To overcome the typical warping and distortion issues from gel to gel especially near the extremities of the pH range and the molecular weight, a common area across all experimental gels that clearly shows the protein spots was selected to assess the proteome differences among the treatments, where proteins in the window of pH 5.1 – 7.8 and 100 – 20 kDa were analyzed (Vuong et al., 2016b; Vuong et al., 2016c). A total of 543 well-resolved protein spots in this common area were compared across all experimental gels, and the identities of 333 of these protein spots were determined using MALDI-TOF-TOF-MS (Vuong et al., 2016b; Vuong et al., 2016c). The protein spots within the gels were matched and quantified with PDQuestTM Advance V8.0.1 (Bio-Rad), where spot volume was quantified using the available "Local regression model (LOESS)" algorithm in PDQuest. The reported spot volume for each protein was used to compare its level of expression across the treatments. In order to calculate the fold change for a protein spot from a treatment group, the treatment/control ratio (n = 3) was first determined. If the treatment/control ratio is between 0 and 1.0, a decreased expression (e.g., 0.5), then the fold-change is calculated by dividing "– 1.0" by the treatment/control ratio (e.g., – 1.0 / 0.5 = – 2.0). If the treatment/control ratio is >1.0, corresponding to increased expression (e.g., 1.5),

then this serves as the fold-change by itself (https://www.qiagen.com/). Such fold-change values are used for bioinformatic analyses (e.g. IPA) as reported in Table IV – S2 and Figures IV – 4, 5, 6 and 7. It should be noted that there is no value between "– 1.0 and 1.0" when the fold-changes are expressed in this manner. For hierarchical cluster analysis, however, fold-changes were calculated based on Log_2(treatment/control) so that the data is continuous (i.e., there is no gap between – 1.0 and 1.0) for the appropriate analysis.

IV.2.11. Statistics.

Hierarchical cluster analysis was conducted using GenePattern (Reich et al., 2006), and the resulting heatmap was generated with Java TreeView (http://www.princeton.edu/~abarysh/treeview/). Two-way analysis of variance (ANOVA) was performed on 2D-GE (n = 3), cytotoxicity assays (n = 4) and cytokine releases (n = 4) data with treatment and dose as factors, using R (R Core Team, 2013). When the assumptions of equal variance or normality were not met, the data were rank transformed. Holm-Sidak was the post-hoc method used for all pairwise comparison procedures, which is a step-down procedure on a sorted set of null hypotheses. The reported p-values have been adjusted for the familywise error rate (FWER) which is the probability of making at least one type I error (incorrect rejection of a true null hypothesis) in the set or family of null hypotheses. A protein was considered as having a significant effect if the Holm-Sidak adjusted *p*-value was less than 0.05. If the Treatment x Dose interaction was significant for a protein spot, its change in expression for a given treatment and dose that was found significant by Holm-Sidak analysis was reported as it is, as presented in Table IV – S2. The same applied for those proteins that were found to have significant Treatment and Dose main effects. If a protein was found to have significant Treatment main effect, fold changes were

estimated using least square mean (Goodnight JH and Harvey WR, 1978; Searle SR et al., 1980). In the case where the Dose main effect was significant, the average FC estimate was reported for each significant dose group.

IV.2.12. Bioinformatics.

It should be noted that multiple protein spots with the same protein ID may have a p-value < 0.05, which suggests different isoforms of the same protein were significantly altered (Table IV – S2). When this was the case, selection for pathway analysis was based on the following order: best matching MW, largest spot volume, highest MOWSE score (molecular weight search) and then greatest FC. Furthermore, protein spots that were deemed as small peptides/fragments (based on MW and unique peptide sequences) of their native proteins were excluded from pathway analysis, unless functional data can be found for such peptides based on UniProt (www.uniprot.org) and PubMed (http://www.ncbi.nlm.nih.gov/pubmed) searches. It should be mentioned that a few cleaved protein products were included in pathway analysis in this study because they are known to serve functional purposes. For example, the precursor of HTRA2 is a 50 kDa mitochondrial membrane protein that became a mature serine protease of 36 kDa (SSP6208, see Table IV – S2) in the cytosol after 133 of its N-terminal amino acids has been proteolytically cleaved (Suzuki et al., 2001), where the mature peptide serves as an inhibitor of XIAP and IAPs (Suzuki et al., 2001). Furthermore, an arbitrary ±1.10 FC cut-off was also applied on all significant proteins (adjusted p-value <0.05) when conducting pathway and network analyses. Protein interaction network and pathway analyses were conducted using Ingenuity Pathway Analysis (www.ingenuity.com).

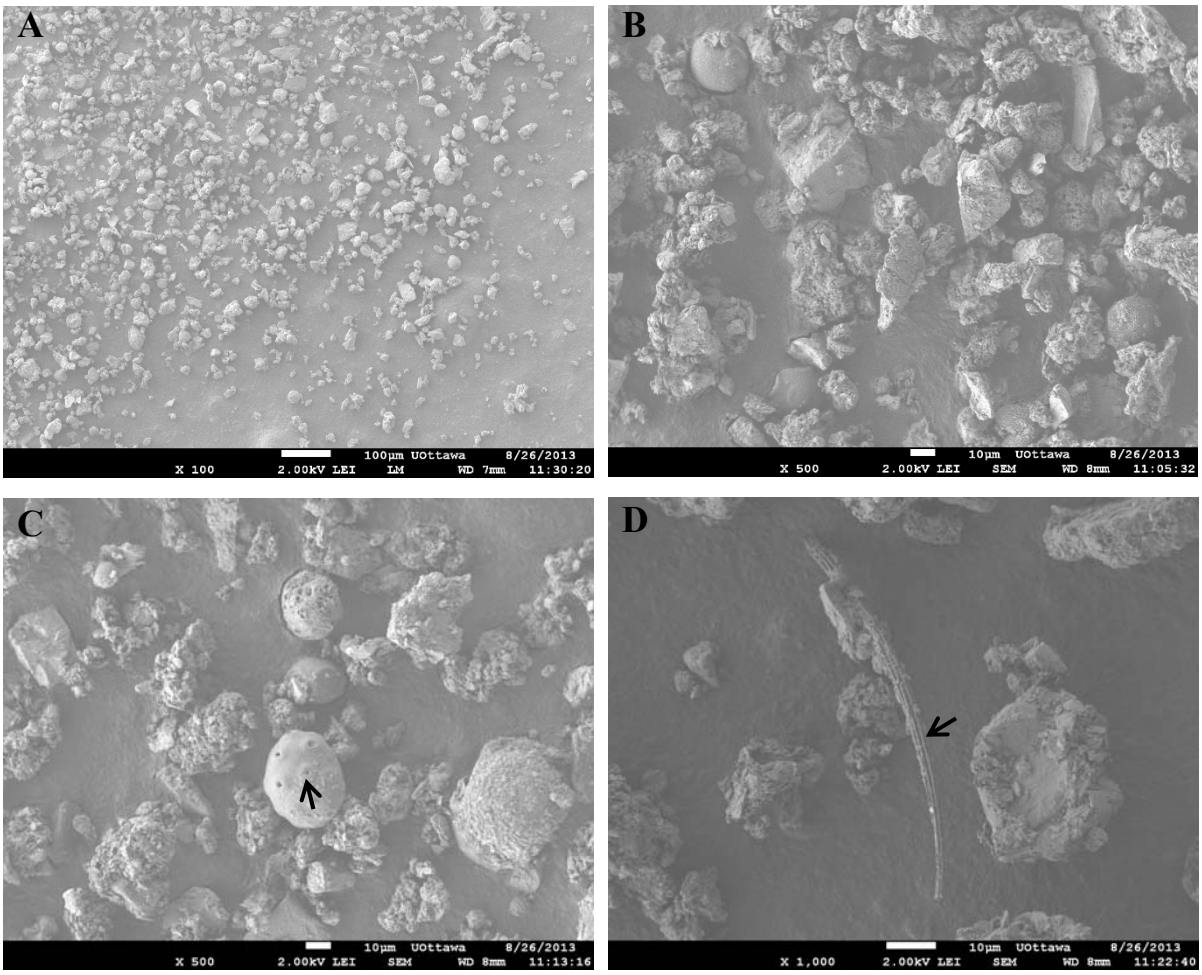

Figure IV – 1. The particles in the EHC-93 sample observed by scanning electron microscopy at various magnifications to show the contents in the particulate matter.
A is a 100X magnification image of the particles. B and C are 500X magnification images of the particles that shows the majority of the particles have the appearance of mineral particles, where the arrow in C points to a spherical ordered particle (biological origin). D is a 1,000X magnification image, and it shows a thin rod (arrow) in the middle of the image.

IV.3. Results

IV.3.1. Physicochemical characterization of the EHC-93 particles.

The electron micrographs in Figure IV – 1 show that the EHC-93 Ottawa urban dust is a complex mixture of particles with a broad range of size, shape, crystallinity, aggregation, porosity and surface structure. Majority of the materials appear to be crystalline particles with a wide range of sizes, where most particles possess flat non-porous plains and sharp edges. Some particles found in small quantities appeared as long thin rods (Figure IV – 1D), and as spherical non-porous, spherical porous and spherical ordered porous (biological origin) (Figure IV – 1C) materials. X-ray diffraction data in Table IV – 1 showed that calcite ($CaCO_3$), α-quartz (SiO_2), gypsum ($CaSO_4$) and dolomite ($CaMg(CO_3)_2$) were the major crystalline particles in EHC-93, which constituted of 41, 18, 13 and 13 % of the crystalline particles, respectively. The EDX analysis revealed that Ca (31.9 % by mass), Si (23.2 % by mass) and S (11.4 % by mass) are the three dominant elements in EHC-93 (Table IV – 2). This EDX result is similar to that of the IPC-MS result from a previous study which also showed that Ca and Si are major elements in EHC-93 total (Table IV – S1) (Vincent et al., 2001). The combined results suggested that majority of the insoluble components in EHC-93 are calcite followed by α-quartz and gypsum.

The results in Table IV – 3 showed that EHC-93 total particles contain a very small amount of endotoxin (100.0 EU/kg material). Almost all of the endotoxin was found in the insoluble fraction of EHC-93 (91.6 ± 1.4 EU/kg equivalent mass to the total). Only a trace quantity of endotoxin can be found in the soluble fraction of EHC-93 (2.5 ± 1.0 EU/kg equivalent mass to the total).

Table IV – 1. The percentage distribution of the major mineral crystals in the EHC-93 Ottawa urban dust detected by X-ray diffraction.

Mineral crystal	**% Distribution**
Calcite ($CaCO_3$)	41
α-quartz (SiO_2)	18
Gypsum ($CaSO_4$)	13
Dolomite ($CaMg(CO_3)_2$)	13
Albite ($NaAlSi_3O_8$)	10
Halite (NaCl)	5

Table IV – 2. The percentage distribution of the major elements in the EHC-93 Ottawa urban dust detected by energy dispersive X-ray spectroscopy.

Element	**Weight %**	**Atomic %**
Na	6.99	9.96
Mg	2.72	3.66
Al	6.46	7.84
Si	23.17	27.04
S	11.41	11.66
Cl	7.74	7.16
K	3.70	3.10
Ca	31.89	26.08
Fe	5.94	3.49

Table IV – 3. Endotoxin levels in EHC-93 total and its water-insoluble and soluble fractions.

PM	**Endotoxin (EU/kg material[a])**
Total[b]	100.0 ± 1.0
Insoluble	91.6 ± 1.4
Soluble	2.5 ± 1.0

[a]The quantity of endotoxin unit (EU) was expressed in relative to EHC-93 total for direct comparison (i.e., 91.6 and 2.5 EU can be detected from 0.83 and 0.17 kg of materials from the insoluble and soluble fractions, respectively)
[b]Data has been published (Breznan et al., 2016).

IV.3.2. Cytotoxic effects of EHC-93, and its insoluble and soluble components in A549 cells.

The cytotoxicity assays in Figure IV – 2 indicated that EHC-93 Ottawa urban air particles (total) had mild cytotoxic effect on A549 cells at low level of exposure (60 μg/cm^2). However, EHC-93 total were cytotoxic to A549 cells at higher doses (140 and 200 μg/cm^2), where they were capable of causing significant damage to the cell membrane based on LDH release assay (Figure IV – 2A), reducing cell proliferation based on BrdU incorporation assay (Figure IV – 2B) and decreasing metabolic energy content based on cellular ATP (Figure IV – 2C). Resazurin reduction assay did not detect any significant effect by EHC-93 total or its sub-fractions (Figure IV – 2D). It was observed that the trend of cytotoxicity of the insoluble fraction was remarkably similar to that of total PM, suggesting that the insoluble components drove most of the toxic effects of EHC-93 in A549 cells. Nevertheless, subtle cytotoxicity differences between the insoluble fraction and total PM can be observed in most assays, where the insoluble components appeared even more potent than EHC-93 total, and a significant difference between the two exposures was observed in the level of cellular ATP at the highest dose (two-way ANOVA: *Treatment x Dose* interaction at 200 μg/cm^2, $p < 0.05$) (Figure IV – 2C). The soluble materials were relatively non-toxic to A549 cells, and their effects were significantly different than the total and insoluble components in most assays.

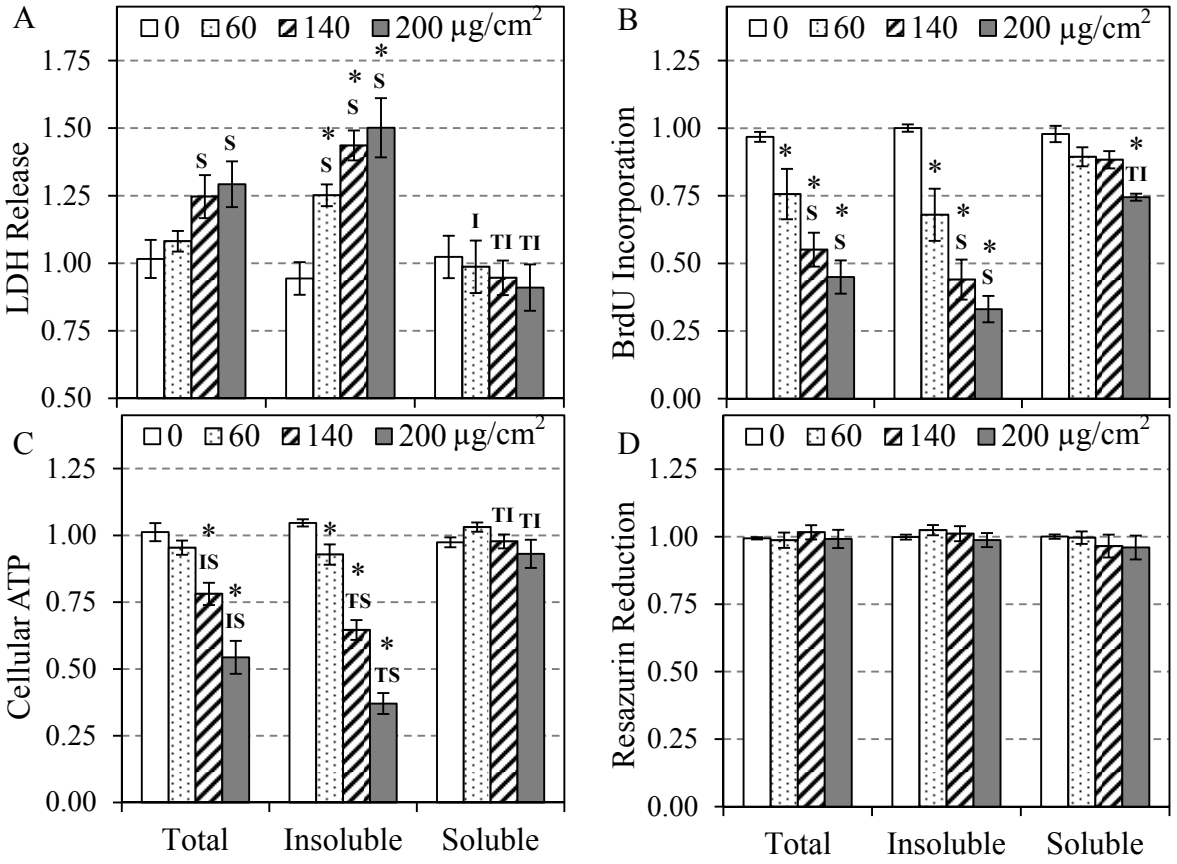

Figure IV – 2. The cytotoxicities of EHC-93 total and its water-insoluble (insoluble) and water-soluble (soluble) fractions in A549 cells after 24 hours of exposure were assessed by LDH release (A), BrdU incorporation (B), cellular ATP (C) and resazurin reduction(D) assays.

Data are expressed as mean fold effect +/- standard error, relative to the control (0 µg/cm^2), n = 4. Two-way ANOVA was used to determine significant effects of the particles, where Holm-Sidak was the post-hoc method used for all pairwise comparison procedures. * indicates significant difference compared to control. ^{T} indicates significant difference compared to EHC-93 total. ^{I} indicates significant difference compared to the insoluble fraction. ^{S} indicates significant difference compared to the soluble fraction.

IV.3.3. Changes in the expression of proteins in A549 cells following exposures to EHC-93 and its insoluble and soluble fractions.

Two-way ANOVA results in Table IV – S2 indicated that 206 protein spots were differentially altered significantly by the treatments (adjusted *p*-value < 0.05), and 154 of these protein spots have been identified via MALDI-TOF-TOF-MS. The effects of particle treatments on most of these protein spots (i.e., 126 out of 154 identified proteins) were particle-specific (i.e., *Treatment* main effect, *Treatment & Dose* main effects, and *Treatment X Dose* interaction). It should be kept in mind that two-way ANOVA results are meant to identify significant differential changes in protein expression among the treatments, and these changes are not always significantly different from the control. For example, all of the *Treatment* main effects in Table IV – S2 were not due to significant difference from the control after particle exposures. Rather, most of the Treatment main effects were significant differences between the soluble fraction and the total and/or insoluble fraction based on Holm-Sidak multiple pair-wise comparison tests (adjusted *p*-values were not shown), and some were due to differences between the total and insoluble fraction. On the other hand, significant differences from the control as well as among the treatments can be identified by *Treatment & Dose* main effect and *Treatment X Dose* interaction as demonstrated in Table IV – S2. Holm-Sidak multiple pair-wise comparison tests showed that EHC-93 total and its insoluble fraction affected the expression of most protein spots similarly (e.g., same direction of expression), and that their effects were differed from the soluble materials (e.g., opposite directions of expression) (Table IV – S2). Despite their similarity, differences between the total and insoluble fraction can be identified based on their FCs and adjusted *p*-values (not shown) following Holm-Sidak analysis. It should be noted that the two-way ANOVA results

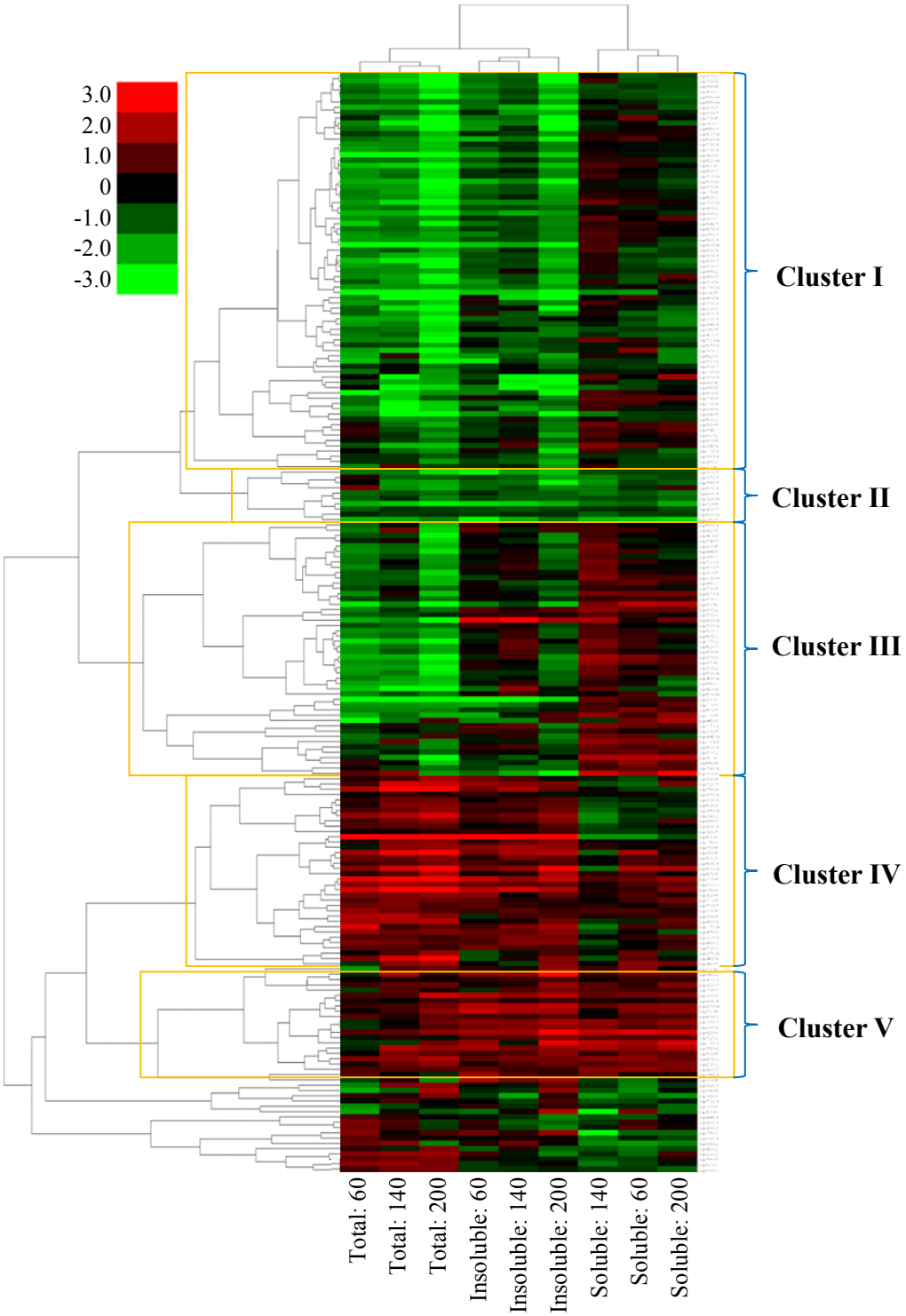

Figure IV – 3. Unsupervised hierarchical cluster analysis of the protein spots that were significantly affected due to particle exposures (Two-way ANOVA: $p < 0.05$).
The expression of each protein spot was calculated by Log_2(Treatment/Control), n=3. Red is coded for increased expression and green is coded for decreased expression. The number indicates the dose in μg/cm^2.

in Table IV – S2 revealed multiple significant protein spots with the same protein ID, an indication of different isoforms of the same protein and/or post-translational modification of the native protein. A large portion of the significant protein spots were small fragments of their native proteins (based on MW and unique peptide sequences).

Hierarchical cluster analysis was conducted to visually compare changes in the proteome of A549 cells following 24 hours of exposure to EHC-93 and its insoluble and soluble fractions. The results based on all 543 protein spots examined by 2D-GE (Figure IV – S1) or only the significantly altered protein spots (Figure IV – 3) showed that the insoluble fraction and EHC-93 total formed a cluster that is separate from the soluble fraction. Such observations indicated that the total EHC-93 mixture and its insoluble components affected the proteome of A549 cells similarly, and that their effects differed from those of the soluble materials. It should be noted that the effects of the total PM and the insoluble were different enough that the two treatments formed two separate sub-clusters (Figures IV – S1 and 3). The significantly altered protein spots in Figure IV – 3 appeared to form five interesting clusters (I – V). Cluster I was dominated by those protein spots that were down regulated by the total and insoluble fraction; and these proteins were found to be involved in cellular movement, cell growth and proliferation, cell death and survival, molecular transport and small molecule biochemistry pathways (Table IV – S3). Cluster II was a small group of protein spots that were decreased in expression by all treatments, but the number of protein in this cluster was not large enough to conduct a reliable bioinformatics analysis. Cluster III displayed the protein spots that the total and insoluble fraction treatments generally decreased their expressions, while the soluble fraction generally increased their expressions; these proteins were involved predominantly in cellular movement, carbohydrate metabolism, cell growth and proliferation, cell death and survival, and cell morphology pathways (Table

Table IV – 4. Biological functions indicated by Ingenuity Pathway Analysis (IPA) that were likely impacted by the particles based on the proteins that were significantly affected.
The # indicate the number of proteins that were significantly affected by each treatment (EHC-93 total, insoluble and soluble at 60 μg/cm^2), and the *p*-value indicate the significance of the biological function based on IPA's calculations. Only the significant functions that were influenced by more than 5 proteins in any particle treatment group are presented.

	Total		**Insoluble**		**Soluble**	
Biological Function	#	*p*-value	#	*p*-value	#	*p*-value
Cell Death and Survival	22	$1.51x10^{-05}$	24	$4.39x10^{-09}$	19	$4.29x10^{-05}$
Cell Growth and Proliferation	21	$2.42x10^{-04}$	22	$6.91x10^{-05}$	18	$5.85x10^{-04}$
Cellular Movement	17	$1.83x10^{-05}$	18	$3.89x10^{-06}$	16	$6.56x10^{-06}$
Acute Inflammation	10	$1.45x10^{-03}$	9	$5.30x10^{-03}$	8	$6.33x10^{-03}$
Chronic Inflammation	10	$1.62x10^{-04}$	8	$3.39x10^{-03}$	9	$2.15x10^{-04}$
Cytoplasm Organization	9	$2.03x10^{-02}$	10	$6.95x10^{-03}$	9	$6.90x10^{-03}$
Protein Metabolism	7	$1.07x10^{-02}$	10	$1.24x10^{-04}$	11	$3.80x10^{-06}$
ROS Metabolism	6	$1.40x10^{-03}$	8	$2.74x10^{-05}$	5	$3.83x10^{-03}$
Allergic Response	7	$5.18x10^{-05}$	6	$4.31x10^{-04}$	6	$1.71x10^{-04}$
Nucleic Acid Metabolism	6	$1.62x10^{-03}$	7	$8.05x10^{-05}$	5	$1.95x10^{-03}$
Mitochondrial Transmembrane Potential	5	$1.22x10^{-04}$	6	$8.52x10^{-06}$	5	$5.47x10^{-05}$

It should be noted that about half of the proteins used in pathway analysis derived from Treatment main effect, where the effect of the soluble fraction on these protein spots were typically opposite that of the total and insoluble fraction. The directions of protein expressions of several selected functions were demonstrated as heatmaps in Figure IV – S2.

IV – S3). Cluster IV consisted of those protein spots that were strongly increased by most total and insoluble exposures but were weakly increased or decreased by the soluble treatments. The proteins in this cluster were found to be in the lipid metabolism, small molecule biochemistry, and cell growth and proliferation pathways. Cluster V showed the protein spots that were increased in expression by all treatments; these proteins are involved in cellular morphology, cellular function and maintenance, cellular assembly and organization, and cell death and survival.

IV.3.4. Effects of EHC-93 and its insoluble and soluble components on various pathways and networks in A549 cells.

Ingenuity Pathway Analysis results in Table IV – 4 revealed that EHC-93 and its insoluble and soluble fractions can affect the expression of the proteins involved in a number of biological functions including cell death, cell proliferation, cell differentiation, cellular movement, inflammatory response, protein metabolism and reactive oxygen species (ROS) metabolism. In these pathways, the patterns of protein expression in A549 cells influenced by the soluble fraction were noticeably different from the total and insoluble fraction, and the differences between the latter two are more subtle but distinguishable (Figure IV – S2). Generally, most of these proteins were altered by the total and insoluble fraction treatments in the same direction but varying in magnitude, whereas the soluble fraction exposure may cause no effect or opposite effects to that of the total and insoluble fraction treatments. For example, the networks of cell death and proliferation in Figure IV – 4 showed that the expressions of proteins such as YWHAE, SRSF1, PKM, HSPA9 and ENO1 were down-regulated in the total and insoluble fraction but were up-regulated or unaffected by the soluble fraction. The expression of proteins such as VCP, TREM1 and BUB3 were up-

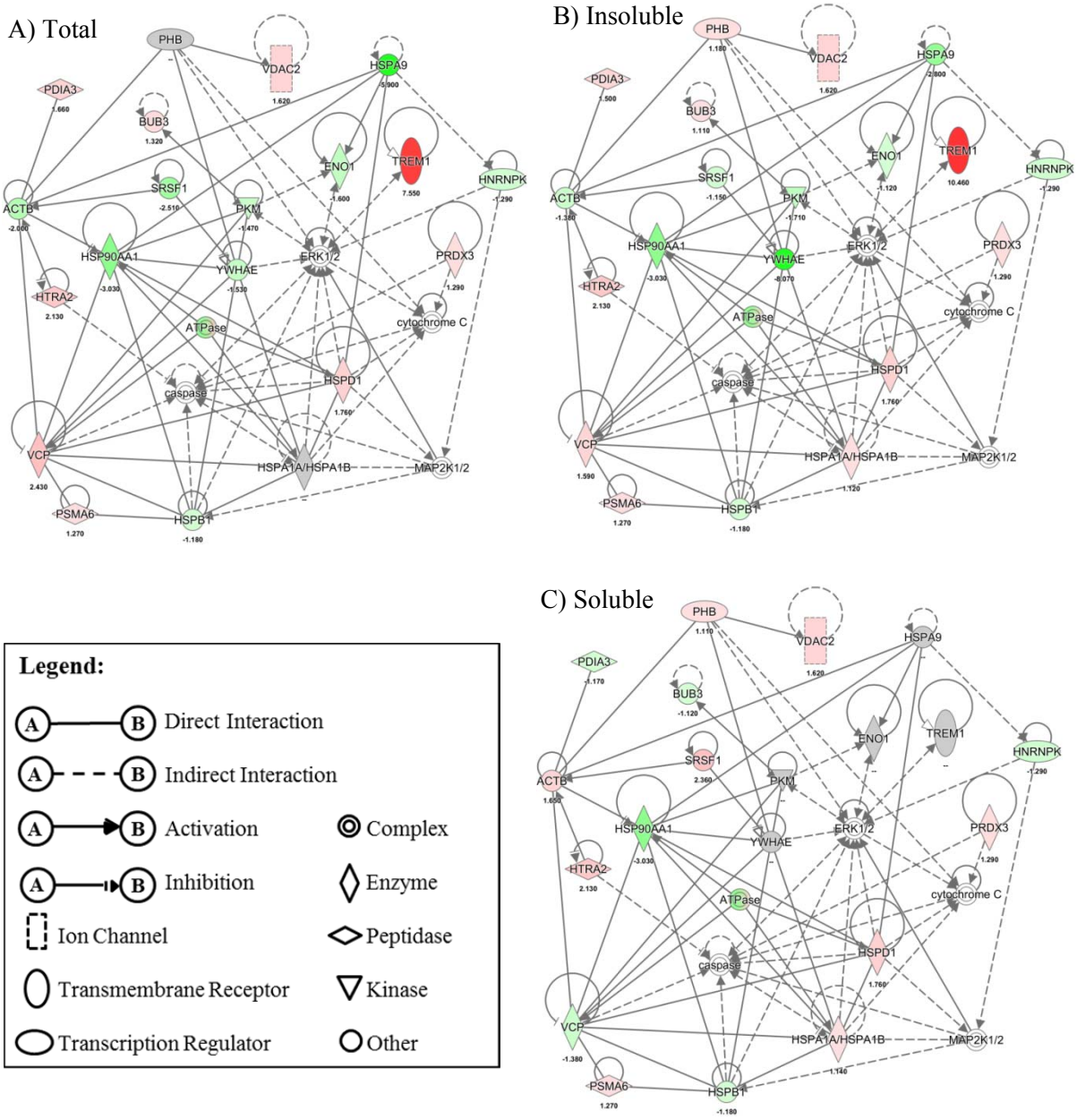

Figure IV – 4. Protein profiles in the network of cell death and cell proliferation pathway in A549 cells following EHC-93 total (A) and its insoluble (B) and soluble (C) fractions treatments at 60 μg/cm^2.
Red indicates increased expression, green stands for decreased expression, grey implies non-significant change and white indicates the protein was not examined in this study. The color scale, representing fold-change, was set at a maximum and minimum of 8 (deepest red) and -6 (darkest green).

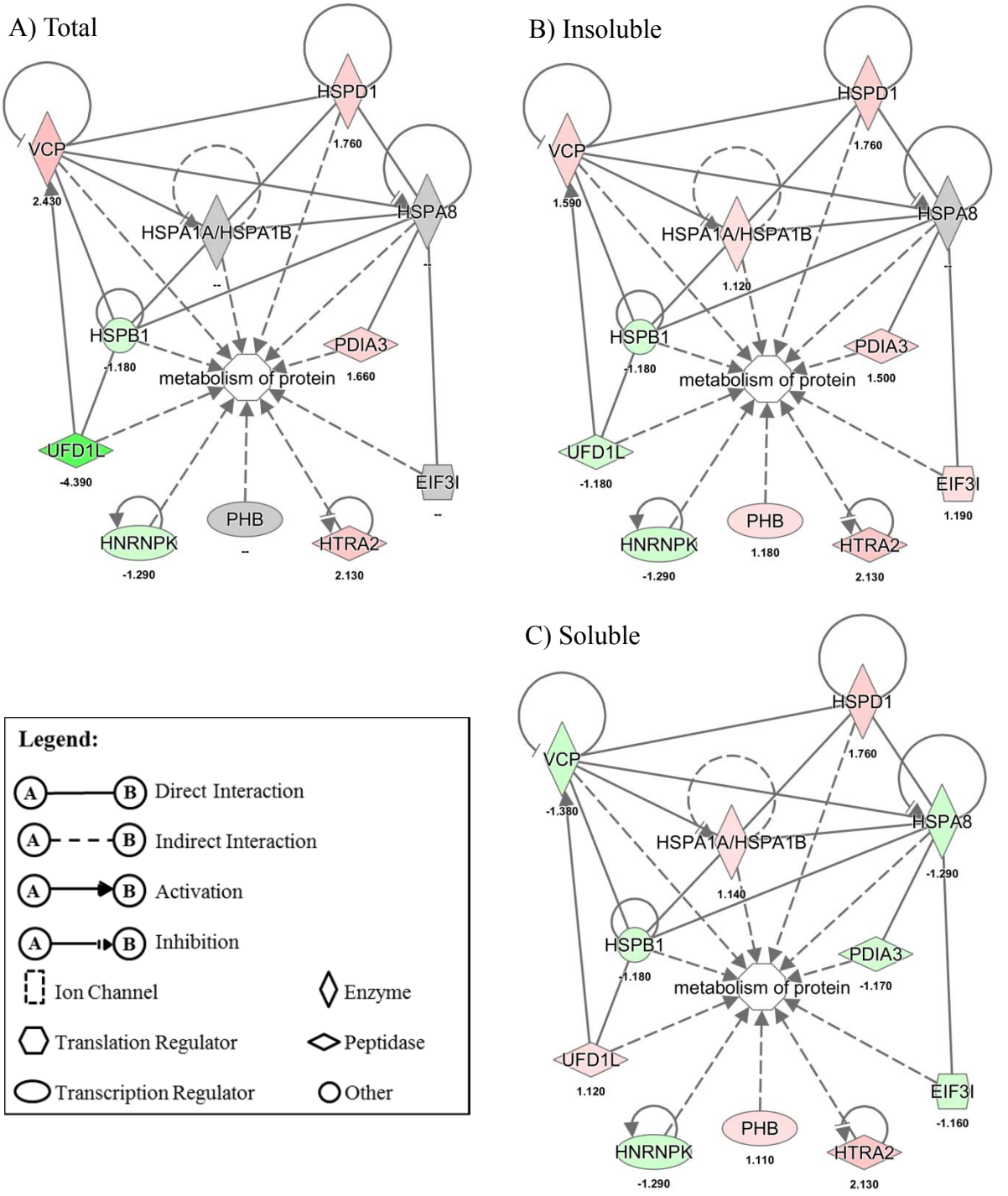

Figure IV – 5. Protein profiles in the network of protein metabolism pathway in A549 cells following EHC-93 total (A) and its insoluble (B) and soluble (C) fractions treatments at 60 μg/cm^2.
Red indicates increased expression, green stands for decreased expression and grey implies non-significant change. The color scale, representing fold-change, was set at a maximum and minimum of 8 (deepest red) and -6 (darkest green).

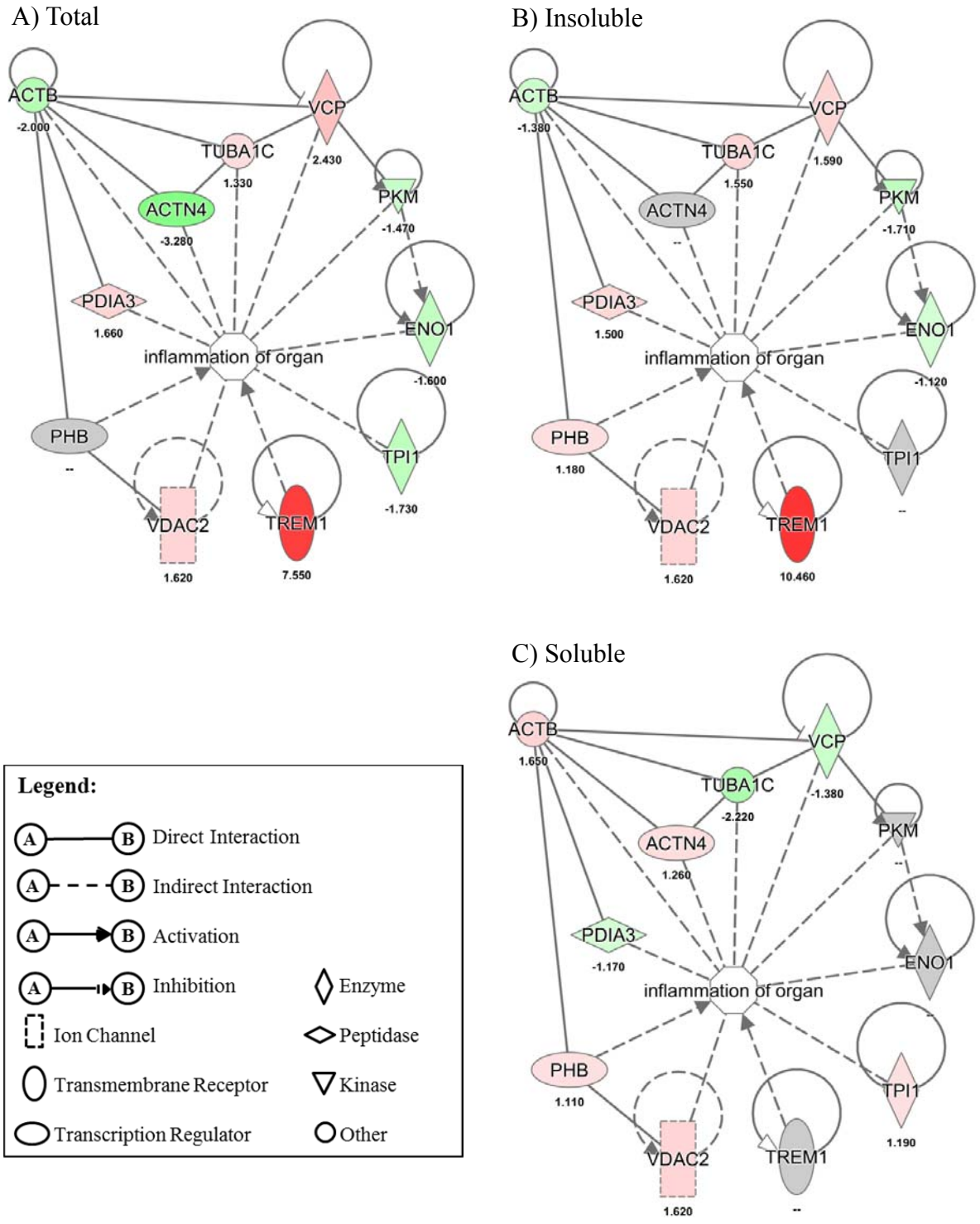

Figure IV – 6. Protein profiles in the network of organ inflammation pathway in A549 cells following EHC-93 total (A) and its insoluble (B) and soluble (C) fractions treatments at 60 μg/cm^2.
Red indicates increased expression, green stands for decreased expression and grey implies non-significant. The color scale, representing fold-change, was set at a maximum and minimum of 8 (deepest red) and -6 (darkest green).

regulated in the total and insoluble fraction but down-regulated or unaffected in the soluble fraction. All these proteins were affected by the total and insoluble fraction in the same direction but varying magnitude. Similarly, the network of protein metabolism in Figure IV – 5 showed that the expression of PDIA3, HSPA8 and EIF3I were down-regulated due to the soluble fraction exposure, but these proteins were either up-regulated or unaffected by the total and insoluble fraction exposures to varying magnitude. The expression of UFD1L was up-regulated by the soluble fraction, but it was down-regulated by the total and insoluble fraction to different degrees. Of all the networks examined, the network of organ inflammation in Figure IV – 6 showed the most contrasting effect between the total or insoluble fraction against the soluble fraction, where 10/11 and 9/11 proteins in the network were distinctly altered, respectively. In this network, the total and insoluble fraction significantly increased the expression of PDIA3, TREM1, TUBA1C and VCP to various degrees in A549 cells, whereas exposure to the soluble fraction either did not affect or decreased the expression of these proteins. On the other hand, the expression of ACTB, ENO1 and PKM were significantly decreased in A549 cells to varying magnitude following exposure to the total and insoluble fraction, but these proteins were either unaffected or increased after exposing to the soluble fraction.

IV.3.5. Secretion levels of IL-8, MCP-1 and VEGF from A549 cells due to exposures to EHC-93 and its insoluble and soluble fractions.

From a panel of 11 cytokines assessed, only 3 cytokines (IL-8, MCP-1 and VEGF) were found to secret at a reliable detection level (> 5 pg/ml) and were significantly altered due to particle exposures (Figure IV – 7). It was found that EHC-93 total and its insoluble fraction displayed a similar trend in stimulating the secretion of IL-8, MCP-1 and VEGF

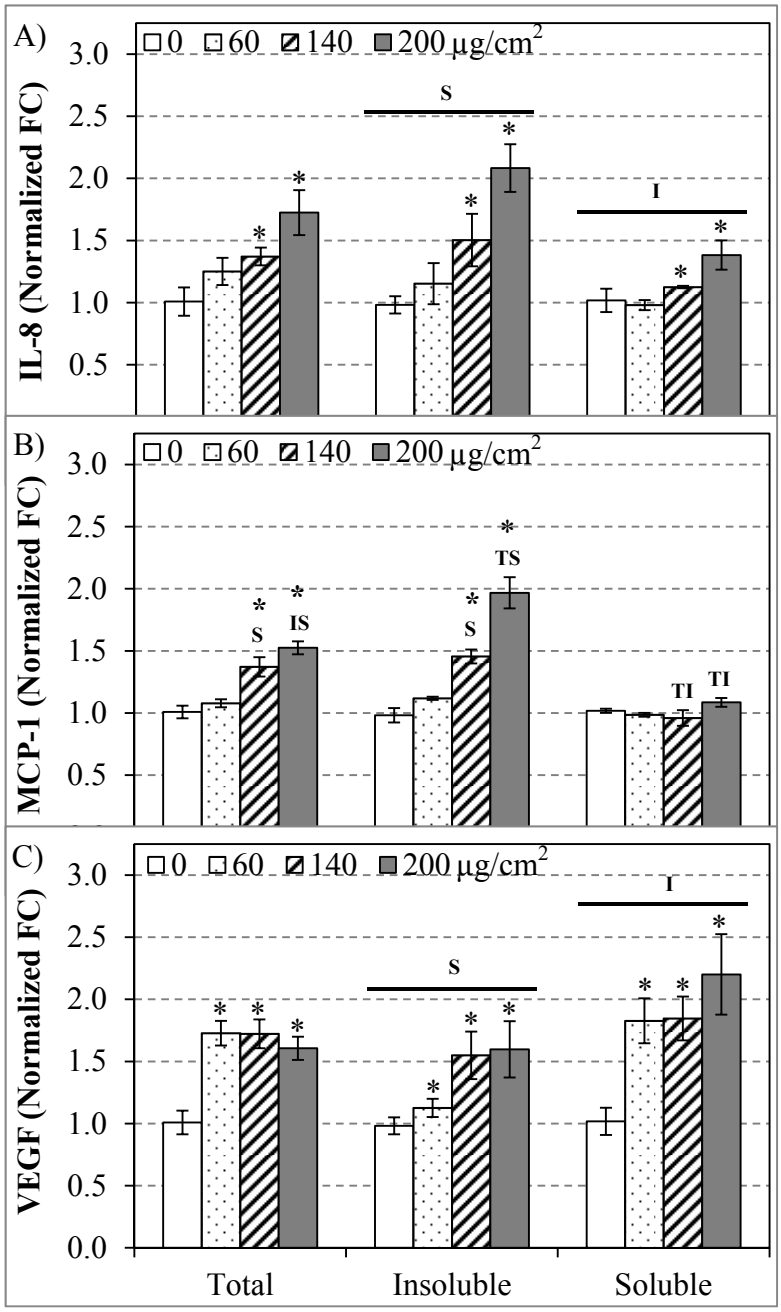

Figure IV – 7. Comparing the secretion of cytokines such as IL-8 (A), MCP-1 (B) and VEGF (C) by A549 cells after 24 hr exposure to EHC-93 total and its insoluble and soluble components.

Data are expressed as normalized fold-change (FC) ± standard error, relative to the control (0 µg/cm^2), n = 4. Two-way ANOVA was used to determine significant effects of the particles, where Holm-Sidak was the post-hoc method used for all pairwise comparison procedures. * indicates significant difference compared to control. ^{T} indicates significant compared to EHC-93 total. ^{I} indicates significant difference compared to the insoluble fraction. ^{S} indicates significant difference compared to the soluble fraction. The bar on top of a treatment group indicates significant *Treatment* main effect.

from A549 cells that is different from the soluble fraction. The insoluble fraction is significantly more potent than the soluble fraction in stimulating the releases of the pro-inflammatory cytokines interleukin-8 (IL-8) and monocyte chemoattractant protein-1 (MCP-1) from A549 cells (Figures IV – 7A and B). The insoluble fraction appeared more potent than the total in inducing the secretion of IL-8 and MCP-1 from A549 cells, and it reached statistical significant for MCP-1 at the highest dose (Figure IV – 7B). Contrarily, the soluble fraction is significantly more potent than the insoluble fraction in causing the release of vascular endothelial growth factor (VEGF) from A549 cells (Figure IV – 7C). The total and insoluble fraction can stimulate significant release of VEGF from A549 cells, but their potencies were not significantly different.

Discussion

Understanding the mechanisms of particle toxicity of urban air PM is a challenge, because airborne PM is a complex mixture of particles with a wide range of physicochemical properties. In an attempt to assess the in vitro toxicity of urban air particles, we previously fractionated EHC-93 (Ottawa urban air particles) into water-insoluble and soluble fractions, and used A549 cells to examine the PM exposure-related effects on a few selected genes and secretory proteins in the endothelin system (Chauhan et al., 2005). The current study focuses on integration of multiple cytotoxicity assay and untargeted proteomic analysis results to gain insight into toxicity mechanisms underlying total and fractionated PM exposure- related changes in A549 cells.

This is the first time that multiple cytotoxicity assays were used to investigate the cytotoxic effects of EHC-93 and its insoluble and soluble fraction in the same in vitro study.

The results from LDH release, cellular ATP and BrdU incorporation assays indicated that EHC-93 total and its insoluble fraction were both similarly cytotoxic to A549 cells, while the soluble fraction caused very little toxic effect to the cells (Figure IV – 2). It could be argued that the cells were actually dosed with low concentrations of soluble materials (0, 10, 24 and 34 μg/cm^2), which were 17 % mass equivalent to the dosing concentrations of the total (0, 60, 140 and 200 μg/cm^2), and thus such low quantities of the soluble materials were not high enough to exhibit a significant effect. However, this is the actual proportion of the soluble materials present in EHC-93 total, and the present study focused on comparing the cytotoxic effects of the insoluble and soluble fractions in the mass proportion as they were found in the environment. Similarly, A549 cells were dosed with 0, 50, 116 and 166 μg/cm^2 insoluble materials, which are 83 % mass equivalent to EHC-93 total concentrations. Nevertheless, the insoluble fraction appeared even more toxic than the total in every equivalent dose of every cytotoxicity assay, and reached statistical significance at the highest dose in ATP assay (two-way ANOVA: *Treatment x Dose* interaction at 200 μg/cm^2, $p < 0.05$) (Figure IV – 2C). Evidently, the toxic potency of EHC-93 total is not equal to the sum of its insoluble and soluble fractions, suggesting that there were interactions between the insoluble and soluble materials. It is possible that the soluble materials coated the surface of the insoluble components and reduced some of their cytotoxic effects. Such inhibitory coating effect has been previously reported in nano-silica particles (Sun et al., 2015a). Alternatively, biological effects caused by the soluble materials in A549 cells may be antagonistic to some of those effects elicited by the insoluble materials.

The effects of EHC-93 and its insoluble and soluble fractions on the proteome of A549 cells were examined via 2D-GE and mass spectrometry as previously described (Vuong et al., 2016b; Vuong et al., 2016c). Two-way ANOVA and Holm-Sidak (post-hoc)

were the statistical methods used to determine significant effects of particles across treatments. The results in Table IV – S2 indicated that there was a significant Treatment main effect for BUB3 (SSP9301), where the total and insoluble components of EHC-93 affected the expression of BUB3 similarly but their effects were different from the soluble materials. On average, the expression of BUB3 in A549 cells due to EHC-93 total, insoluble and soluble materials exposures were listed as 1.32, 1.11 and -1.12, respectively. It is important to understand that such FCs were relative to the control. More importantly, it must be recognized that the net difference between the effects of the total and soluble fraction was 44 % (from 1.32 to -1.12) and the net difference between the effects of the insoluble and soluble fractions was 23 % (from 1.11 to -1.12). Thus, such magnitudes of changes between treatments should not be overlooked, particularly when the adjusted *p*-value is very small (adjusted $p = 0.003$), and especially the goal of this study is to identify the differential responses of A549 cells to EHC-93 particles and its insoluble and soluble components. When conducting pathway and network analyses, we believe that a ±1.10 FC cut-off on all significant proteins (adjusted *p*-value < 0.05) is sufficient to remove nuanced expressions that may not contribute to any biological impact.

Two-way ANOVA results in Table IV – S2 identified 206 protein spots were significantly altered by the treatments (adjusted *p*-value <0.05), and 154 of these protein spots have been identified via MALDI-TOF-TOF-MS, which can potentially be used for pathway analysis. Unsupervised hierarchical cluster analysis based on all the significantly altered protein spots showed that the total and insoluble fraction treatments clustered together (Figures IV – 3), suggesting that these two treatments had similar effects on the proteome of A549 cells. Such result holds true regardless if cluster analysis was conducted based both non-significantly and significantly altered protein spots (Figure IV – S1). In

addition, the total and insoluble fraction treatments formed separate sub-clusters, implying that their effects on the proteome of A549 cells were distinguishable (Figure IV – 3 and S1). These findings were similar to those in an earlier study in our laboratory that demonstrated that the expression of a selected set of genes (e.g., MMP2, ECE1 and EDN1) and secretory proteins (e.g., IL-8 and VEGF) in A549 cells were similarly affected by the total and insoluble components of EHC-93, and that their effects differed from those of the soluble materials (Chauhan et al., 2005). Results from two-way ANOVA and Holm-Sidak multiple comparisons analyses in Table IV – S2 were in line with the above observations. The total and insoluble fraction PM exposures were observed to alter the proteome of A549 cells more than the soluble fraction, and these changes were not additive. In brief, all proteomic and cytotoxicity assay results in this study unanimously pointed out that the toxic effects of EHC-93 in A549 cells were mainly driven by its insoluble components.

Unsupervised hierarchical cluster analysis revealed that all the doses of the same treatment clustered together, and the highest dose of the total and insoluble fraction exposures induced the greatest change to most protein spots (Figure IV – 3). These findings suggested that the effects of the total and insoluble fraction would eventually converge to the same outcome as the dose increases. Interestingly, majority of these significantly altered protein spots were not full length native proteins or isoforms based on their molecular weights and unique peptide sequences (Table IV – S2). These peptides (e.g., SSP2010, 8302, 3104, 4108, 305 and 8109) were possibly cleavage or degradation products of their native proteins, and they may be derived from dying or dead cells that have undergone or have committed to apoptosis or necrosis. This is plausible because functional annotation for the proteins in different clusters in Figure IV – 3 revealed that cell death and survival and cell growth and proliferation were the two dominant cellular functions affected by particle

exposures (Table IV – S3). In addition, the LDH release, cellular ATP and BrdU incorporation assays indicated that A549 cells were adversely impacted at the higher doses (Figure IV – 2). Altogether, these results suggested that the A549 cells exposed to the higher doses of PM (140 and 200 μg/cm^2) engaging into terminal stage of particle toxicity (i.e., dead or dying cells), and the lowest dose (60 μg/cm^2) revealing an early stage of particle toxicity (i.e., live cells). It should be noted that the chosen exposure doses for most in vitro toxicology studies, including the current study, are well beyond the actual environmental levels in order to obtain measurable responses. Therefore, there is more value to examine the effect of the particles on A549 cells at the low toxicity dose to capture the early signs of particle toxicity.

Pathway analysis revealed that the significantly altered proteins in A549 cells following exposure to the particles at 60 μg/cm^2 dose were involved in pathways such as ROS metabolism, inflammatory response, cytoplasm organization, cellular movement, cell growth and proliferation, and cell death and survival (Table IV – 4). These pathways were likely the mechanisms employed by A549 cells to handle the effects of the exposed particles at a low toxicity level. It should be noted that about half of the significantly altered proteins in these pathways were derived from Treatment main effect, where their expressions were not necessarily different from the control significantly. Rather, their expression were mostly opposite in direction between the soluble fraction and the total or insoluble fraction (Figure IV – S2). It should be clarified that the proteomic results based on 2D-GE data were not strong enough to confidently determine if any of the pathways in Table IV – 4 was actually activated or inactivated. Rather, we relied on the cytokine release (Figure IV – 7) and cytotoxicity assays (Figure 2) data to determine the phenotypic effects of the particles.

It is interesting to note that a large number of significantly altered proteins were involved in the cell death and survival pathways (Figure IV – S2), suggesting that this dose (60 μg/cm^2) was sufficient to cause such effects. This is consistent with the cytotoxicity assay results (Figure IV – 2A, B, C). Examining the pattern of proteins expressed in the networks of cell death and cell proliferation pathways in Figure IV – 4 may provide insights to the molecular mechanisms that dictate the contrasting effects of the insoluble and soluble fractions. In this network, the extracellular signal-regulated kinase 1/2 (ERK1/2) was found in one of the main nodes, where this protein is known to modulate a broad biological functions in cells, including cell death and cell proliferation (Roskoski, Jr., 2012). It was noticeable that the soluble fraction treatment did not significantly alter the expression of a number of proteins up- and down-stream of ERK1/2. For example, only the total and insoluble treatments significantly decreased the expression of 14-3-3 protein epsilon (YWHAE), pyruvate kinase (PKM) and enolase-1 (ENO1) and significantly increased the expression of triggering receptor expressed on myloid cells 1 (TREM1). Down regulation of ENO1 and PKM may explain the decreased ATP levels in A549 cells follow the total and insoluble fraction exposures in Figure 2C (significant only in the insoluble fraction treatment at dose 60 μg/cm2) as these two proteins are known to serve distinct enzymatic functions in the last two steps of glycolysis (Voet and Voet, 2010). Interestingly, these proteins are known to serve several other biological functions such as cell death, cell proliferation and stress response, and their expressions can be modulated in response to various stimuli (Yang et al., 2012;Zhou et al., 2013). ENO1 has been reported to regulate the kinase activity of ERK1/2 in A549 cells (Zhou et al., 2013), and ERK1/2 can modulate the nuclear translocation of PKM in U251 human glioblastoma cells that is necessary for PKM's auto-regulation of expression (Yang et al., 2012). Knockdown of PKM expression PKM (via

siRNA) have been shown to decrease the production of ATP and induce apoptosis and autophagy in A549 cells (Chu et al., 2015;Sun et al., 2015b), which is consistent with the LDH release and BrdU incorporation trends (Figures IV – 2A and B). These findings were similar to the proteomic results observed for the total and insoluble fraction exposures and were also consistent with the cytotoxicity data (Figure IV – 2C) in this study. Furthermore, PKM has been shown to phosphorylate the mitotic checkpoint protein BUB3, which is essential for the BUB3-BUB1 complex to be recruited to the kinetochore spindle during mitosis (Jiang et al., 2014). The expression of BUB3 in A549 cells was increased by the total and insoluble fraction treatments, but its expression was decreased by the soluble fraction (Figure IV – 4). It is evident that the cytotoxicity assay and proteomic results were mutually complementary in explaining the toxic effects of the particles, extensive investigations would be required to better understand the PM-driven mechanisms of particle toxicity in the cell death and cell proliferation pathways.

Of all the networks examined, the network related to inflammatory process in Figure 6 showed the most contrasting effect between the total or insoluble fraction against the soluble fraction, where 10/11 and 9/11 proteins in the network were distinctly altered, respectively. It should be caution that the relationships of the proteins involved in this network are not straight forward to interpret because inflammation is a process that is involved with multiple cell types such as epithelial cells, neutrophils and macrophages. Interestingly, inflammatory stimuli are known to increase the expression of triggering receptor expressed on myeloid cells 1 (TREM1) on neutrophils, monocytes and macrophages, where this receptor is known to amplify the secretion of pro-inflammatory mediators such as IL-1β, IL-6, IL-8, MCP-1 and TNFα from these cells (Bouchon et al., 2001;Schenk et al., 2007). Furthermore, TREM1 has been reported to be expressed in lung

cancer epithelial cells. For instance, A549 cells exposed to silica nano-particle has been associated TREM1 signaling (Pisani et al., 2015). Increased expression of this receptor in the cells exposed to the total and insoluble fraction is a possible mechanism for the release of IL-8 and MCP-1 in A549 cells (Figure IV – 7). In addition, a recent mouse lung injury model demonstrated that increased expression of protein disulfide-isomerase associated 3 (PDIA3) and ENO1 were important for alveolar epithelial type II (AT-II) cells to repair bleomycin-induced injury in the lung of mice (Mutze et al., 2015). Over-expression of PDIA3 in murine embryonic fibroblast cells is known to exacerbate apoptosis via Bak signaling (Zhao et al., 2015). Mutze et al (2015) and Zhao et al (2015) hinted that increased level of PDIA3 in injured cells may determine whether the cells would commit to injury repair or apoptosis. As increased level of PDIA3 (Figure IV – 6) in A549 cells in the present study coincided with increased LDH release and decreased BrdU incorporation and cellular ATP levels (Figure IV – 2) after exposure to the total and insoluble fraction at the 60 μg/cm2 dose, the results point perhaps to an inflammatory process directed-apoptosis. EHC-93 is known to contain inflammatogenic particles such as silica (Table IV – 1) and endotoxins (Table IV – 3). Moreover, previous studies have shown that EHC-93 was capable of stimulating the release of pro-inflammatory cytokines such as IL-8 (Breznan et al., 2016; Chauhan et al., 2005; Fujii et al., 2001; Sakamoto et al., 2007) and MCP-1 (Breznan et al., 2016) from bronchial or lung epithelial cells. Sakamoto et al (2007) demonstrated that the secretion of IL-8 from human epithelial bronchial cells by EHC-93 total was induced by the influx of calcium from the extracellular media, where the signalling was suspected to be mediated by a membrane receptor and/or ion channel (Sakamoto et al., 2007). Whether EHC-93 total or its insoluble components induced secretion of IL-8 and MCP-1 from A549 epithelial cells were mediated

by calcium influx, and the involvement of a membrane receptor/ion channel, will be explored in future studies.

It should be noted that correlating the *in vitro* results in this study to those *in vivo* results from previous studies is not straight forward. When EHC-93 total particles were inhaled by rats, the inhalation did not result in lung injury but it elicited inflammatory responses and cardiovascular effects (Bouthillier et al., 1998; Thomson et al., 2005; Vincent et al., 1997a; Vincent et al., 2001). These results suggested that the efficient clearance mechanism in the respiratory tract of healthy animals and humans would make the inhaled particles only mildly toxic. Intriguingly, the data based on *in vitro* and intratracheal instillation studies suggested that the particles can be toxic if they were deposited and retained in the lungs. For example, the *in vitro* results in the present study demonstrated that A549 human type II lung epithelial cells were sensitive to the cytotoxic effects of EHC-93 and its water-insoluble components upon exposure, where the particles are potent in stimulating proteins involved in inflammatory responses and cell death, while decreasing cellular ATP and cell proliferation. On the other hand, direct injection of either EHC-93, its soluble or insoluble fractions into the lungs of rats via intratracheal instillation triggered inflammation based on the number of cells and protein levels in lavaged lung fluid (Adamson et al., 1999). However, exposure to EHC-93 and its soluble, but not insoluble, fraction caused mild lung injury in rats based on the observed necrosis to type I alveolar cells and the subsequent 3H-thymidine uptake by type II alveolar cells (Adamson et al., 1999), which would proliferate and differentiate to replace type I cells. It is not clear why the instilled insoluble fraction did not induce lung injury even when it contains varying amount of insoluble minerals (Table IV – 1), endotoxins (Table IV – 3), PAHs and metals (Vincent et al., 1997b). It is possible that the insoluble particles were cleared from the lung. As for the

instilled soluble materials, they can be readily absorbed by the cardiovascular system and affect various cell types, where the observed lung injury was attributed to the presence of soluble zinc and copper (Adamson et al., 2000; Prieditis and Adamson, 2002). In addition, the immunoassay results in this study showed that the soluble materials had greater potency than the insoluble materials in stimulating the secretion of a potent vasculogenic/angiogenic signaling protein vascular endothelial growth factor (VEGF) from A549 cells (Figure IV – 7C), which are type II alveolar cells. In this point of view, the effects of the soluble materials could be mediated by type II alveolar cells via paracrine signalling.

In summary, most of the results in this study and previous *in vitro* study (Chauhan et al., 2005) consistently showed that the cytotoxic effects of EHC-93(total) and its insoluble fraction in A549 cells were similar to each other and their effects were differed from the soluble fraction. These results indicated that the insoluble materials in EHC-93 are the drivers of toxic potency in A549 human lung epithelial cells. The culminated physicochemical characterizations from the previous (Vincent et al., 1997b; Vincent et al., 2001) and present studies have built a repertoire of identified insoluble components in EHC-93 including metals (e.g., iron, lead, magnesium and zinc), minerals (e.g., calcite, silica and gypsum), carbonaceous materials (e.g., phenanthrene, pyrene, fluoranthene and benzo[b]fluoranthene) and endotoxins at defined quantities or relative quantities. This repertoire would allow present and future studies to better assess the contribution of toxic potency and assess the pathways of effects of one or a combination of particles. The majority of the insoluble components are mineral crystal particles such as calcite ($CaCO_3$), α-quartz (SiO_2), gypsum ($CaSO_4$) and dolomite ($CaMg(CO_3)_2$) (Table IV – 1). As these insoluble mineral particles can contribute to the total cytotoxic effects of EHC-93, other minor insoluble components such as endotoxins (Table 3), metals (e.g., Fe, Al, Pb, Mg, Sn and Ti)

(Table IV – S1) and PAHs (Vincent et al., 1997b) may also add significant cytotoxicity to A549 cells. The insoluble materials in EHC-93 affected markers of inflammatory responses (Figures IV – 6 & 7) as well as cell death and proliferation in A549 cells (Figures IV – 2 & 4 and Table IV – 4). Importantly, the proteomic results in this study provided molecular details associated with the toxicity of EHC-93 and its insoluble fraction.

Conclusion

To our knowledge, this is the first study that used in tandem multiple cytotoxicity assays and proteomic analyses to assess the phenotypic outcomes and molecular mechanisms of particle toxicity of an urban air PM (i.e., EHC-93) and its insoluble and soluble fractions on human lung epithelial cells (A549). Both cytotoxicity assays and proteomic results consistently indicated that the insoluble materials explained most of the toxic effects of the total PM. Furthermore, the toxic potency of EHC-93 total is not equal to the sum of its insoluble and soluble fractions, implying inter-component interactions between insoluble and soluble materials that may be reflected through synergistic or antagonistic in vitro responses. Finally, this study demonstrated that in vitro toxicoproteomics is a valuable tool in delineating the toxicity mechanisms of environmental air particles.

Ethics approval and consent to participate

Not applicable.

Consent for publication

All authors consent to publication of this manuscript.

Availability of data and material

All data generated or analyzed during this study are included in this published article and its supplementary information files.

Competing interests

All authors declare that they have no competing interests.

Fundings

This work was supported by the Clean Air Regulatory Agenda at Health Canada (Grant # 4340565) and Ontario Graduate Scholarship in Science and Technology and Ontario Graduate Scholarship (funding for Ngoc Vuong).

Authors' contributions

Ngoc Q. Vuong: Wrote the manuscript, analyzed all data, prepared all tables and figures, and conducted most of the experimental works (e.g., cell culture, particle exposures, cytotoxicity assays, 2D-GE, MS, statistical analysis, bioinformatic analysis, pathway analysis).

Dalibor Breznan: Assisted conducting cytotoxicity assays, conducted endotoxin analysis and contributed to the writing of manuscript.

Patrick Goegan: Assisted in the preparation of 2D gels from exposed cells.

Julie S. O'Brien: Conducted physical analyses of the EHC-93 particles

Andrew Williams: Assisted in statistical analysis

Subramanian Karthikeyan: Assisted in statistical analysis

Premkumari Kumarathasan: Helped design experiments, supported data interpretation and contributed to the writing of manuscript.

Renaud Vincent: Helped design experiments, contributed to the writing of manuscript and supported data interpretation.

Acknowledgements

We would like to thank Drs. Vinita Chauhan and Pahdi Bhaja Krushna for their helpful comments.

References

Adamson IY, Prieditis H, Hedgecock C and Vincent R (2000) Zinc Is the Toxic Factor in the Lung Response to an Atmospheric Particulate Sample. Toxicol Appl Pharmacol 166:111-119.

Adamson IY, Vincent R and Bjarnason S G (1999) Cell Injury and Interstitial Inflammation in Rat Lung After Inhalation of Ozone and Urban Particulates. Am J Respir Cell Mol Biol 20:1067-1072.

Ailshire JA and Crimmins E M (2014) Fine Particulate Matter Air Pollution and Cognitive Function Among Older US Adults. Am J Epidemiol 180:359-366.

Amatullah H, North M L, Akhtar U S, Rastogi N, Urch B, Silverman F S, Chow C W, Evans G J and Scott J A (2012) Comparative Cardiopulmonary Effects of Size-Fractionated Airborne Particulate Matter. Inhal Toxicol 24:161-171.

Bell ML, Ebisu K, Leaderer B P, Gent J F, Lee H J, Koutrakis P, Wang Y, Dominici F and Peng R D (2014) Associations of PM(2).(5) Constituents and Sources With Hospital Admissions: Analysis of Four Counties in Connecticut and Massachusetts (USA) for Persons >/= 65 Years of Age. Environ Health Perspect 122:138-144.

Bouchon A, Facchetti F, Weigand M A and Colonna M (2001) TREM-1 Amplifies Inflammation and Is a Crucial Mediator of Septic Shock. Nature 410:1103-1107.

Bouthillier L, Vincent R, Goegan P, Adamson I Y, Bjarnason S, Stewart M, Guenette J, Potvin M and Kumarathasan P (1998) Acute Effects of Inhaled Urban Particles and Ozone: Lung Morphology, Macrophage Activity, and Plasma Endothelin-1. Am J Pathol 153:1873-1884.

Breznan D, Karthikeyan S, Phaneuf M, Kumarathasan P, Cakmak S, Denison M S, Brook J R and Vincent R (2016) Development of an Integrated Approach for Comparison of in Vitro and in Vivo Responses to Particulate Matter. Part Fibre Toxicol 13:41.

Brook RD, Cakmak S, Turner M C, Brook J R, Crouse D L, Peters P A, van D A, Villeneuve P J, Brion O, Jerrett M, Martin R V, Rajagopalan S, Goldberg M S, Pope C A, III and Burnett R T (2013) Long-Term Fine Particulate Matter Exposure and Mortality From Diabetes Mellitus in Canada. Diabetes Care 36:3313-20.

Burnett RT, Brook J, Dann T, Delocla C, Philips O, Cakmak S, Vincent R, Goldberg M S and Krewski D (2000) Association Between Particulate- and Gas-Phase Components of Urban Air Pollution and Daily Mortality in Eight Canadian Cities. Inhal Toxicol 12 Suppl 4:15-39.

Canova C, Dunster C, Kelly F J, Minelli C, Shah P L, Caneja C, Tumilty M K and Burney P (2012) PM10-Induced Hospital Admissions for Asthma and Chronic Obstructive Pulmonary Disease: the Modifying Effect of Individual Characteristics. Epidemiology 23:607-615.

Chauhan V, Breznan D, Thomson E, Karthikeyan S and Vincent R (2005) Effects of Ambient Air Particles on the Endothelin System in Human Pulmonary Epithelial Cells (A549). Cell Biol Toxicol 21:191-205.

Chu B, Wang J, Wang Y and Yang G (2015) Knockdown of PKM2 Induces Apoptosis and Autophagy in Human A549 Alveolar Adenocarcinoma Cells. Mol Med Rep 12:4358-4363.

Fujii T, Hayashi S, Hogg J C, Vincent R and van Eeden S F (2001) Particulate Matter Induces Cytokine Expression in Human Bronchial Epithelial Cells. Am J Respir Cell Mol Biol 25:265-271.

Gan WQ, FitzGerald J M, Carlsten C, Sadatsafavi M and Brauer M (2013) Associations of Ambient Air Pollution With Chronic Obstructive Pulmonary Disease Hospitalization and Mortality. Am J Respir Crit Care Med 187:721-727.

Gonzalez RJ and Tarloff J B (2001) Evaluation of Hepatic Subcellular Fractions for Alamar Blue and MTT Reductase Activity. Toxicol In Vitro 15:257-259.

Goodnight JH and Harvey WR. Least-Squares Means in the Fixed-Effects General Linear Models. SAS Technical Report R-103. 1978. SAS Institute Inc., SAS Technical Report. SAS Technical Report R-103.

Guan L, Rui W, Bai R, Zhang W, Zhang F and Ding W (2016) Effects of Size-Fractionated Particulate Matter on Cellular Oxidant Radical Generation in Human Bronchial Epithelial BEAS-2B Cells. Int J Environ Res Public Health 13.

Huang Q, Zhang J, Peng S, Tian M, Chen J and Shen H (2014) Effects of Water Soluble PM2.5 Extracts Exposure on Human Lung Epithelial Cells (A549): A Proteomic Study. J Appl Toxicol 34:675-687.

Huang W, Zhu T, Pan X, Hu M, Lu S E, Lin Y, Wang T, Zhang Y and Tang X (2012) Air Pollution and Autonomic and Vascular Dysfunction in Patients With Cardiovascular Disease: Interactions of Systemic Inflammation, Overweight, and Gender. Am J Epidemiol 176:117-126.

Jedrychowski WA, Perera F P, Camann D, Spengler J, Butscher M, Mroz E, Majewska R, Flak E, Jacek R and Sowa A (2014) Prenatal Exposure to Polycyclic Aromatic Hydrocarbons and Cognitive Dysfunction in Children. Environ Sci Pollut Res Int 22:3631-9.

Jiang Y, Li X, Yang W, Hawke D H, Zheng Y, Xia Y, Aldape K, Wei C, Guo F, Chen Y and Lu Z (2014) PKM2 Regulates Chromosome Segregation and Mitosis Progression of Tumor Cells. Mol Cell 53:75-87.

Julvez J, Ribas-Fito N, Torrent M, Forns M, Garcia-Esteban R and Sunyer J (2007) Maternal Smoking Habits and Cognitive Development of Children at Age 4 Years in a Population-Based Birth Cohort. Int J Epidemiol 36:825-832.

Kumarathasan P, Blais E, Saravanamuthu A, Bielecki A, Mukherjee B, Bjarnason S, Guenette J, Goegan P and Vincent R (2015) Nitrative Stress, Oxidative Stress and Plasma Endothelin Levels After Inhalation of Particulate Matter and Ozone. Part Fibre Toxicol 12:28.

Kumarathasan P, Breznan D, Das D, Salam M A, Siddiqui Y, Mackinnon-Roy C, Guan J, de S N, Simard B and Vincent R (2014) Cytotoxicity of Carbon Nanotube Variants: A Comparative in Vitro Exposure Study With A549 Epithelial and J774 Macrophage Cells. Nanotoxicology 9:148-61.

Liu L, Yu L Y, Mu H J, Xing L Y, Li Y X and Pan G W (2014) Shape of Concentration-Response Curves Between Long-Term Particulate Matter Exposure and Morbidities of Chronic Bronchitis: a Review of Epidemiological Evidence. J Thorac Dis 6:S720-S727.

MacIntyre EA, Brauer M, Melen E, Bauer C P, Bauer M, Berdel D, Bergstrom A, Brunekreef B, Chan-Yeung M, Klumper C, Fuertes E, Gehring U, Gref A, Heinrich J, Herbarth O, Kerkhof M, Koppelman G H, Kozyrskyj A L, Pershagen G, Postma D S, Thiering E, Tiesler C M and Carlsten C (2014) GSTP1 and TNF Gene Variants and Associations Between Air Pollution and Incident Childhood Asthma: the Traffic, Asthma and Genetics (TAG) Study. Environ Health Perspect 122:418-424.

Merlo F, Costantini M, Reggiardo G, Ceppi M and Puntoni R (1991) Lung Cancer Risk Among Refractory Brick Workers Exposed to Crystalline Silica: a Retrospective Cohort Study. Epidemiology 2:299-305.

Mutze K, Vierkotten S, Milosevic J, Eickelberg O and Konigshoff M (2015) Enolase 1 (ENO1) and Protein Disulfide-Isomerase Associated 3 (PDIA3) Regulate Wnt/Beta-Catenin-Driven Trans-Differentiation of Murine Alveolar Epithelial Cells. Dis Model Mech 8:877-890.

Peng RD, Dominici F, Pastor-Barriuso R, Zeger S L and Samet J M (2005) Seasonal Analyses of Air Pollution and Mortality in 100 US Cities. Am J Epidemiol 161:585-594.

Pisani C, Gaillard J C, Nouvel V, Odorico M, Armengaud J and Prat O (2015) High-Throughput, Quantitative Assessment of the Effects of Low-Dose Silica Nanoparticles on Lung Cells: Grasping Complex Toxicity With a Great Depth of Field. BMC Genomics 16:315.

Pope CA, III, Burnett R T, Krewski D, Jerrett M, Shi Y, Calle E E and Thun M J (2009) Cardiovascular Mortality and Exposure to Airborne Fine Particulate Matter and Cigarette Smoke: Shape of the Exposure-Response Relationship. Circulation 120:941-948.

Pope CA, III, Burnett R T, Turner M C, Cohen A, Krewski D, Jerrett M, Gapstur S M and Thun M J (2011) Lung Cancer and Cardiovascular Disease Mortality Associated With Ambient Air Pollution and Cigarette Smoke: Shape of the Exposure-Response Relationships. Environ Health Perspect 119:1616-1621.

Prieditis H and Adamson I Y (2002) Comparative Pulmonary Toxicity of Various Soluble Metals Found in Urban Particulate Dusts. Exp Lung Res 28:563-576.

R Core Team. R: A language and environment for statistical computing. 2013. http://www.R-project.org/.

Rao X, Patel P, Puett R and Rajagopalan S (2015) Air Pollution As a Risk Factor for Type 2 Diabetes. Toxicol Sci 143:231-241.

Reich M, Liefeld T, Gould J, Lerner J, Tamayo P and Mesirov J P (2006) GenePattern 2.0. Nat Genet 38:500-501.

Roskoski R, Jr. (2012) ERK1/2 MAP Kinases: Structure, Function, and Regulation. Pharmacol Res 66:105-143.

Sakamoto N, Hayashi S, Gosselink J, Ishii H, Ishimatsu Y, Mukae H, Hogg J C and van Eeden S F (2007) Calcium Dependent and Independent Cytokine Synthesis by Air Pollution Particle-Exposed Human Bronchial Epithelial Cells. Toxicol Appl Pharmacol 225:134-141.

Schenk M, Bouchon A, Seibold F and Mueller C (2007) TREM-1--Expressing Intestinal Macrophages Crucially Amplify Chronic Inflammation in Experimental Colitis and Inflammatory Bowel Diseases. J Clin Invest 117:3097-3106.

Schneider A, Hampel R, Ibald-Mulli A, Zareba W, Schmidt G, Schneider R, Ruckerl R, Couderc J P, Mykins B, Oberdorster G, Wolke G, Pitz M, Wichmann H E and Peters A (2010) Changes in Deceleration Capacity of Heart Rate and Heart Rate Variability Induced by Ambient Air Pollution in Individuals With Coronary Artery Disease. Part Fibre Toxicol 7:29.

Scott JA (1953) Fog and Deaths in London, December 1952. Public Health Rep 68:474-479.
Searle SR, Speed FM and Miliken GA (1980) The Population Marginal Means in the Linear Model: An Alternative to Least Squares Means. The American Statistician 34:216-221.

Siemiatycki J, Dewar R, Lakhani R, Nadon L, Richardson L and Gerin M (1989) Cancer Risks Associated With 10 Inorganic Dusts: Results From a Case-Control Study in Montreal. Am J Ind Med 16:547-567.

Snow SJ, De Vizcaya-Ruiz A, Osornio-Vargas A, Thomas R F, Schladweiler M C, McGee J and Kodavanti U P (2014) The Effect of Composition, Size, and Solubility on Acute Pulmonary Injury in Rats Following Exposure to Mexico City Ambient Particulate Matter Samples. J Toxicol Environ Health A 77:1164-1182.

Stocks P (1959) Cancer and Bronchitis Mortality in Relation to Atmospheric Deposit and Smoke. Br Med J 1:74-79.

Su MW, Tsai C H, Tung K Y, Hwang B F, Liang P H, Chiang B L, Yang Y H and Lee Y L (2013) GSTP1 Is a Hub Gene for Gene-Air Pollution Interactions on Childhood Asthma. Allergy 68:1614-1617.

Sun B, Pokhrel S, Dunphy D R, Zhang H, Ji Z, Wang X, Wang M, Liao Y P, Chang C H, Dong J, Li R, Madler L, Brinker C J, Nel A E and Xia T (2015a) Reduction of Acute Inflammatory Effects of Fumed Silica Nanoparticles in the Lung by Adjusting Silanol Display Through Calcination and Metal Doping. ACS Nano 9:9357-9372.

Sun H, Zhu A, Zhang L, Zhang J, Zhong Z and Wang F (2015b) Knockdown of PKM2 Suppresses Tumor Growth and Invasion in Lung Adenocarcinoma. Int J Mol Sci 16:24574-24587.

Suzuki Y, Imai Y, Nakayama H, Takahashi K, Takio K and Takahashi R (2001) A Serine Protease, HtrA2, Is Released From the Mitochondria and Interacts With XIAP, Inducing Cell Death. Mol Cell 8:613-621.

Thomson E, Kumarathasan P, Goegan P, Aubin R A and Vincent R (2005) Differential Regulation of the Lung Endothelin System by Urban Particulate Matter and Ozone. Toxicol Sci 88:103-113.

Thomson EM, Breznan D, Karthikeyan S, Mackinnon-Roy C, Charland J P, Dabek-Zlotorzynska E, Celo V, Kumarathasan P, Brook J R and Vincent R (2015) Cytotoxic and Inflammatory Potential of Size-Fractionated Particulate Matter Collected Repeatedly Within a Small Urban Area. Part Fibre Toxicol 12:24.

Thomson EM, Vladisavljevic D, Mohottalage S, Kumarathasan P and Vincent R (2013) Mapping Acute Systemic Effects of Inhaled Particulate Matter and Ozone: Multiorgan Gene Expression and Glucocorticoid Activity. Toxicol Sci 135:169-181.

Tonne C, Elbaz A, Beevers S and Singh-Manoux A (2014) Traffic-Related Air Pollution in Relation to Cognitive Function in Older Adults. Epidemiology 25:674-681.

Verma V, Rico-Martinez R, Kotra N, King L, Liu J, Snell T W and Weber R J (2012) Contribution of Water-Soluble and Insoluble Components and Their Hydrophobic/Hydrophilic Subfractions to the Reactive Oxygen Species-Generating Potential of Fine Ambient Aerosols. Environ Sci Technol 46:11384-11392.

Vincent R, Bjarnason S G, Adamson I Y, Hedgecock C, Kumarathasan P, Guenette J, Potvin M, Goegan P and Bouthillier L (1997a) Acute Pulmonary Toxicity of Urban Particulate Matter and Ozone. Am J Pathol 151:1563-1570.

Vincent R, Goegan P, Johnson G, Brook J R, Kumarathasan P, Bouthillier L and Burnett R T (1997b) Regulation of Promoter-CAT Stress Genes in HepG2 Cells by Suspensions of Particles From Ambient Air. Fundam Appl Toxicol 39:18-32.

Vincent R, Kumarathasan P, Goegan P, Bjarnason S G, Guenette J, Berube D, Adamson I Y, Desjardins S, Burnett R T, Miller F J and Battistini B (2001) Inhalation Toxicology of Urban Ambient Particulate Matter: Acute Cardiovascular Effects in Rats. Res Rep Health Eff Inst5-54.

Voet D and Voet J G (2010) Biochemistry, 4th Edition. Wiley, New Jersey.

Vora R, Zareba W, Utell M J, Pietropaoli A P, Chalupa D, Little E L, Oakes D, Bausch J, Wiltshire J and Frampton M W (2014) Inhalation of Ultrafine Carbon Particles Alters Heart Rate and Heart Rate Variability in People With Type 2 Diabetes. Part Fibre Toxicol 11:31.

Vuong NQ, Goegan P, De R F, Breznan D, Thomson E M, O'Brien J S, Karthikeyan S, Williams A, Vincent R and Kumarathasan P (2016a) Responses of A549 Human Lung Epithelial Cells to Cristobalite and Alpha-Quartz Exposures Assessed by Toxicoproteomics and Gene Expression Analysis. J Appl Toxicol 37:721-731.

Vuong NQ, Goegan P, Mohottalage S, Breznan D, Ariganello M, Williams A, Elisma F, Karthikeyan S, Vincent R and Kumarathasan P (2016b) Human Lung Epithelial Cell A549 Proteome Data After Treatment With Titanium Dioxide and Carbon Black. Data Brief 8:687-691.

Vuong NQ, Goegan P, Mohottalage S, Breznan D, Ariganello M, Williams A, Elisma F, Karthikeyan S, Vincent R and Kumarathasan P (2016c) Proteomic Changes in Human Lung Epithelial Cells (A549) in Response to Carbon Black and Titanium Dioxide Exposures. J Proteomics 149:53-63.

Yang W, Zheng Y, Xia Y, Ji H, Chen X, Guo F, Lyssiotis C A, Aldape K, Cantley L C and Lu Z (2012) ERK1/2-Dependent Phosphorylation and Nuclear Translocation of PKM2 Promotes the Warburg Effect. Nat Cell Biol 14:1295-1304.

Yi S, Zhang F, Qu F and Ding W (2014) Water-Insoluble Fraction of Airborne Particulate Matter (PM10) Induces Oxidative Stress in Human Lung Epithelial A549 Cells. Environ Toxicol 29:226-233.

Zanobetti A, Franklin M, Koutrakis P and Schwartz J (2009) Fine Particulate Air Pollution and Its Components in Association With Cause-Specific Emergency Admissions. Environ Health 8:58.

Zhao G, Lu H and Li C (2015) Proapoptotic Activities of Protein Disulfide Isomerase (PDI) and PDIA3 Protein, a Role of the Bcl-2 Protein Bak. J Biol Chem 290:8949-8963.

Zhou X, Zhang Y, Han N, Guo S, Xiao T, Cheng S, Gao Y and Zhang K (2013) [Alpha-Enolase (ENO1) Inhibits Epithelial-Mesenchymal Transition in the A549 Cell Lineby Suppressing ERK1/2 Phosphorylation]. Zhongguo Fei Ai Za Zhi 16:221-226.

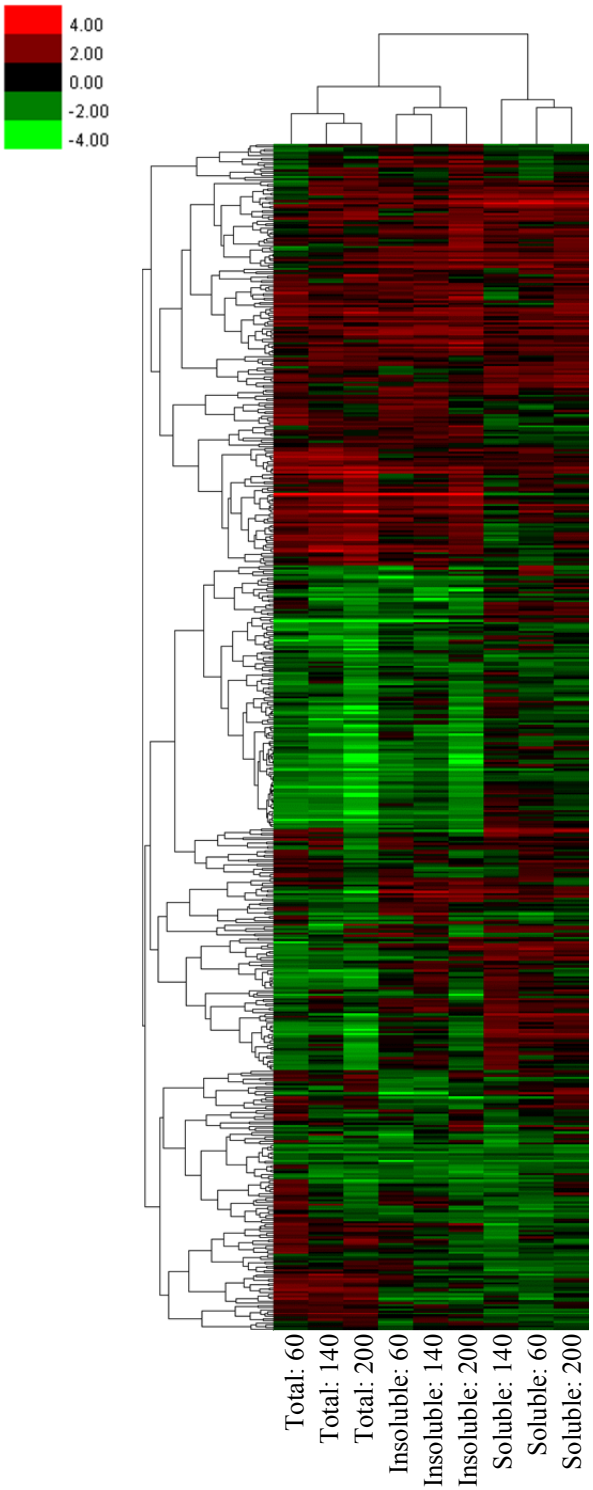

Figure IV – S1. Unsupervised hierarchical cluster analysis demonstrating the effect of all the tested particles on the proteome of A549 cells.
The expressions of all the well-defined protein spots in the 2D gels were examined. The expression of each protein spot was calculated by Log_2(Treatment/Control), n = 3. Red is coded for increased expression and green is coded for decreased expression. The number indicates the dose in μg/cm^2.

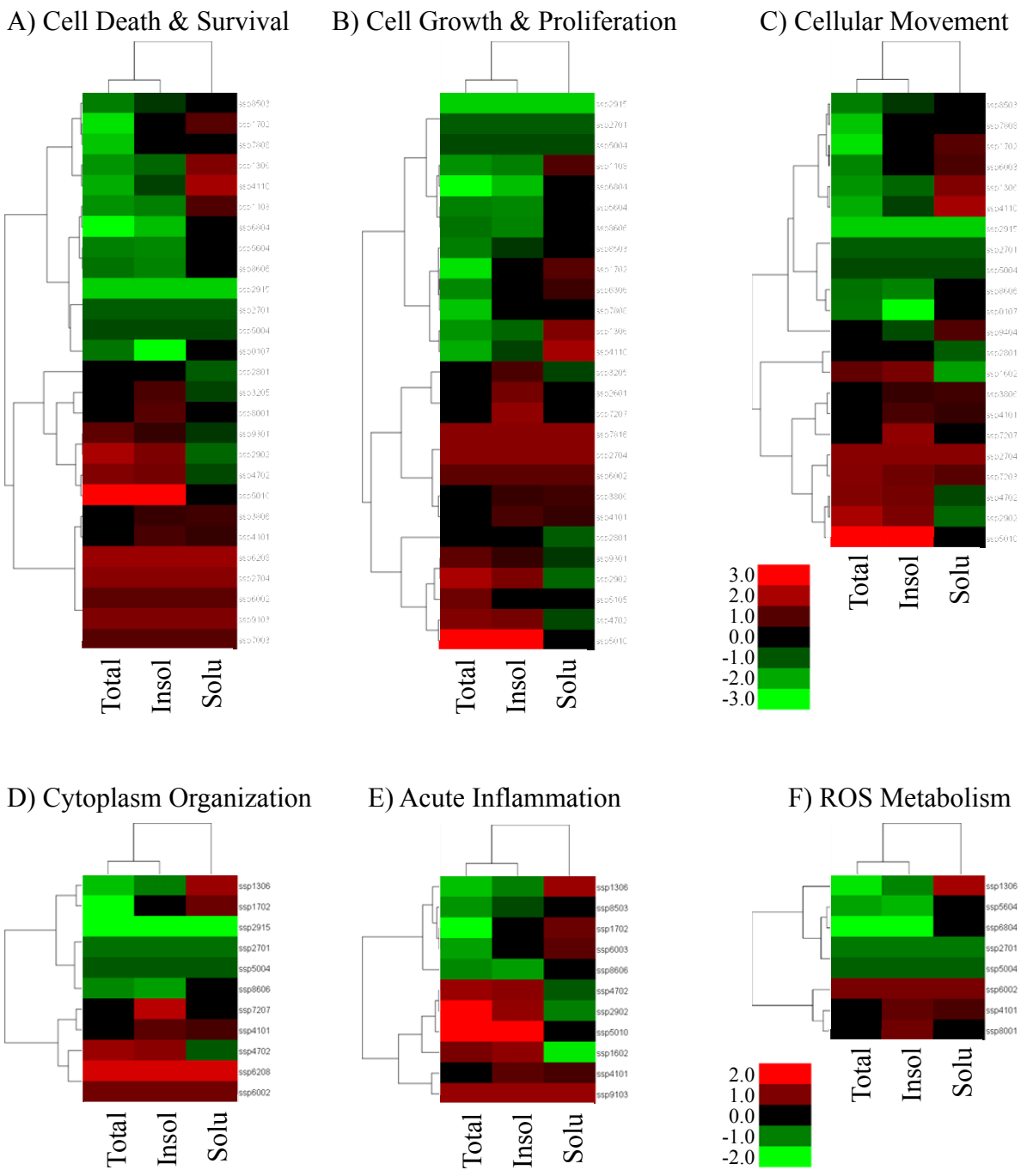

Figure IV – S2. Changes in the expression of proteins in various pathways in A549 cells that were exposed to EHC-93 total and its insoluble and soluble fractions (at 60 μg/cm^2).
These selected pathways were based on the top biological functions identified by Ingenuity Pathway Analysis (in Table IV – 4). The color scales that show fold-changes, Log_2 (Treatment/Control), were set between -3 to 3 in panels A – C and -2 to 2 in panels D – F.

Table IV – S1. Elemental content of EHC-93 and its water-insoluble and soluble fractions were examined by IPC-MS (Vincent et al., 2001).

	Total		Insoluble		Soluble	
Element	**(µg/g)**	**Mass %**	**(µg/g)**	**Mass %**	**(µg/g)**	**Mass %**
Aluminum (Al)	23,700	7.3	25,400	8.1	650	0.6
Barium (Ba)	411	0.1	470	0.1	123	0.1
Boron (B)	61	0.0	48	0.0	20	0.0
Cadmium (Cd)	23	0.0	8	0.0	16	0.0
Calcium (Ca)	122,000	37.7	114,000	36.3	65,000	64.6
Chromium (Cr)	70	0.0	71	0.0	0	0.0
Cobalt (Co)	11	0.0	9	0.0	2	0.0
Copper (Cu)	763	0.2	742	0.2	500	0.5
Iron Fe)	20,200	6.2	22,500	7.2	350	0.3
Lead (Pb)	6,780	2.1	7,210	2.3	1,500	1.5
Magnesium (Mg)	15,200	4.7	15,800	5.0	3,000	3.0
Manganese (Mn)	594	0.2	584	0.2	220	0.2
Molybdenum (Mo)	19	0.0	18	0.0	1	0.0
Nickel (Ni)	60	0.0	66	0.0	20	0.0
Silicon (Si)	95,400	29.5	112,000	35.6	0	0.0
Sodium (Na)	23,900	7.4	6,480	2.1	19,000	18.9
Strontium (Sr)	363	0.1	378	0.1	225	0.2
Tin (Sn)	1,230	0.4	1,300	0.4	25	0.0
Titanium (Ti)	1,830	0.6	2,010	0.6	10	0.0
Vanadium (V)	120	0.0	140	0.0	20	0.0
Zinc (Zn)	11,200	3.5	5,230	1.7	10,000	9.9
Total	323,935	100.0	314,464	100.0	100,682	100.0

It should be noted that the mass of each element presented did not take into account that the insoluble and soluble fractions corresponded to 83 and 17 mass % of the total.

Table IV – S2. Two-way ANOVA results for the A549 protein spots that changed significantly due to particle exposures (n = 3). The SSP number corresponds to the identifier number that PDQuest used to identify the spot based on its coordinate in the gel. The number below *Treatment* main effect (Trt), *Dose* main effect (Dose) or interaction between *Treatment and Dose* (T x D) corresponds to the *p*-value, where the bolded number emphasized *p*-value < 0.05. Only the protein spots identified by MALDI-TOF-TOF-MS/MS are provided here (Vuong et al., 2016a; Vuong et al., 2016b). The proteins indicated in red (likely degradation product of the native protein) and fold-change indicated in blue (cut-off at ±1.10) were excluded from pathway analysis. Orange colored spots were used for pathway analysis in the 60 μg/cm^2 dose. The yellow highlight shows multiple protein spots with the same protein ID. See the Materials and Methods section for more information on the protein spot selection criteria for pathway analysis.

		$ET (μg/cm^2)			$EI (μg/cm^2)			$ES (μg/cm^2)			2WayANOVA			†ET (μg/cm^2)			†EI (μg/cm^2)			†ES (μg/cm^2)			Spot	Obs/Theor	Observed		Theoretical		MOWSE
SSP	ID	60	140	200	60	140	200	60	140	200	Trt	Dose	TxD	60	140	200	60	140	200	60	140	200	Volume	MW ratio	MW	pI	MW	pI	Score
2010	ARMCX1	-10.14	-13.80	-10.44	-6.93	-9.23	-2.97	1.22	1.43	1.19	**0.000**	**0.000**	**0.000**	-10.14	-13.80	-10.44	-6.93	-9.23	-2.97				229,493	50.9%	25,040	5.6	49,150	9.3	59
8302	CCT2	-1.85	-2.55	-4.50	-1.54	-1.37	-6.14	-1.37	1.01	-1.23	**0.000**	**0.000**	**0.010**	-1.85	-2.55	-4.50			-6.14				155,115	70.1%	40,300	7.4	57,452	6.0	85
5010	TREM1	7.55	16.03	23.36	10.46	21.01	32.61	-1.94	-1.95	-1.26	**0.000**	**0.000**	**0.000**	7.55	16.03	23.36	10.46	21.01	32.61				53,697	86.4%	22,780	6.5	26,370	6.4	72
8506	ENO1	2.02	3.24	5.58	1.53	2.26	2.45	2.24	-1.40	1.05	**0.003**	**0.005**	**0.019**			5.58							83,320	105.4%	49,690	7.3	47,139	7.7	201
3104	HSP90AB3P	-2.07	-3.07	-4.93	-1.76	-1.72	-1.87	1.17	1.48	1.06	**0.000**	**0.044**	**0.027**	-2.07	-3.07	-4.93	-1.76	-1.72			1.48		231,963	47.5%	32,400	5.9	68,282	4.6	48
3705	INA	1.25	1.25	2.76	2.41	1.76	2.41	1.54	1.43	1.62	**0.019**	**0.000**	**0.013**			2.76							117,488	112.5%	62,290	5.9	55,357	5.2	302
7207	LASP1	1.23	2.96	2.78	1.95	1.68	1.62	-1.44	-1.29	1.56	**0.000**	**0.003**	**0.014**		2.96	2.78	1.95						170,775	125.1%	37,140	7.1	29,698	6.7	60
6309	METTL18	-3.76	-2.74	-1.94	-1.64	-1.28	-5.71	1.15	1.27	1.01	**0.000**	**0.042**	**0.041**	-3.76	-2.74		-1.64	-1.28	-5.71				147,958	95.2%	40,080	6.7	42,122	6.3	31
8606	PKM	-1.47	-2.19	-3.46	-1.71	-1.39	-2.67	-1.14	-1.29	-1.28	**0.000**	**0.000**	**0.009**	-1.47	-2.19	-3.46	-1.71		-2.67				664,391	97.7%	56,550	7.4	57,900	9.0	286
4108	SYNCRIP	-1.30	-1.19	-3.38	1.04	-1.01	-1.74	1.03	1.21	1.04	**0.000**	**0.000**	**0.017**			-3.38			-1.74				182,365	48.2%	33,560	6.2	69,560	9.1	65
2802	ACTG1	1.63	1.88	2.02	1.22	-1.07	-1.66	-1.43	-1.13	1.26	**0.015**	0.567	**0.022**			2.02			-1.66				409,216	160.8%	67,180	5.7	41,766	5.2	197
305	HSPA1A	1.09	-1.50	-2.40	-1.15	-1.10	-1.59	1.21	1.48	1.32	**0.004**	0.095	**0.024**			-2.40							1,357,282	59.9%	41,960	5.4	70,009	5.4	234
5701	PKM	-1.41	-1.04	-2.49	1.20	1.02	1.17	-1.01	1.17	1.05	**0.042**	0.161	**0.013**			-2.49							162,132	110.3%	63,840	6.3	57,900	9.0	73
8304	PCBP2	-1.28	-1.40	-1.44	1.20	1.06	-1.20	1.00	1.23	1.00	**0.003**	0.050	**0.016**		-1.40						1.23		228,483	109.3%	42,160	7.4	38,556	10.1	67
104	IPO4	1.02	-3.69	-1.99	-1.25	-3.49	-3.63	1.02	1.40	2.14	**0.003**	0.423	**0.033**			-1.99			-3.63			2.14	324,908	24.2%	28,730	5.3	118,640	5.1	46
3704	HNRNPK	1.03	1.28	1.95	-1.28	-1.05	1.26	1.40	-1.03	-1.16	0.353	0.175	**0.044**			1.95						-1.16	288,171	128.1%	65,250	5.9	50,944	5.3	278
9401	IDH1	1.25	1.16	1.01	-1.05	-1.15	-1.68	-1.31	-1.31	-1.00	0.421	0.218	**0.013**						-1.68				493,723	98.0%	45,700	7.5	46,630	6.6	278
8809	LMNA	1.12	1.29	2.07	1.48	1.27	-1.06	-1.24	-1.08	1.10	0.073	0.201	**0.014**			2.07							149,249	104.6%	77,530	7.4	74,095	6.6	115
8109	SEPT9	-1.93	-1.98	-5.73	-1.44	-1.24	-2.46	-1.07	-1.05	-1.18	**0.000**	**0.000**	0.290	-1.93	-1.98	-5.73	-1.44	-1.24	-2.46				180,146	49.9%	32,600	7.4	65,361	9.7	104
3009	ALDH1A1	-2.13	-2.85	-8.75	-1.52	-1.34	-6.96	-1.29	1.23	-1.29	**0.002**	**0.036**	0.632			-8.75			-6.96				167,406	47.7%	26,150	6.0	54,827	6.3	134
7608	ALDH1A1	2.78	3.71	4.82	2.52	2.96	2.36	1.17	1.08	1.60	**0.004**	**0.011**	0.273		3.71	4.82							158,569	103.0%	56,450	7.0	54,827	6.3	187
2001	ANXA1	-1.84	-1.76	-2.62	-1.12	-1.12	-1.64	-1.02	1.01	-1.06	**0.000**	**0.003**	0.083			-2.62			-1.64				1,771,082	69.6%	26,940	5.6	38,690	6.7	558
1001	ANXA1	-2.10	-1.81	-2.63	-1.39	-1.11	-1.69	-1.02	1.03	-1.05	**0.000**	**0.022**	0.296			-2.63			-1.69				613,766	69.0%	26,680	5.5	38,690	6.7	498
2106	ANXA1	3.04	3.35	3.83	2.72	1.85	2.67	1.43	1.30	1.90	**0.005**	**0.005**	0.576				2.72	1.85	2.67				177,777	72.1%	27,910	5.6	38,690	6.7	234
4109	ANXA3	-1.74	-8.44	-11.72	1.09	-2.93	-4.86	1.26	1.02	-1.12	**0.009**	**0.002**	0.285		-8.44	-11.72							156,920	89.0%	32,350	6.1	36,353	5.5	84
6502	ANXA7	-1.63	-1.79	-2.27	-1.30	1.07	-1.68	-1.16	1.12	-1.14	**0.004**	**0.049**	0.473						-1.68				302,446	92.1%	48,560	6.8	52,706	5.4	89
2007	ARMCX1	-2.35	-2.16	-5.09	-1.48	-2.53	-3.44	1.10	-1.16	-1.38	**0.000**	**0.000**	0.111	-2.35	-2.16	-5.09	-1.48	-2.53	-3.44				719,199	47.0%	23,120	5.7	49,150	9.3	68
4208	ARMCX1	-4.25	-4.64	-10.17	-2.18	-1.47	-2.83	-1.04	1.10	-1.06	**0.000**	**0.031**	0.406	-4.25	-4.64	-10.17	-2.18	-1.47	-2.83				146,949	79.8%	39,220	6.1	49,150	10.1	40
7001	C14orf166	1.14	1.49	1.50	1.00	1.19	1.32	-1.09	-1.18	-1.04	**0.000**	**0.025**	0.190			1.50			1.32				395,225	94.8%	26,600	7.0	28,051	6.2	217
3206	CIAPIN1	-1.23	-2.37	-2.14	-1.09	-3.24	-5.48	-1.19	1.08	-1.07	**0.003**	**0.035**	0.272						-5.48				163,277	118.4%	39,750	5.9	33,561	5.3	119
5604	DLST	-1.64	-2.12	-4.47	-1.78	-1.32	-2.91	-1.24	-1.18	-1.37	**0.004**	**0.001**	0.605	-1.64	-2.12	-4.47	-1.78	-1.32	-2.91				396,951	110.0%	53,600	6.5	48,724	9.9	121
2008	EEF1D	-1.36	-3.19	-6.79	-1.08	1.05	-4.12	-1.06	1.06	-1.39	**0.038**	**0.044**	0.677			-6.79			-4.12			-1.39	266,974	77.1%	23,990	5.8	31,103	4.8	111
8107	EEF2	-2.04	-1.82	-3.45	-1.23	-1.23	-2.30	-1.18	1.13	-1.30	**0.000**	**0.013**	0.685			-3.45			-2.30				413,269	29.6%	28,190	7.2	95,277	6.4	178
3203	EIF3I	-1.67	-3.31	-10.92	-1.84	-1.59	-7.48	1.03	-1.14	-1.38	**0.007**	**0.020**	0.760						-7.48				535,369	103.3%	37,700	5.9	36,479	5.3	48
9405	ENO1	-1.78	-1.43	-3.16	-1.10	1.07	-1.57	1.22	1.43	-1.14	**0.000**	**0.010**	0.254			-3.16			-1.57				704,299	92.3%	43,500	7.7	47,139	7.7	338
6201	ENO1	-2.00	-1.87	-2.09	-1.30	-1.25	-1.66	1.09	1.24	-1.19	**0.000**	**0.046**	0.250			-2.09			-1.66				420,493	84.3%	39,720	6.6	47,139	7.7	162
8504	ENO1	1.23	1.47	1.90	1.14	1.14	1.44	-1.08	-1.41	-1.24	**0.000**	**0.033**	0.064			1.90			1.44				2,108,093	107.3%	50,580	7.4	47,139	7.7	432
8503	ENO1	-1.53	-1.23	-2.04	1.01	1.09	-1.46	-1.08	1.31	-1.19	**0.004**	**0.024**	0.668	-1.60	-1.60	-1.60	-1.12	-1.12	-1.12	1.01	1.01	1.01	578,887	109.7%	51,730	7.4	47,139	7.7	237
7509	ENO1	2.24	4.58	3.38	1.52	2.19	1.38	-1.21	1.03	-1.24	**0.023**	**0.006**	0.200					2.19					193,070	107.9%	50,850	7.1	47,139	7.7	203

6010	EPHX3	-2.58	-2.86	-9.31	-1.64	-1.39	-2.63	1.14	1.30	-1.03	**0.000**	**0.020**	0.129			-9.31			-2.63				196,626	52.8%	21,600	7.0	40,882	8.7	35
7609	GART	-1.10	2.32	1.92	2.18	1.50	1.96	1.71	2.20	2.37	**0.005**	**0.001**	0.124	**-1.10**	2.32	1.92	2.18	1.50	1.96	1.71	2.20	2.37	68,884	50.0%	53,810	7.2	107,699	6.3	114
2006	CRK	-1.07	1.79	1.99	1.81	2.17	1.92	1.03	1.17	1.14	**0.038**	**0.001**	0.119		1.79	1.99		2.17	1.92		**1.17**	**1.14**	269,480	75.3%	25,470	5.8	33,810	5.3	68
2201	HSP90AA1	-2.28	-2.24	-4.13	-1.41	-1.30	-1.04	-1.20	-1.01	-1.65	**0.027**	**0.032**	0.299			-4.13							743,932	42.5%	36,000	5.6	84,607	4.8	130
1804	HSPA5	-1.91	-1.84	-2.01	-1.67	-1.44	-2.04	1.04	-1.08	-1.16	**0.009**	**0.016**	0.533						-2.04				170,968	96.7%	69,930	5.6	72,288	5.1	74
8106	HSPA8	-1.75	-1.42	-2.52	1.05	-1.01	-1.24	1.01	1.52	-1.07	**0.001**	**0.042**	0.145	-1.90	-1.90	-1.90	**-1.07**	**-1.07**	**-1.07**	**1.15**	**1.15**	**1.15**	408,038	39.6%	28,030	7.3	70,854	5.2	357
5203	IDH3A	-1.80	-1.66	-2.25	1.03	1.16	-1.38	1.15	1.32	-1.13	**0.000**	**0.029**	0.148			-2.25							583,564	100.4%	39,720	6.4	39,566	6.5	241
4303	MSN	-1.36	-1.66	-2.78	-1.46	-1.20	-2.02	-1.29	-1.22	-1.32	**0.037**	**0.000**	0.450	-1.36	-1.66	-2.78	-1.46	**-1.20**	-2.02	-1.29	**-1.22**	-1.32	1,804,595	62.9%	42,660	6.2	67,778	6.0	134
6007	AKR1C2	-2.54	-3.33	-5.58	-1.34	-1.20	-2.65	-1.29	1.10	-1.53	**0.001**	**0.014**	0.520			-5.58			-2.65				411,705	58.3%	21,400	6.7	36,712	8.5	56
3204	PDHB	1.29	1.34	1.20	1.32	1.56	1.58	1.13	-1.02	1.30	**0.030**	**0.005**	0.204				1.32	1.56	1.58				507,694	90.6%	35,530	6.0	39,208	6.2	119
5109	PGP	-2.23	-2.37	-11.19	-2.49	-1.72	-4.50	-1.07	1.07	-1.30	**0.000**	**0.000**	0.352	-2.23		-11.19	-2.49		-4.50				209,506	99.8%	33,920	6.3	33,985	5.8	80
3007	PHB	-1.14	-1.01	1.46	1.73	1.67	2.26	1.47	1.82	1.82	**0.024**	**0.019**	0.665						2.26				178,576	92.3%	27,500	6.0	29,786	5.5	257
7204	PKM	-1.86	-1.46	-2.92	-1.14	-1.16	-1.74	1.05	1.21	-1.14	**0.000**	**0.025**	0.573			-2.92			-1.74				621,084	66.1%	38,270	7.2	57,900	9.0	233
5204	PKM	-1.51	-1.48	-2.41	-1.29	-1.07	-1.53	1.16	1.12	-1.19	**0.000**	**0.012**	0.366			-2.41			-1.53				885,786	63.2%	36,570	6.5	57,900	9.0	349
6203	PKM	-1.91	-1.56	-2.93	-1.16	-1.06	-1.74	-1.00	1.15	-1.13	**0.000**	**0.022**	0.514			-2.93			-1.74				508,286	67.2%	38,890	7.0	57,900	9.0	190
5504	PKM	-1.36	-1.47	-1.67	-1.45	-1.18	-2.09	-1.09	1.01	-1.26	**0.002**	**0.011**	0.821			-1.67			-2.09				292,702	89.3%	51,710	6.5	57,900	9.0	191
5208	PKM	-2.25	1.16	-2.81	-1.90	-1.33	-2.18	-1.04	1.11	-1.66	**0.016**	**0.020**	0.828				-1.90	-1.33	-2.18				262,691	61.3%	35,510	6.3	57,900	9.0	117
8502	PLIN2	1.23	1.48	1.85	1.15	1.27	1.65	-1.15	-1.69	1.31	**0.000**	**0.000**	0.065			1.85			1.65				109,370	109.6%	52,680	7.3	48,045	6.4	140
5105	PSMB7	1.42	1.49	1.77	1.12	1.51	1.43	1.25	-1.02	1.21	**0.010**	**0.001**	0.088	1.42	1.49	1.77							585,590	94.4%	28,260	6.4	29,946	7.6	47
1508	PSMC3	1.10	1.67	1.70	1.12	1.38	1.69	1.03	1.05	-1.01	**0.024**	**0.010**	0.269						1.69				256,400	103.9%	51,070	5.5	49,172	5.1	239
1006	RBM8A	-1.09	-2.10	-4.54	-1.56	-1.41	-3.67	1.52	1.02	-1.04	**0.014**	**0.018**	0.364						-3.67				223,798	116.7%	23,200	5.6	19,877	5.4	42
7203	RGS1	1.72	2.24	1.85	1.43	1.40	1.44	1.27	1.06	1.40	**0.034**	**0.010**	0.512	1.72	2.24	1.85	1.43	1.40	1.44	1.27	**1.06**	1.40	198,141	159.7%	38,080	7.0	23,843	9.5	41
6407	SFPQ	-2.84	-1.52	-3.46	-1.54	-1.25	-1.77	1.15	1.14	1.05	**0.000**	**0.013**	0.078	-2.84		-3.46	-1.54		-1.77				120,670	62.0%	47,200	6.8	76,102	9.9	49
9503	SFPQ	-1.40	-1.25	-2.46	1.03	-1.25	-1.47	1.39	1.28	1.12	**0.000**	**0.039**	0.164	-1.40	-1.25	-2.46				1.39	1.28	**1.12**	561,886	64.9%	49,370	7.6	76,102	9.9	305
3201	TUBB	-1.54	-2.27	-2.58	-1.27	-1.24	-2.08	-1.17	1.11	-1.19	**0.000**	**0.001**	0.067	-1.54	-2.27	-2.58	-1.27	**-1.24**	-2.08				2,149,465	70.5%	35,010	5.9	49,639	4.6	413
5201	TUBB	-1.54	-1.44	-1.86	-1.17	-1.23	-1.57	1.10	1.19	-1.00	**0.000**	**0.006**	0.075			-1.86			-1.57				315,588	79.0%	39,220	6.3	49,639	4.6	303
4102	VCP	-1.69	-1.51	-2.71	-1.29	-1.24	-1.47	-1.09	-1.05	-1.03	**0.000**	**0.002**	0.096	-1.69	-1.51	-2.71	-1.29	**-1.24**	-1.47				1,048,678	37.8%	33,700	6.1	89,266	5.0	204
1706	VCP	-1.61	-2.05	-3.28	-1.40	-1.27	-2.21	1.05	1.08	-1.08	**0.002**	**0.001**	0.089			-3.28			-2.21				680,342	72.1%	64,320	5.5	89,266	5.0	374
107	YWHAE	-1.53	-1.57	-3.06	-8.07	-2.08	-2.68	-1.21	-1.25	-1.23	**0.003**	**0.005**	0.222	-1.53	-1.57	-3.06	-8.07	-2.08	-2.68				231,369	105.1%	30,640	5.4	29,155	4.5	94
7304	ACAT2	-1.38	-1.35	-2.46	-1.24	1.09	-1.03	1.25	1.65	1.26	**0.000**	0.186	0.096	-1.73	-1.73	-1.73	**-1.06**	**-1.06**	**-1.06**	1.39	1.39	1.39	159,527	100.5%	41,540	7.0	41,324	6.5	55
1306	ACTB	-2.23	-1.45	-2.33	-2.37	-1.07	1.29	1.22	1.86	1.87	**0.001**	0.153	0.140	-2.00	-2.00	-2.00	-1.38	-1.38	-1.38	1.65	1.65	1.65	259,237	101.8%	42,460	5.5	41,710	5.5	111
1702	ACTN4	-3.01	-2.46	-4.38	-1.06	1.36	-1.02	1.19	1.58	1.02	**0.001**	0.271	0.192	-3.28	-3.28	-3.28	**1.09**	**1.09**	**1.09**	1.26	1.26	1.26	290,581	59.2%	62,060	5.4	104,788	5.2	293
2005	ANXA1	-1.22	1.01	-1.14	1.25	1.15	-1.23	1.04	1.22	1.07	**0.006**	0.380	0.647				**1.06**	**1.06**	**1.06**	**1.11**	**1.11**	**1.11**	483,661	70.4%	27,240	5.8	38,690	6.7	434
6106	ANXA1	-1.04	-1.20	-1.48	-1.02	1.13	-1.39	-1.04	1.17	1.05	**0.028**	0.471	0.822				**-1.09**	**-1.09**	**-1.09**	**1.06**	**1.06**	**1.06**	177,548	82.9%	32,070	6.7	38,690	6.7	297
8108	ARMCX1	-2.41	-2.36	-7.73	-1.11	1.24	-1.93	1.62	2.17	1.27	**0.000**	0.092	0.066	-4.17	-4.17	-4.17	-1.27	-1.27	-1.27	1.69	1.69	1.69	126,891	58.0%	28,490	7.4	49,150	10.1	39
6111	MRS2	-1.79	1.09	-2.73	1.05	1.01	-1.51	1.49	1.57	1.51	**0.000**	0.103	0.059	-1.81	-1.81	-1.81	**-1.15**	**-1.15**	**-1.15**	1.52	1.52	1.52	113,234	57.8%	29,080	6.8	50,285	6.2	66
7008	ATP5A1	-1.39	-1.27	-1.12	1.18	1.19	1.09	1.14	1.36	1.06	**0.017**	0.803	0.642	-1.26	-1.26	-1.26				**1.19**	**1.19**	**1.19**	203,990	40.8%	24,390	7.2	59,714	9.6	170
5205	AUH	-1.74	-1.75	-1.68	-1.21	-1.20	-1.05	1.60	1.30	1.23	**0.001**	0.826	0.129	-1.72	-1.72	-1.72	**-1.15**	**-1.15**	**-1.15**	1.38	1.38	1.38	237,214	112.0%	39,870	6.5	35,586	10.2	31
9301	BUB3	1.29	1.34	1.33	-1.02	1.04	1.30	-1.10	-1.24	-1.00	**0.003**	0.192	0.401	1.32	1.32	1.32	**1.11**	**1.11**	**1.11**	**-1.12**	**-1.12**	**-1.12**	221,901	112.8%	41,880	7.5	37,131	6.4	96
1108	C1QTNF9B	-1.91	-1.93	-2.04	-2.20	-1.56	-1.11	1.08	1.22	1.37	**0.008**	0.414	0.531	-1.96	-1.96	-1.96	-1.62	-1.62	-1.62	**1.22**	**1.22**	**1.22**	217,430	86.8%	30,100	5.5	34,691	9.1	37
4202	CAPZA2	1.13	-1.09	1.58	-1.36	1.10	-1.36	-1.52	-1.32	-1.26	**0.034**	0.712	0.323	**1.21**	**1.21**	**1.21**				-1.37	-1.37	-1.37	225,841	106.9%	35,190	6.2	32,929	5.5	300
5008	CYB5R3	1.09	1.60	1.65	1.22	1.25	1.39	-1.22	-1.27	-1.08	**0.023**	0.093	0.196	1.45	1.45	1.45				**-1.19**	**-1.19**	**-1.19**	296,740	71.8%	24,580	6.4	34,213	7.9	47
1011	DLST	-1.36	1.42	-1.78	-1.04	-1.07	-1.42	1.60	1.91	1.54	**0.002**	0.227	0.490	**-1.24**	**-1.24**	**-1.24**	**-1.18**	**-1.18**	**-1.18**	1.68	1.68	1.68	149,091	46.0%	22,400	5.5	48,724	9.9	83
7107	ECH1	1.46	1.60	1.25	1.34	1.16	1.10	1.06	1.12	1.19	**0.044**	0.082	0.570				**1.20**	**1.20**	**1.20**	**1.13**	**1.13**	**1.13**	196,345	89.4%	32,010	7.2	35,793	9.2	279
6304	EEF2	-1.17	-1.30	-2.45	-1.10	-1.18	-1.98	1.08	1.12	1.09	**0.002**	0.053	0.369	-1.64	-1.64	-1.64	-1.42	-1.42	-1.42	**1.10**	**1.10**	**1.10**	688,440	43.6%	41,560	6.9	95,277	6.4	129
3205	EIF3I	1.05	1.06	1.15	1.18	1.12	1.26	-1.19	-1.20	-1.08	**0.003**	0.401	0.548				**1.19**	**1.19**	**1.19**	**-1.16**	**-1.16**	**-1.16**	804,804	102.4%	37,360	6.0	36,479	5.3	420
7205	ENO1	-1.35	-1.30	-2.93	-1.03	1.05	-1.06	1.12	1.52	1.07	**0.001**	0.216	0.368	-1.86	-1.86	-1.86	**-1.01**	**-1.01**	**-1.01**	**1.24**	**1.24**	**1.24**	219,034	84.7%	39,930	7.1	47,139	7.7	125
1008	GLRX3	-1.51	-2.64	-1.33	1.09	-1.04	-1.70	1.30	1.34	1.36	**0.001**	0.727	0.076	-1.82	-1.82	-1.82	**-1.22**	**-1.22**	**-1.22**	1.34	1.34	1.34	290,884	67.1%	25,110	5.5	37,408	5.2	39
9004	HNRNPA1L2	-2.29	-1.83	-7.04	3.13	3.68	2.18	1.11	2.24	1.47	**0.022**	0.391	0.384	-3.72	-3.72	-3.72	3.00	3.00	3.00	1.61	1.61	1.61	133,772	61.7%	21,090	7.5	34,204	9.6	56
7005	HNRNPH1	-1.26	1.00	-1.47	1.04	-1.09	-1.22	1.10	1.13	-1.03	**0.001**	0.087	0.558	**-1.24**	**-1.24**	**-1.24**	**-1.09**	**-1.09**	**-1.09**	**1.07**	**1.07**	**1.07**	1,391,050	51.6%	25,410	7.2	49,198	5.9	389
8002	HSPA1A	-2.14	-2.07	-3.43	1.10	-1.03	-1.64	1.03	1.43	1.14	**0.000**	0.169	0.098	-2.55	-2.55	-2.55	**-1.19**	**-1.19**	**-1.19**	**1.20**	**1.20**	**1.20**	253,850	39.2%	27,470	7.3	70,009	5.4	318
3806	HSPA1A	2.32	2.40	1.72	-1.13	1.22	1.26	1.14	1.11	1.18	**0.043**	0.235	0.410				**1.12**	**1.12**	**1.12**	**1.14**	**1.14**	**1.14**	200,887	98.0%	68,580	5.9	70,009	5.5	82
301	HSPA2	-2.00	-1.79	-2.80	1.10	-1.39	-1.82	1.04	1.23	-1.11	**0.033**	0.145	0.496	-2.20	-2.20	-2.20				**1.05**	**1.05**	**1.05**	246,403	60.7%	42,470	5.3	69,978	5.4	124
7102	HSPA5	-1.26	-1.07	-1.38	1.06	1.01	-1.17	1.44	1.34	1.21	**0.001**	0.278	0.247	**-1.24**	**-1.24**	**-1.24**	**-1.03**	**-1.03**	**-1.03**	1.33	1.33	1.33	538,874	42.3%	30,590	7.0	72,288	4.9	287

102	HSPA5	-1.66	-1.15	-1.54	1.30	1.10	1.35	1.43	1.80	1.41	**0.007**	0.642	0.322	-1.45	-1.45	-1.45	1.25	1.25	1.25	1.54	1.54	1.54	276,531	40.1%	28,970	5.4	72,288	4.9	157
2801	HSPA8	1.36	1.08	1.06	1.02	1.06	1.03	-1.08	-1.56	-1.24	**0.021**	0.622	0.713				**1.04**	**1.04**	**1.04**	-1.29	-1.29	-1.29	231,884	103.2%	73,090	5.6	70,854	5.2	166
6804	HSPA9	-6.53	-5.08	-6.09	-2.72	-2.26	-3.42	-1.08	1.24	-1.32	**0.000**	0.054	0.388	-5.90	-5.90	-5.90	-2.80	-2.80	-2.80	**-1.05**	**-1.05**	**-1.05**	189,640	99.2%	73,020	6.8	73,635	5.8	69
1711	HSPA9	-1.13	1.09	-1.16	1.22	1.39	-1.72	1.45	1.71	1.29	**0.008**	0.101	0.670	**-1.07**	**-1.07**	**-1.07**	**-1.04**	**-1.04**	**-1.04**	1.48	1.48	1.48	177,004	86.7%	63,870	5.6	73,635	5.8	222
8117	IDH1	-1.78	-1.07	-1.80	1.09	1.20	-1.37	-1.02	1.43	-1.03	**0.009**	0.126	0.823	-1.55	-1.55	-1.55	**-1.03**	**-1.03**	**-1.03**	**1.13**	**1.13**	**1.13**	207,072	65.9%	30,730	7.2	46,630	6.6	119
4304	IDH3A	-1.58	-2.08	-2.48	-1.12	-1.02	-1.41	-1.01	1.23	-1.27	**0.019**	0.188	0.622	-2.04	-2.04	-2.04	**-1.19**	**-1.19**	**-1.19**	**-1.02**	**-1.02**	**-1.02**	254,496	101.7%	40,230	6.2	39,566	6.5	126
1009	JARID2	-1.44	-4.05	-2.75	-1.48	-1.54	-1.37	1.24	1.24	-1.02	**0.006**	0.136	0.189	-2.75	-2.75	-2.75	-1.47	-1.47	-1.47	**1.15**	**1.15**	**1.15**	280,001	18.7%	25,970	5.5	138,648	10.2	50
2601	KRT7	1.34	1.01	-1.12	2.05	1.30	1.19	1.05	1.52	1.08	**0.037**	0.200	0.430	**1.08**	**1.08**	**1.08**	1.51	1.51	1.51				191,581	108.2%	55,540	5.6	51,354	5.3	111
7808	LMNA	-2.05	-3.86	-2.80	-1.12	-2.29	-1.70	-1.06	1.22	-1.06	**0.005**	0.160	0.363	-2.90	-2.90	-2.90				**1.03**	**1.03**	**1.03**	142,552	102.8%	76,150	7.0	74,095	6.6	55
7302	NONO	-1.25	-1.08	-1.58	1.04	-1.02	-1.18	1.23	1.16	1.21	**0.000**	0.417	0.199	-1.30	-1.30	-1.30	**-1.05**	**-1.05**	**-1.05**	**1.20**	**1.20**	**1.20**	613,065	77.0%	41,720	7.1	54,197	9.6	104
7211	OSBPL8	-1.49	-1.01	-1.99	-1.06	1.11	-1.29	1.17	1.52	1.02	**0.000**	0.088	0.775	-1.50	-1.50	-1.50	**-1.08**	**-1.08**	**-1.08**	**1.24**	**1.24**	**1.24**	141,140	35.6%	36,020	7.1	101,132	6.5	54
4702	PDIA3	1.92	1.46	1.59	1.45	1.38	1.66	1.05	-1.23	-1.32	**0.001**	0.128	0.444	1.66	1.66	1.66	1.50	1.50	1.50	**-1.17**	**-1.17**	**-1.17**	535,433	105.0%	59,590	6.2	56,747	5.9	264
8110	PDIA3	-1.84	-1.76	-2.97	1.09	1.00	-1.59	1.39	1.90	1.25	**0.002**	0.516	0.568	-2.19	-2.19	-2.19	**-1.17**	**-1.17**	**-1.17**	1.51	1.51	1.51	177,911	52.2%	29,620	7.3	56,747	5.9	91
6306	PGK1	-1.93	-1.31	-2.16	1.05	1.25	-1.24	1.06	1.31	1.03	**0.003**	0.099	0.423	-1.80	-1.80	-1.80	**1.02**	**1.02**	**1.02**	**1.13**	**1.13**	**1.13**	323,291	91.1%	40,600	7.0	44,586	9.2	275
5207	PGK1	-1.93	-1.48	-2.23	1.00	1.41	-1.22	1.20	1.55	-1.12	**0.004**	0.156	0.577	-1.88	-1.88	-1.88	**1.06**	**1.06**	**1.06**	**1.21**	**1.21**	**1.21**	140,379	88.4%	39,430	6.6	44,586	9.2	108
4101	PHB	1.04	1.10	1.04	1.11	1.17	1.25	1.16	1.05	1.13	**0.024**	0.428	0.917				**1.18**	**1.18**	**1.18**	**1.11**	**1.11**	**1.11**	1,520,426	95.8%	28,540	6.0	29,786	5.6	775
206	PHB	1.59	1.62	1.84	1.78	1.02	1.42	1.29	1.10	1.10	**0.035**	0.066	0.546				1.40	1.40	1.40	**1.16**	**1.16**	**1.16**	714,153	131.4%	39,150	5.4	29,786	5.5	370
5003	PKM	-1.62	-1.86	-3.03	-1.28	-1.09	-1.95	1.08	1.16	-1.06	**0.000**	0.051	0.425	-2.17	-2.17	-2.17	-1.44	-1.44	-1.44	**1.06**	**1.06**	**1.06**	449,384	45.8%	26,540	6.5	57,900	9.0	177
6605	PKM	-1.78	-2.15	-4.20	-1.40	-1.27	-2.54	-1.27	-1.08	1.36	**0.004**	0.336	0.228	-2.71	-2.71	-2.71	-1.73	-1.73	-1.73	**1.01**	**1.01**	**1.01**	520,191	95.0%	55,020	6.9	57,900	9.0	335
5904	PNMA6A	-1.46	-1.70	-2.92	-2.48	-1.49	-3.60	1.33	1.15	1.05	**0.009**	0.190	0.558				-2.53	-2.53	-2.53	**1.18**	**1.18**	**1.18**	135,164	187.9%	82,390	6.4	43,847	5.1	43
7904	PPP1R7	1.05	-1.22	-1.47	-1.18	-1.44	-1.41	1.38	1.20	1.29	**0.000**	0.143	0.122	**-1.21**	**-1.21**	**-1.21**	-1.34	-1.34	-1.34	1.29	1.29	1.29	226,167	203.6%	84,560	7.1	41,539	10.1	58
5507	SDHAF1	-1.47	-2.02	-5.25	-1.96	-1.10	-3.71	1.05	-1.08	1.08	**0.009**	0.059	0.246	-2.91	-2.91	-2.91	-2.26	-2.26	-2.26	**1.02**	**1.02**	**1.02**	124,954	397.2%	50,840	6.5	12,799	12.0	45
8507	SFPQ	-1.93	-1.61	-2.21	-1.63	-1.19	-1.72	1.13	1.29	1.02	**0.000**	0.066	0.317	-1.92	-1.92	-1.92	-1.51	-1.51	-1.51	**1.15**	**1.15**	**1.15**	186,216	64.3%	48,930	7.3	76,102	9.9	113
4110	SRSF1	-1.08	-1.87	-4.59	-1.10	-1.33	-1.01	2.39	2.42	2.28	**0.001**	0.730	0.225	-2.51	-2.51	-2.51	**-1.15**	**-1.15**	**-1.15**	2.36	2.36	2.36	129,112	121.9%	33,810	6.0	27,728	10.8	91
6003	TPI1	-1.66	-1.43	-2.10	-1.13	1.19	-1.34	1.19	1.27	1.10	**0.001**	0.155	0.304	-1.73	-1.73	-1.73	**-1.09**	**-1.09**	**-1.09**	**1.19**	**1.19**	**1.19**	1,117,908	83.8%	25,800	6.8	30,772	5.6	266
8007	TPI1	-1.33	-1.32	-2.41	-1.11	-1.91	-2.31	-1.14	1.08	-1.08	**0.023**	0.063	0.419	-1.69	-1.69	-1.69				**-1.05**	**-1.05**	**-1.05**	167,408	88.5%	27,230	7.4	30,772	5.6	60
1602	TUBA1C	1.69	1.03	1.26	1.52	1.15	1.97	-1.42	-3.79	-1.45	**0.006**	0.235	0.543	1.33	1.33	1.33	1.55	1.55	1.55	-2.22	-2.22	-2.22	1,663,093	114.6%	57,160	5.5	49,863	4.8	425
113	TUBB	-1.88	-1.62	-2.02	-1.14	-1.20	-1.65	1.02	1.39	1.36	**0.002**	0.554	0.267	-1.84	-1.84	-1.84	-1.33	-1.33	-1.33	1.26	1.26	1.26	361,526	63.2%	31,390	5.4	49,639	4.6	252
6101	TUFM	-1.10	-1.20	-1.73	1.14	1.24	-1.17	1.28	1.45	1.35	**0.021**	0.200	0.213	-1.35	-1.35	-1.35	**1.07**	**1.07**	**1.07**	1.36	1.36	1.36	310,204	64.1%	31,760	6.7	49,510	7.9	462
7214	UFD1L	-1.63	-1.75	-9.79	-1.04	-1.35	-1.16	1.16	1.48	-1.29	**0.002**	0.133	0.303	-4.39	-4.39	-4.39	**-1.18**	**-1.18**	**-1.18**	**1.12**	**1.12**	**1.12**	118,902	115.2%	39,730	7.2	34,478	6.3	206
9404	UGDH	-1.49	-1.23	1.26	-1.07	1.15	-1.66	1.40	1.48	-1.22	**0.049**	0.780	0.340				**-1.19**	**-1.19**	**-1.19**	**1.22**	**1.22**	**1.22**	254,675	81.8%	44,970	7.6	54,989	6.9	330
8001	UQCRFS1	1.08	1.03	1.26	1.39	1.13	1.24	1.04	1.09	1.12	**0.039**	0.074	0.505				1.25	1.25	1.25	**1.08**	**1.08**	**1.08**	600,541	86.2%	25,560	7.3	29,649	9.4	162
2902	VCP	1.93	2.32	3.04	1.32	1.47	1.99	-1.22	-1.79	-1.13	**0.002**	0.051	0.302	2.43	2.43	2.43	1.59	1.59	1.59	-1.38	-1.38	-1.38	185,353	107.2%	95,730	5.6	89,266	5.0	124
7607	ALDH1A1	-1.00	-1.93	-2.21	-1.40	-1.50	-3.44	-1.22	-1.90	-1.39	0.720	**0.008**	0.703		-1.78	-2.35		-1.78	-2.35		-1.78	-2.35	10,928,604	100.5%	55,080	7.2	54,827	6.3	271
7816	CSTF2	1.03	1.23	1.86	2.73	2.22	2.15	1.60	-1.02	1.77	0.513	**0.019**	0.316	1.78		1.93	1.78		1.93	1.78		1.93	246,739	112.3%	68,440	7.1	60,920	6.4	85
9502	DIS3L	-1.14	-1.14	-2.07	-1.25	-1.37	-2.42	-1.19	1.00	-1.21	0.092	**0.007**	0.690			-1.90			-1.90			-1.90	490,554	44.3%	53,480	7.6	120,711	6.1	53
6001	ECHS1	1.23	1.29	1.55	1.28	1.14	1.31	1.27	1.01	1.18	0.135	**0.017**	0.694	1.26		1.35	1.26		1.35	1.26		1.35	757,526	87.9%	27,570	6.6	31,367	8.3	221
3505	EZR	-1.45	-1.55	-2.89	-1.01	-1.04	-1.58	-1.17	-1.28	-1.21	0.050	**0.001**	0.206		-1.29	-1.89		-1.29	-1.89		-1.29	-1.89	2,080,083	71.7%	49,710	6.0	69,370	5.9	156
8811	GMPS	-1.13	-1.14	-1.33	-1.11	-1.28	-1.67	-1.18	-1.13	-1.30	0.309	**0.021**	0.966			-1.44			-1.44			-1.44	385,935	98.2%	75,270	7.4	76,667	6.4	475
207	HNRNPC	1.19	1.39	1.42	1.06	1.10	1.91	1.15	1.31	1.69	0.736	**0.050**	0.936			1.67			1.67			1.67	519,104	118.6%	39,920	5.4	33,650	5.0	115
3707	HNRNPK	1.11	-1.42	-1.36	-1.21	-1.36	-2.03	-1.35	-1.66	-1.23	0.495	**0.013**	0.432		-1.48	-1.54		-1.48	-1.54		-1.48	-1.54	873,963	127.1%	64,770	5.9	50,944	5.3	135
2701	HNRNPK	-1.44	-1.29	-1.46	-1.12	-1.34	-1.39	-1.32	-1.57	-1.55	0.493	**0.030**	0.966	-1.29	-1.40	-1.47	-1.29	-1.40	-1.47	-1.29	-1.40	-1.47	1,039,838	129.4%	65,930	5.6	50,944	5.4	196
2915	HSP90AA1	-4.31	-3.72	-5.58	-2.72	-2.88	-4.59	-2.07	-1.84	1.02	0.080	**0.011**	0.607	-3.03	-2.81	-3.38	-3.03	-2.81	-3.38	-3.03	-2.81	-3.38	219,580	107.3%	90,760	5.8	84,607	4.8	175
2206	HSP90AB1	-2.40	-2.71	-3.19	-3.01	-2.82	-2.43	-1.43	-1.55	-2.31	0.135	**0.011**	0.984	-2.28	-2.36	-2.65	-2.28	-2.36	-2.65	-2.28	-2.36	-2.65	216,453	45.5%	37,900	5.8	83,212	4.8	89
401	HSPA8	-1.98	-1.62	-3.13	-1.10	-1.28	-1.37	-1.32	-1.06	-1.61	0.313	**0.028**	0.754			-2.04			-2.04			-2.04	1,196,183	61.3%	43,430	5.2	70,854	5.2	420
5004	HSPB1	-1.11	-1.18	-1.14	-1.22	-1.14	-1.12	-1.21	-1.39	-1.19	0.507	**0.022**	0.878	**-1.18**	**-1.24**	**-1.15**	**-1.18**	**-1.24**	**-1.15**	**-1.18**	**-1.24**	**-1.15**	2,997,085	117.3%	26,710	6.6	22,768	6.0	446
6011	HSPB1	-2.63	-1.30	-4.24	-3.28	-1.17	-1.62	-1.14	-1.17	-1.70	0.076	**0.033**	0.707	-2.35		-2.52	-2.35		-2.52	-2.35		-2.52	164,719	117.8%	26,810	6.7	22,768	6.0	79
2704	HSPD1	1.17	1.23	1.48	2.42	2.25	2.65	1.68	1.36	1.74	0.631	**0.009**	0.786	1.76	1.61	1.95	1.76	1.61	1.95	1.76	1.61	1.95	5,804,994	99.2%	60,500	5.7	61,016	5.6	305
6208	HTRA2	1.30	1.38	1.83	2.14	2.06	3.86	2.95	2.62	2.71	0.707	**0.001**	0.452	2.13	2.02	2.80	2.13	2.02	2.80	2.13	2.02	2.80	134,109	73.5%	35,870	6.8	48,811	10.5	125
9207	METTL18	-1.36	-1.15	-1.21	-1.27	-1.33	-1.21	-1.11	-1.14	-1.28	0.796	**0.050**	0.871		**-1.21**	**-1.23**		**-1.21**	**-1.23**		**-1.21**	**-1.23**	639,668	83.4%	35,110	7.6	42,122	6.3	38
7202	MRPS22	-1.05	1.12	-1.03	1.29	1.31	1.73	1.33	1.37	1.38	0.713	**0.039**	0.261			1.36			1.36			1.36	363,309	95.7%	39,470	7.0	41,254	8.7	358
8303	NANS	-1.14	-1.02	-1.58	-1.20	-1.01	-1.42	-1.21	-1.13	-1.12	0.130	**0.009**	0.545			-1.37			-1.37			-1.37	188,709	101.4%	40,860	7.4	40,281	6.3	127
1101	NCAPD3	1.01	-1.43	-1.80	1.07	-1.09	-3.14	-1.12	1.28	-1.48	0.555	**0.012**	0.526			-2.14			-2.14			-2.14	523,714	19.3%	32,550	5.5	168,783	8.0	39
2809	NDUFS1	-1.17	1.06	1.29	1.49	1.64	1.87	1.30	1.65	1.48	0.756	**0.043**	0.779			1.55			1.55			1.55	143,988	98.0%	77,820	5.8	79,417	5.8	73

5006	NDUFV2	1.03	1.67	1.39	1.20	1.29	1.73	1.47	1.17	1.37	0.323	**0.006**	0.115		1.38	1.50		1.38	1.50		1.38	1.50	258,970	92.0%	25,190	6.5	27,374	9.2	181
3101	OFD1	-1.36	-1.88	-2.86	1.14	-1.28	-1.94	-1.42	1.10	-1.52	0.555	**0.006**	0.245			-2.11			-2.11			-2.11	592,406	26.1%	30,460	5.9	116,599	5.8	61
8204	PDLIM1	-1.35	-1.14	-1.70	-1.24	-1.37	-1.36	-1.23	-1.28	-1.44	0.592	**0.033**	0.961			-1.50			-1.50			-1.50	2,901,166	103.9%	37,460	7.4	36,049	6.6	101
6002	PRDX3	1.31	1.11	1.35	1.28	1.21	1.39	1.27	1.04	1.28	0.062	**0.022**	0.993	1.29		1.34	1.29		1.34	1.29		1.34	1,082,225	90.5%	25,050	6.7	27,675	7.7	247
7003	PSMA6	1.33	1.31	1.16	1.47	1.29	1.22	1.02	-1.09	1.25	0.096	**0.042**	0.188	1.27			1.27			1.27			564,995	99.3%	27,200	7.1	27,382	6.4	328
5704	SF3B1	-1.20	-1.23	-2.29	-1.01	-1.28	-1.20	1.08	-1.06	-1.13	0.062	**0.008**	0.236			-1.54			-1.54			-1.54	328,062	43.5%	63,350	6.4	145,738	6.7	92
9103	VDAC2	1.60	1.86	2.39	1.36	1.55	1.51	1.88	1.75	1.41	0.177	**0.003**	0.354	1.62	1.72	1.77	1.62	1.72	1.77	1.62	1.72	1.77	221,772	103.7%	32,730	7.6	31,547	8.7	175

§ Spot volume intensity normalized to the control (n = 3).

† Significant change in protein expression identified by multiple comparison based on Holm-Sidak method (see Materials and Methods), which was used for pathway analysis, and the blank entries imply non-significant changes as compared to the control (i.e., fold-change = 1.0). Those protein spots with *p*-value < 0.05 (based on Two-way ANOVA) but did not pass Holm-Sidak test were excluded.

Table IV – S3. Top cellular functions in which the proteins in various clusters (in Figure IV – 3) were involved based on IPA.
Only those functions that were significantly ($p < 0.05$) influenced by more than 5 proteins were presented.

Cluster	**Cellular Function**
Cluster I	Cellular Movement
	Cellular Growth and Proliferation
	Cell Death and Survival
	Molecular Transport
	Small Molecule Biochemistry
Cluster II	*Too few protein available for analysis
Cluster III	Cellular Movement
	Carbohydrate Metabolism
	Cellular Growth and Proliferation
	Cell Death and Survival
	Cell Morphology
Cluster IV	Lipid Metabolism
	Small Molecule Biochemistry
	Cellular Growth and Proliferation
Cluster V	Cell Morphology
	Cellular Function and Maintenance
	Cellular Assembly and Organization
	Cell Death and Survival

Chapter V. Discussion

V.1. Overview

There is an association between particle composition in ambient air particulate matter (PM) and adverse health effects (Burnett et al., 2000; Dockery et al., 1993; Scott, 1953). In order to develop regulatory measures to reduce the negative impact of air pollution, it is necessary to disentangle the driver(s) of toxic potency in ambient air particles and identify their mechanisms of effects. However, such a task is challenging, because PM composition in different environments varies, depending on the local sources of release (Vincent et al., 1997b). In attempt to assess the toxic effects of different components in ambient air PM via *in vitro* models, earlier studies in our laboratory fractionated Ottawa urban air particles (EHC-93) into water-insoluble and water-soluble fractions, and used A549 cells to examine the PM exposure-related effects on a few selected genes and/or proteins of targeted pathways (Chauhan et al., 2005; Thomson et al., 2015; Thomson et al., 2016). As a continuing effort to our previous studies, my Ph.D. research project focuses on integrating multiple cytotoxicity assays and untargeted shotgun proteomic analyses to gain insight into toxicity mechanisms underlying total and fractionated PM exposure-related changes in A549 cells.

The work conducted in this Ph.D. thesis investigated the impact of EHC-93 (total) and its insoluble and soluble fractions and several occupational health-relevant particles, such as titanium dioxide (TiO_2), carbon black (CB), cristobalite (CR) and α–quartz (MI: Min-U-Sil 5), on A549 cells, in three separate studies (Chapters II – IV). It should be noted that A549 cells were exposed to these particles at the same time (i.e., blocked together) when cytotoxicity assays and proteomic experiments were conducted. This experimental set up

allowed all of these particles to be appropriately analyzed as individuals, pairs or groups. The differential effects of TiO_2 and CB (Chapter IIa,b), CR and MI (Chapter III), EHC-93 (total) and its insoluble and soluble fractions (Chapter IV) have already been discussed in detail in three separate research manuscripts. This discussion section focuses mainly on comparing the toxic effects of EHC-93 and its sub-fractions against the occupational health-relevant particles based on the published/submitted cytotoxicity assays and proteomic data.

V.2. Contrasting cytotoxic potencies of the tested particles in A549 cells.

The toxic potencies of all tested particles were compared based on multiple cytotoxicity assays (Figure V – 1). All cytotoxicity assays in Figure V – 1 showed that the soluble fraction and TiO_2 elicited little or no toxic effect on A549 cells at the doses tested. In contrast, carbon black, silica (both CR and MI), EHC-93 total and its insoluble fraction were substantially cytotoxic to A549 cells. It was noticeable that the total and insoluble fraction had similar toxic potencies on A549 cells, where both caused extensive damage to the cell membrane based on the LDH release assay (Figure V – 1A), reduced cell proliferation based on the BrdU incorporation assay (Figure V – 1B) and decreased metabolic energy content based on the cellular ATP assay (Figure V – 1C). These observations indicated that the insoluble components drove most of the toxic effects of EHC-93 in A549 cells. Nevertheless, subtle differences between the insoluble fraction and total PM can be observed in most assays, where the insoluble fraction was more potent than EHC-93 total. It is plausible that soluble materials in EHC-93 total may impose some inhibitory effects or damper some of the acute effects of the insoluble fraction, as the total particles were less cytotoxic than the insoluble fraction. The soluble materials may coat or mask potency determinants at the

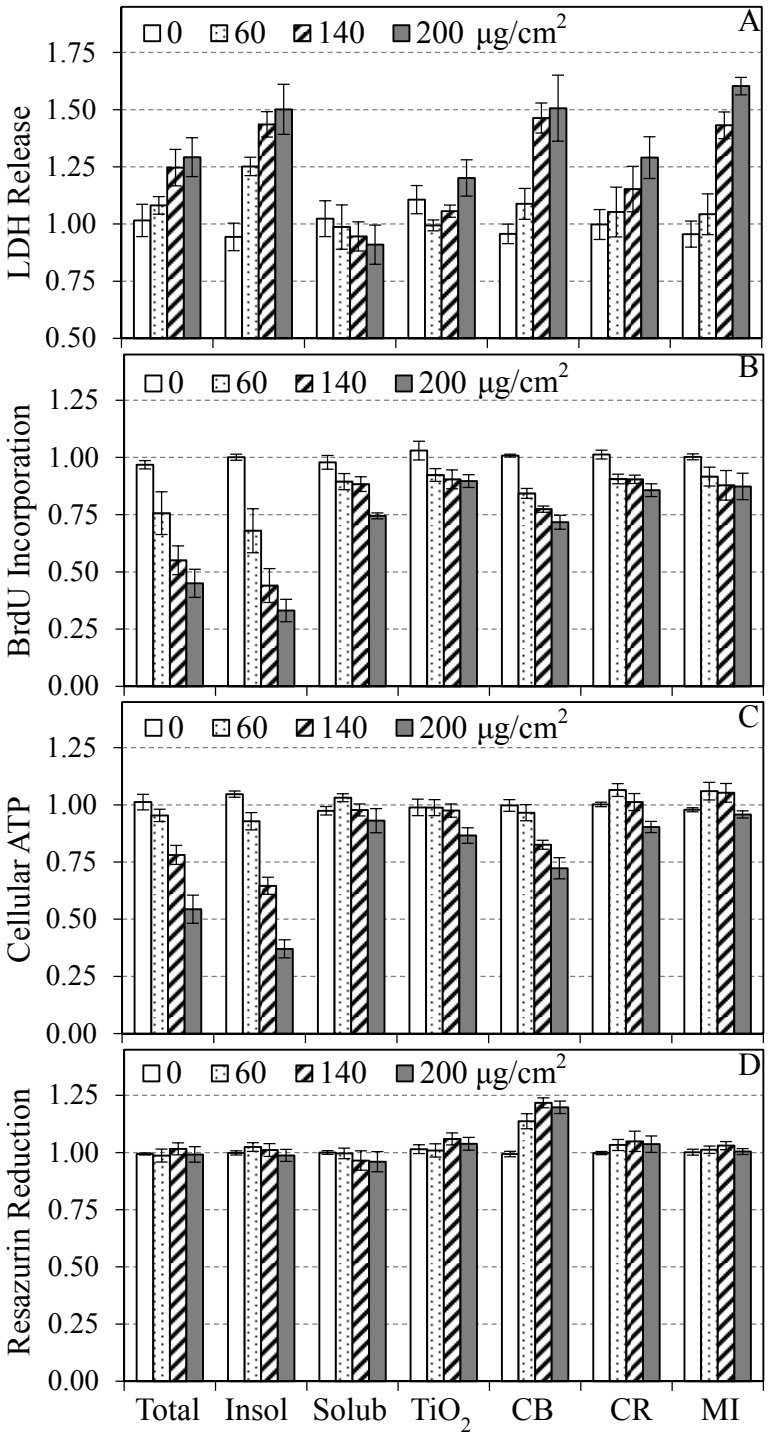

Figure V – 1. Contrasting cytotoxic potencies of all tested particles.
A549 cells were exposed to EHC-93 total, its insoluble and soluble fractions, titanium dioxide (TiO_2), carbon black (CB), crisobalite and Min-U-Sil 5 (MI) for 24 hr and cellular toxicities were assessed by LDH release (A), BrdU incorporation (B), cellular ATP (C) and resazurin reduction (D) assays. Data are expressed as mean fold effect +/- standard error, relative to the control (0 $\mu g/cm^2$), n = 4.

surface of the insoluble materials and reduce some of their cytotoxic effects. Such an inhibitory coating effect has been reported in nano-silica particles (Sun et al., 2015a), where it was demonstrated that the inflammatory effects of amorphous nano-silica particles can be reduced through calcination (high heat treatment) and metal doping. In brief, the cytotoxic potency of EHC-93 total is not equal to the sum of potencies of its insoluble and soluble fractions, revealing toxicological interactions at the cellular level between particle components.

The trends and magnitudes of LDH release induced by the insoluble particles, such as silica (CR and MI) and elemental carbon (CB), appeared similar to those of the total and insoluble fraction (Figure V – 1A). Thus, silica (Table IV – 1) and elemental carbon present in ambient air and urban particles may account for some of the impacts of EHC-93 on the plasma membrane of A549 cells. Silica and carbon black are known to cause apoptotic cell death to macrophages (Chao et al., 2001; Iyer et al., 1996) and bronchial epithelial cells (Hussain et al., 2010), respectively. Despite the strong potencies of silica and elemental carbon in causing LDH release from A549 cells, other insoluble component in EHC-93, such as minerals other than silica, metals, PAHs and endotoxins, could also have induced the release of LDH from the exposed cells.

The potencies of the particles to reduce ATP content and BrdU incorporation in A549 cells were low by CR and MI exposures, moderate by CB exposure, and high by the total and insoluble fraction exposures (Figure V – 1). This suggests that silica as a component in EHC-93 may have a limited role in affecting energy production and cellular proliferation pathways in A549 cells. Elemental carbon may have some influences on these pathways if it was present in an appreciable amount in EHC-93, which is unlikely, since the levels of resazurin reduction in the total and insoluble fraction treatments appeared negligible as compared to

the CB exposures. Thus, the observed marked reduction in cellular ATP and BrdU incorporation in A549 cells may be influenced by a combination of insoluble materials in EHC-93.

V.3. Proteomic analyses using 2D-GE and MALDI-TOF-TOF-MS/MS.

Changes in the proteome of A549 cells following particle exposures were assessed by 2D-GE followed by protein identification with MALDI-TOF-TOF-MS/MS. Since 2D gels tend to warp and distort near the extremities of the pH and the molecular weight ranges, a defined area away from these extremities (Figure IIa – 2; pH 5.1 - 7.8 and 100 - 20 kDa) was selected to investigate exposure-related changes in the proteome of cells across experimental treatments. This area allowed 543 well resolved protein spots across all experimental gels to be cross-examined. Of the 543 protein spots, the identities of 333 protein spots were determined via MALDI-TOF-TOF-MS/MS. To my knowledge this is the largest repository of A549 cellular proteome identified by 2D-GE. This 2D-GE map of A549 cells was compared with those that were published by two independent groups of investigators (Malard et al., 2005; Morbt et al., 2009). Of the protein spots identified by 2D-GE that were matched to two published maps based on their coordinate and constellation, the identities agreed well with each other (Table V-1).

It was noticeable that the same protein was annotated in multiple spots in the 2D-GE map of A549 cells in the data set (Table IIa – S2) and those that have been previously published (Malard et al., 2005; Morbt et al., 2009). These multiple identifications of the same protein were likely due to post-translational modifications, isoforms or degradation products. This is an advantage of using 2D-GE to examine changes in the proteome of cells as

Table V – 1. Comparing the IDs of the protein spots in the 2D-GE map of A549 cells in this study to two independently published data sets (Malard et al., 2005; Morbt et al., 2009). Comparison was only done on the well-defined protein spots, and the comparison was based on the matching constellation and coordinate of spots in the 2D gels. Uncertain spots were either not compared or were given blank spaces. MASCOT scores of each spot from the three studies are provided for comparison purpose.

	Vuong *et al.*, 2015[a]		Morbt *et al.*, 2009[b]		Malard *et al.*, 2005[c]	
SSP	**ID**	**Score**	**ID**	**Score**	**ID**	**Score**
SSP2303	ACTB	417	ACTB	520	ACTB	83
SSP7605	ALDH1A1	232			RUVBL1	76
SSP7607	ALDH1A1	271	ALDH1A1	844	ALDH1A1	110
SSP7602	ALDH1A1	385	ALDH1A1	325	ALDH3A1	144
SSP7603	ALDH1A1	424			ALDH1A1	74
SSP8201	ANXA1	198			ANXA1	123
SSP1501	ATP5B	206			ATP5B	136
SSP0001	CAPNS1	158			CAPNS1	70
SSP4105	CAPZB	242	ANXA4	830	ANXA4	69
SSP6604	CCT2	475	ALDH1A1	322		
SSP3708	CCT5	137			CCT5	69
SSP4701	CCT5	206			CCT5	55
SSP7701	CCT6A	139	CCT6A	138	CCT6A	140
SSP8504	ENO1	432	ENO1	894		
SSP6103	ERP29	382	ERP29	104		
SSP7903	EZR	95			MSN	107
SSP4001	GSTP1	367	GSTP1	622	GSTP1	70
SSP7005	HNRNPH1	389	HNRNPH1	236		
SSP2701	HNRNPK	196			HNRNPK	83
SSP0803	HSPA5	224	HSPA5	1437	HSPA5	148
SSP3801	HSPA8	138			HSPA8	69
SSP2804	HSPA8	486			HSPA8	173
SSP4802	HSPA9	604			HSPA9	99
SSP4002	HSPB1	273			HSPB1	54
SSP2704	HSPD1	305			HSPD1	177
SSP9401	IDH1	278	IDH1	640		
SSP8703	IMPDH2	447	G6PD	753		
SSP4604	KRT8	488			KRT8	156
SSP5002	NME1	294	NME1	345		
SSP7009	PAFAH1B3	301	PAFAH1B3	299		
SSP1513	PDIA6	75			PDIA6	75
SSP9101	PGAM1	255	PGAM1	296		
SSP4101	PHB	775	PHB	263		
SSP6002	PRDX3	247	PRDX3	288		
SSP7002	PRDX6	404	PRDX6	528		
SSP6005	PSMB3	249	PSMB3	138		
SSP5704	SF3B1	92			TCP1	73
SSP9503	SFPQ	305	PGD	234		
SSP4005	SOD1	76	SOD1	230		
SSP8805	STIP1	243			STIP1	185
SSP7006	TPI1	185	TPI1	97		
SSP9001	TPI1	246			TPI1	65
SSP1602	TUBA1C	425	VIM	662	VIM	143
SSP0603	TUBB	562			TUBB	143
SSP8402	TUFM	543	TUFM	861		
SSP3002	UCHL1	240	UCHL1	344	UCHL1	58
SSP2904	VCP	416	VCP	240	VCP	152
SSP6906	ZYX	160			EZR	196

Protein identification was done by:

[a] MALDI-TOF-TOF-MS/MS

[b] MALDI-TOF-TOF-MS/MS or nano-LC-ESI ion trap MS

[c] MALDI-TOF-MS

compared to non-gel-based shotgun proteomic methods (e.g., LC-MS), where 2D-GE can clearly identify different isoforms and post-translational modification products of proteins. For future studies, however, non-gel based proteomic methods will be used to assess various environmental air particles, as they possess higher sensitivity, reproducibility and proteome coverage.

V.4. Impacts of the particles on the proteome of A549 cells.

The influences of all tested particles on the expression of proteins in A549 cells were compared, based on unsupervised hierarchical cluster analysis. The result in Figure V – 2 revealed that the total and insoluble fraction treatments form a small cluster, suggesting that their effects on the proteome of A549 cells are closely related. Yet, their effects can be distinguished, because they formed separate sub-clusters. These two treatments are part of a larger cluster that includes CR and CB, implying that the particle components in these four treatments may share a commonality in impacting the expression of proteins in A549 cells, in contrast to the other particle exposures including the soluble fraction, TiO_2 and MI exposures, which clustered separately. Based on the clustering distance, CR and CB resembled the effects of the total and insoluble fraction the most. In brief, the soluble fraction altered the expression of proteins in A549 cells differently than the total or insoluble fraction. Thus, the proteomic results are in line with the cytotoxicity assay data. Intriguingly, individual impacts of the insoluble and soluble fractions on majority of the protein spots examined by 2D-GE did not sum up to same magnitude of effect of the total. It is likely that there are inter-component interactions between insoluble and soluble materials that may be synergistic or antagonistic in terms of *in vitro* effects.

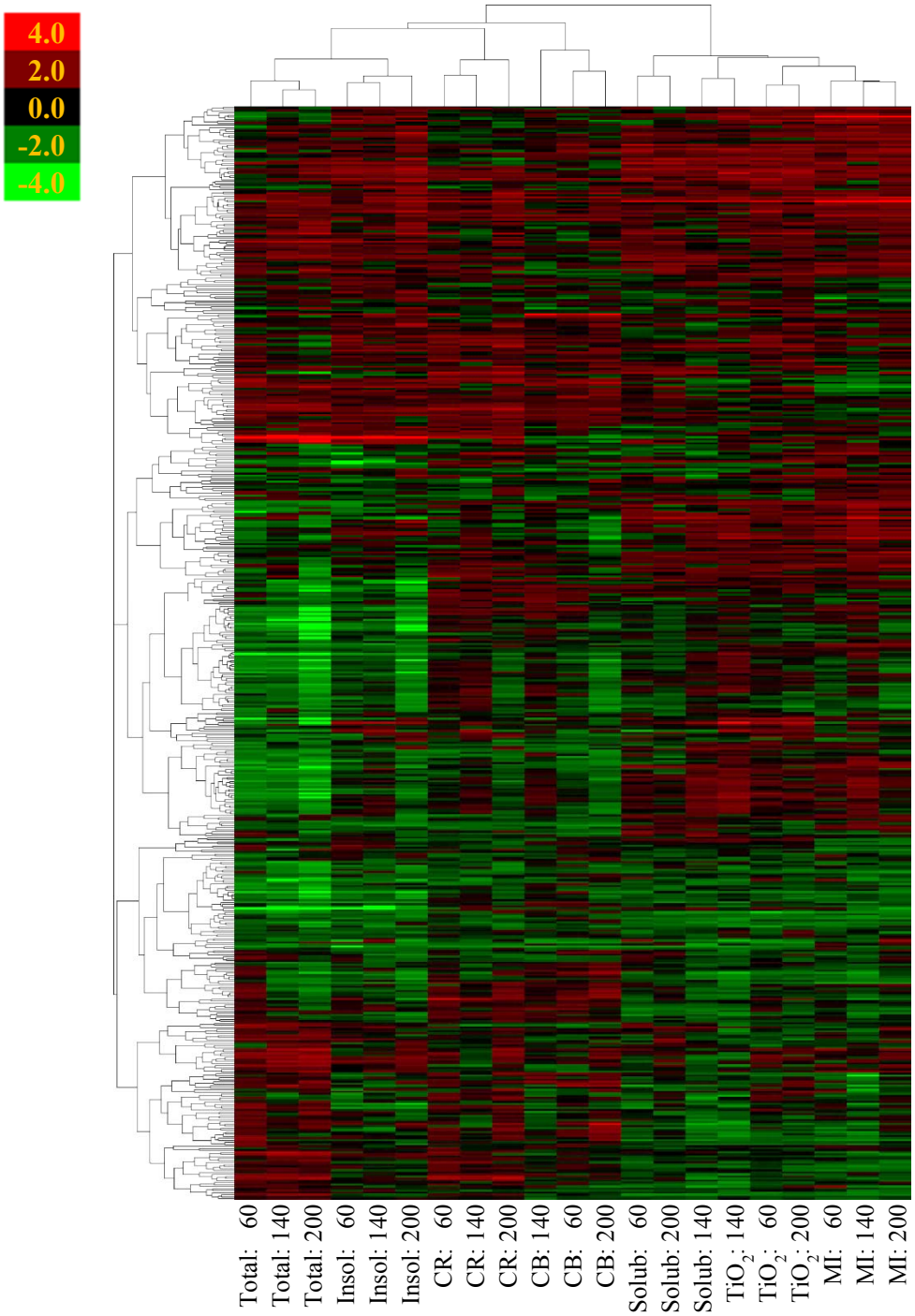

Figure V – 2. Characteristic effects of all tested particles on the proteome of A549 cells. A549 cells were exposed to EHC-93 total, its insoluble and soluble fractions, titanium dioxide (TiO_2), carbon black (CB), crisobalite and Min-U-Sil 5 (MI) for 24 hr, and the effects of the particles on the proteome of the exposed cells were examined via 2D-GE, where all 543 protein spots were assessed. The expression of each protein spot was calculated by Log_2(Treatment/Control), n=3. The number indicates the dose in $\mu g/cm^2$.

It was noticeable that the silica particles CR and MI did not cluster together, which indicated that they likely affected the proteome of A549 cells distinctly. The observation was in line with the RT-PCR results in Table III – S3, showing that these two silica particles perturbed the transcriptome of A549 cells differently, despite their similarity in toxic potencies (Figure III – 2). This contrast in their effect on the proteome and expression of genes in A549 cells was attributed to their differences in physical properties, such as crystalline structure (cristobalite Vs. α–quartz) and median size (5.0 Vs. 2.5 μm). Thereby, proteomic analysis is sensitive in distinguishing the effects of similar and distinctive particles.

V.5. Statistical analyses

Two-way ANOVA coupled with Holm-Sidak (post-hoc) analysis were the statistical methods used to determine significant effects of particles across treatments on cytotoxicity assays, proteomic (2D-GE) and gene expression (RT-PCR) data. The *Treatment* main effect assessed by two-way ANOVA is particularly sensitive for detecting a significant net difference in effect in opposite directions between two treatments, where the effect of each treatment compared to its own control is not significantly changed. For example, the results in Table IV – S2 indicated that there was a significant *Treatment* main effect for BUB3 (SSP9301), where the total and insoluble components of EHC-93 affected the expression of BUB3 similarly but their effects were different from the soluble materials. On average, the expression of BUB3 in A549 cells due to EHC-93 total, insoluble and soluble materials exposures were listed as 1.32, 1.11 and -1.12, respectively. It is important to understand that such fold-changes (FCs) were relative to the control. More importantly, the net difference

between the effects of the total and soluble fraction was 44 % (from 1.32 to -1.12) and the net difference between the effects of the insoluble and soluble fractions was 23 % (from 1.11 to -1.12). Such magnitudes of changes between treatments should not be overlooked, particularly when the *p*-value is very small ($p = 0.003$), and especially since the goal of this study is to identify the differential responses of A549 cells to various airborne particles.

The proteomic results in Table IV – S2 showed that almost all of the significant changes in expression due to *Treatment* and *Dose* main effect and *Treatment X Dose* interaction were strong changes, where the FCs were typically greater than ±1.5. However, the changes that were due to significant *Treatment* main effects were more subtle, and a FC cut-off strategy that can help to remove the noises from data prior to conducting pathway analysis was needed. The changes in expression of proteins in A549 cells that were caused by the total and insoluble fraction were mostly in the same direction, but their expression was in opposite direction between the soluble and insoluble/total. Hypothetically, a FC cut-off set at ± 1.50 has the potential to remove differential effects ranging from 50 – 98 % (e.g., FC from 1.49 to -1.01 and FC from 1.49 to -1.49). Similarly, a cut-off at ± 1.25 has the potential to filter out differential effects ranging from 25 – 48 % (e.g., FC from 1.24 to -1.01 and FC from 1.24 to -1.24). A cut-off at ± 1.10 can potentially remove all differential effects below 10 % (e.g., FC from 1.09 to -1.01) and up to 18 % (e.g., FC from 1.09 to -1.09). Based on this logic, a cut-off of ± 1.10 FC was selected for those proteins with *p*-value < 0.05, so as to sufficiently filter out nuanced expressions that may not contribute to any significant biological effect. Furthermore, proteins do not act on their own in a cell; they normally interact with one another in a network or pathway to carry out a particular function. Thus, when a group of proteins in a particular pathway were identified as significantly altered with $p < 0.05$ and FC > ± 1.10, such changes in a group of proteins are not likely to occur by

chance. Importantly, this notion is well supported by a concordance between the proteomic and pathway analysis and the cytotoxicity assays data.

V.6. Pathway analysis on sub-lethal doses

The effects of airborne PM on various pathways in A549 cells were examined only at a sub-toxic dose. The toxic concentrations were not assessed because pathway analysis outcomes would be dominated by cell death pathways, such as apoptosis and necrosis. This rationale was based on the cytotoxicity results (Figure V – 1) and pathway analysis (Table IV – S3). The cytotoxicity assay results in Figure V – 1 indicate that the higher doses of the total and insoluble fraction caused substantial release of LDH and decrease of cellular ATP and BrdU incorporation. Functional annotation analysis (Table IV – S3) for different protein clusters (Figure IV – 3) revealed that cell death and survival, and cell growth and proliferation were the two dominant cellular functions that were affected by the total and insoluble fraction. In addition, the chosen exposure doses for most *in vitro* toxicology studies, including the current study, are well beyond the actual environmental levels in order to obtain measurable responses. Therefore, there is more value to examine the effect of the particles on A549 cells at a sub-toxic dose, to capture the early signs of particle toxicity.

Pathway analysis demonstrated that the sub-toxic dose (60 $\mu g/cm^2$) of insoluble and soluble fractions of EHC-93 distinctly affected the expression of a number of proteins involved in various pathways in A549 cells, such as cell death and proliferation, protein metabolism and inflammatory response (Figure IV – S2 and Figures IV – 4, 5, 6). For example, the networks of cell death and proliferation in Figure IV – 4 showed that the expressions of YWHAE, SRSF1, PKM, HSPA9 and ENO1 were down-regulated in the

insoluble fraction but were up-regulated or unaffected by the soluble fraction. On the other hand, the expressions of VCP, TREM1 and BUB3 were up-regulated by the insoluble fraction but down-regulated or unaffected by the soluble fraction. Such contrasting patterns of protein expressed in A549 cells after exposure to the insoluble and soluble fractions provided the molecular insight to interpret the differential phenotypic outcomes that were observed by cytotoxicity assays. For example, down-regulation of ENO1 and PKM could explain the decreased ATP levels in A549 cells following the insoluble fraction exposures (Figure IV – 2C), as these two proteins serve distinct enzymatic functions in the last two steps of glycolysis (Voet and Voet, 2010). However, this interpretation would have to be experimentally tested. Knockdown of PKM expression (via siRNA) decreases the production of ATP and induce apoptosis and autophagy in A549 cells (Chu et al., 2015; Sun et al., 2015b). These findings were similar to the proteomic results observed for the insoluble fraction exposure and were also consistent with the cellular ATP and LDH release assays (Figure IV – 2C and A). The results for cytotoxicity assays and proteomic analyses were coherent in interpreting the toxic effects of the insoluble fraction of EHC-93.

V.7. Conclusions

In conclusion, the results in this Ph.D. thesis demonstrated that multiple cytotoxicity assays and proteomic analyses have the capacity to discriminate the phenotypic outcomes and toxic mechanisms of respirable ambient air particles. This is the first time that such a proof of principle is observed. The biological effects of occupational health-relevant particles that are different (i.e., TiO_2 and CB) or similar (i.e., CR and MI) in toxic potency, based on cytotoxicity assays, can both be distinguished by proteomic analyses. Importantly, sub-

fractions of urban dust PM (i.e., insoluble and soluble fractions of EHC-93 Ottawa urban dust) that are different in toxic potency can also be distinguished by proteomic analyses, which provides the molecular basis to understand the toxicity of environmental air particles of defined physicochemical properties. Therefore, *in vitro* toxicoproteomics and multiple cytotoxicity assays are valuable tools to assess the toxicity mechanisms of environmental air pollutants.

V.8. Future direction.

The results in this study indicated that individual particles or mixtures of particles induced differential toxicity profiles in A549 human lung epithelial cells which were observed through multiple cytotoxicity assays, protein and gene expression. These observations demonstrate that *in vitro* toxicoproteomics can differentiate the toxic effect of PM at the molecular level, and the pathways of effect can be interpreted. In this study, cellular responses to a selection of occupational health-relevant respirable materials (i.e., CB, TiO_2, CR and MI) and an urban PM (EHC-93) and its insoluble and soluble fractions were characterized. For future work, the established *in vitro* toxicoproteomic and multiple cytotoxicity assays approach could be utilized to assess the toxic effects of environmental particles in the air that were collected in various Canadian cities that are specifically linked to defined sources of emission as mention in Section I.6. in the Clean Air Regulatory Agenda project. Such work would allow the toxic effects of ambient air PM from different Canadian cities to be estimated and compared, and also the work would provide important data for clean air regulatory purpose.

Contributions of collaborators

Premkumari Kumarathasan: Head of the Analytical Biochemistry and Proteomics Laboratory. She provided instruments such as EXQuest 2D-gel spot picker and MALDI-TOF-MS to conduct most of the proteomic work. She also helped in designing proteomic experiments, supported data interpretation and contributed to the writing of all manuscripts.

Dalibor Breznan: He designed the integrated cytotoxicity assays for high-throughput assessment of particle toxicity. He also conducted endotoxin analysis and contributed to the writing of all manuscripts.

Errol Thomson: He designed a high-throughput RT-PCR platform, which was used to assess the expression of genes in A549 cells following exposures to cristobalite and Min-U-Sil 5. He also contributed to the writing of the manuscript documented in Chapter III.

Julie S. O'Brien: She conducted physical analyses such as SEM, EDX and pXRD for the tested particles (i.e., EHC-93, carbon black, TiO_2, cristobalite and Min-U-Sil 5).

Andrew Williams: He wrote R code for statistical analysis.

Patrick Goegan: Assisted in the preparation of 2D gels from exposed cells.

Subramanian Karthikeyan: Assisted in statistical analysis in all the works.

References

Adamson,I.Y., Vincent,R., and Bjarnason,S.G. (1999). Cell injury and interstitial inflammation in rat lung after inhalation of ozone and urban particulates. Am. J. Respir. Cell Mol. Biol. *20*, 1067-1072.

Barkauskas,C.E., Cronce,M.J., Rackley,C.R., Bowie,E.J., Keene,D.R., Stripp,B.R., Randell,S.H., Noble,P.W., and Hogan,B.L. (2013). Type 2 alveolar cells are stem cells in adult lung. J. Clin. Invest. *123*, 3025-3036.

Borman,S., Russell,H., and Slaga,T.J. (2003). A Mass Spec Timeline. Today's Chemist at Work 47-49.

Bouthillier,L., Vincent,R., Goegan,P., Adamson,I.Y., Bjarnason,S., Stewart,M., Guenette,J., Potvin,M., and Kumarathasan,P. (1998). Acute effects of inhaled urban particles and ozone: lung morphology, macrophage activity, and plasma endothelin-1. Am. J. Pathol. *153*, 1873-1884.

Breznan,D., Karthikeyan,S., Phaneuf,M., Kumarathasan,P., Cakmak,S., Denison,M.S., Brook,J.R., and Vincent,R. (2016). Development of an integrated approach for comparison of in vitro and in vivo responses to particulate matter. Part Fibre. Toxicol. *13*, 41.

Burnett,R.T., Brook,J., Dann,T., Delocla,C., Philips,O., Cakmak,S., Vincent,R., Goldberg,M.S., and Krewski,D. (2000). Association between particulate- and gas-phase components of urban air pollution and daily mortality in eight Canadian cities. Inhal. Toxicol. *12 Suppl 4*, 15-39.

Cassel,S.L., Eisenbarth,S.C., Iyer,S.S., Sadler,J.J., Colegio,O.R., Tephly,L.A., Carter,A.B., Rothman,P.B., Flavell,R.A., and Sutterwala,F.S. (2008). The Nalp3 inflammasome is essential for the development of silicosis. Proc. Natl. Acad. Sci. U. S. A *105*, 9035-9040.

Chao,S.K., Hamilton,R.F., Pfau,J.C., and Holian,A. (2001). Cell surface regulation of silica-induced apoptosis by the SR-A scavenger receptor in a murine lung macrophage cell line (MH-S). Toxicol. Appl. Pharmacol. *174*, 10-16.

Chauhan,V., Breznan,D., Goegan,P., Nadeau,D., Karthikeyan,S., Brook,J.R., and Vincent,R. (2004). Effects of ambient air particles on nitric oxide production in macrophage cell lines. Cell Biol. Toxicol. *20*, 221-239.

Chauhan,V., Breznan,D., Thomson,E., Karthikeyan,S., and Vincent,R. (2005). Effects of ambient air particles on the endothelin system in human pulmonary epithelial cells (A549). Cell Biol. Toxicol. *21*, 191-205.

Chen,R., Zhang,Y., Yang,C., Zhao,Z., Xu,X., and Kan,H. (2013). Acute effect of ambient air pollution on stroke mortality in the China air pollution and health effects study. Stroke *44*, 954-960.

Chu,B., Wang,J., Wang,Y., and Yang,G. (2015). Knockdown of PKM2 induces apoptosis and autophagy in human A549 alveolar adenocarcinoma cells. Mol. Med. Rep. *12*, 4358-4363.

Clarke,S.W. and Pavia,D. (1980). Lung mucus production and mucociliary clearance: methods of assessment. Br. J. Clin. Pharmacol. *9*, 537-546.

Crapo,J.D., Barry,B.E., Gehr,P., Bachofen,M., and Weibel,E.R. (1982). Cell number and cell characteristics of the normal human lung. Am. Rev. Respir. Dis. *126*, 332-337.

Dockery,D.W., Pope,C.A., III, Xu,X., Spengler,J.D., Ware,J.H., Fay,M.E., Ferris,B.G., Jr., and Speizer,F.E. (1993). An association between air pollution and mortality in six U.S. cities. N. Engl. J. Med. *329*, 1753-1759.

Dostert,C., Petrilli,V., Van,B.R., Steele,C., Mossman,B.T., and Tschopp,J. (2008). Innate immune activation through Nalp3 inflammasome sensing of asbestos and silica. Science *320*, 674-677.

Evans,M.J., Cabral,L.J., Stephens,R.J., and Freeman,G. (1973). Renewal of alveolar epithelium in the rat following exposure to NO2. Am. J. Pathol. *70*, 175-198.

Ferin,J. (1972). Observations concerning alveolar dust clearance. Ann. N. Y. Acad. Sci. *200*, 66-72.

Giard,D.J., Aaronson,S.A., Todaro,G.J., Arnstein,P., Kersey,J.H., Dosik,H., and Parks,W.P. (1973). In vitro cultivation of human tumors: establishment of cell lines derived from a series of solid tumors. J. Natl. Cancer Inst. *51*, 1417-1423.

Goldberg,M.S., Burnett,R.T., Bailar,J.C., III, Tamblyn,R., Ernst,P., Flegel,K., Brook,J., Bonvalot,Y., Singh,R., Valois,M.F., and Vincent,R. (2001). Identification of persons with cardiorespiratory conditions who are at risk of dying from the acute effects of ambient air particles. Environ. Health Perspect. *109 Suppl 4*, 487-494.

Goldberg,M.S., Burnett,R.T., Stieb,D.M., Brophy,J.M., Daskalopoulou,S.S., Valois,M.F., and Brook,J.R. (2013). Associations between ambient air pollution and daily mortality among elderly persons in Montreal, Quebec. Sci. Total Environ. *463-464C*, 931-942.

Goldstein,E. (1886). Über eine noch nicht untersuchte Strahlungsform an der Kathodeinducirter Entladungen. Berlin Akd. Monatsber *II*, 691.

Hales,S., Blakely,T., and Woodward,A. (2012). Air pollution and mortality in New Zealand: cohort study. J. Epidemiol. Community Health *66*, 468-473.

Harmsen,A.G., Mason,M.J., Muggenburg,B.A., Gillett,N.A., Jarpe,M.A., and Bice,D.E. (1987). Migration of neutrophils from lung to tracheobronchial lymph node. J. Leukoc. Biol. *41*, 95-103.

Harmsen,A.G., Muggenburg,B.A., Snipes,M.B., and Bice,D.E. (1985). The role of macrophages in particle translocation from lungs to lymph nodes. Science. *230*, 1277-1280.

Hassoun,E.A. and Stohs,S.J. (1996). Cadmium-induced production of superoxide anion and nitric oxide, DNA single strand breaks and lactate dehydrogenase leakage in J774A.1 cell cultures. Toxicology *112*, 219-226.

Hornung,V., Bauernfeind,F., Halle,A., Samstad,E.O., Kono,H., Rock,K.L., Fitzgerald,K.A., and Latz,E. (2008). Silica crystals and aluminum salts activate the NALP3 inflammasome through phagosomal destabilization. Nat. Immunol. *9*, 847-856.

Hunt,D.F., Yates,J.R., III, Shabanowitz,J., Winston,S., and Hauer,C.R. (1986). Protein sequencing by tandem mass spectrometry. Proc. Natl. Acad. Sci. U. S. A. *83*, 6233-6237.

Hussain,S., Thomassen,L.C., Ferecatu,I., Borot,M.C., Andreau,K., Martens,J.A., Fleury,J., Baeza-Squiban,A., Marano,F., and Boland,S. (2010). Carbon black and titanium dioxide nanoparticles elicit distinct apoptotic pathways in bronchial epithelial cells. Part Fibre. Toxicol. *7*, 10.

IARC (1997). IARC Working Group on the Evaluation of Carcinogenic Risks to Humans: Silica, Some Silicates, Coal Dust and Para-Aramid Fibrils. Lyon, 15-22 October 1996. IARC Monogr Eval. Carcinog. Risks Hum. *68*, 1-475.

Iyer,R., Hamilton,R.F., Li,L., and Holian,A. (1996). Silica-induced apoptosis mediated via scavenger receptor in human alveolar macrophages. Toxicol. Appl. Pharmacol. *141*, 84-92.

Johannson,K.A., Vittinghoff,E., Lee,K., Balmes,J.R., Ji,W., Kaplan,G.G., Kim,D.S., and Collard,H.R. (2014). Acute exacerbation of idiopathic pulmonary fibrosis associated with air pollution exposure. Eur. Respir. J. *43*, 1124-1131.

Johnston,H.J., Hutchison,G.R., Christensen,F.M., Peters,S., Hankin,S., and Stone,V. (2009). Identification of the mechanisms that drive the toxicity of TiO(2)particulates: the contribution of physicochemical characteristics. Part Fibre. Toxicol. *6*, 33.

Kreyling,W.G., Semmler,M., Erbe,F., Mayer,P., Takenaka,S., Schulz,H., Oberdorster,G., and Ziesenis,A. (2002). Translocation of ultrafine insoluble iridium particles from lung epithelium to extrapulmonary organs is size dependent but very low. J. Toxicol. Environ. Health. A. *65*, 1513-1530.

Kumarathasan,P., Blais,E., Saravanamuthu,A., Bielecki,A., Mukherjee,B., Bjarnason,S., Guenette,J., Goegan,P., and Vincent,R. (2015). Nitrative stress, oxidative stress and plasma endothelin levels after inhalation of particulate matter and ozone. Part Fibre. Toxicol. *12*, 28.

Kumarathasan,P., Mohottalage,S., Goegan,P., and Vincent,R. (2005). An optimized protein in-gel digest method for reliable proteome characterization by MALDI-TOF-MS analysis. Anal. Biochem. *346*, 85-89.

Laden,F., Neas,L.M., Dockery,D.W., and Schwartz,J. (2000). Association of fine particulate matter from different sources with daily mortality in six U.S. cities. Environ. Health. Perspect. *108*, 941-947.

Landahl,H.D. and Black,S. (1947). Penetration of air-borne particulates through the human nose. J. Ind. Hyg. Toxicol. *29*, 269-277.

Landahl,H.D. and Tracewell,T. (1949). Penetration of air-borne particulates through the human nose. J. Ind. Hyg. Toxicol. *31*, 55-59.

Lieber,M., Smith,B., Szakal,A., Nelson-Rees,W., and Todaro,G. (1976). A continuous tumor-cell line from a human lung carcinoma with properties of type II alveolar epithelial cells. Int. J. Cancer *17*, 62-70.

Malard,V., Prat,O., Darrouzet,E., Berenguer,F., Sage,N., and Quemeneur,E. (2005). Proteomic analysis of the response of human lung cells to uranium. Proteomics. *5*, 4568-4580.

McLafferty,F.W. (1981). Tandem mass spectrometry. Science. *214*, 280-287.

Merkus,F.W., Verhoef,J.C., Schipper,N.G., and Marttin,E. (1998). Nasal mucociliary clearance as a factor in nasal drug delivery. Adv. Drug Deliv. Rev. *29*, 13-38.

Morbt,N., Mogel,I., Kalkhof,S., Feltens,R., Roder-Stolinski,C., Zheng,J., Vogt,C., Lehmann,I., and von,B.M. (2009). Proteome changes in human bronchoalveolar cells following styrene exposure indicate involvement of oxidative stress in the molecular-response mechanism. Proteomics. *9*, 4920-4933.

Morbt,N., Tomm,J., Feltens,R., Mogel,I., Kalkhof,S., Murugesan,K., Wirth,H., Vogt,C., Binder,H., Lehmann,I., and von,B.M. (2011). Chlorinated benzenes cause concomitantly oxidative stress and induction of apoptotic markers in lung epithelial cells (A549) at nonacute toxic concentrations. J. Proteome. Res. *10*, 363-378.

Oberdorster,G., Ferin,J., and Lehnert,B.E. (1994). Correlation between particle size, in vivo particle persistence, and lung injury. Environ. Health. Perspect. *102 Suppl 5*, 173-179.

Oberdorster,G., Maynard,A., Donaldson,K., Castranova,V., Fitzpatrick,J., Ausman,K., Carter,J., Karn,B., Kreyling,W., Lai,D., Olin,S., Monteiro-Riviere,N., Warheit,D., and Yang,H. (2005). Principles for characterizing the potential human health effects from exposure to nanomaterials: elements of a screening strategy. Part Fibre. Toxicol. *2*, 8.

Pope,C.A., III (1989). Respiratory disease associated with community air pollution and a steel mill, Utah Valley. Am. J. Public. Health. *79*, 623-628.

Proctor,D.F., Andersen,I.B., and Lundqvist,G. (1973). Clearance of Inhaled Particles From the Human Nose. Arch. Intern. Med. *131*, 132.

Raabe,O.G., Al-Bayati,M.A., Teague,S.V., and Rasolt,A. (1988). Regional deposition of inhaled monodisperse coarse and fine aerosol particles in small laboratory animals. Ann. Occup. Hyg. *32*, 53-63.

Sager,T.M. and Castranova,V. (2009). Surface area of particle administered versus mass in determining the pulmonary toxicity of ultrafine and fine carbon black: comparison to ultrafine titanium dioxide. Part Fibre. Toxicol. *6*, 15.

Scott,J.A. (1953). Fog and deaths in London, December 1952. Public Health Rep. *68*, 474-479.

Serita,F., Kyono,H., and Seki,Y. (1999). Pulmonary clearance and lesions in rats after a single inhalation of ultrafine metallic nickel at dose levels comparable to the threshold limit value. Ind. Health. *37*, 353-363.

Sterling,J.B. and Hanke,C.W. (2005). Dioxin toxicity and chloracne in the Ukraine. J. Drugs. Dermatol. *4*, 148-150.

Suckau,D., Resemann,A., Schuerenberg,M., Hufnagel,P., Franzen,J., and Holle,A. (2003). A novel MALDI LIFT-TOF/TOF mass spectrometer for proteomics. Anal. Bioanal. Chem. *376*, 952-965.

Sun,B., Pokhrel,S., Dunphy,D.R., Zhang,H., Ji,Z., Wang,X., Wang,M., Liao,Y.P., Chang,C.H., Dong,J., Li,R., Madler,L., Brinker,C.J., Nel,A.E., and Xia,T. (2015a). Reduction of Acute Inflammatory Effects of Fumed Silica Nanoparticles in the Lung by Adjusting Silanol Display through Calcination and Metal Doping. ACS. Nano. *9*, 9357-9372.

Sun,H., Zhu,A., Zhang,L., Zhang,J., Zhong,Z., and Wang,F. (2015b). Knockdown of PKM2 Suppresses Tumor Growth and Invasion in Lung Adenocarcinoma. Int. J. Mol. Sci. *16*, 24574-24587.

Sun,Q., Yue,P., Ying,Z., Cardounel,A.J., Brook,R.D., Devlin,R., Hwang,J.S., Zweier,J.L., Chen,L.C., and Rajagopalan,S. (2008). Air pollution exposure potentiates hypertension through reactive oxygen species-mediated activation of Rho/ROCK. Arterioscler. Thromb. Vasc. Biol. *28*, 1760-1766.

Syka,J.E., Coon,J.J., Schroeder,M.J., Shabanowitz,J., and Hunt,D.F. (2004). Peptide and protein sequence analysis by electron transfer dissociation mass spectrometry. Proc. Natl. Acad. Sci. U. S. A. *101*, 9528-9533.

Thomson,E.M., Breznan,D., Karthikeyan,S., Mackinnon-Roy,C., Charland,J.P., Dabek-Zlotorzynska,E., Celo,V., Kumarathasan,P., Brook,J.R., and Vincent,R. (2015). Cytotoxic

and inflammatory potential of size-fractionated particulate matter collected repeatedly within a small urban area. Part Fibre. Toxicol. *12*, 24.

Thomson,E.M., Breznan,D., Karthikeyan,S., Mackinnon-Roy,C., Vuong,N.Q., Dabek-Zlotorzynska,E., Celo,V., Charland,J.P., Kumarathasan,P., Brook,J.R., and Vincent,R. (2016). Contrasting biological potency of particulate matter collected at sites impacted by distinct industrial sources. Part Fibre. Toxicol. *13*, 65.

Thomson,J.J. (1913). Rays of positive electricity. Proceedings of the Royal Society A *89*, 1-20.

Vincent,R., Bjarnason,S.G., Adamson,I.Y., Hedgecock,C., Kumarathasan,P., Guenette,J., Potvin,M., Goegan,P., and Bouthillier,L. (1997a). Acute pulmonary toxicity of urban particulate matter and ozone. Am. J. Pathol. *151*, 1563-1570.

Vincent,R., Goegan,P., Johnson,G., Brook,J.R., Kumarathasan,P., Bouthillier,L., and Burnett,R.T. (1997b). Regulation of promoter-CAT stress genes in HepG2 cells by suspensions of particles from ambient air. Fundam. Appl. Toxicol. *39*, 18-32.

Vincent,R., Kumarathasan,P., Goegan,P., Bjarnason,S.G., Guenette,J., Berube,D., Adamson,I.Y., Desjardins,S., Burnett,R.T., Miller,F.J., and Battistini,B. (2001). Inhalation toxicology of urban ambient particulate matter: acute cardiovascular effects in rats. Res. Rep. Health Eff. Inst. 5-54.

Voet,D. and Voet,J.G. (2010). Biochemistry, 4th Edition. (New Jersey: Wiley).

Zhang,Y., Ji,X., Ku,T., Li,G., and Sang,N. (2016). Heavy metals bound to fine particulate matter from northern China induce season-dependent health risks: A study based on myocardial toxicity. Environ. Pollut. *216*, 380-390.

Zhang,Y., Xu,D., Li,W., Yu,J., and Chen,Y. (2012). Effect of Size, Shape, and Surface Modification on Cytotoxicity of Gold Nanoparticles to Human HEp-2 and Canine MDCK Cells. Hindawi *2012*, 1-7.

Zubarev,R.A., Kelleher,N.L., and McLafferty,F.W. (1998). Electron Capture Dissociation of Multiply Charged Protein Cations. A Nonergodic Process. J. Am. Chem. Soc. *120*, 3265-3266.

Appendices

Articles' copyright distribution

Co-author manuscripts

JOURNAL OF PROTEOMICS 100 (2014) 136–146

Available online at www.sciencedirect.com

ScienceDirect

www.elsevier.com/locate/jprot

Applicability of a high-throughput shotgun plasma protein screening approach in understanding maternal biological pathways relevant to infant birth weight outcome☆

P. Kumarathasan[a,*], R. Vincent[b], D. Das[a], S. Mohottalage[a], E. Blais[a], K. Blank[a], S. Karthikeyan[b], N.Q. Vuong[b], T.E. Arbuckle[c], W.D. Fraser[d]

[a]Analytical Biochemistry and Proteomics Laboratory, Mechanistic Studies Division, Health Canada, Ottawa, ON, K1A 0K9, Canada
[b]Inhalation Toxicology Laboratory, Hazard Identification Division, Health Canada, Ottawa, ON, K1A 0K9, Canada
[c]Population Studies Division, Environmental Health Science and Research Bureau, Healthy Environments and Consumer Safety Branch, Health Canada, Ottawa, ON, K1A 0K9, Canada
[d]St-Justine Hospital, Montreal, QC, H3T 1C5, Canada

ARTICLE INFO

Available online 14 December 2013

Keywords:
Birth weight
Shot-gun proteomic
Mass spectrometry
Biomarkers

ABSTRACT

There are reports linking maternal nutritional status, smoking and environmental chemical exposures to adverse pregnancy outcomes. However, biological bases for association between some of these factors and birth outcomes are yet to be established. The objective of this preliminary work is to test the capability of a new high-throughput shotgun plasma proteomic screening in identifying maternal changes relevant to pregnancy outcome. A subset of third trimester plasma samples (N = 12) associated with normal and low-birth weight infants were fractionated, tryptic-digested and analyzed for global proteomic changes using a MALDI-TOF–TOF-MS methodology. Mass spectral data were mined for candidate biomarkers using bioinformatic and statistical tools. Maternal plasma profiles of cytokines (e.g. IL8, TNF-α), chemokines (e.g. MCP-1) and cardiovascular endpoints (e.g. ET-1, MMP-9) were analyzed by a targeted approach using multiplex protein array and HPLC-Fluorescence methods. Target and global plasma proteomic markers were used to identify protein interaction networks and maternal biological pathways relevant to low infant birth weight. Our results exhibited the potential to discriminate specific maternal physiologies relevant to risk of adverse birth outcomes. This proteomic approach can be valuable in understanding the impacts of maternal factors such as environmental contaminant exposures and nutrition on birth outcomes in future work.

Biological significance
We demonstrate here the fitness of mass spectrometry-based shot-gun proteomics for surveillance of biological changes in mothers, and for adverse pathway analysis in

☆ This article is part of a Special Issue entitled: Can Proteomics Fill the Gap Between Genomics and Phenotypes?

* *Corresponding author at:* Room 233A, Environmental Health Centre, 0803C Tunney's Pasture, Ottawa, Ontario, K1A 0K9 Canada. Tel.: +1 613 957 0209; fax: +1 613 946 2600.
E-mail address: premkumari.kumarathasan@hc-sc.gc.ca (P. Kumarathasan).

http://dx.doi.org/10.1016/j.jprot.2013.12.003

combination with target biomarker information. This approach has potential for enabling early detection of mothers at risk for low infant birth weight and preterm birth, and thus early intervention for mitigation and prevention of adverse pregnancy outcomes.
This article is part of a Special Issue entitled: Can Proteomics Fill the Gap Between Genomics and Phenotypes?

1. Introduction

There is rising concern due to association between pregnancy outcomes and onset of childhood and adult diseases [1,2]. Perinatal health outcomes are important markers of future child and adult health [3]. Maternal determinants of adverse pregnancy outcomes can include maternal nutrition, age, smoking, disease, and environmental contaminant exposure levels [4–9]. For instance, there are reports on maternal nutrition in different stages of pregnancy affecting placental and infant size [10] as well as preterm birth and fetal growth retardation [11]. Similarly, diet in pregnancy has been shown to affect offspring's blood pressure in their early adulthood [12]. Previous works have shown that both extremely young and advanced maternal ages can lead to poor pregnancy outcomes [13,14]. Maternal smoking has been implicated in miscarriage, perinatal mortality, birth defects, low birth weight and premature births [15,16]. Also, heart disease has been associated with maternal and neonatal complications in pregnancy [17]. Exposures to diesel exhausts during pregnancy can lead to pathologies similar to autism in infants [18]. There are also studies suggesting pregnancy time-dependant vulnerability to different components of air pollutants [19,20].

Mechanistic understanding of the maternal biological pathways which play a role in adverse pregnancy outcome is critical in terms of managing the risk during pregnancy. Elevated circulating endothelin-1 (ET-1) levels and high blood pressure in pregnant women are associated with intrauterine growth restriction (IUGR) resulting in low infant birth weights [21]. Similarly, oxidative stress has been reported to cause maternal and fetal morbidities [22–26], and is implicated as a major factor in preeclampsia [27]. Molecular mechanisms by which maternal factors influence fetal development are still poorly characterized.

Traditionally, most of the methodologies that are used to understand maternal biological mechanisms involved in poor pregnancy outcome are based on target endpoint analyses, a reductionist approach [28]. Proteomic analyses exhibit a greater potential in viewing changes at a global level. One such approach is shotgun proteomic analysis [29,30]. This refers to rapid and direct analysis of multiple proteins simultaneously in a protein mixture permitting qualitative and quantitative assessment of their changes in biological systems. There are various methodologies employed to conduct shotgun proteomic analyses including analyses based on two-dimensional gel electrophoresis separation followed by mass spectrometry by both MALDI-TOF–TOF-MS and ESI-MS/MS platforms, multidimensional LC based separations followed by tandem mass spectrometry. However, there are reports on limitations associated with global analysis of proteins when applied to real biological systems [31].

Our objective was to test the ability of a simple high-throughput shotgun plasma proteomic screening approach to discriminate between maternal physiologies relevant to different types of pregnancy outcomes. For this purpose, we used a very small subset of third trimester plasma samples from a mother–infant cohort (Maternal-infant Research on Environmental Chemicals-(MIREC) Study). Plasma proteomic changes were assessed by a global MS-based proteomic analysis method and the m/z data was used for protein profiling. Meanwhile, an array of target protein markers were analyzed in a second set of matched 3rd trimester maternal plasma samples. Information on these target marker levels and candidate protein marker results obtained by the global proteomic method were used for exploring maternal mechanisms relevant to low infant birth weight outcome.

2. Methods

2.1. Materials

Dulbecco's phosphate-buffered saline (PBS, calcium and magnesium free), ethylenediaminetetraacetic acid (EDTA), diethylenetriaminepentaacetic acid (DETPA), phenylmethylsulfonyl fluoride (PMSF), trifluoroacetic acid (TFA), 3,4-dichloroisocoumarin, molecular weight cut-off filters (30, 50 and 100 kDa) and endothelin isoform standards for the HPLC-Fluorescence analyses namely, endothelin-1 (ET-1), endothelin-2 (ET-2) and endothelin-3 (ET-3) were purchased from Sigma (St. Louis, MO, USA). The big endothelin-1 (BET-1) isoform was from Bachem Americas (Torrance, CA, USA). Reagent-grade acetone, acetonitrile, and methanol were from ThermoFisher (Ottawa, ON, Canada). Butylatedhydroxytoluene (BHT) was from United States Biochemical Corporation (Cleveland, OH, USA). Deionzed water (DI water) was obtained from a super-Q plus high purity water system (Millipore, Bedford, MA, USA). UHP-grade compressed nitrogen was supplied by Matheson Gas products (Whitby, ON, Canada). Amber glass vials and screw caps with septa were purchased from Chromatographic Specialties Inc. (Brockville, ON, Canada). Antiprotease (Halt protease inhibitor) cocktail was obtained from ThermoFisher (Ottawa, ON, Canada). Peptide/protein calibration standards and the matrix α-cyano-4-hydroxy cinnamic acid were purchased from Bruker Daltonics (Bremen, Germany). Sequence grade trypsin was obtained from Promega Corporations (Madison, WI, USA). Bioplex kits were purchased from either Millipore (Billerica, MA, USA) or BioRad (Mississauga, ON, Canada).

2.2. Maternal plasma samples associated with low and healthy birth weight infants

Third trimester maternal plasma samples were obtained from the MIREC study cohort described by Arbuckle et al. [32]. A

very small subset of samples (N = 12/group) of cases and controls (mothers associated with infants of low (<2700 g) and normal (2700–4300 g) birth weights) were used in this study since this is an exploratory high throughput shotgun proteomic analysis undertaken to determine its use in future screening of maternal samples for adverse outcome pathways. For the purpose of this analysis and to increase our study power, low birth weight was defined as less than the 10th percentile of all birth weights in the cohort (i.e. <2700 g). Infant birth weights and gestational ages were abstracted from the medical charts at delivery. Systolic and diastolic blood pressure values were measured during the third trimester clinic visit when the blood samples were collected.

2.3. Ethics

The details of the ethics review of the MIREC study are described by Arbuckle et al. [32]. Briefly, the research protocol, questionnaires, consent forms and recruitment posters and pamphlets were reviewed and approved by human studies research ethics committees, including the Research Ethics Board at Health Canada and the ethics committee at the coordinating center at St-Justine's Hospital in Montreal, as well as more than ten academic and hospital ethics committees across Canada.

2.4. Plasma sample preparation

Aliquots of plasma samples derived from the 3rd trimester maternal whole blood samples (N = 12/group, low vs. normal infant birth weight groups) stabilized with preservatives (EDTA, PMSF) [33], were treated with DETPA, BHT and antiprotease cocktail, were vortexed, and frozen for storage. Matching sets of aliquots of plasma were analyzed for target biomarkers namely, circulating vasoregulatory peptides (endothelins), inflammatory cytokines, chemokines, other cardiovascular markers including acute phase proteins, and for global biomarkers using a MS-based shotgun proteomic analysis method (Scheme 1).

2.5. Sample preparation for global proteomic analysis

The plasma samples for global proteomic biomarker analysis were fractionated using molecular weight cut-off filters (Millipore, Billerica, MA, USA) to obtain <30 kDa, 30–50 kDa and 50–100 kDa fractions as described previously by Kumarathasan et al., 2012 [34]. Briefly, 60 μL aliquots of plasma samples were thawed on ice, diluted with 200 μL of deionized H_2O, and were vortexed. Molecular weight cut-off (MWCO) filters (30 kDa) were pre-wetted by passing 200 μL deionized water at 14,000 ×g for 10 min. The filtrate was discarded and the above diluted plasma samples were transferred into the pre-wetted MWCOs. The content was centrifuged at 14,000 ×g for 10 min. The filtrates (<30 kDa fractions) were collected, and the residues were diluted with 200 μL deionized H_2O, vortexed gently and the filter units were inverted and the residue samples were collected into fresh clean tube by centrifugation at 14,000 ×g for 10 min. The filter unit was washed with additional 75 μL of deionized H_2O, vortexed gently, inverted and centrifuged again to transfer the wash into the same collection tube. These >30 kDa residue samples were transferred into a pre-wetted 50 kDa MWCO filters and centrifuged at 14,000 ×g for 10 min. The filtrates (30–50 kDa) were collected, and the residues from this step were subjected to the process above to obtain the 50–100 kDa and the subsequent

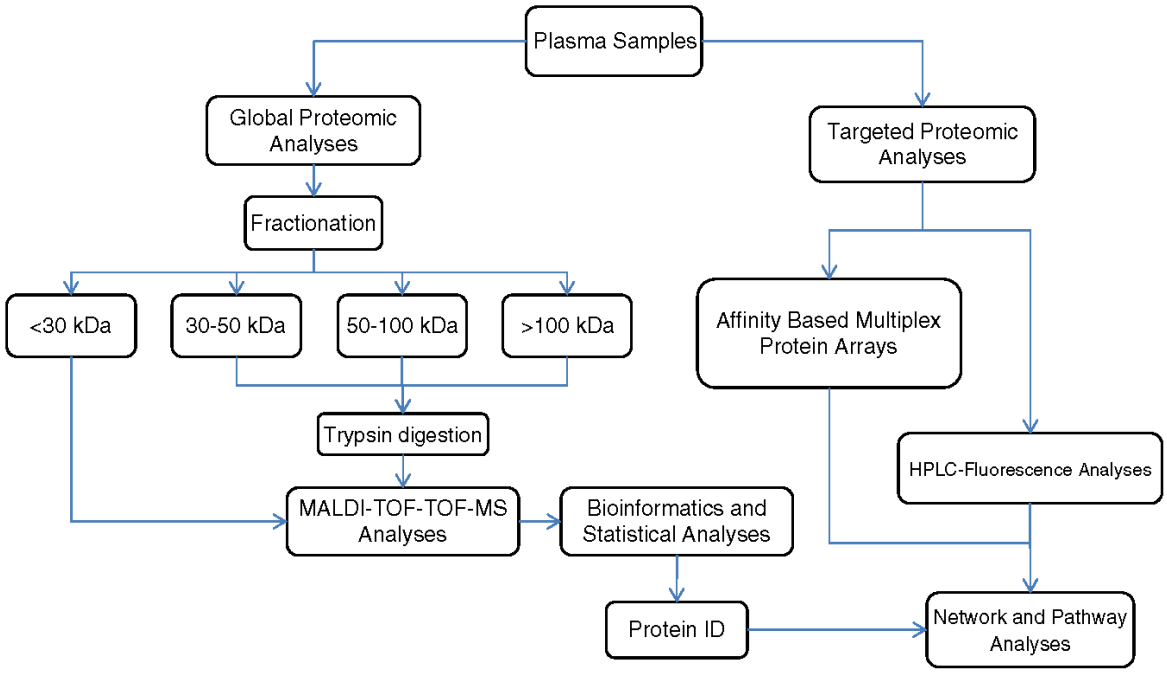

Scheme 1 – Work flow for sample preparation, analyses and data processing.

>100 kDa fractions using the appropriate pre-wetted MWCO filters. The plasma fractions other than the <30 kDa were digested with trypsin following the procedure reported earlier [34,35]. <30 kDa fractions were saved for endogenous peptides analyses. All tryptic digested and non-digested fractions of the plasma samples were evaporated under a flow of nitrogen, and were stored at −80 °C prior to being analyzed.

2.6. MALDI-TOF–TOF-MS analysis of plasma samples

Frozen, dry tryptic-digested and non-digested plasma fractions were thawed at room temperature and were reconstituted (50 μL) using 0.1% TFA in 30% ACN (aq). One μL of the above processed samples (n = 12/group) was spotted (N = 8) on a 384/600 anchor chip target plate (Bruker Daltonics, Bremen, Germany). One μL of matrix solution (10 mg/mL α-cyano-4-hydroxy cinnamic acid in 50% acetonitrile, 0.1% TFA) was added on the sample spot and was mixed as described previously [34,35]. An on-target washing of the sample spot was carried out by placing 2.5 μL of cold 1% TFA in water on the dried sample spot, and the liquid was removed after 10 s. Washed spots were dried and analyzed by MALDI-TOF–TOF-MS using a Bruker Daltonics Autoflex III time-of-flight mass spectrometer (Bruker Daltonics, Bremen, Germany) equipped with a Smart BeamTM laser (355 nm wavelength), a 1 GHz sampling rate digitizer, a pulsed ion extraction source, and a TOF–TOF-MS analyzer. Calibration was done using external protein and peptide calibration standards (m/z range of 1000 to 6000 Da; Bruker). Detection was carried out both in linear and reflectron positive modes. In a typical experiment, a composite spectrum (total of 4000 shots) was obtained by summation of twenty 200-shots of individual spectra. The sampling sites were selected randomly for every sample in order to obtain homogenous sampling. Eight spots/sample were analyzed to enhance overall homogeneity of sampling to obtain the optimal representative mass spectra of the sample (for spot to spot reproducibility among samples please see Supplementary Fig. 1). The data acquisition and processing were carried out using the Flex Control 3.3 and Flex analysis 3.3 software (Bruker Daltonics, Bremen, Germany), respectively. Post-processed mass spectral data (m/z values from the MS scan) were mined for candidate biomarkers [34] by building discriminatory models (ClinPro Tools software version 2.2, Bruker Daltonics, Bremen, Germany), and by statistical analysis. Potential markers were subjected to MS/MS analyses in "Lift" mode for protein identification. Lift conditions used in this study were, ion source 1–6.00 kV; ion source 2–5.30 kV; lens – 3.00 kV; reflectron 1–26.94 kV; reflectron 2–11.48; lift 1–18.97 kV; lift 2 – 3.77 kV. The MS/MS data were queried against SwissProt, NCBInr databases with BioTools software (Bruker Daltonics, Bremen, Germany) using the MASCOT search engine for protein identification. Number of allowed missed cleavages was 1 and the variable modification allowed was methionine oxidation, also decoy sequences were included (FDR < 1).

2.7. Target protein marker analysis

Target markers included in this study were protein markers relevant to inflammatory and endothelial injury pathways which are some of the mechanisms associated with adverse birth outcomes, especially low birth weight outcome, based on previous work as stated above.

2.8. Affinity-based multiplex protein array analyses

Analysis of maternal plasma samples for target markers related to endothelial dysfunction, inflammation and oxidative stress such as cytokines (TNF-α, IFN-γ, IL-2, IL-6, IL-8, IL10, IL12), chemokines (MCP-1, MIP-1β), cellular adhesion molecules (VCAM, ICAM), matrix metalloproteinases (MMP-1, MMP-2, MMP7, MMP-9, MMP-10) and vascular endothelial growth factor (VEGF) were conducted by affinity-based multiplex protein array analysis (Biorad, Millipore) based on the procedure reported by Surronen et al., 2010 [36].

2.9. Circulating endothelin isoforms

This procedure was conducted as described before [33]. Briefly, aliquots of 3rd trimester maternal plasma samples (250 μL) were treated with 3,4-dichloroisocoumarin solution in isopropanol to prevent conversion of big ET-1 to ET-1 during sample processing. These samples were then deproteinized with acidified acetone, followed by clean-up using molecular weight cut-off filters (30 kDa). Clarified samples were dried under a N_2 flow, and were reconstituted in the mobile phase A (composition is given below), and were analyzed by a reversed phase HPLC-Fluorescence system. Initial separation of endothelin isoforms (Big ET-1, ET-1, ET2 and ET-3) were carried out on a LC-318 column (25 cm length, 4.6 mm id, 5 μm particle size; Supelco, Oakville, ON) by gradient elution using water-acetonitrile mobile phase (A-30% acetonitrile (aq); B-90% acetonitrile (aq)) with 0.19% of TFA used as the ion-pair reagent. Analytes were measured by fluorescence detection at excitation and emission wavelengths of 240 nm and 380 nm, respectively.

2.10. Statistics and bioinformatic analyses

Post-processed 3rd trimester maternal plasma global proteomic (m/z) data were mined for significant peptide changes and discriminatory model building (ClinPro Tools version 2.0, Bruker) and candidate biomarker identification [34]. Target protein biomarker levels in the corresponding maternal plasma samples were tested by one-way ANOVA using infant birth weight (low vs normal) as a factor (SigmaStat v3.5, SPSS Inc., Chicago, IL). Differences between the maternal plasmatic proteomic changes for the target biomarkers were determined by one-way analysis of variance (ANOVA) using infant birth weight (low vs normal) as a factor (SigmaStat v3.5, SPSS Inc., Chicago, IL). In order to visualize the differential pattern of responses a heat map with hierarchical clustering was constructed using the Heat map software (Los Alamos National Laboratory, Los Alamos, NM, USA; http://www.hiv.lanl.gov/content/sequence/HEATMAP/heatmap_mainpage.html). Protein interaction networks and biofunctions were identified using Ingenuity Pathway Analysis (IPA) (Ingenuity Systems, www.ingenuity.com) based on target and global protein marker ($p < 0.05$) changes.

3. Results and discussion

Adverse pregnancy outcomes such as fetal growth restriction, preterm birth, low birth weight, birth defects, perinatal and infant death have been associated to a number of maternal and prenatal factors including environmental contaminant exposures [4–20,37–39]. Moreover, maternal physiological changes have been shown to influence birth outcomes [13,17]. In this study, a small subset of maternal plasma samples from the MIREC cohort were analyzed by global shotgun screening and targeted analyses for proteomic changes to determine the efficiency of these biomarker approaches in discriminating maternal physiological conditions relevant to adverse pregnancy outcomes. Here, we have defined the low infant birth weight as the low 10th percentile of birth weight in this mother–infant cohort, <2.7 kg to gain power in the low infant birth weight group (Fig. 1). Also, in this preliminary work, we have attempted to use equal number of cases (mothers with infants of low birth weights) and controls (mothers with infants of normal birth weights). Gestational age and maternal blood pressure profiles associated with these two groups are illustrated in Fig. 1. These results suggest comparably low gestational age ($p < 0.001$) in the low birth weight group as compared to the controls. Also, both mean systolic and diastolic blood pressure levels in mothers are relatively higher in the low infant birth weight group compared to the control group, but did not reach statistical significance in this small sample size.

For the shotgun proteomic screening analysis of plasma, we chose to conduct a very simple plasma fractionation strategy with minimal sample handling steps, and used adequate stabilizers to prevent any post-sample collection changes to avoid any experimental artifacts and potential sample losses due to any recovery issues. Retaining the integrity of plasma proteins was essential in order to gain a clear preliminary understanding of maternal physiological changes that can be specific to adverse birth outcomes. Our results on global high content proteomic data from the MS scans of maternal plasma suggested that there were up or down regulation of various proteins in mothers with low infant birth weights compared to the ones with normal birth weight babies. The m/z data was post-processed using ClinProTools software from Bruker Daltonics with subsequent discriminatory model building as mentioned above. Post-processing of raw mass spectral data included normalization with respect to total ion counts (TIC). Also, significant changes were verified by additional independent statistical analysis (one-way ANOVA) for heat map construction. Statistically significant ($p < 0.05$) proteomic changes summarized as tryptic peptide heat maps with hierarchical clustering (Fig. 2) indicated that maternal plasma global proteomic information at the third trimester can discriminate between those mothers who subsequently gave birth to infants with low birth weights, by comparison to mothers who gave birth to normal birth weight infants. Our results suggest that misclassification into low or normal birth weight groups can be identified by comparing these proteomic patterns (Fig. 2), for example, mothers with the infant birth weights of 2672 g and 3750 g appear to be misclassified based on the infant birth weight concept. However, their proteomic patterns suggest that the classification should be reversed. This reversal of classification can be due to various factors. It is plausible that if the mother and the father had relatively small body mass, the infant can be of lower birth weight at term. Similarly, larger parents may have infants with larger birth weight for gestational age. Such discrepancies can be verified by

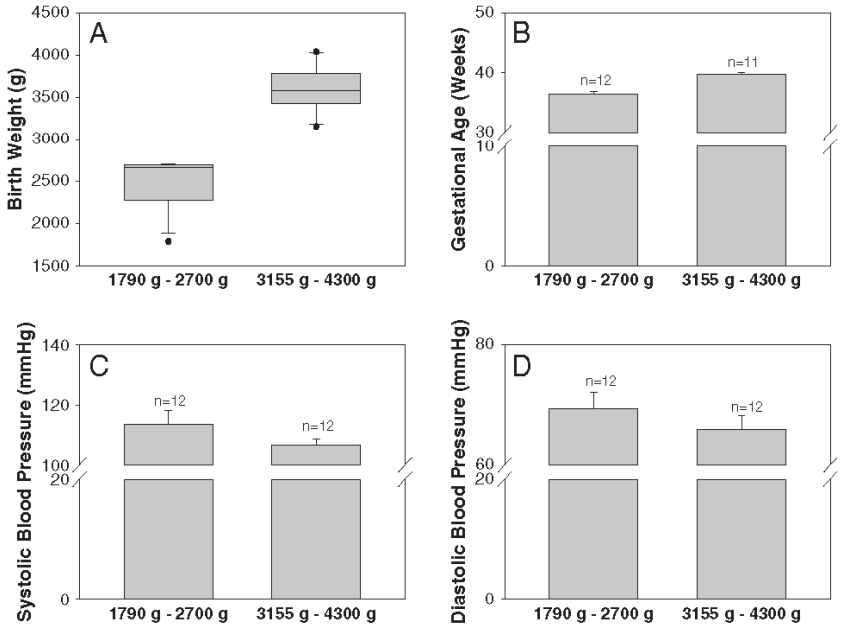

Fig. 1 – Profiles of A. birth weight, B. gestational age and maternal C. systolic and D. diastolic blood pressure levels for the two (low vs normal) infant birth weight groups. Results are expressed as mean ± standard error.

assessment of maternal physiological indices, questionnaires, target marker profiles and other infant parameters. Future analyses of the MIREC data sets will incorporate maternal age, ethnicity and other parameters to determine the causes of similar discrepancies.

A number of candidate tryptic peptide markers (e.g., obtained by discriminatory model building using ClinPro Tools software from Bruker Daltonics, as well as by one-way ANOVA analysis) were subjected to MS/MS analysis, and the fragmentation spectra were matched against SwissProt or/and

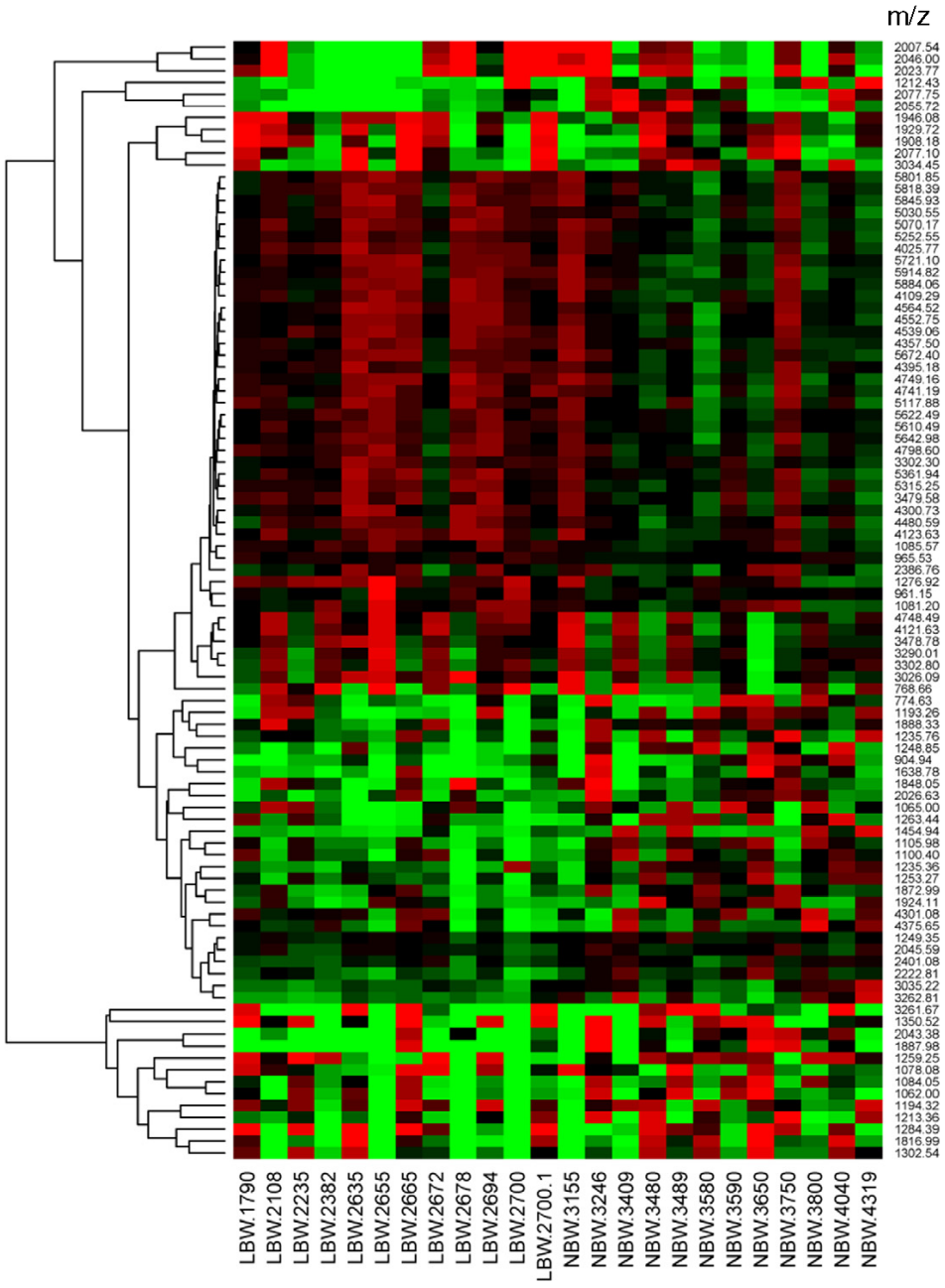

Fig. 2 – Heat map of plasma peptide (m/z) expressions revealed significant ($p < 0.05$) differences between mothers of low birth weight (LBW) and normal birth weight (NBW) infants. Hierarchical clustering of the data reveal clusters of candidate peptides differentially expressed between the two groups. Green indicates down regulation and red indicates up regulation. A yellow-red version of the heatmap is available in supplementary material. Note: (If the yellow–red figure is considered then, yellow indicates down regulation and red indicates up regulation).

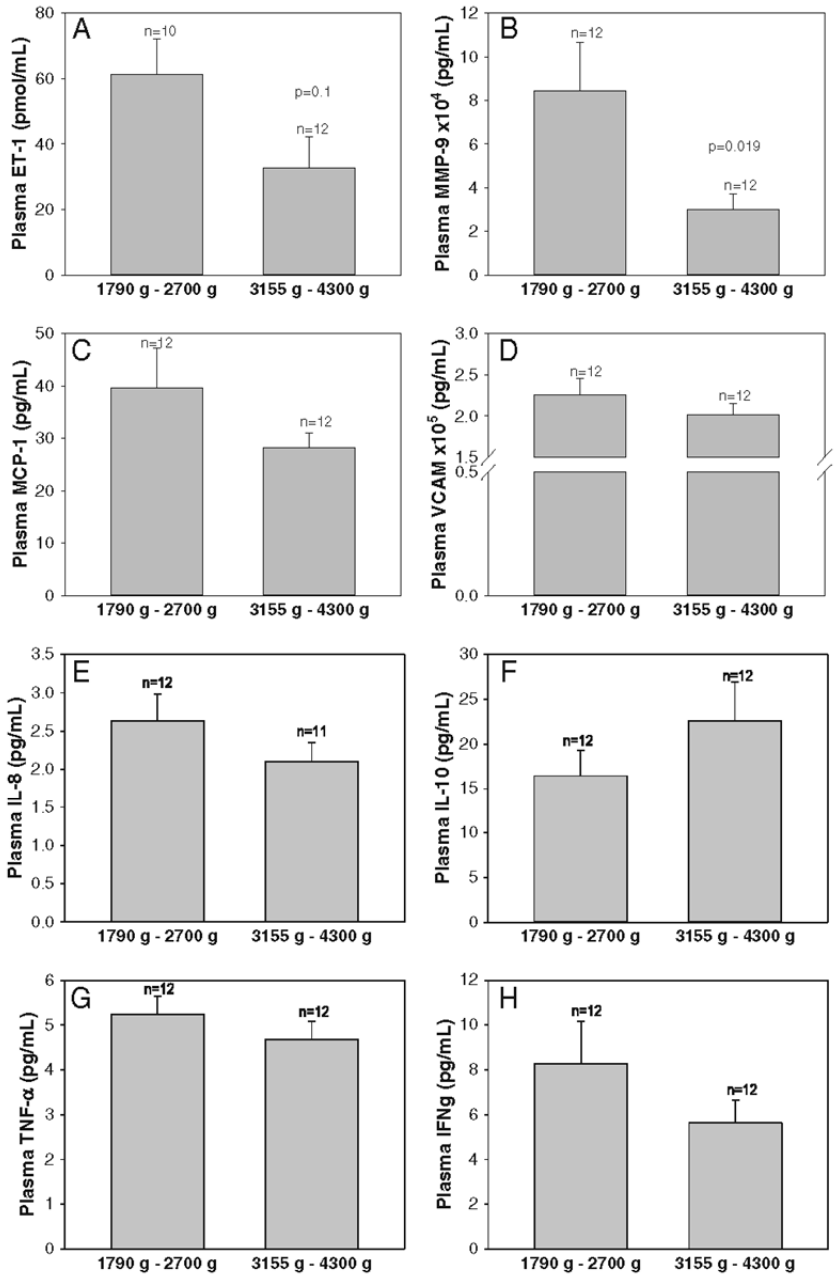

Fig. 3 – Antibody-based multiplex protein array analysis results for the 3rd trimester maternal plasma samples. A. ET-1 B. MMP-9C. MCP-1 D. VCAM E. IL-8F. IL-10G. TNF-α H. IFN-gamma. Results are expressed as mean ± standard error.

NCBInR databases, using MASCOT search engine, for protein identification. Although statistically strongest assignments with the highest ions score, low expect value and unique peptide were used as criteria for potential protein identification, the best matches with low scores were retained if they were unique peptides and were biologically relevant or significant (Supplementary material, Table S1). In this work, our primary aim was to test the discriminatory capability of the global proteomic strategy. In this proof-of-principle effort, the most significant candidate protein markers identified as mentioned above were used as secondary addition to the primary data on target protein markers to enhance the confidence in the networks selected by the IPA analysis.

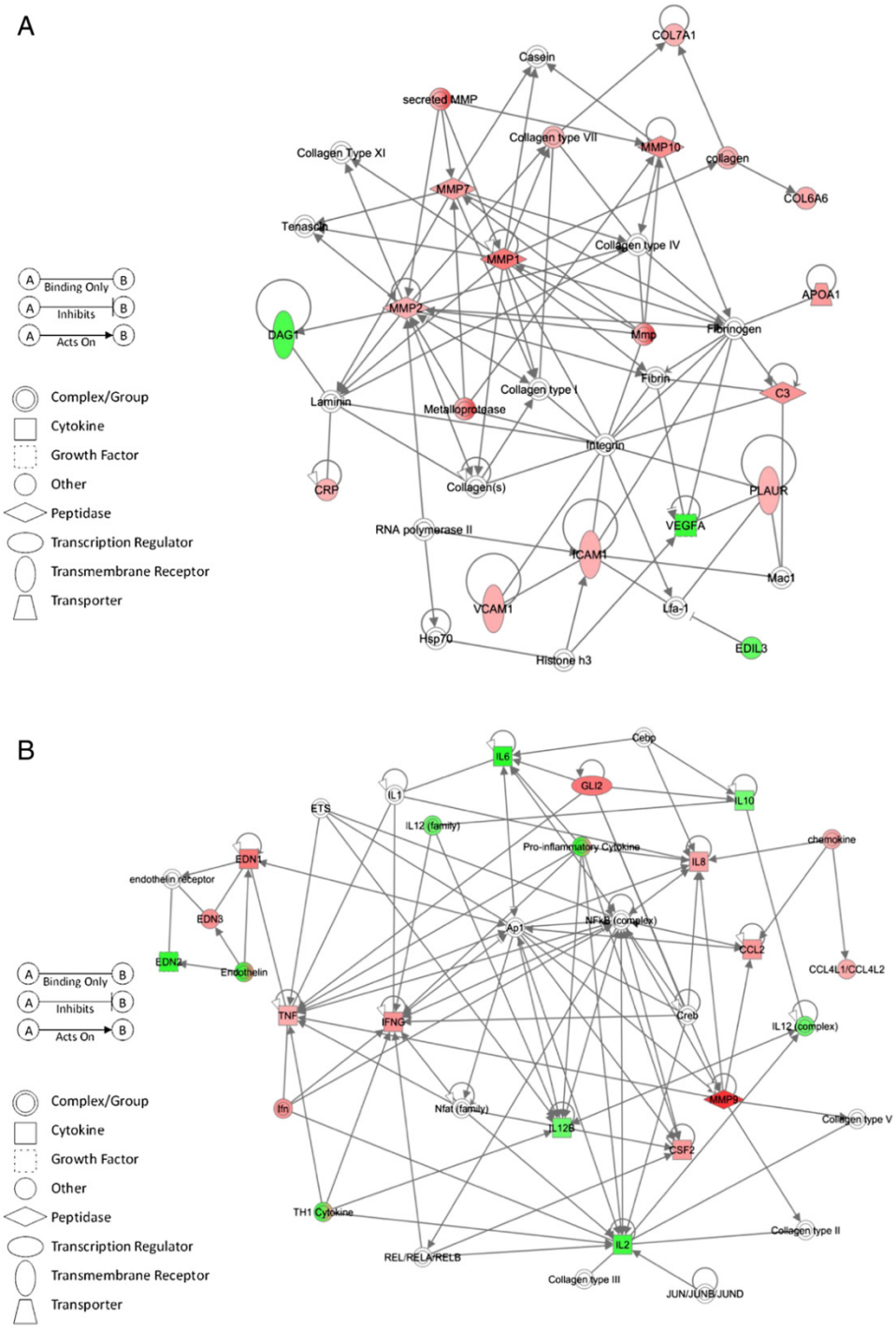

Fig. 4 – Results of IPA analysis performed based on fold changes in maternal plasma levels (low vs normal infant birth weight groups) of both target and global protein biomarkers (A) NETWORK 1: Ophthalmic Disease, Cardiac Stenosis, Cardiovascular Disease (Score 30). (B) NETWORK 2: Cellular Movement, Hematological System Development and Function, Immune Cell Trafficking (Score 29). Green indicates down regulation and red indicates up regulation.

Of the target markers analyzed, a subset of marker profiles are illustrated in Fig. 3. The proinflammatory cytokines IL-8, TNF-alpha, and IFN-gamma were all increased, while the anti-inflammatory cytokine IL-10 was decreased, in plasma of mothers associated with low birth weight infants suggesting a proinflammatory state in these mothers. Similarly, plasmatic ET-1, matrix metalloproteinase (e.g. MMP-9), MCP-1 and VCAM implicated in cardiovascular diseases were elevated [40]. We have previously shown [33,41,42] that in animals and humans exposed to air pollutants there is an increase in circulating endothelin isoforms (ET-1). ET-1 is a potent vasoconstrictor peptide and is formed as a result of the cleavage of its precursor peptide big ET-1 that is comparably less potent by the action of endothelin converting enzyme (ECE).[33] ET-1 is implicated in gestational hypertension and gestational diabetes [43]. Similarly, matrix metalloproteinases are evolving as new set of markers of endothelial injury and are implicated in downstream signaling of vasoregulatory events such as increase in circulating ET-1 levels [44,45].

IPA analysis with target and global protein biomarker information generated several protein interaction networks. Two of these networks with the highest scores are illustrated in Fig. 4A–B. The networks identified here are associated with ophthalmic, cardiovascular, dermatological and neurological conditions, cellular movement, immune cell trafficking, hematological system development, small molecule biochemistry, lipid metabolism and molecular transport. It is noteworthy to see that urokinase plasminogen activator receptor (PLAUR) in network 1 (cardiovascular diseases; Fig. 4A) is up-regulated in mothers with low birth weight infants in our preliminary work. It has been shown by others that elevated levels of plasma urokinase plasminogen activator receptor in mothers infected with malaria (pro-inflammatory condition) is predictive of low infant birth weight.[46] Also, our results exhibit that matrix metalloproteinases (MMPs) are up-regulated (network 1, cardiovascular diseases, Fig. 4A; network 2, immune cell trafficking, Fig. 4B) in mothers with low birth weight infants. This is in line with the report by Sundrani et al., 2011, where MMPs are implicated in the pathophysiology of adverse pregnancy outcomes such as preterm labor that may result in low birth weight infants.[47] The networks that we have observed in this study also trigger detailed analysis of their components for which we do not have data currently but can be achieved through future affinity-based analyses. Furthermore, when related to information on biological functions and diseases, IPA analyses yielded profiles of molecular and cellular functions, diseases/disorders and physiological system development and functions with associated significance values. These preliminary results imply cell signaling, cellular movement, molecular transport, organismal injury and abnormalities, inflammatory, respiratory and cardiovascular effects-related changes in mothers with low birth weight infants compared to the ones with normal birth weight babies. Nevertheless, these findings have to be further investigated through future work on much larger set of samples.

Shot-gun proteomic methodologies face challenges in terms of protein recoveries and experimental artifacts due to intensive sample processing steps, issues of internal standards, necessity of high-end analytical platforms and bottle neck in data handling due to explosion in data generation [31]. Nevertheless, our results demonstrate that global shotgun proteomic approach is a promising tool in understanding negative pregnancy outcomes. We intend to apply this approach to advance our knowledge of environmental contaminant exposure-mediated toxicity mechanisms that can potentially lead to adverse pregnancy outcomes, and impacts of nutritional intervention on these mechanistic pathways, through future work. Increased sample size along with LC-based separation of plasma followed by MS/MS analyses and enhanced protein identification/validation processes with emerging analytical and bioinformatics tools can advance the application of such global proteomic analyses to similar complex investigations.

4. Conclusion

High-throughput shotgun screening of global plasma proteomic changes is useful in discriminating mothers with different physiologies that are related to low birth weight (<2700 g), a potentially adverse pregnancy outcome. Considerable metabolic control is executed at the metabolite as well as the protein levels including post-translational modifications, constituting phenotypic plasticity. Our results indicate that a mass spectrometry-based proteomic approach can capture molecular phenotypes and can be of utility for the identification of prognostic biomarkers of adverse pregnancy outcomes. Combined use of the information from target biomarkers and high-content global proteomics should provide valuable insight into adverse outcome pathways.

Supplementary data to this article can be found online at http://dx.doi.org/10.1016/j.jprot.2013.12.003.

Acknowledgments

We would like to thank Dr. Dalibor Breznan and Dr. Guillaume Pelletier for their helpful comments. This work was supported by the Chemical Management Plan and the Clean Air Regulatory Agenda at Health Canada. The MIREC Research Platform is supported by the Chemicals Management Plan of Health Canada, the Canadian Institutes for Health Research (grant # MOP—81285), and the Ontario Ministry of the Environment. We also acknowledge the valuable contribution of all other MIREC Research Platform Investigators: Peter von Dadelszen, Denise Hemmings, Jingwei Wang, Michael Helewa, Shayne Taback, Mathew Sermer, Warren Foster, Greg Ross, Paul Fredette, Graeme Smith, Mark Walker, Roberta Shear, Linda Dodds, Adrienne Ettinger, Jean-Philippe Weber, Melissa Legrand, Zhong-Cheng Luo, Robert Platt, Grant Mitchell, Kevin Cockell, Maya Villeneuve, Sheryl Tittlemier, Pierre Julien, Denise Avard, Nick Hidiroglou, Hope Weiler, Alain LeBlanc, Mandy Fisher, Monique D'Amour, Bob Dabeka, Thea Rawn, Xu-Liang Cao, Adam Becalski, Nimal Ratnayake, Genevieve Bondy, Dawn Jin, Zhongwen Wang, Gina Muckle, Bruce Lanphear, Jean Séguin, Pierre Ayotte, Dave Saint-Amour, Éric Dewailly, Patricia Monnier, Gideon Koren, and Emmanuel Ouellet.

REFERENCES

[1] Stillerman KP, Mattison DR, Giudice LC, Woodruff TJ. Environmental exposures and adverse pregnancy outcomes: a review of the science. Reprod Sci 2008;15(7):631–50.

[2] Perera FP, Tang D, Rauh V, Tu YH, Tsai WY, Becker M, et al. Relationship between polycyclic aromatic hydrocarbon-DNA adducts, environmental tobacco smoke, and child development in the World Trade Center cohort. Environ Health Perspect 2007;115(10):1497–502.

[3] Woodruff TJ, Parker JD, Darrow LA, Slama R, Bell ML, Choi H, et al. Methodological issues in studies of air pollution and reproductive health. Environ Res 2009;109(3):311–20.

[4] Wigle DT, Arbuckle TE, Turner MC, Berube A, Yang Q, Liu S, et al. Epidemiologic evidence of relationships between reproductive and child health outcomes and environmental chemical contaminants. J Toxicol Environ Health B Crit Rev 2008;11(5–6):373–517.

[5] Mathews F, Yudkin P, Neil A. Influence of maternal nutrition on outcome of pregnancy: prospective cohort study. BMJ 1999;319(7206):339–43.

[6] Jolly M, Sebire N, Harris J, Robinson S, Regan L. The risks associated with pregnancy in women aged 35 years or older. Hum Reprod 2000;15(11):2433–7.

[7] Gelson E, Johnson M. Effect of maternal heart disease on pregnancy outcomes. Expert Rev Obstet Gynecol 2010;5(5):605–17.

[8] Alsuwaida A, Mousa D, Al-Harbi A, Alghonaim M, Ghareeb S, Alrukhaimi MN. Impact of early chronic kidney disease on maternal and fetal outcomes of pregnancy. J Matern Fetal Neonatal Med 2011;24(12):1432–6.

[9] Abu-Saad K, Fraser D. Maternal nutrition and birth outcomes. Epidemiol Rev 2010;32(1):5–25.

[10] Godfrey K, Robinson S, Barker DJ, Osmond C, Cox V. Maternal nutrition in early and late pregnancy in relation to placental and fetal growth. BMJ 1996;312(7028):410–4.

[11] King JC. The risk of maternal nutritional depletion and poor outcomes increases in early or closely spaced pregnancies. J Nutr 2003;133(5 Suppl 2):1732S–6S.

[12] Campbell DM, Hall MH, Barker DJ, Cross J, Shiell AW, Godfrey KM. Diet in pregnancy and the offspring's blood pressure 40 years later. Br J Obstet Gynaecol 1996;103(3):273–80.

[13] Kenny LC, Lavender T, McNamee R, O'Neill SM, Mills T, Khashan AS. Advanced maternal age and adverse pregnancy outcome: evidence from a large contemporary cohort. PLoS One 2013;8(2):e56583.

[14] Chantrapanichkul P, Chawanpaiboon S. Adverse pregnancy outcomes in cases involving extremely young maternal age. Int J Gynaecol Obstet 2013;120(2):160–4.

[15] Howe LD, Matijasevich A, Tilling K, Brion MJ, Leary SD, Smith GD, et al. Maternal smoking during pregnancy and offspring trajectories of height and adiposity: comparing maternal and paternal associations. Int J Epidemiol 2012;41(3):722–32.

[16] Hackshaw A, Rodeck C, Boniface S. Maternal smoking in pregnancy and birth defects: a systematic review based on 173 687 malformed cases and 11.7 million controls. Hum Reprod Update 2011;17(5):589–604.

[17] Stangl V, Schad J, Gossing G, Borges A, Baumann G, Stangl K. Maternal heart disease and pregnancy outcome: a single-centre experience. Eur J Heart Fail 2008;10(9):855–60.

[18] Sugamata M, Ihara T, Sugamata M, Takeda K. Maternal exposure to diesel exhaust leads to pathological similarity to autism in newborns. J Health Sci 2006;52(4):486–8.

[19] Lin YY, Hwang YH, Chen PC, Chen BY, Wen HJ, Liu JH, et al. Contribution of gestational exposure to ambient traffic air pollutants to fetal cord blood manganese. Environ Res 2012;112:1–7.

[20] Maroziene L, Grazuleviciene R. Maternal exposure to low-level air pollution and pregnancy outcomes: a population-based study. Environ Health 2002;1(1):6.

[21] Arslan M, Yazici G, Erdem A, Erdem M, Arslan EO, Himmetoglu O. Endothelin 1 and leptin in the pathophysiology of intrauterine growth restriction. Int J Gynaecol Obstet 2004;84(2):120–6.

[22] Triche EW, Hossain N. Environmental factors implicated in the causation of adverse pregnancy outcome. Semin Perinatol 2007;31(4):240–2.

[23] Tabacova S, Baird DD, Balabaeva L. Exposure to oxidized nitrogen: lipid peroxidation and neonatal health risk. Arch Environ Health 1998;53(3):214–21.

[24] Gitto E, Reiter RJ, Karbownik M, Tan DX, Gitto P, Barberi S, et al. Causes of oxidative stress in the pre- and perinatal period. Biol Neonate 2002;81(3):146–57.

[25] Cindrova-Davies T. Gabor Than Award Lecture 2008: pre-eclampsia—from placental oxidative stress to maternal endothelial dysfunction. Placenta 2009;30(Suppl. A):S55–65.

[26] Bell ML, Ebisu K, Belanger K. Ambient air pollution and low birth weight in Connecticut and Massachusetts. Environ Health Perspect 2007;115(7):1118–24.

[27] Burton GJ, Jauniaux E. Placental oxidative stress: from miscarriage to preeclampsia. J Soc Gynecol Investig 2004;11(6):342–52.

[28] Madazli R, Atis A, Uzun H, Aksu F. Mid-trimester amniotic fluid angiogenin, lactate dehydrogenase and fibronectin in the prediction of preterm delivery. Eur J Obstet Gynecol Reprod Biol 2003;106(2):160–4.

[29] Gilmore JM, Washburn MP. Advances in shotgun proteomics and the analysis of membrane proteomes. J Proteomics 2010;73(11):2078–91.

[30] Fabietti A, Gaspari M, Krishnan S, Quirino A, Liberto MC, Cuda G, et al. Shotgun proteomic analysis of two Bartonella quintana strains. Proteomics 2013;13(8):1375–8.

[31] Wu CC, MacCoss MJ. Shotgun proteomics: tools for the analysis of complex biological systems. Curr Opin Mol Ther 2002;4(3):242–50.

[32] Arbuckle TE, Fraser WD, Fisher M, Davis K, Liang CL, Lupien N, et al. Cohort profile: the maternal-infant research on environmental chemicals research platform. Paediatr Perinat Epidemiol 2013;27(4):415–25.

[33] Kumarathasan P, Goegan P, Vincent R. An automated high-performance liquid chromatography fluorescence method for the analyses of endothelins in plasma samples. Anal Biochem 2001;299(1):37–44.

[34] Kumarathasan P, Das D, Salam MA, Mohottalage S, DeSilva N, Simard B, et al. Mass spectrometry-based proteomic assessment of the in vitro toxicity of carbon nanotubes. Curr Top Biochem Res 2012;14(1):15–27.

[35] Kumarathasan P, Mohottalage S, Goegan P, Vincent R. An optimized protein in-gel digest method for reliable proteome characterization by MALDI-TOF-MS analysis. Anal Biochem 2005;346(1):85–9.

[36] Suuronen EJ, Hazra S, Zhang P, Vincent R, Kumarathasan P, Zhang Y, et al. Impairment of human cell-based vasculogenesis in rats by hypercholesterolemia-induced endothelial dysfunction and rescue with L-arginine supplementation. J Thorac Cardiovasc Surg 2010;139(1):209–16.

[37] Shah NR, Bracken MB. A systematic review and meta-analysis of prospective studies on the association between maternal cigarette smoking and preterm delivery. Am J Obstet Gynecol 2000;182(2):465–72.

[38] Grandjean P, Bellinger D, Bergman A, Cordier S, Davey-Smith G, Eskenazi B, et al. The faroes statement: human health effects of developmental exposure to chemicals in our environment. Basic Clin Pharmacol Toxicol 2008;102(2):73–5.

[39] Bellinger DC. A strategy for comparing the contributions of environmental chemicals and other risk factors to neurodevelopment of children. Environ Health Perspect 2012;120(4):501–7.
[40] Boyle JJ. Macrophage activation in atherosclerosis: pathogenesis and pharmacology of plaque rupture. Curr Vasc Pharmacol 2005;3(1):63–8.
[41] Vincent R, Kumarathasan P, Goegan P, Bjarnason SG, Guenette J, Berube D, et al. Inhalation toxicology of urban ambient particulate matter: acute cardiovascular effects in rats. Res Rep Health Eff Inst 2001;104:5–54.
[42] Calderon-Garciduenas L, Vincent R, Mora-Tiscareno A, Franco-Lira M, Henriquez-Roldan C, Barragan-Mejia G, et al. Elevated plasma endothelin-1 and pulmonary arterial pressure in children exposed to air pollution. Environ Health Perspect 2007;115(8):1248–53.
[43] Lygnos MC, Pappa KI, Papadaki HA, Relakis C, Koumantakis E, Anagnou NP, et al. Changes in maternal plasma levels of VEGF, bFGF, TGF-beta1, ET-1 and sKL during uncomplicated pregnancy, hypertensive pregnancy and gestational diabetes. In Vivo 2006;20(1):157–63.
[44] Xu J, Zou MH. Molecular insights and therapeutic targets for diabetic endothelial dysfunction. Circulation 2009;120(13):1266–86.
[45] Schafers M, Schober O, Hermann S. Matrix-metalloproteinases as imaging targets for inflammatory activity in atherosclerotic plaques. J Nucl Med 2010;51(5):663–6.
[46] Ostrovsky SR, Shulman CE, Peshu N, Staalsoe T, Hoyer-Hansen G, Pedersen BK, et al. Elevated plasma urokinase receptor predicts low birth weight in maternal malaria. Parasite Immunol 2007;29:37–46.
[47] Sundrani DP, Chavan Gautam PM, Mehendale SS, Joshi SR. Altered metabolism of maternal micronutrients and omega 3 fatty acids epigenetically regulate matrix metalloproteinases in preterm pregnancy: a novel hypothesis. Med Hypotheses 2011;77:878–83.

Thomson et al. Particle and Fibre Toxicology (2016) 13:65
DOI 10.1186/s12989-016-0176-y

Particle and Fibre Toxicology

RESEARCH Open Access

Contrasting biological potency of particulate matter collected at sites impacted by distinct industrial sources

Errol M. Thomson[1*], Dalibor Breznan[1], Subramanian Karthikeyan[1], Christine MacKinnon-Roy[1], Ngoc Q. Vuong[1], Ewa Dabek-Zlotorzynska[2], Valbona Celo[2], Jean-Pierre Charland[2], Prem Kumarathasan[1], Jeffrey R. Brook[3] and Renaud Vincent[1*]

Abstract

Background: Industrial sources contribute a significant proportion of anthropogenic particulate matter (PM) emissions, producing particles of varying composition that may differentially impact health. This study investigated the in vitro toxicity of ambient PM collected near industrial sites in relation to particle size and composition.

Methods: Size-fractionated particles (ultrafine, $PM_{0.1–2.5}$, $PM_{2.5–10}$, $PM_{>10}$) were collected in the vicinity of steel, copper, aluminium, and petrochemical industrial sites. Human lung epithelial-like A549 and murine macrophage-like J774A.1 cells were exposed for 24 h to particle suspensions (0, 30, 100, 300 μg/cm^2). Particle potency was assessed using cytotoxic (resazurin reduction, lactate dehydrogenase (LDH) release) and inflammatory (cytokine release) assays, and regressed against composition (metals, polycyclic aromatic hydrocarbons (PAHs), endotoxin).

Results: Coarse ($PM_{2.5–10}$, $PM_{>10}$) particle fractions were composed primarily of iron and aluminium; in contrast, ultrafine and fine ($PM_{0.1–2.5}$) fractions displayed considerable variability in metal composition (especially water-soluble metals) across collection sites consistent with source contributions. Semi-volatile and PM-associated PAHs were enriched in the fine and coarse fractions collected near metal industry. Cell responses to exposure at equivalent mass concentrations displayed striking differences among sites (*SITE x SIZE* and *SITE x DOSE* interactions, $p < 0.05$), suggesting that particle composition, in addition to size, impacted particle toxicity. While both J774A.1 and A549 cells exhibited clear particle size-dependent effects, site-dependent differences were more pronounced in J774A.1 cells, suggesting greater sensitivity to particle composition. Plotting particle potency according to cytotoxic and inflammatory response grouped particles by size and site, and showed that particles of similar composition tended to cluster together. Cytotoxic effects in J774A.1 cells correlated with metal and PAH content, while inflammatory responses were associated primarily with endotoxin content in coarse particles.

Conclusions: Industrial sources produce particulate emissions with varying chemical composition that differ in their in vitro potency in relation to particle size and the levels of specific constituents.

Keywords: Air pollution, Particle, Size, Source, Industry, Toxicity, Inflammation, Metals, Polycyclic aromatic hydrocarbons, Endotoxin

* Correspondence: errol.thomson@canada.ca; renaud.vincent@canada.ca
[1]Environmental Health Science and Research Bureau, Health Canada, Ottawa, Ontario K1A 0K9, Canada
Full list of author information is available at the end of the article

Background

On the basis of associations between particulate matter levels and morbidity and mortality [1–4], air quality standards in North America and Europe are expressed as mass concentrations for a given size range (i.e., PM_{10} and $PM_{2.5}$; particles with an aerodynamic diameter less than 10 μm and 2.5 μm respectively). It is clear, however, that biological responses to particulate matter are dependent not only on size, but also on other physicochemical characteristics such as inorganic and organic composition, which are impacted by mode of generation, and therefore source. Industrial sources are major contributors of particulate matter pollution, and in Canada account for an estimated 64% of total emitted particulate matter and 39% of PM_{10} (Environment Canada (2012)). An understanding of the relative contribution of sources and specific particle constituents to the toxic potency of airborne particulate matter could complement epidemiological studies and exposure data to ultimately inform regulatory initiatives aimed at targeting specific emission sources [5].

Particulate matter is a heterogeneous mixture composed of carbonaceous combustion materials such as polycyclic aromatic hydrocarbons, biogenic material, salts, and other inorganic materials such as transition metals. Particle composition varies geographically and temporally both in chemical composition and size distribution, and these differences are associated with variance in the magnitude of health impacts observed in epidemiological studies [3, 6, 7]. Differences in effects elicited by sub-components of the same particle mix may reflect particle size (e.g., the increased surface area to mass ratio of smaller particles resulting in more surface activity or adsorbed substances; differential particle deposition in the respiratory tract), particle number, composition, or combinations of these factors. We and others have shown previously that the potency of respirable fine particles from different geographical locations is related to their physicochemical characteristics, in particular to the profiles of bioavailable transition metals and polycyclic aromatic hydrocarbons (e.g., [8–12]. While soluble metals appear to play a key role in both acute lung injury [13, 14] and cardiovascular effects [15, 16] of particle exposure in rodents, some studies have found that insoluble particle components are more closely associated with cytotoxic and inflammatory responses in vivo and in vitro [17, 18]. Microbial components (e.g., endotoxin) associated with particles have also been shown to contribute to biological effects of ambient particles, in particular to their inflammogenic potential [9, 19]. Responses of cells that have direct contact with inhaled particles, such as alveolar macrophages and lung epithelial cells, may therefore depend on various particle properties (e.g., size, composition) and their interaction with cell-type-specific characteristics.

Several studies suggest that particulate emissions from specific industrial sources have significant population health impacts. Closure of a steel mill in Utah was associated with a reduction in respiratory and cardiovascular mortality, with daily mortality associated with PM_{10} levels [20]. Comparison of the biological potency of aqueous extracts of particulate samples collected on filters before, during, and after closure and resumption of mill activity revealed increased toxicity (according to lactate dehydrogenase, interleukin (IL)-6 and IL-8 release) associated with higher levels of lead, copper, zinc, and iron (each 2-3-fold higher) when the mill was operating [21]. A study examining health effects of living within pollution gradients of steel industry in Hamilton, Ontario, found increased relative risk of premature mortality associated with higher levels of total suspended particulate matter [22]. Proximity to copper refineries was associated with higher levels of lead, copper, arsenic, and zinc in ambient particles, and increased respiratory mortality [23], and closure of a copper refinery was associated with reduced respiratory and cardiovascular mortality [24]. This was attributed to reduced sulfate levels, although it was noted that transition metals (for which data were not available) would also have been expected to decrease during this period [25]. Changes in heart rate and heart rate variability observed in mice exposed to concentrated fine particulate matter in Tuxedo, New York, were associated with nickel, with 72 h back trajectories suggesting that the air mass passed over the nickel smelter in Sudbury, Ontario [26]. These studies implicate industrial emissions in the health impacts associated with exposure to particulate air pollution. However, to our knowledge there has been no direct comparison of the composition and relative toxicity of size-fractionated particles collected in the vicinity of multiple distinct industrial point sources. Such a study could provide valuable information on the links between sources, physicochemical characteristics of the particles, and toxic potency that underlie associations between exposure to particulate matter and adverse health effects.

Ambient particulate matter at any given site would be expected to be impacted by fixed regional sources, mobile transportation sources, and long-range transit of particles, in addition to local point sources. Nevertheless, airborne particulate matter collected downwind of specific industrial sources for an extended period of time should be enriched for particles generated by that source. In vitro models provide an effective platform for screening and comparing biological responses to materials of differing composition. Using such models, we have previously shown that particles collected at

industrial, high traffic, and residential sites within a small urban area can vary significantly in their composition and potency [12]. In the present study our objective was to compare the relative toxic potency of size-fractionated ambient particles collected at sites impacted by distinct industrial emission sources and investigate determinants of toxicity. We hypothesised that particles collected in the vicinity of different industrial sources would differ in their composition and in their toxic potency in biological systems. By sampling the air at sites in close proximity to specific industrial sources, our intention was to collect size-fractionated samples with distinct chemical composition that reflected a strong signal from the industrial site in question. A panel of cytotoxic and inflammatory assays was used to generate a response signature for each particulate sample, enabling regression of biological endpoints against particle constituents to investigate potency drivers. Our results show that particles collected in the vicinity of industrial sites display clear size- and site-dependent differences in composition and biological potency.

Methods

Particle collection and extraction

A ChemVol High Volume Cascade Impactor [27] was used to collect size-fractionated particles at ground level in the vicinity of five industrial sites. These were: a steel mill in Hamilton (Hamilton Beach, HB), Ontario (5 samples between October 24 and December 6, 2007); a petrochemical refinery in Sarnia (SR), Ontario (7 samples between January 25 and March 11, 2008), and another in Montréal (MA), Québec (5 samples between May 4 and June 8, 2009); a copper smelter in Montréal (MC), Québec (5 samples between February 24 and March 30, 2009); and an aluminum refinery in Shawinigan (SW), Québec (5 samples between June 18 and July 23, 2009). The sampler employed three impaction stages with polyurethane foam collection surfaces with target cut points at 10, 2.5, and 0.1 μm mass median aerodynamic diameter followed by collection of ultrafine particles on polypropylene filters, producing particle fractions with aerodynamic diameter >10 μm ($PM_{>10}$ or super-coarse), between 2.5 and 10 μm ($PM_{2.5-10}$ or coarse), between 0.1 and 2.5 μm ($PM_{0.1-2.5}$ or fine), and <0.1 μm (ultrafine particles, UFP). Collection efficiency curves for the ChemVol impaction stages were reported previously by Demokritou et al. (2002). A high capacity Roots™ Universal RAI Rotary Positive Blower was used to maintain the highest flow rate possible through the ChemVol impaction slits. The main restriction and greatest pressure drop was provided by the 0.1 μm cut stage, which limited the flow rate to the design flow of about 900 L/min according to the manufacturer (Rupprecht and Patashnick, Albany, NY). Samples were collected over a period of five weeks at each site, with the exception of Sarnia where the collection period was for seven weeks, with collection substrates replaced each week. Field blank filters were transported to each site, but remained unexposed to ambient air. They underwent all other steps followed by the samples (i.e., cleaning, handling in the laboratory, shipping, storage at the field site and in the laboratory, and extraction). All collection surfaces were precleaned prior to sampling with repeated sonication in Milli-Q-grade deionized, sterile water (18.2 MOhm.cm resistivity), and Omnisolv HR-GC-grade methanol (EMD Millipore, Etobicoke, ON, Canada), followed by drying under nitrogen and final evaporation of solvent in drying oven. Cleaned substrates were stored in sterile sample bags wrapped in foil to protect from photodegradation.

Particles were recovered from polyurethane foam and filters by aqueous extraction and sonication as previously described [12]. Samples collected across weeks at each site were extracted together, such that the extracted particles represent the full collection period. Extracted particles were vacuum-dried (22 h, 37 °C) using MiVac SpeedTrap™ vacuum concentrator (Genevac Ltd., Ipswitch, Suffolk, UK). Extraction efficiencies of particle mass determined by comparing filter masses pre- and post-extraction were 96 ± 19% from polyurethane foam and 37 ± 13% polypropylene filters. Ultrasonic agitation and mechanical manipulation of the substrates during particle extraction resulted in generation of a small amount of debris that would contribute to the extracted particle mass. Extraction of field blank (unexposed) polyurethane foam and polypropylene filters indicated that such filter material contributed 1–8% of extracted mass. Debris were removed by filtration of the polyurethane foam extracts using a sterile 40 μm nylon filter (BD Falcon Cell Strainer, Corning Life Sciences, Corning, NY), while polypropylene filter extracts were filtered sequentially through 40 μm and 5 μm filters (Target Syringe Filter, National Scientific Co., Rockwood, TN). Average particle yields (final particle mass recovered relative to initial mass extracted) from polyurethane foam and polypropylene filters were 90 ± 7% and 86 ± 9% respectively. Standard reference materials (SRM) TiO_2 (SRM-154b) and SiO_2 (SRM-1879a) were obtained from the National Institute of Standards and Technology (NIST, Gaithersburg, MD). Preparation and characterisation of the urban particulate matter standard EHC-6802 was described previously [28].

Characterisation of particle composition

All analyses of particle composition were performed on particles extracted as described above. For metals analyses, samples were first ultrasonically extracted with 2 mL of double deionized water (DDW, resistivity > 18

MOhm cm) for 30 min at room temperature. Both solid material and aqueous extract were quantitatively transferred to a centrifuge tube followed by dilution to 9 mL using DDW, and centrifuged for 5 min at 5000 rpm. An aliquot of supernatant (8 mL) was taken and acidified with 1% (v/v) HNO_3 [29, 30] for further analysis of water-soluble metals using ICP-MS. The remainder of the sample (solid residue and aqueous extract) was quantitatively transferred into a digestion vial and evaporated to almost dryness. Samples were then digested and analyzed by ICP-MS as previously described [12]. The obtained results were corrected for the water-soluble metals present in the analyzed samples (1 mL aqueous extract) to calculate the concentration of non-water-soluble metals. All measurements were performed using a 7500ce ICP–MS system (Agilent Technologies, Wilmington, DE, USA). The octopole collision/reaction system (ORS), was pressurized with He gas for analysis of V, As and Cr, and with H_2 for analysis of Fe and Se. Internal standardization with 0.5 mg/L solution of ^{45}Sc, ^{89}Y, ^{115}In, and ^{165}Ho was used to correct for instrument drift and nonspectral interferences. Quality control samples were used to determine the accuracy and precision of chemical analysis, and to diagnose contamination.

For polycyclic aromatic hydrocarbons (PAHs), particle samples were spiked with 50 μL of isotopically labeled PAH surrogate standards for recovery correction. PAH analyses were performed on $PM_{0.1-2.5}$, $PM_{2.5-10}$ and $PM_{>10}$ fractions but not ultrafine ($PM_{<0.1}$) particles due to lack of material for this size fraction. Samples were extracted by Soxhlet apparatus in 350 mL of cyclohexane for 16 to 20 h. Following evaporation to ~5 mL, the extract was subjected to activated silica gel column chromatography for fractionation of the desired target analytes using a suite of solvents of increasing polarity as previously described [12]. The purified extract, to which 50 μL d10-fluoranthene (10 ng/μL) was added, was analysed for PAHs by GC/MS using low resolution Agilent 7890A GC interfaced directly to Agilent 5975C Mass Selective Detector under conditions previously described [12]. Quality control samples were used to determine the accuracy and precision of the chemical analyses. Field blank filter samples were used to assess and correct for background concentrations.

Endotoxin levels were assessed using the Limulus Amebocyte Lysate (LAL) chromogenic quantitation kit (Lonza, Walkersville, MD, USA) and quantified with a Synergy 2 multi-mode plate reader (Bio-Tek, Winooski, VT, USA) as described previously [12].

In vitro exposures

Human lung epithelial-like (A549; ATCC, CCL-185) and murine macrophage-like (J774A.1; ATCC, TIB-67) cell lines (American Type Culture Collection, Manassas, VA, USA) were propagated in Dulbecco's Modified Eagle's Medium (Fisher Scientific) containing phenol red and 4.5 g/L glucose and supplemented with FBS (10% v/v, non-heat inactivated; Fisher Scientific) and Pen Strep (100 U/ml penicillin-G, 100 mg/ml streptomycin; Sigma-Aldrich Canada, Oakville, ON) for A549 cells and Gentamicin (50 μg/mL; Sigma-Aldrich Canada, Oakville, ON) for J774A.1 cells respectively, in 75 cm^2 tissue culture flasks (Corning, NY, USA) at 37 °C, 5% CO2, and 95% relative humidity. Phenol red was excluded for particle exposures and bioassays to avoid interference with the detection methods. Cells were seeded in 96-well black-walled clear-bottom cell culture plates (BD Biosciences, Mississauga, ON) at 100 μL/well (A549, 2 x 10^4 cells/well, 6 x 10^4 cells/cm^2; J774A.1, 4 x 10^4 cells/well, 12 x 10^4 cells/cm^2) of complete medium, and incubated at 37 °C for 24 h. On the day of exposure, particle suspensions were thawed, sonicated for 20 min in an ice-cold ultrasonic water bath, diluted in complete media devoid of serum, and sonicated for a further 5 min immediately prior to cell dosing. Cell monolayers were exposed to 100 μl particle suspensions resulting in 0, 30, 100, and 300 μg/cm^2 in a final volume of 200 μl (with a 5% final concentration of serum). Polyurethane foam and polypropylene field blank filter extracts resuspended according to the mean volume used to resuspend extracted particles for each size fraction were compared alongside particles for all toxicity experiments to test for biological effects of any residues from collection substrates. Doses were selected to range from levels that produce negligible effects to levels that produce measurable effects according to the cytotoxicity assays employed so that dose–response relationships could be evaluated [12]. Cells were incubated at 37 °C for 24 h prior to assessment of cytotoxicity and inflammatory effects, a time point selected to allow for cytotoxic and inflammatory responses to develop [12]. Three independent exposure experiments were conducted for each cell line, with duplicate technical replicates included on each plate.

Cytotoxicity assays

Aliquots of supernatants clarified by centrifugation at 350 × g for 5 min were used in the lactate dehydrogenase (LDH) release and inflammatory cytokine assays. Metabolic activity was assessed in cells after the addition of the resazurin reagent mixture (Alamar Blue, Fisher Scientific). Reduction of the dye resazurin to resorufin was calculated by fluorescence reading at 3 h minus baseline fluorescence measured at λEx = 530–540 nm and λEm = 590–600 nm. Following removal of the supernatant, cells were washed in serum-free medium (15 min incubation at 37 °C), lysed in a buffer containing 100 mM $MgCl_2$ and 0.025% Triton X-100 in PBS at room temperature for 5 min, and centrifuged

for 10 min at 1700 × g. The obtained supernatants and lysates were transferred to 96-well conical bottom plates and clarified by centrifugation for 5 min at 350 × g. LDH levels were measured using the CytoTox 96 colorimetric assay (Promega Corporation, Madison, WI) as previously described [12], and LDH release was calculated as a fraction of total LDH activity recovered in supernatant and cell lysate.

Cytokines

Levels of IL-1α, IL-1β, IL-2, IL-3, IL-4, IL-5, IL-6, IL-9, IL-10, IL-12 p70, IL-13, IL-17, eotaxin, G-CSF, GM-CSF, IFNγ, KC, MCP1, MIP-1α, MIP-1β, RANTES, and TNF were assessed in J774A.1 cell supernatants using the Bio-Plex Pro Mouse Cytokine 23-plex Assay (Bio-Rad Laboratories (Canada) Ltd., Mississauga, Ontario, Canada) on a Bio-Plex 200 multiplex luminescence assay system (Bio-Rad Laboratories (Canada) Ltd.) following the manufacturer's protocol.

Potency estimates

Cytotoxicity endpoints (resazurin reduction, lactate dehydrogenase release) and cytokine levels were normalized to the mean of the respective controls to generate fold-change values for each particle dose. Potency estimates (β) of the exposure-response relationship were derived from the following equation: fold-change = $(\text{Dose} + 1)^{\beta}$ where β is the slope of the relationship on the logarithmic scale [8]. As higher potency is reflected by a greater negative slope in the resazurin reduction assay and a positive slope in the LDH release assay, potency estimates for resazurin reduction were multiplied by −1 prior to averaging of cytotoxic potencies across assays to generate a consensus cytotoxic potency for each particle.

Statistical analyses

Cytotoxicity and cytokine dose–response data for the size-fractionated particle exposures were assessed for statistically significant effects by three-way ANOVA with *Dose* (0, 10, 30, 100 μg/cm^2), *Site* (Hamilton beach (HB), Montréal petrochemical industry (MA), Montréal copper refinery (MC), Sarnia petrochemical industry (SR), Shawinigan aluminium smelter (SW)) and *Size* (UFP, $PM_{0.1-2.5}$, $PM_{2.5-10}$, $PM_{>10}$) as factors. For the particle standards, two-way ANOVA was performed with *Particle* (EHC-6802, TiO_2, SiO_2) and *Dose* (0, 10, 30, 100 μg/cm^2) as factors. Datasets not meeting the assumptions of normality and equal variance for ANOVA were transformed prior to analyses. Pairwise multiple comparisons were carried out using the Holm-Sidak procedure as directed by significant factor interactions or main effects in the ANOVA to elucidate the pattern of significant effects ($\alpha = 0.05$). Correlations were performed between toxicological endpoints and particle chemistry using Pearson's Product Moment Correlation and Best Subset Regression. All statistical analyses were conducted using SigmaPlot version 13 (Systat Software, Inc., San Jose, CA, USA). Clustering of particles based on composition was conducted using Minitab, version 15 (Minitab Inc., State College, PA, USA). Heatmap software was used to visualise inflammatory cytokine potency data (http://www.hiv.lanl.gov/content/sequence/HEATMAP/heatmap.html; Los Alamos National Laboratory, Los Alamos, NM, USA).

Results

Chemical analyses of particles from sites impacted by industrial sources

Levels of metals, PAHs, and endotoxin were analysed in each particle (summarised in Table 1).

There was considerable variability in the concentration of metals per unit mass of particulate sample across sites. Hamilton (HB) and Shawinigan (SW) had the highest total metal content across size fractions (with the exception of high levels in the fine fraction from the Montréal petrochemical site (MA)), followed by the two Montréal sites (MA, MC), and lastly Sarnia (SR), which had considerably lower metal content than all other sites. The amount of PAHs in extracted particles was also variable, with no clear trends across size fractions or sites beyond relatively high levels recovered in the coarse and super-coarse fractions in Shawinigan. Endotoxin was detected in all samples, and tended to increase with particle size (*Size* main effect, $p < 0.001$), with significantly higher levels in $PM_{2.5-10}$ and $PM_{>10}$ compared to the ultrafine fraction ($p < 0.05$, Holm-Sidak pairwise comparison). Detailed data on metal and PAH content are provided in Additional files 1 and 2 respectively.

Comparison of metal content across sites revealed size-dependent contrasts in composition and solubility (Fig. 1). Compared on an equivalent mass concentration basis, $PM_{2.5-10}$ and $PM_{>10}$ fractions displayed total metal content 2–3 times higher than UFP and $PM_{0.1-2.5}$ fractions. However, whereas metals in the $PM_{2.5-10}$ and $PM_{>10}$ fractions consisted largely of non-water-soluble iron and aluminium, metal solubility was markedly higher in UFP and $PM_{0.1-2.5}$ fractions. The UFP and $PM_{0.1-2.5}$ fractions were also considerably more variable in composition, with the most striking differences in composition observed in the water-soluble fractions. Notable differences included relatively high levels of zinc, manganese, and arsenic in samples collected near Hamilton steel industry; copper, arsenic, and lead in samples collected near the Montréal copper refinery and to a lesser extent in samples collected near Montréal petrochemical industry; higher cadmium and cobalt in samples collected near the Montréal petrochemical site;

Table 1 Composition of size-fractionated particles collected in the vicinity of industrial sites: total metals, endotoxin, polycyclic aromatic hydrocarbons

	Total Metals[a] (μg/g)				Endotoxin (EU/ml/μg PM)				PAHs[b] (μg/g of PM)		
	UFP	$PM_{0.1-2.5}$	$PM_{2.5-10}$	$PM_{>10}$	UFP	$PM_{0.1-2.5}$	$PM_{2.5-10}$	$PM_{>10}$	$PM_{0.1-2.5}$	$PM_{2.5-10}$	$PM_{>10}$
Hamilton Beach (HB)	29512	32675	86365	72230	0.017	0.038	0.082	0.072	151	90	22
Montréal (MA)	12827	39228	59533	56430	0.019	0.047	0.074	0.080	28	74	40
Montréal (MC)	14467	19758	44853	36381	0.009	0.051	0.053	0.019	100	79	93
Sarnia (SR)	5346	9965	28264	18842	0.006	0.005	0.037	0.054	40	51	96
Shawinigan (SW)	19612	36537	87836	110990	0.010	0.044	0.046	0.078	111	413	305

[a]See Additional file 1 for complete description of metals analysed
[b]See Additional file 2 for complete description of PAHs analysed

and the predominance of aluminum in samples collected near the Shawinigan aluminium refinery (complete metal analyses provided in Additional file 1). Clustering of particles according to the composition of water-soluble metals showed that UFP and $PM_{0.1-2.5}$ particles were more different from each other and from all other particles than any of the $PM_{2.5-10}$ and $PM_{>10}$ samples (Additional file 3). Similar clustering according to size fraction was observed for total metals and non-water-soluble metals, although clusters were less defined. Analysis of covariance of water-soluble elements revealed good correlations (>85% covariance) among a number of sets of elements, including aluminum and beryllium; chromium, cobalt, molybdenum, and cadmium; vanadium, arsenic, lead, and copper; and manganese, zinc, and thallium (Additional file 4).

PAHs were grouped based on their volatility (volatile: acenaphthene, fluorine, phenanthrene, anthracene; semi-volatile: fluoranthene, pyrene, retene, benz(a)anthracene, chrysene; and particle-associated: benzo(b)fluoranthene, benzo(k)fluoranthene, benzo(a)pyrene, indeno(123-cd)pyrene, dibenz(a,h)anthracene, benzo(ghi)perylene) and compared across sites and size fractions (Fig. 2). Semi-volatile and particle-associated PAHs tended to be enriched in the fine and coarse fractions collected near metal industry sites in Hamilton (HB), Montreal (MC), and Shawinigan (SW) compared to petrochemical sites in Sarnia (SR) and Montreal (MA). Volatile PAHs tended to be enriched in the coarse and super-coarse fractions across most sites with the exception of Shawinigan, which displayed the highest levels of semi-volatile and particle-associated PAHs in these fractions.

Cytotoxic responses

Particle-induced cytotoxicity was assessed across a range of doses by measuring resazurin reduction, an indicator

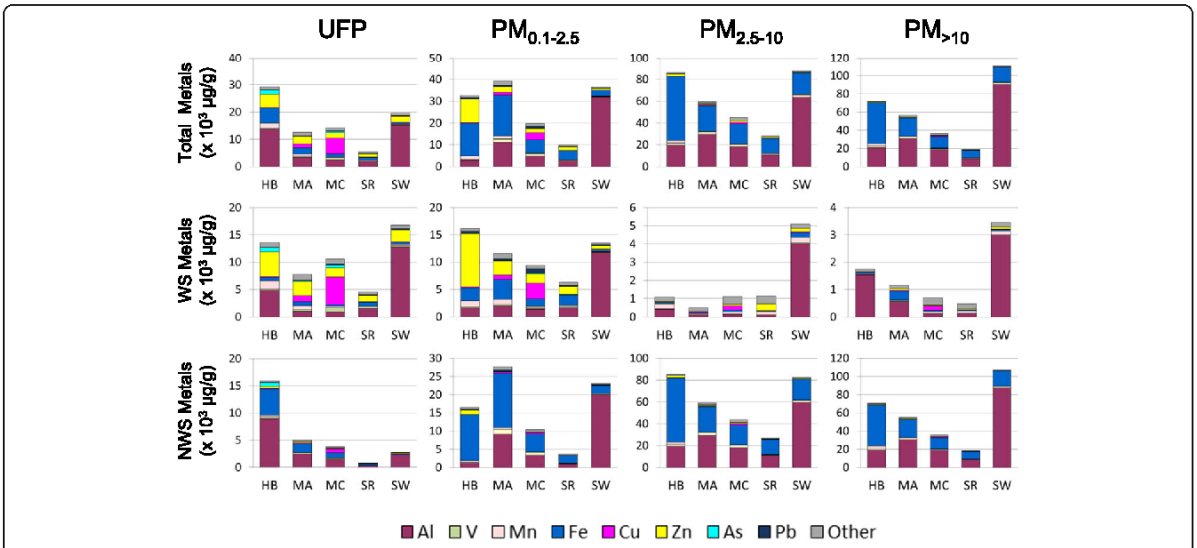

Fig. 1 Metal composition of particles collected in the vicinity of industrial sites. The elemental composition of particulate samples according to total metals, water-soluble (WS) metals, and non-water-soluble (NWS) metals was assessed across particle size-fractions. HB, Hamilton Beach steel mill; MA, Montréal petrochemical refinery; MC, Montréal copper smelter; SR, Sarnia petrochemical refinery; SW, Shawinigan aluminum smelter

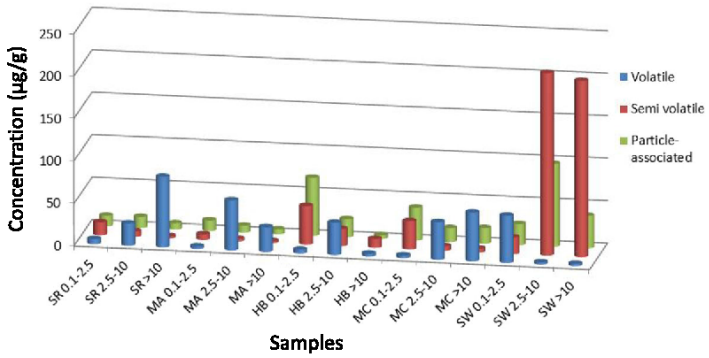

Fig. 2 Polycyclic aromatic hydrocarbon (PAH) content of particles collected in the vicinity of industrial sites. PAHs were grouped according to volatility (volatile: acenaphthene, fluorine, phenanthrene, anthracene; semi-volatile: fluoranthene, pyrene, retene, benz(a)anthracene, chrysene; particulate-associated: benzo(b)fluoranthene, benzo(k)fluoranthene, benzo(a)pyrene, indeno(123-cd)pyrene, dibenz(a,h)anthracene, benzo(ghi)perylene) and compared across sites and size-fractions. HB, Hamilton Beach steel mill; MA, Montréal petrochemical refinery; MC, Montréal copper smelter; SR, Sarnia petrochemical refinery; SW, Shawinigan aluminum smelter

of metabolic activity, and LDH release, an indicator of membrane permeability, in two cell lines: macrophage-like J774A.1 cells and A549 lung epithelial-like cells (Additional files 5, 6, 7 and 8, left panels). Particles produced dose–response relationships across the sites and size-fractions (*SIZE* x *DOSE* interaction, $p < 0.05$ for all assays; see figure legends for statistical analyses). Effects of particles differed across sites, however, as revealed by significant *SITE* x *SIZE* and *SITE* x *DOSE* interactions ($p < 0.05$). In contrast, exposure to extracts of field blank filters produced minimal response across cell lines and assays (Additional files 5, 6, 7 and 8, right panels) with the exception of the LDH response in A549 cells in which the blank filter extracts produced a small but significant dose-related response. In this cell line the UFP and $PM_{0.1-2.5}$ fractions did not elicit a significantly greater LDH response than was observed for the corresponding blank filter extracts; however, $PM_{2.5-10}$ and $PM_{>10}$ samples produced a markedly greater response compared to blank filter extracts.

To reduce complexity and facilitate comparison of the pattern of effects, cytotoxic potencies according to resazurin reduction and LDH release assays were estimated using the slope of dose–response relationships observed for each assay. Potency estimates for both J774A.1 and A549 cells varied considerably across sites and sizes (Fig. 3). The pattern of potency estimates in J774A.1 cells was generally consistent for resazurin reduction and LDH assays ($r = 0.78$, $p < 0.001$). Sarnia particles of all size fractions exhibited low potency according to both cytotoxicity assays in J774A.1 cells compared to particles from other sites (Fig. 3a, b). The ultrafine fraction produced negligible cytotoxicity in resazurin reduction and LDH assays, with the exception of Hamilton and Shawinigan UFP which produced modest cytotoxic responses. For the remaining size fractions, potency estimates were variable across sites, with the fine ($PM_{0.1-2.5}$) or coarse ($PM_{2.5-10}$) fractions generally more potent than the super-coarse ($PM_{>10}$) fraction. Whereas fine, coarse, and super-coarse particles from Hamilton steel, Montréal petrochemical, and Montréal copper exhibited significant size-dependent contrasts in potency according to both cytotoxic assays, Sarnia petrochemical and Shawinigan aluminum site particles tended to exhibit more similar potency across size-fractions.

Exposure of A549 cells produced a similar profile of resazurin reduction (Fig. 3c) to that observed in J774A.1 cells ($r = 0.84$, $p < 0.001$). In contrast, the pattern of LDH release in A549 cells (Fig. 3d) differed significantly from the pattern of resazurin reduction in the same cells ($r = 0.23$, $p = 0.34$) and with the LDH response in J774A.1 cells ($r = 0.33$, $p = 0.16$), with less evidence of site-dependent differences and more uniform size-dependent effects. For example, whereas Sarnia particles exhibited little capacity to provoke LDH release in J774A.1 cells (Fig. 3b), in A549 cells the LDH profile was similar to that seen for other sites (Fig. 3d). Potency measured by A549 LDH release tended to increase with particle size ($UFP \leq PM_{0.1-2.5} < PM_{2.5-10} \leq PM_{<10}$).

Cytokine release

The inflammatory potential of particles was assessed by measuring cytokine levels released by J774A.1 cells into cell culture media. In contrast to exposures to field blank filter extracts (Additional file 9), particle exposures altered cytokine levels in a dose-dependent manner characterised by clear size- and site-dependent effects (Fig. 4). For example, IL-6 responded strongly to the $PM_{2.5-10}$ and $PM_{>10}$ size-fractions, but less so to the fine $PM_{0.1-2.5}$ fraction with the exception of Shawinigan

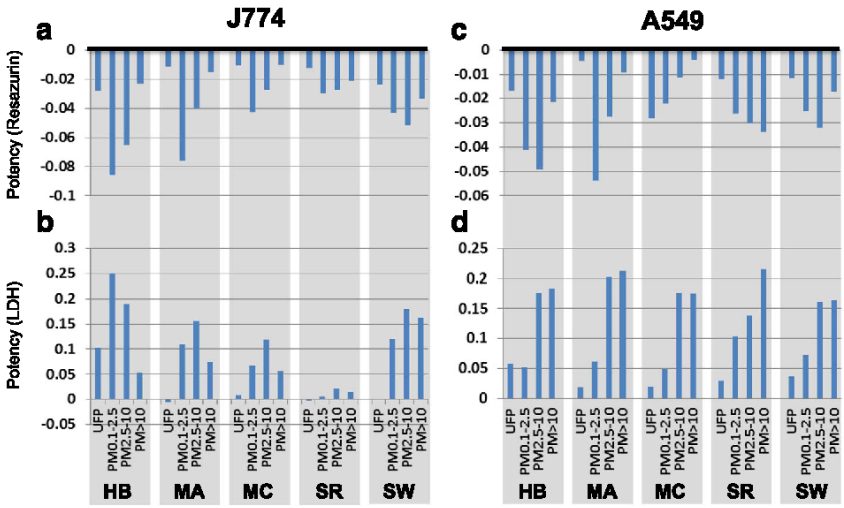

Fig. 3 Cytotoxic potency of size-fractionated particles from industrial sites. Cytotoxic potency (β) was estimated using the slope of the dose-effect relationship from $n = 3$ independent experiments as described in the Methods section. Potency was assessed according to resazurin reduction and lactate dehydrogenase (LDH) release in J774A.1 macrophage-like cells (**a**, **b**) and A549 epithelial-like cells (**c**, **d**) respectively. For both assays, the height of the bar represents the potency, with greater negative numbers in the resazurin reduction assay and greater positive numbers in the LDH release assay corresponding to increased potency. HB, Hamilton Beach steel mill; MA, Montréal petrochemical refinery; MC, Montréal copper smelter; SR, Sarnia petrochemical refinery; SW, Shawinigan aluminum smelter

$PM_{0.1-2.5}$ (*Site* x *Size* x *Dose* interaction, $p = 0.002$; Fig. 4a). To facilitate comparison of inflammatory signaling across samples, particle inflammatory potency was estimated using the slope of the dose–response curve for each cytokine. Two-way clustering of cytokines and samples according to potency for the most part separated particles by size, with some evidence of clustering according to site (Fig. 4b). Hamilton and Montréal petrochemical site $PM_{2.5-10}$ and $PM_{>10}$ samples formed a cluster characterised by strong inflammatory response, characterised by markedly higher levels of IL-6, RANTES, MCP-1, IL-1α, and KC. Sarnia and Montréal copper refinery $PM_{>10}$ samples also produced a strong response, and clustered with the urban standard EHC-93 and with Montréal petrochemical site $PM_{0.1-2.5}$. The remaining fine $PM_{0.1-2.5}$ fractions (Montréal copper refinery, Hamilton steel, Sarnia petrochemical) clustered together and were generally of lower potency. The two mineral dusts TiO_2 and SiO_2, included as standard reference materials, clustered together with most UFP. TiO_2 elicited little inflammatory response, while cytokine release tended to decrease with increasing dose of SiO_2. UFP exposure produced a unique profile of cytokine response compared to other particles, characterised by decreased IL-10 (*Size* x *Dose* interaction, $p < 0.001$; *Site* x *Size* interaction, $p = 0.035$) and RANTES (*Site* x *Size* x *Dose* interaction, $p = 0.025$), as well as a modest increase of G-CSF (*Site* x *Size* x *Dose* interaction, $p < 0.001$). In contrast to the size-dependent effects, three Shawinigan samples ($PM_{0.1-2.5}$, $PM_{2.5-10}$, $PM_{>10}$) elicited a similar inflammatory response and clustered together, while Shawinigan UFP tended to decrease cytokine expression to a greater extent than other sites.

Integrated estimate of potency

Contrasts in particle effects across sites and sizes may be better visualised by integrating particle potency assessed by cytotoxicity and inflammatory measures [12]. As J774A.1 cells appeared to be more sensitive to site-dependent differences, integrated potency estimates were generated for responses measured using cytotoxic (resazurin reduction, LDH release) and inflammatory (mean of all cytokines) responses in these cells. Plotting cytotoxic and inflammatory potency for all particles (Fig. 5) showed that UFP exhibited the lowest cytotoxic and inflammatory potency, with the exception of Hamilton UFP, which exhibited relatively high cytotoxic potency but little inflammatory potency. All remaining size fractions from Shawinigan clustered together (relatively high cytotoxic and inflammatory potential), as did fractions from Sarnia (relatively low cytotoxic and inflammatory potential). Particles from the two Montréal sites generally clustered together, with fractions from the petrochemical site tending to have slightly higher cytotoxic and inflammatory potency than the corresponding size fraction from the copper refinery site across size fractions. In contrast to these groupings, potency estimates

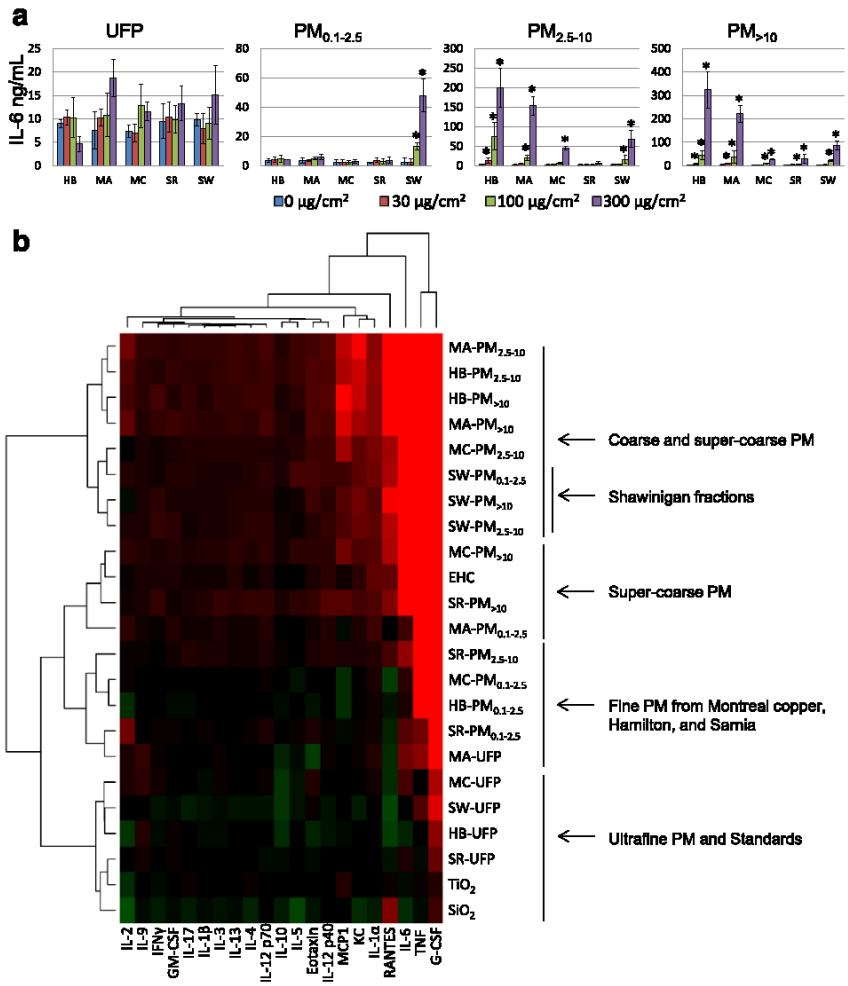

Fig. 4 Inflammatory response to particles collected at industrial sites. Cytokine responses were measured in cell culture supernatants of J774A.1 cells exposed to size-fractionated particles ($n = 3$ independent experiments). **a** Interleukin (IL)-6 levels released by J774A.1 cells in response to a 24 h exposure to UFP, $PM_{0.1-2.5}$, $PM_{2.5-10}$ and $PM_{>10}$ from industrial sites. Three-way ANOVA, *Dose x Site x Size* interaction, $p = 0.002$. For simplicity, only significant dose effects relative to 0 µg/cm^2 within a *Site* and *Size* are presented (*$p < 0.05$, Holm-Sidak). **b** Hierarchical clustering of particles according to cytokine response in J774A.1 cells. The heat map displays particle potency estimates determined for each cytokine from the slope of the dose-effect relationship. General descriptions of the clusters are presented on the right. Red, increased expression; green, decreased expression. HB, Hamilton Beach steel mill; MA, Montréal petrochemical refinery; MC, Montréal copper smelter; SR, Sarnia petrochemical refinery; SW, Shawinigan aluminum smelter

for particles from Hamilton varied considerably across size fractions and were distributed around the periphery of the plot, exhibiting high cytotoxic/low inflammatory potency (fine $PM_{0.1-2.5}$), high cytotoxic and inflammatory potency ($PM_{2.5-10}$), or low cytotoxic/high inflammatory potency ($PM_{>10}$).

Regressions against total metals, PAH, and endotoxin content

The observation that plotting particle potency according to average cytotoxic and inflammatory responses grouped particles of similar composition (e.g., Shawinigan particles) suggested that composition, in addition to size, is an important determinant of potency. To explore the link between particle composition and in vitro response, potency estimates were regressed against metals (total, water-soluble, non-water-soluble), PAHs, and endotoxin content. In J774A.1 cells, metal content within each size fraction tended to be associated with potency according to both LDH release and resazurin reduction, but associations differed according to metal solubility (Fig. 6). Ultrafine particles exhibited little potency, and associations with metal content were driven by the response to the Hamilton sample. For the remaining size fractions, the slope describing

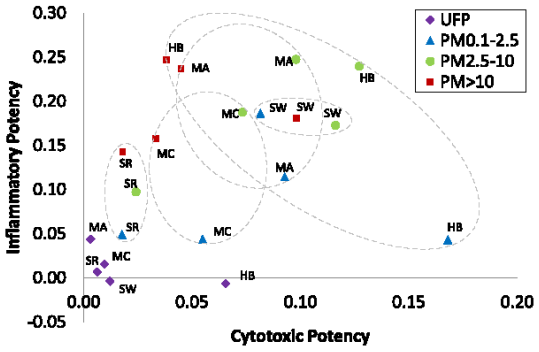

Fig. 5 Integrated assessment of particle potency as a function of cytotoxic and inflammatory potency estimates. Potency estimates were calculated for responses of J774. A1 cells to particles described in the Methods. Groupings of particles (excluding UFP) from the same site are indicated by dashed lines. HB, Hamilton Beach steel mill; MA, Montréal petrochemical refinery; MC, Montréal copper smelter; SR, Sarnia petrochemical refinery; SW, Shawinigan aluminum smelter

the association between total metals and potency tended to decrease with increasing particle size (Fig. 6a, d), and mirrored the trends observed in the non-water-soluble fraction (Fig. 6c, f). In general, the potency of $PM_{0.1-2.5}$ particles was more closely associated with water-soluble metals (Fig. 6b, e) while the potency of $PM_{2.5-10}$ was more closely associated with non-water-soluble metals (Fig. 6c, f); associations between $PM_{>10}$ potency and metals tended to be independent of solubility. Association of cytotoxic response with metals were generally weaker and non-significant in A549 cells (Additional file 10). Inflammatory potential in J774A.1 cells was positively correlated with total metals ($r = 0.74$, $p < 0.001$), non-water-soluble metals ($r = 0.80$, $p < 0.001$), and negatively correlated with water-soluble metals ($r = -0.67$, $p = 0.001$) when data from all size fractions were included. However, there was little evidence for associations between metals and inflammatory potential when size fractions were assessed individually (data not shown).

Total PAH content was associated with LDH release in J774A.1 cells ($r = 0.52$, $p = 0.045$) when all size fractions were included in the analysis. With the exception of a marginal association between PAHs in the $PM_{>10}$ fraction and LDH release ($r = 0.81$, $p = 0.09$), associations were weak and non-significant when analysed within each size fraction (Additional file 11). Stratification of PAHs according to volatility showed that while cytotoxic responses were not associated with volatile PAH content, LDH release was associated with super-coarse fraction

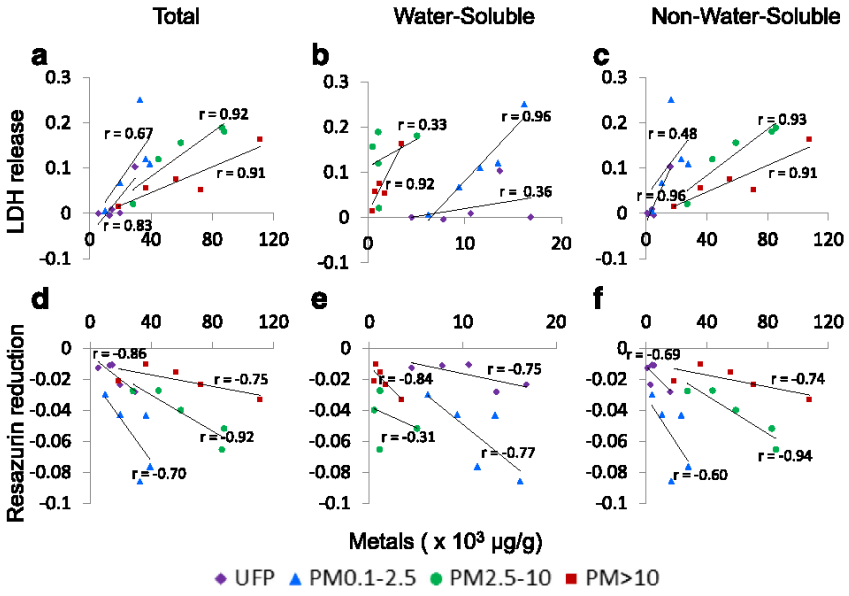

Fig. 6 Association of cytotoxic potency in J774A.1 cells with metal content in size-fractionated particles. Cytotoxic potencies according to lactate dehydrogenase (LDH) release and resazurin reduction were regressed against total, water-soluble, and non-water-soluble metals. Pearson product–moment correlation coefficient r-values are presented. LDH release. **a** Total metals. UFP, $r = 0.83$, $p = 0.08$; $PM_{0.1-2.5}$, $r = 0.67$, $p = 0.22$; $PM_{2.5-10}$, $r = 0.92$, $p = 0.03$; $PM_{>10}$, $r = 0.91$, $p = 0.03$. **b** Water-soluble metals. UFP, $r = 0.36$, $p = 0.55$; $PM_{0.1-2.5}$, $r = 0.96$, $p < 0.01$; $PM_{2.5-10}$, $r = 0.33$, $p = 0.59$; $PM_{>10}$, $r = 0.92$, $p = 0.02$. **c** Non-water-soluble metals. UFP, $r = 0.96$, $p = 0.01$; $PM_{0.1-2.5}$, $r = 0.48$, $p = 0.42$; $PM_{2.5-10}$, $r = 0.93$, $p = 0.02$; $PM_{>10}$, $r = 0.91$, $p = 0.03$. Resazurin reduction. **d** Total metals. UFP, $r = -0.86$, $p = 0.06$; $PM_{0.1-2.5}$, $r = -0.70$, $p = 0.19$; $PM_{2.5-10}$, $r = -0.92$, $p = 0.02$; $PM_{>10}$, $r = -0.75$, $p = 0.15$. **e** Water-soluble metals. UFP, $r = -0.75$, $p = 0.14$; $PM_{0.1-2.5}$, $r = -0.77$, $p = 0.13$; $PM_{2.5-10}$, $r = -0.31$, $p = 0.61$; $PM_{>10}$, $r = -0.84$, $p = 0.07$. **f** Non-water-soluble metals. UFP, $r = -0.69$, $p = 0.20$; $PM_{0.1-2.5}$, $r = -0.60$, $p = 0.28$; $PM_{2.5-10}$, $r = -0.94$, $p = 0.02$; $PM_{>10}$, $r = -0.74$, $p = 0.15$

semi-volatile PAHs ($r = 0.92$, $p = 0.03$; $r = 0.46$, $p = 0.09$ when including data for all size fractions) and PM-associated PAHs ($r = 0.85$, $p = 0.07$; $r = 0.63$, $p = 0.01$ when including data for all size fractions). Resazurin reduction and inflammatory potential were not consistently associated with PAH content (Additional file 11).

Endotoxin was most strongly associated with inflammatory potency (J774A.1, $r = 0.85$, $p < 0.001$) and LDH release (J774A.1, $r = 0.55$, $p = 0.01$; A549, $r = 0.71$, $p < 0.001$), but not with resazurin reduction (J774A.1, $r = 0.40$, $p = 0.08$; A549, NS) when all size fractions were evaluated together. When size fractions were evaluated individually, the only significant association was with inflammatory potency in the $PM_{2.5-10}$ fraction ($r = 0.94$, $p = 0.02$, Additional file 11).

Regressions against specific metals

Given the overall positive correlations between metals and cytotoxicity endpoints, best subset regressions were performed on metal composition to identify potential drivers of toxicity. Analyses were performed on abundant metals (those exceeding 100 μg/g in at least one particle size/sample) in the water-soluble fraction (Al, V, Mn, Fe, Ni, Cu, Zn, As, Sr, Cd, Ba, Pb) and non-water-soluble fraction (Al, Ti, V, Cr, Mn, Fe, Ni, Cu, Zn, Sr, Sn, Ba, Pb). UFP were excluded from these analyses as they did not exhibit strong contrasts in potency across sites. Potency according to resazurin reduction in J774A.1 cells could be predicted by the linear combination of the concentration of water-soluble Mn, Fe, Cu, Zn, and Pb ($\beta = 0.0168 + [0.000155 \times Mn] - [0.0000178 \times Fe] - [0.0000547 \times Cu] - [0.0000156 \times Zn] + [0.000246 \times Pb]$; $r^2 = 0.90$, $p < 0.05$ for all elements). However, water-soluble Mn alone was sufficient to explain a significant proportion of the variance in potency ($\beta = 0.0235 + [0.0000634 \times \text{soluble Mn}]$; $r^2 = 0.75$, $p < 0.001$). Resazurin reduction in A549 cells was also most closely associated with Mn ($\beta = 0.0189 + [0.0000317 \times \text{soluble Mn}]$; $r^2 = 0.47$, $p = 0.005$). LDH release in J774A.1 cells was predicted by a linear combination of water-soluble manganese and iron ($\beta = 0.0684 + [0.000334 \times \text{soluble Mn}] - [0.0000676 \times \text{soluble Fe}]$; $r^2 = 0.69$, Mn $p = 0.002$, Fe $p = 0.011$), with manganese again being the best single predictor ($\beta = 0.0743 + [0.000122 \times \text{soluble Mn}]$; $r^2 = 0.26$, $p = 0.05$). No soluble element predicted LDH release in A549, although there was a significant inverse relationship with nickel ($\beta = 0.198 - [0.000860 \times \text{soluble Ni}]$; $r^2 = 0.81$, $p < 0.001$).

Regressing against non-water-soluble metal levels, resazurin reduction in J774A.1 cells was predicted by a linear combination of lead, zinc, and strontium ($\beta = 0.023 + [0.000145 \times Pb] + [0.0000127 \times Zn] - [0.0000799 \times Sr]$; $r^2 = 0.90$, Pb $p < 0.001$, Zn $p = 0.013$, Sr $p < 0.001$), which could be simplified to lead alone ($\beta = 0.0176 + [0.000155 \times Pb]$; $r^2 = 0.571$, $p = 0.001$). In A549 cells, resazurin reduction was predicted by the concentration of non-water-soluble lead, iron, and strontium ($\beta = 0.0192 + 0.0000696 \times Pb] + [0.000000322 \times Fe] - [0.0000548 \times Sr]$; $r^2 = 0.73$, Pb $p = 0.006$, Fe $p = 0.055$, Sr $p = 0.002$). Lactate dehydrogenase release in J774A.1 cells was predicted by a linear combination of non-water-soluble lead, zinc, and aluminium ($\beta = -0.0151 \times [0.000381 \times Pb] + [0.0000526 \times Zn] + [0.00000158 \times Al]$, $r^2 = 0.698$, Pb $p = 0.008$, Zn $p = 0.040$, Al $p = 0.012$], and in A549 cells by non-water-soluble titanium and tin ($\beta = 0.146 + [0.0000647 \times Ti] - [0.00119 \times Sn]$; $r^2 = 0.60$, Ti $p = 0.004$, Sn $p = 0.022$].

Discussion

Industrial emissions are important contributors to particulate air pollution levels, and may contribute to geographical disparities in the health impacts of particulate matter identified in epidemiological studies [3, 6, 7]. There has, however, been little direct comparison of the toxicity of particles from multiple industrial sources. In the present study, particles collected in the vicinity of industrial sources were compared across size fractions on an equal mass basis, across a range of doses, in two cell lines, using a panel of cytotoxic and inflammatory assays to characterise the profile of response. Our results demonstrate that particles collected near distinct industrial sites display strong contrasts in composition and in vitro toxicity, substantiating the hypothesis that industrial sources differentially impact the toxicity of airborne particulate matter.

The distinct composition of particles collected in the vicinity of industrial sites, notably with respect to metals, suggests that emissions from dominant local sources were enriched in our samples collected over a period of weeks, as expected. All size-fractions displayed differences in the total concentration of metals, but the extent to which constituent metals varied depended on the size-fraction. Metal composition of coarse ($PM_{2.5-10}$) and super-coarse ($PM_{>10}$) fractions was similar across sites, consisting mostly of the common crustal elements aluminium and iron. In contrast, UFP and fine ($PM_{0.1-2.5}$) particles exhibited considerable variability across sites generally consistent with significant impact of the local sources targeted by our sampling (e.g., elevated zinc, manganese and arsenic near the Hamilton steel mills; elevated copper, arsenic, and lead near the Montréal copper refinery; elevated aluminum near the Shawinigan aluminium smelter; [31, 32]). Relatively high levels of copper were also detected at the Montréal petrochemical site, itself downwind of the copper refinery, illustrating how multiple sources can contribute to the composition of particles collected at a given site, particularly in a complex location like East Montréal. Contrasts were especially

evident in the water-soluble fraction, which represented a significant proportion of total metals in ultrafine and fine particles (45 ± 13% and 70 ± 17% average water-solubility respectively compared to 2–3% average water-solubility of metals in the coarse fractions). While most sites displayed considerable variability in composition across size ranges, size-fractionated particles in Shawinigan were remarkably similar, with aluminium being the dominant metal in all samples. Importantly, the data show that differences in metal composition were most prominent in the water-soluble fraction of ultrafine and fine particles, suggesting that industrial emissions can significantly impact levels of bioavailable elements in respirable particles. Semi-volatile and particle-associated PAHs appeared to be enriched in either or both of the fine and coarse particle fractions collected near metal industry sites in Hamilton (HB), Montréal (MC), and Shawinigan (SW) compared to petrochemical industry sites in Montréal (MA) and Sarnia (SR), suggesting inter-site differences in the organic fraction. The presence of volatile PAHs in the coarse and super-coarse fractions may represent absorption onto the collection substrate rather than particle composition [33], as a significant fraction will be in the gas-phase. Collectively, the data confirm that our sampling strategy resulted in the collection of particles of distinct composition related to specific source emissions.

The clear inter-site variability in particle composition provided a basis for examining to what extent source-dependent differences in particle composition altered the potency of particles in biological models. While a number of studies have compared the potency of ambient particles collected in different sites, including urban vs. rural [11] and residential vs. traffic vs. industrial [10, 12], there has been little direct comparison of the toxicity of particles collected at multiple industrial sites. Several key observations were made in the present study. First, particles collected in the vicinity of industrial sites displayed striking differences in overall potency. For example, particles collected near Hamilton steel industry tended to be among the most potent across size fractions, whereas particles collected near Sarnia petrochemical industry were among the least potent. Second, particle potency appeared to be a function of both particle size and particle composition. Whereas samples from Hamilton steel, Montréal petrochemical, and Montréal copper sites exhibited contrasting composition and potency across size fractions within each site, particles collected in the vicinity of the Shawinigan aluminium refinery that were very similar in composition (predominantly aluminium) tended to exhibit similar potency across size-fractions. Third, the cytotoxic and inflammatory potential of particle samples was associated with the levels of specific constituents (metals, PAHs, endotoxin). Fourth, effects differed across cell lines and assays, suggesting differential responsiveness to particle constituents. The contrasting effects of particles compared on an equal mass basis is consistent with the hypothesis that particles collected in the vicinity of distinct sources will exhibit a range of cytotoxic and inflammatory potencies. Collectively, these observations suggest that particle potency is influenced both by particle size and composition, with biological responses being a function of particle properties and cell characteristics.

While coarse particles generally represent a significant proportion of total particle mass, they are less efficiently deposited in the alveolar regions of the lungs and may contain less bioavailable metal content. In contrast, smaller particles may be present in greater number, have a greater reactive surface:volume ratio per unit mass, and tend to contain a greater concentration of soluble metals, characteristics that may increase their potency in vivo. Despite these differences between fine and coarse particles, the coarse fraction of ambient particles can exert relatively high cytotoxic and inflammatory effects in cell culture models or when instilled into the lungs of experimental animals compared to ultrafine and fine particles [12, 17, 19, 34–36]. We observed size-dependent effects on both cytotoxicity and inflammatory potential in our cell culture models: fine and coarse particles tended to be more cytotoxic, whereas coarse and super-coarse particles tended to be more inflammogenic. The cell culture models and assays employed in the present study were less sensitive to UFP than to larger size fractions in terms of the magnitude of response. There are several explanations beyond lower inherent potency of the UFP, including reduced particle-cell interaction resulting from size-dependent differences in phagocytosis by macrophages [37] or differences in particle settling rate that impact the effective dose and timing of effects. However, the effects of UFP on cytokine release confirms that these particles, while not acutely cytotoxic in the present model according to the resazurin reduction and LDH release assays, did impact biological function, and were therefore neither inert nor invisible to the cells.

The significant variability in response across industrial sites within each size fraction indicated that the cell culture models and assays employed were sensitive to particle characteristics other than particle size. Considerable attention has been directed towards elucidating determinants of particle potency, including investigation of the role of metals, PAHs, and endotoxin [35, 38]. Total metal content was associated with cytotoxic potency, and to a lesser extent inflammatory potency, while PAHs and endotoxin were associated with cytotoxicity and inflammatory potency respectively primarily in the coarse

fractions. These results are, in a broad sense, consistent with previous observations by ourselves and others [9, 12, 19, 39]. Despite representing only a fraction of total particle mass, trace metal concentrations explained a significant proportion of the variance in cytotoxic potency. For example, Sarnia particles, which had the lowest metal content across size-fractions, also displayed the lowest cytotoxic potency, whereas the high metal content in the fine fraction of Hamilton, Montréal, and Shawinigan sites was associated with higher toxicity. These results, reflecting strong contrasts in particle composition as a result of sampling in the vicinity of important industrial point sources, are in line with a body of work linking trace metals with particle toxicity through in vitro, in vivo, and population studies [38]. Endotoxin levels were significantly higher in the coarse and super-coarse fractions, and likely account for a portion of the inflammatory and cytotoxic effects, consistent with other studies [9, 19]. While PAHs were not strongly linked to the biological indices evaluated here beyond correlations with LDH release in the super-coarse fraction, they may nevertheless contribute to the overall cytotoxic and inflammatory potency of fine and coarse particles [19, 36, 40].

There is considerable evidence that soluble metal content is an important determinant of pulmonary and systemic impacts of urban and combustion emission particles [13, 14, 16]. However, insoluble metals have also been linked to biological reactivity [18, 41], and effects of this fraction warrant attention given the relative abundance of insoluble metals. As significant associations were found for both water-soluble (fine fraction) and non-water-soluble metals (coarse fractions), it was not possible to unambiguously attribute effects to water-soluble or non-water-soluble metals. The slope of the relationship between non-water-soluble metals and potency appeared to decrease with increasing particle size, suggesting an interaction between physical and chemical characteristics of the particles. This could possibly reflect the actual effective internal dose experienced by cell (i.e., due to differential intake of material [42]), or interactions of independent physical and chemical effects associated with particle size. On the other hand, the concentration of active agents may vary with particle size: as particle size increases, crustal elements of lower solubility predominate and metals derived from anthropogenic sources are less abundant. Particle size likely influences both how cells experience metals (as a result of surface and endocytic interactions), as well as the nature of the metals to which cells are exposed (due to differences in particle composition and metal solubility), which may explain apparent changes in the potency of metals across size fractions.

Given that the size-dependency of the effects could be due to differential distribution of a toxicity determinant across size fractions, we performed a series of regression analyses to evaluate whether specific metals better explained the variance in particle potency. A number of models were generated that contained a variety of metals, with soluble manganese emerging as the factor most closely associated with cytotoxicity across size fractions, particularly with respect to resazurin reduction. Soluble manganese covaried closely with zinc and other metals across sites, and could be a surrogate for other elements, and so caution should be applied in attributing effects to any one element. Nevertheless, these associations are in a broad sense consistent with the overall coherence among in vitro, in vivo, and population studies implicating soluble transition metals in adverse health effects of ambient particles [14, 38, 40, 43]. While manganese is an essential element and deficiency is associated with adverse health impacts, chronic inhalation of manganese is neurotoxic, associated with both cognitive and motor deficits, and may have cardiovascular impacts [44]. Manganese chloride has been shown to inhibit cell proliferation and induce apoptosis in A549 cells [45], demonstrating in vitro toxicity. The acute toxicity resulting from intratracheal instillation of the urban particle standard EHC-93 was reproduced by administration of soluble zinc, implicating zinc in the toxicity of ambient particulate matter [13]. Consistent with a role for soluble zinc in mediating cytotoxic effects of particle exposure, the in vitro cytotoxicity of zinc oxide nanoparticles appears to be at least partly due to levels of free zinc ions [46]. Thus, while associations made on the basis of a small number of samples should be interpreted with caution, the associations appear consistent with the established toxicity of soluble transition metals. It is important to note that the relatively high concentrations of transition metals in UFP compared to other size fractions did not correlate well with cytotoxicity, suggesting that soluble metal content alone does not explain the toxicity of the particles. The failure to find specific metal drivers of LDH release across size fractions may relate to a greater sensitivity of this assay to particle characteristics or constituents (e.g., endotoxin) that co-vary with size, as LDH release correlated reasonably well with metals when analysed within each size fraction.

The J774A.1 macrophage-like and A549 epithelial-like cell lines displayed certain differences in their responses to particle size and constituents according to the cytotoxicity assays (resazurin reduction, LDH release) employed. J774A.1 cells appeared to be sensitive to metal composition in addition to particle size, and although not statistically significant in all comparisons, the relationship appeared to hold across particle sizes. In contrast, A549 cells appeared to be more sensitive to

particle size than to particle composition. This was particularly evident in the similar size-dependent effects of particles on A549 LDH release across sampling sites. These differences between cell lines are consistent with our previous observations using these models [12], and with other comparisons across cell lines [47]. Macrophage-like J774A.1 cells are capable of phagocytising particles at a high rate and thus possibly experience a greater internal dose of metals than A549 cells, which may explain their apparently higher sensitivity to differences in metal composition. It is noteworthy that had we employed only A549 cells, commonly used to assess particle toxicity, and LDH release, an established cytotoxicity assay, we would have likely concluded that there was little evidence of differences in the toxic potency of particles collected in the vicinity of industrial sites. Our findings reinforce the importance of using multiple cell lines and assays to assess particle toxicity, as different cells and assays may be sensitive to distinct particle characteristics [12].

The primary objective of the present work was to evaluate to what extent particles collected in the vicinity of different industrial sources exhibit contrasts in composition and potency. Strengths of the present study include direct comparison of size-fractionated particles with contrasting chemical composition across a range of doses, employment of two cell lines, and assessment of toxic potency using a panel of cytotoxic and inflammatory assays. However, certain factors should be considered when interpreting results. While samples were collected as close as possible to each industrial site, some differences between the locations could be due to seasonal influences. For example, the amount and composition of regionally-transported particles is seasonally dependent, and their variable influence could add noise to the analysis of differential biological responses as has been shown previously [48, 49]. A limitation common to this type of toxicological analysis of environmental samples is that the extracted material will likely differ from the ambient aerosols at the time of sampling. The aqueous extraction of particles, while reasonably efficient at extracting mass from polyurethane foam and less efficient from polypropylene filters, likely modified the composition of the extracted materials compared to the composition of total particulates suspended in the air at the five sampling sites we studied. Poor extraction of non-polar organic constituents may explain the contrast in PAH composition measured in the present work compared with analyses performed using solvent- and acid-based extractions on other urban ambient particles (e.g., [12]). It is also likely that a proportion of volatile and semi-volatile PAHs were lost during the extraction process. In addition, some of the semi-volatile PAHs measured may have been due to the capture of gas phase compounds by the PUF material as opposed to originating on particles [33]. Accordingly, while performing chemical and toxicological analyses on the same extracted material facilitated the association of particle constituents to biological effects, it is clear that the chemical profile of extracted particles to which cells were exposed may differ from that inhaled from ambient air. Nevertheless, the metal composition of the particles is consistent with expected enrichment of source emissions, and the higher PAH levels measured at the Shawinigan site is consistent with aluminium smelters being a significant anthropogenic source of PAHs released to the atmosphere. The cytotoxic and inflammatory indices assessed here were selected to represent distal endpoints that integrate the cellular response as a whole to multiple physical and chemical stressors. While measurement of biological effects at a single time point allowed comparison across sites and particle sizes, the pattern of effects may differ at other time points (e.g., due to differential kinetics of response of individual cytokines). Assays that target specific particle components or enable assessment of the activation of specific biological pathways may identify other exposure and mechanistic signatures [8, 28].

Conclusions

This study confirms that local industrial sources are important producers of particulate constituents that differentially impact biological function and that differ depending on industrial processes. Validation of these findings using multiple complementary assays, manipulation of particle constituents, and blockade of biological pathways should help verify the relative importance of identified factors in driving such effects. Attribution of toxic potency to specific particle constituents will provide critical data for identification of priority sources for regulatory action.

Additional files

Additional file 1: Metal composition of all size-fractionated particles. Table of metal content according to particle size and sampling site. (XLSX 35 kb)

Additional file 2: PAH composition of all size-fractionated particles. Table of PAH content according to particle size and sampling site. (XLSX 15 kb)

Additional file 3: Clustering of particulate matter samples according to metal content. Size-fractionated particles collected in the vicinity of industrial sites were clustered according to A) water-soluble metals, B) total metals, and C) non-water-soluble (NWS) metals (average linkage, Pearson correlation coefficient distance). (PDF 200 kb)

Additional file 4: Clustering of elements according to water soluble, non-water- soluble and total elements. A) Water-soluble (WS), B) non-water soluble (NWS) and C) total metals were clustered to reveal the associations (covariance) among sets of elements. (PDF 22 kb)

Additional file 5: Cytotoxic responses of J774A.1 cells to 24 h exposure to size-fractionated particulate matter collected in the vicinity of industrial sites according to the resazurin reduction assay. Metabolic reduction of non-fluorescent resazurin in J774A.1 cells exposed for 24 h to size-

fractionated and standard reference particles (left side) and extracts from corresponding field blank filters that were transported to each site but remained unexposed to ambient air (right side). Values are presented as average fold-effect (FE) over control ± standard error ($n = 3$ independent experiments). HB, Hamilton Beach steel mill; MA, Montréal petrochemical refinery; MC, Montréal copper smelter; SR, Sarnia petrochemical refinery; SW, Shawinigan aluminum smelter. Size-fractionated and standard reference particles. Three-way ANOVA (Size-fractionated particles): *Site* x *Dose* ($p = 0.002$) and *Size* x *Dose* ($p < 0.001$) interactions. Asterisks represent significant pairwise comparisons (Holm-Sidak) as follows: doses within *Site* significantly different from 0 μg/cm^2, or sites within *Size* significantly different from one another as indicated by brackets (*$p < 0.05$, **$p < 0.001$). Letters (a-e) represent sizes within *Site* significantly different from one another ($p < 0.05$). Two-way ANOVA (Standards): *Particle* ($p < 0.001$) and *Dose* ($p < 0.001$) main effects. Asterisks represent significant pairwise comparisons (Holm-Sidak) as follows: doses significantly different from 0 μg/cm^2, or particles significantly different from one another as indicated by brackets (*$p < 0.05$, **$p < 0.001$). Field blanks. Three-way ANOVA: *Site* x *Size* ($p = 0.05$) interaction. No significant pairwise comparisons (Holm-Sidak) were observed. (PDF 52 kb)

Additional file 6: Cytotoxic responses of J774A.1 cells to 24 h exposure to size-fractionated particulate matter collected in the vicinity of industrial sites according to the LDH release assay. Lactate dehydrogenase (LDH) release into cell culture supernatants of J774A.1 cells exposed for 24 h to size-fractionated and standard reference particles (left-side) and extracts from corresponding field blank filters that were transported to each site but remained unexposed to ambient air (right side). Data represent LDH release adjusted for total cellular LDH content. Values are presented as average fold-effect (FE) over control ± standard error ($n = 3$ independent experiments). HB, Hamilton Beach steel mill; MA, Montréal AIEM petrochemical refinery; MC, Montréal copper smelter; SR, Sarnia petrochemical refinery; SW, Shawinigan aluminum smelter. Size-fractionated and standard reference particles. Three-way ANOVA (Size-fractionated particles): *Site* x *Dose* ($p < 0.001$) and *Size* x *Dose* ($p < 0.001$) interactions. Asterisks represent significant pairwise comparisons (Holm-Sidak) as follows: doses within *Size* significantly different from 0 μg/cm^2 (*$p < 0.05$, **$p < 0.001$). Letters (a-g) represent doses within *Site* significantly different from 0 μg/cm^2 ($p < 0.05$). Bars with the same symbol (#,@,&,^,$) indicate sites within *Dose* that are significantly different from one another ($p < 0.05$). Two-way ANOVA (Standards): *Particle* ($p < 0.001$) and *Dose* ($p < 0.001$) main effects. Asterisks represent significant pairwise comparisons (Holm-Sidak) as follows: doses significantly different from 0 μg/cm^2, or particles significantly different from one another as indicated by brackets (*$p < 0.05$, **$p < 0.001$). Field blanks. Three way ANOVA: *Size* x *Dose* ($p = 0.021$) interaction. Asterisks represent doses within *Size* significantly different from 0 μg/cm^2 (*$p < 0.05$). Letters (a-c) represent sizes within *Dose* significantly different from one another ($p < 0.05$). (PDF 55 kb)

Additional file 7: Cytotoxic responses of A549 cells to 24 h exposure to size-fractionated particulate matter collected in the vicinity of industrial sites according to the resazurin reduction assay. Metabolic reduction of non-fluorescent resazurin in A549 cells exposed for 24 h to size-fractionated and standard reference particles (left-side) and extracts from corresponding field blank filters that were transported to each site but remained unexposed to ambient air (right-side). Values are presented as average fold-effect (FE) over control ± standard error ($n = 3$ independent experiments). HB, Hamilton Beach steel mill; MA, Montréal AIEM petrochemical refinery; MC, Montréal copper smelter; SR, Sarnia petrochemical refinery; SW, Shawinigan aluminum smelter. Size-fractionated and standard reference particles. Three-way ANOVA (Size-fractionated particles): *Site* x *Size* ($p < 0.001$) and *Size* x *Dose* ($p = 0.019$) interactions. Asterisks represent significant pairwise comparisons (Holm-Sidak) as follows: doses within *Site* significantly different from 0 μg/cm^2, or sites within *Size* significantly different from one another as indicated by brackets (*$p < 0.05$, **$p < 0.001$). Letters (a-h) represent sizes within *Site* significantly different from one another ($p < 0.05$). Two-way ANOVA (Standards): *Particle* x *Dose* interaction ($p = 0.012$). Asterisks represent significant pairwise comparisons (Holm-Sidak) as follows: doses within *Particles* significantly different from 0 μg/cm^2 (**$p < 0.001$). Letters (a,b) represent sites within *Dose* significantly different from one another ($p < 0.5$). Field blanks. Three-way ANOVA: *Site* x *Size* ($p < 0.001$) interaction. Asterisks represent significant pairwise comparisons (Holm-Sidak) as follows: sites within *Size* significantly different from one another as indicated by brackets (*$p < 0.05$, **$p < 0.001$). Letters (a-e) represent sizes within *Site* significantly different from one another ($p < 0.05$). (PDF 54 kb)

Additional file 8: Cytotoxic responses of A549 cells to 24 h exposure to size-fractionated particulate matter collected in the vicinity of industrial sites according to the LDH release assay. Lactate dehydrogenase (LDH) release into cell culture supernatants of A549 cells exposed for 24 h to size-fractionated and standard reference particles (left-side) and extracts from corresponding field blank filters that were transported to each site but remained unexposed to ambient air (right side). Data represent LDH release, adjusted for total cellular LDH content. Values are presented as average fold-effect (FE) over control ± standard error ($n = 3$). HB, Hamilton Beach steel mill; MA, Montréal AIEM petrochemical refinery; MC, Montréal copper smelter; SR, Sarnia petrochemical refinery; SW, Shawinigan aluminum smelter. Size-fractionated and standard reference particles. Three-way ANOVA (Size-fractionated particles): *Site* x *Size* ($p = 0.002$) and *Size* x *Dose* ($p = 0.018$) interactions. Asterisks represent significant pairwise comparisons (Holm-Sidak) as follows: doses within *Size* significantly different from 0 μg/cm^2, or sites within *Size* significantly different from one another as indicated by brackets (*$p < 0.05$, **$p < 0.001$). Letters (a-n) represent sizes within *Site* significantly different from one another ($p < 0.05$). Two-way ANOVA (Standards): *Particle* ($p = 0.002$) and *Dose* ($p < 0.001$) main effects. Asterisks represent significant pairwise comparisons (Holm-Sidak) as follows: doses significantly different from 0 μg/cm^2, or particles significantly different from one another as indicated by brackets (*$p < 0.05$, **$p < 0.001$). Field blanks. Three-way ANOVA: *Dose* ($p < 0.001$) main effect. Letter (a) spanned by a line represents doses significantly different from 0 μg/cm^2 ($p < 0.001$). (PDF 55 kb)

Additional file 9: Inflammatory response to field blank filter extracts. Hierarchical clustering of particles according to cytokine response in J774A.1 cells exposed to field blank filter extracts. The heat map displays particle potency estimates determined for each cytokine from the slope of the dose-effect relationship. Red, increased expression; green, decreased expression. bHB, field blank from Hamilton Beach steel mill; bMA, field blank from Montréal petrochemical refinery; MC, field blank from Montréal copper smelter; SR, field blank from Sarnia petrochemical refinery; SW, field blank from Shawinigan aluminum smelter. (PDF 84 kb)

Additional file 10: Association of biological effects in A549 cells with metal content in size-fractionated particles. Cytotoxic potencies according to lactate dehydrogenase (LDH) release and resazurin reduction were regressed against total, water-soluble, and non-water-soluble metals. Pearson product–moment correlation coefficient r-values are presented. LDH release. A) Total metals. UFP, $r = 0.77$, $p = 0.13$; $PM_{0.1–2.5}$, $r = -0.55$, $p = 0.34$; $PM_{2.5–10}$, $r = 0.32$, $p = 0.60$; $PM_{>10}$, $r = -0.68$, $p = 0.21$. B) Water-soluble metals. UFP, $r = 0.51$, $p = 0.38$; $PM_{0.1–2.5}$, $r = -0.64$, $p = 0.25$; $PM_{2.5–10}$, $r = -0.35$, $p = 0.57$; $PM_{>10}$, $r = -0.68$, $p = 0.20$. C) Non-water-soluble metals. UFP, $r = 0.75$, $p = 0.14$; $PM_{0.1–2.5}$, $r = -0.46$, $p = 0.43$; $PM_{2.5–10}$, $r = 0.36$, $p = 0.55$; $PM_{>10}$, $r = -0.68$, $p = 0.21$. Resazurin reduction. D) UFP, $r = -0.19$, $p = 0.76$; $PM_{0.1–2.5}$, $r = -0.63$, $p = 0.26$; $PM_{2.5–10}$, $r = -0.60$, $p = 0.28$; $PM_{>10}$,$r = 0.18$, $p = 0.78$. Water-soluble metals. UFP, $r = -0.20$, $p = 0.74$; $PM_{0.1–2.5}$, $r = -0.41$, $p = 0.49$; $PM_{2.5–10}$, $r = -0.09$, $p = 0.88$; $PM_{>10}$, $r = 0.04$, $p = 0.95$. Non-water-soluble metals. UFP, $r = -0.12$, $p = 0.84$; $PM_{0.1–2.5}$, $r = -0.65$, $p = 0.24$; $PM_{2.5–10}$, $r = -0.62$, $p = 0.26$; $PM_{>10}$, $r = 0.18$, $p = 0.77$. (PDF 43 kb)

Additional file 11: Regressions of biological potency against total metals, water-soluble metals, non-water-soluble metals, endotoxin, and PAHs. Table of Pearson correlations and *p*-values. (PDF 71 kb)

Acknowledgments

We wish to acknowledge the technical assistance of Gang Lu, Sandy Benetti, and Paul Daszko for sample collection, Alain Filiatreault, Djordje Vladisavljevic, James Crispo, and Marianne Ariganello for particle extraction and conduct of biological assays, and Michelle Golub, Joel Bennoit, and Avril Metcalfe-Roach for preparation of figures. We thank Andy Nong and Phil Blagden for their insightful comments on the manuscript.

Funding

This work was funded by the Clean Air Regulatory Agenda (Health Canada).

Availability of data and material
All data generated or analysed during this study are included in this published article and its Additional files 1, 2, 3, 4, 5, 6, 7, 8, 9, 10 and 11.

Authors' contributions
EMT participated in the design and coordination of the study, analysed the data, and drafted the manuscript. DB participated in the design of the study and contributed to the cell culture experiments and endotoxin analyses. SK participated in the design of the study and performed the hierarchical clustering. CMR carried out the cell culture experiments. NQV prepared filters for particle collection and extracted the particulate matter samples. EDZ and VC were responsible for trace metal analysis. JPC was responsible for the analysis of organic species. PK participated in the design of the study and contributed to the particle extraction procedure. JRB participated in the design of the study and was responsible for site selection and particle collection. RV conceived of the study, and participated in its design and coordination. All authors participated in revision of the manuscript, and read and approved the final draft.

Competing interests
The authors declare that they have no competing interests.

Consent for publication
Not applicable.

Ethics approval and consent to participate
Not applicable.

Author details
[1]Environmental Health Science and Research Bureau, Health Canada, Ottawa, Ontario K1A 0K9, Canada. [2]Analysis and Air Quality Section, Air Quality Research Division, Atmospheric Science and Technology Directorate, Environment and Climate Change Canada, Ottawa, ON K1A 0H3, Canada. [3]Air Quality Processes Research Section, Air Quality Research Division, Atmospheric Science and Technology Directorate, Environment and Climate Change Canada, Toronto, ON M3H 5T4, Canada.

Received: 14 July 2016 Accepted: 23 November 2016
Published online: 01 December 2016

References

1. Dockery DW, Pope III CA, Xu X, Spengler JD, Ware JH, Fay ME, Ferris Jr BG, Speizer FE. An association between air pollution and mortality in six U.S. cities. N Engl J Med. 1993;329:1753–9.
2. Pope III CA, Burnett RT, Thurston GD, Thun MJ, Calle EE, Krewski D, Godleski JJ. Cardiovascular mortality and long-term exposure to particulate air pollution: epidemiological evidence of general pathophysiological pathways of disease. Circulation. 2004;109:71–7.
3. Burnett RT, Brook J, Dann T, Delocla C, Philips O, Cakmak S, Vincent R, Goldberg MS, Krewski D. Association between particulate- and gas-phase components of urban air pollution and daily mortality in eight Canadian cities. Inhal Toxicol. 2000;12 Suppl 4:15–39.
4. Crouse DL, Peters PA, van DA, Goldberg MS, Villeneuve PJ, Brion O, Khan S, Atari DO, Jerrett M, Pope CA, et al. Risk of nonaccidental and cardiovascular mortality in relation to long-term exposure to low concentrations of fine particulate matter: a Canadian national-level cohort study. Environ Health Perspect. 2012;120:708–14.
5. Grahame TJ, Schlesinger RB. Health effects of airborne particulate matter: do we know enough to consider regulating specific particle types or sources? Inhal Toxicol. 2007;19:457–81.
6. Zanobetti A, Franklin M, Koutrakis P, Schwartz J. Fine particulate air pollution and its components in association with cause-specific emergency admissions. Environ Health. 2009;8:58.
7. Peng RD, Dominici F, Pastor-Barriuso R, Zeger SL, Samet JM. Seasonal analyses of air pollution and mortality in 100 US cities. Am J Epidemiol. 2005;161:585–94.
8. Vincent R, Goegan P, Johnson G, Brook JR, Kumarathasan P, Bouthillier L, Burnett RT. Regulation of promoter-CAT stress genes in HepG2 cells by suspensions of particles from ambient air. Fundam Appl Toxicol. 1997; 39:18–32.
9. Steenhof M, Gosens I, Strak M, Godri KJ, Hoek G, Cassee FR, Mudway IS, Kelly FJ, Harrison RM, Lebret E, et al. In vitro toxicity of particulate matter (PM) collected at different sites in the Netherlands is associated with PM composition, size fraction and oxidative potential—the RAPTES project. Part Fibre Toxicol. 2011;8:26.
10. Dergham M, Lepers C, Verdin A, Billet S, Cazier F, Courcot D, Shirali P, Garcon G. Prooxidant and proinflammatory potency of air pollution particulate matter (PM(2). (5)(−)(0). (3)) produced in rural, urban, or industrial surroundings in human bronchial epithelial cells (BEAS-2B). Chem Res Toxicol. 2012;25:904–19.
11. Mirowsky J, Hickey C, Horton L, Blaustein M, Galdanes K, Peltier RE, Chillrud S, Chen LC, Ross J, Nadas A, et al. The effect of particle size, location and season on the toxicity of urban and rural particulate matter. Inhal Toxicol. 2013;25:747–57.
12. Thomson EM, Breznan D, Karthikeyan S, MacKinnon-Roy C, Charland JP, Dabek-Zlotorzynska E, Celo V, Kumarathasan P, Brook JR, Vincent R. Cytotoxic and inflammatory potential of size-fractionated particulate matter collected repeatedly within a small urban area. Part Fibre Toxicol. 2015;12:24.
13. Adamson IY, Prieditis H, Hedgecock C, Vincent R. Zinc is the toxic factor in the lung response to an atmospheric particulate sample. Toxicol Appl Pharmacol. 2000;166:111–9.
14. Dreher KL, Jaskot RH, Lehmann JR, Richards JH, McGee JK, Ghio AJ, Costa DL. Soluble transition metals mediate residual oil fly ash induced acute lung injury. J Toxicol Environ Health. 1997;50:285–305.
15. Vincent R, Kumarathasan P, Goegan P, Bjarnason SG, Guenette J, Berube D, Adamson IY, Desjardins S, Burnett RT, Miller FJ et al.. Inhalation toxicology of urban ambient particulate matter: acute cardiovascular effects in rats. Res Rep Health Eff Inst. 2001;104:5–54.
16. Wallenborn JG, Schladweiler MJ, Richards JH, Kodavanti UP. Differential pulmonary and cardiac effects of pulmonary exposure to a panel of particulate matter-associated metals. Toxicol Appl Pharmacol. 2009;241:71–80.
17. Schins RP, Lightbody JH, Borm PJ, Shi T, Donaldson K, Stone V. Inflammatory effects of coarse and fine particulate matter in relation to chemical and biological constituents. Toxicol Appl Pharmacol. 2004;195:1–11.
18. Imrich A, Ning Y, Kobzik L. Insoluble components of concentrated air particles mediate alveolar macrophage responses in vitro. Toxicol Appl Pharmacol. 2000;167:140–50.
19. Guastadisegni C, Kelly FJ, Cassee FR, Gerlofs-Nijland ME, Janssen NA, Pozzi R, Brunekreef B, Sandstrom T, Mudway I. Determinants of the proinflammatory action of ambient particulate matter in immortalized murine macrophages. Environ Health Perspect. 2010;118:1728–34.
20. Pope III CA, Schwartz J, Ransom MR. Daily mortality and PM10 pollution in Utah Valley. Arch Environ Health. 1992;47:211–7.
21. Frampton MW, Ghio AJ, Samet JM, Carson JL, Carter JD, Devlin RB. Effects of aqueous extracts of PM(10) filters from the Utah valley on human airway epithelial cells. Am J Physiol. 1999;277:L960–7.
22. Jerrett M, Buzzelli M, Burnett RT, DeLuca PF. Particulate air pollution, social confounders, and mortality in small areas of an industrial city. Soc Sci Med. 2005;60:2845–63.
23. Mattson ME, Guidotti TL. Health risks associated with residence near a primary copper smelter: a preliminary report. Am J Ind Med. 1980;1:365–74.
24. Pope III CA, Rodermund DL, Gee MM. Mortality effects of a copper smelter strike and reduced ambient sulfate particulate matter air pollution. Environ Health Perspect. 2007;115:679–83.
25. Grahame TJ. Mortality from copper smelter emissions circa 1967. Environ Health Perspect. 2007;115:A439–40.
26. Lippmann M, Ito K, Hwang JS, Maciejczyk P, Chen LC. Cardiovascular effects of nickel in ambient air. Environ Health Perspect. 2006;114:1662–9.
27. Demokritou P, Kavouras IG, Ferguson ST, Koutrakis P. Development of a high volume cascade impactor for toxicological and chemical characterization studies. Aerosol Sci Technol. 2002;36:925–33.
28. Thomson EM, Williams A, Yauk CL, Vincent R. Toxicogenomic analysis of susceptibility to inhaled urban particulate matter in mice with chronic lung inflammation. Part Fibre Toxicol. 2009;6:6.
29. Fang T, Guo H, Verma V, Peltier RE, Weber RJ. PM2.5 water-soluble elements in the southeastern United States: Automated analytical method development, spatiotemporal distributions, source apportionment, and implications for health studies. Atmos Chem Phys. 2015;15:11667–82.
30. Oakes MM, Burke JM, Norris GA, Kovalcik KD, Pancras JP, Landis MS. Near-road enhancement and solubility of fine and coarse particulate matter trace elements near a major interstate in Detroit, Michigan. Atm Env. 2016;145:213–24.

31. Jeong C-H, McGuire M, Herod D, Dann T, Dabek-Zlotorzynska E, Wang D, Ding L, Celo V, Mathieu D, Evans G. Receptor model based identification of PM2.5 sources in Canadian cities. Atm Poll Res. 2012;2:158–71.
32. Celo V, Dabek-Zlotorzynska E. Concentration and Source Origin of Trace Elements in PM2.5 Collected at Selected sites within the Canadian National Air Pollution Surveillance PM2.5 Speciation Program. In: Zereini F, Wiseman C, editors. Urban Airborne Particulate Matter: Origins,Chemistry, Fate and Health Impact. 2010. p. 19–38.
33. Galarneau E, Patel M, Brook JR, Charland J-P, Glasius R, Hung H: Artefacts in semivolatile organic compound sampling with polyurethane foam (PUF) substrates in high volume cascade impactors. Aerosol Science and Technology. 2016. In press.
34. Becker S, Mundandhara S, Devlin RB, Madden M. Regulation of cytokine production in human alveolar macrophages and airway epithelial cells in response to ambient air pollution particles: further mechanistic studies. Toxicol Appl Pharmacol. 2005;207:269–75.
35. Schwarze PE, Ovrevik J, Hetland RB, Becher R, Cassee FR, Lag M, Lovik M, Dybing E, Refsnes M. Importance of size and composition of particles for effects on cells in vitro. Inhal Toxicol. 2007;19 Suppl 1:17–22.
36. Monn C, Becker S. Cytotoxicity and induction of proinflammatory cytokines from human monocytes exposed to fine (PM2.5) and coarse particles (PM10-2.5) in outdoor and indoor air. Toxicol Appl Pharmacol. 1999;155: 245–52.
37. Oberdorster G, Oberdorster E, Oberdorster J. Nanotoxicology: an emerging discipline evolving from studies of ultrafine particles. Environ Health Perspect. 2005;113:823–39.
38. Chen LC, Lippmann M. Effects of metals within ambient air particulate matter (PM) on human health. Inhal Toxicol. 2009;21:1–31.
39. Wang B, Li K, Jin W, Lu Y, Zhang Y, Shen G, Wang R, Shen H, Li W, Huang Y, et al. Properties and inflammatory effects of various size fractions of ambient particulate matter from Beijing on A549 and J774A.1 cells. Environ Sci Technol. 2013;47:10583–90.
40. Gerlofs-Nijland ME, Rummelhard M, Boere AJ, Leseman DL, Duffin R, Schins RP, Borm PJ, Sillanpaa M, Salonen RO, Cassee FR. Particle induced toxicity in relation to transition metal and polycyclic aromatic hydrocarbon contents. Environ Sci Technol. 2009;43:4729–36.
41. Ghio AJ, Stonehuerner J, Dailey LA, Carter JD. Metals associated with both the water-soluble and insoluble fractions of an ambient air pollution particle catalyze an oxidative stress. Inhal Toxicol. 1999;11:37–49.
42. Gliga AR, Skoglund S, Wallinder IO, Fadeel B, Karlsson HL. Size-dependent cytotoxicity of silver nanoparticles in human lung cells: the role of cellular uptake, agglomeration and Ag release. Part Fibre Toxicol. 2014;11:11.
43. Dye JA, Lehmann JR, McGee JK, Winsett DW, Ledbetter AD, Everitt JI, Ghio AJ, Costa DL. Acute pulmonary toxicity of particulate matter filter extracts in rats: coherence with epidemiologic studies in Utah Valley residents. Environ Health Perspect. 2001;109 Suppl 3:395–403.
44. O'Neal SL, Zheng W. Manganese toxicity upon overexposure: a decade in review. Curr Environ Health Rep. 2015;2:315–28.
45. Zhao P, Zhong W, Ying X, Yuan Z, Fu J, Zhou Z. Manganese chloride-induced G0/G1 and S phase arrest in A549 cells. Toxicology. 2008;250:39–46.
46. Kim YH, Fazlollahi F, Kennedy IM, Yacobi NR, Hamm-Alvarez SF, Borok Z, Kim KJ, Crandall ED. Alveolar epithelial cell injury due to zinc oxide nanoparticle exposure. Am J Respir Crit Care Med. 2010;182:1398–409.
47. Riley MR, Boesewetter DE, Turner RA, Kim AM, Collier JM, Hamilton A. Comparison of the sensitivity of three lung derived cell lines to metals from combustion derived particulate matter. Toxicol In Vitro. 2005;19:411–9.
48. Becker S, Dailey LA, Soukup JM, Grambow SC, Devlin RB, Huang YC. Seasonal variations in air pollution particle-induced inflammatory mediator release and oxidative stress. Environ Health Perspect. 2005;113:1032–8.
49. Hetland RB, Cassee FR, Lag M, Refsnes M, Dybing E, Schwarze PE. Cytokine release from alveolar macrophages exposed to ambient particulate matter: heterogeneity in relation to size, city and season. Part Fibre Toxicol. 2005;2:4.

NANOTOXICOLOGY, 2017
VOL. 11, NO. 2, 223–235
http://dx.doi.org/10.1080/17435390.2017.1287313

Taylor & Francis
Taylor & Francis Group

ORIGINAL ARTICLE

OPEN ACCESS

Differential cytotoxic and inflammatory potency of amorphous silicon dioxide nanoparticles of similar size in multiple cell lines

Dalibor Breznan[a], Dharani D. Das[a], Julie S. O'Brien[a], Christine MacKinnon-Roy[a], Surendra Nimesh[a], Ngoc Q. Vuong[a], Stéphane Bernatchez[b], Nimal DeSilva[c], Myriam Hill[b], Prem Kumarathasan[a] and Renaud Vincent[a]

[a]Environmental Health Science and Research Bureau, Health Canada, Tunney's Pasture, Ottawa, Canada; [b]New Substances Assessment and Control Bureau, Health Canada, Tunney's Pasture, Ottawa, Canada; [c]Department of Earth and Environmental Sciences, University of Ottawa, Ottawa, Canada

ABSTRACT

The likelihood of environmental and health impacts of silicon dioxide nanoparticles (SiNPs) has risen, due to their increased use in products and applications. The biological potency of a set of similarly-sized amorphous SiNPs was investigated in a variety of cells to examine the influence of physico-chemical and biological factors on their toxicity. Cellular LDH and ATP, BrdU incorporation, resazurin reduction and cytokine release were measured in human epithelial A549, human THP-1 and mouse J774A.1 macrophage cells exposed for 24 h to suspensions of 5–15, 10–20 and 12 nm SiNPs and reference particles. The SiNPs were characterized in dry state and in suspension to determine their physico-chemical properties. The dose-response data were simplified into particle potency estimates to facilitate the comparison of multiple endpoints of biological effects in cells. Mouse macrophages were the most sensitive to SiNP exposures. Cytotoxicity of the individual cell lines was correlated while the cytokine responses differed, supported by cell type-specific differences in inflammation-associated pathways. SiNP (12 nm), the most cytotoxic and inflammogenic nanoparticle had the highest surface acidity, dry-state agglomerate size, the lowest trace metal and organics content, the smallest surface area and agglomerate size in suspension. Particle surface acidity appeared to be the most significant determinant of the overall biological activity of this set of nanoparticles. Combined with the nanoparticle characterization, integration of the biological potency estimates enabled a comprehensive determination of the cellular reactivity of the SiNPs. The approach shows promise as a useful tool for first-tier screening of SiNP toxicity.

ARTICLE HISTORY
Received 15 September 2016
Revised 5 January 2017
Accepted 20 January 2017

KEYWORDS
Nanoparticles; silica; cytotoxicity; cytokines; pathway analysis

Introduction

Synthetic, amorphous silicon dioxide nanoparticles (SiNPs) have a growing use in coatings, paints, adhesives, composites, cosmetics, food additives and in the biomedical field in drug delivery and diagnostics (Kim et al., 2010; Napierska et al., 2010; Park et al., 2009). Despite the rapid introduction of nanomaterials to markets and extensive investigations of their toxicological properties, their safety has not yet been well established. Safety assessments of the silica-based nanomaterials in food and consumer applications have been attempted and appear reasonable (Jacobs et al., 2015; Michel et al., 2013). However, it has also been stressed to consider each nanomaterial on a case-by-case basis due to the heterogeneity in their properties, which can influence their biological activity. These properties include surface chemistry, polarity, porosity, particle size and morphology, solubility and chemical purity (Fruijtier-Pölloth, 2012; Rabolli et al., 2010, 2011). Therefore, systematic studies with well characterized nanomaterials and defined protocols are necessary to obtain an understanding of the influence of physico-chemical and biological factors on their toxicity.

Macrophages and epithelial cells of the bronchi and alveoli are the critical cells involved in processing inhaled particulates. The cells respond by locally releasing inflammatory mediators for chemotaxis and inducing the phagocytic/endocytic uptake of the particles from the airways. When particles are present in large amounts or are highly noxious, antigen presentation and inflammation are utilized to recruit cells from the systemic circulation to aid in resolving the heightened lung insult (Miyata & van Eeden, 2011). These processes are thereby implicated in the clearance of foreign materials from the respiratory system. However, with high lung burden the cellular clearance activities can become inadequate and can result in pathologies, such as those observed in chronic occupational exposures to crystalline silicon dioxide leading to silicosis, a progressive fibrotic lung disease (Davis, 1986; Ding et al., 2002; Hnizdo & Sluis-Cremer, 1993). Overall, these studies establish a clear paradigm linking inhaled particulates with morbidity and mortality in humans. Moreover, in the context of air pollution, exposures to high levels of ambient particulate matter also contribute to cardiovascular disease and mortality (Hnizdo & Sluis-Cremer, 1993; Pope et al., 2009).

Although chronic exposures to micro-sized crystalline silicon dioxide result in silicosis in humans (Davis, 1986; Ding et al., 2002; Hnizdo & Sluis-Cremer, 1993), synthesized amorphous silicon dioxide particles such as precipitated or colloidal particles are thought to be less toxic and non-fibrogenic in animal models (Johnston

CONTACT Renaud Vincent renaud.vincent@canada.ca; Dalibor Breznan dalibor.breznan@canada.ca Environmental Health Science and Research Bureau, Health Canada, Tunney's Pasture, Ottawa, Ontario K1A 0K9, Canada

Supplemental data for this article can be accessed here.

et al., 2000; Lee & Kelly, 1992). However, the body of evidence from both *in vitro* and *in vivo* toxicological studies shows that amorphous nano forms of silicon dioxide particles present some toxicological hazards to human health. Based on *in vitro* findings, the effects of exposure to amorphous SiNPs include cytotoxicity, reactive oxygen species (ROS) production and pro-inflammatory effects, while the *in vivo* studies report a generally reversible pulmonary inflammation, localized emphysema, granulomatous lesions and silicotic nodules with a potential for establishment of a pro-fibrotic milieau (Byrne & Baugh, 2008; Chen et al., 2014; Choi et al., 2008; Napierska et al., 2010). Limited evidence for a genotoxic potential of SiNPs also exists (Golbamaki et al., 2015; Kwon et al., 2014).

Since silica-based nanoparticles are already commercially available, they may present a potential for exposure in occupational settings, including during synthesis, transportation and use. A strong linkage between the SiNP physico-chemical characteristics and toxicological effects has been established (Napierska et al., 2010). However, a clear understanding of the contributions and roles of specific SiNP characteristics in inducing toxicity is an area of fervent investigation. This study aimed to determine the cytotoxic and inflammatory potential of a set of commercially available amorphous SiNPs in cells of distinct origin (human vs. murine) and type (epithelial vs. macrophage), which are the primary cell types included in processing of inhaled particles *in vivo*. The determination of the SiNP physico-chemical parameters associated with the biological effects was subsequently sought.

Methods

Particles

Amorphous silicon dioxide nanoparticles (SiNPs); SiNP (10–20 nm, cat # 637238), SiNP (5–15 nm, cat # 637246) and SiNP (12 nm, cat # 718483) were obtained from Sigma-Aldrich (ON, Canada). The Standard Reference Material (SRM)-1879a (respirable cristobalite, CRI SiO_2) and SRM-154b (titanium dioxide, TiO_2) were obtained from the National Institute of Standards and Technology (NIST; MD). The SRM-1879a was used as supplied, while SRM-154b was washed three times with methanol, and three times with phosphate-buffered saline (Vincent et al., 1997). The NIST SRMs were included for comparative purposes, based on their historical use across studies, for cellular responses to mineral particles.

Characterization of particles

Detailed description of particle physico-chemical analyses is provided in the supplemental section. Briefly, the following methods were conducted;

Surface area and pore volume

All SiNPs were measured by nitrogen adsorption at 77 K using the ASAP 2020 adsorption analyzer (Micromeritics, GA) following procedure reported previously (Das et al., 2007, 2014).

Determination of surface organic content

The weight loss from the SiNP samples was determined by thermogravimetric analysis (TGA) using a TA Instruments Q5000 IR instrument (Waters Limited, ON, Canada) following a previously reported method (Das et al., 2014).

Determination of elemental concentration

The SiNP samples were acid-digested following procedure provided in the supplemental section. The metal contents of the acid-digested solutions were measured using Inductively Coupled Plasma-Atomic Emission Spectroscopy (ICP-AES; Varian Vista-Pro, Australia) and -Mass Spectrometry (ICP-MS; Agilent 7700×, MA). Samples were diluted where the concentration was above the upper limit of the calibration (100 ppb).

Quantitation of surface acidity

The total acidity of the surface of SiNPs was quantified following the acid-base titration procedure reported earlier (Eitan et al., 2003; Kumarathasan et al., 2015).

Particle size and morphology in dry state

The size of the SiNPs was assessed by Transmission Electron Microscope (TEM; JEOL JEM-2100F field emission, MA) equipped with an ultra-high resolution pole-piece operating at 200 kV, while the presence of agglomerates and their morphology were assessed by Scanning Electron Microscope (SEM; JSM-7500F FESEM (JEOL), MA) equipped with a Field Emission Gun (Das et al., 2014).

Particle size and surface potential in liquid media

The hydrodynamic diameter of SiNPs in liquid media was determined by Dynamic Light Scattering (DLS) using Zetasizer Nano ZS (Malvern Instruments, UK) as reported earlier (Das et al., 2014). The analysis of SiNP size and the electrokinetic potential of particle dispersions was conducted in ultrapure water, Dulbecco's Modified Eagle's Medium (DMEM; phenol red-free, 4.5 g/L glucose) and DMEM +5% (v/v) fetal bovine serum FBS (Fisher Scientific, ON, Canada) at particle concentrations corresponding to the 30 and 100 μg/cm^2 doses per well surface area.

Cell culture

Human lung epithelial (A549), human peripheral blood monocytes (THP-1) and murine macrophage (J774A.1) cell lines were obtained from American Type Culture Collection (ATCC; VA). The cells were maintained as described in the supplemental section. All cells were cultured in 75 cm^2 tissue culture flasks (Corning, NY) at 37 °C with 5% CO_2 and 95% relative humidity.

For experiments, A549 and J774A.1 cells were cultured in DMEM (phenol red-free) with 10% FBS, in 96-well plates at 10,000 and 20,000 cells/well (~0.32 cm^2 surface area; 100 μL medium) respectively, using a repeater pipette. J774A.1 cell suspensions were strained through a 100 μm cell strainer prior to counting and seeding. Cell counts were determined using the Multisizer 3 Coulter Counter (Beckman Coulter, ON, Canada). The cell monolayers were cultured for 24 h prior to exposure to particles. THP-1 monocytes were seeded in 96-well plates at 120,000 cells/well, in 100 μL of complete RPMI-1640 medium (phenol red-free) supplemented as described above. THP-1 cells were seeded in the presence of phorbol-12-myristate-13-acetate (PMA, 10 ng/mL; Sigma-Aldrich) to induce their differentiation into macrophages. The medium was replaced the next day with 100 μL of fresh media and the cells were incubated for 24 h prior to SiNP exposure.

Preparation of particle suspensions

Stock suspensions of SiNPs (3 mg/mL) and SRMs (10 mg/mL) were prepared in particle buffer (0.19% NaCl, 25 μg/mL Tween-80; Sigma-Aldrich). The final concentration of Tween-80 in a 96-well is below 0.4 ug/mL in the culture medium, with no impact on cytotoxicity or inflammatory cytokine release in cells. The particle suspensions were vortexed for 30 s, sonicated on ice for 20 min using a Branson 2510 water bath sonicator (Branson Ultrasonics, CT) and dispersed by 25 strokes of the homogenizer piston in a Dounce

glass-glass micro-homogenizer (Nadeau et al., 1996). Particle suspensions were aliquoted into sterile microcentrifuge tubes with o-ring seal screw caps and heated to 56 °C for 30 min. Stock suspensions were stored at −80 °C until use.

Cell exposure to SiNPs

Particle suspensions were thawed to room temperature (RT), sonicated for 20 min and working suspensions were prepared in 100 µL of serum-free medium and re-sonicated for 10 min before adding them at 3, 10, 30 and 100 µg/cm^2 of well surface area to the cell monolayers in 100 µL of DMEM +10% FBS using Liquidator 96 (Mettler Toledo, ON, Canada) for A549 and J774A.1 cells and RPMI-1640 + 10% FBS for THP-1 cells. The equivalent exposure concentration was 5, 16, 50 and 160 µg/mL of media +5% FBS (final conc.). After exposure, the cells were incubated at 37 °C with 5% CO_2 and 95% relative humidity for 24 h prior to commencement of the integrated assay.

Endotoxin analysis

Stock samples of particles were analyzed for the presence of bacterial endotoxin using the chromogenic Limulus Amebocyte Lysate (LAL; Lonza, MD) test, as described by the supplier, with modification to prevent potential interference of particles with test kit reagents. The procedure is described in the supplemental section.

Sequence of assays

The cytotoxicity of SiNPs was assessed using the integrated bioassay which enabled the analysis of the redox state (resazurin reduction), energy metabolism (cellular ATP) and cell membrane integrity (LDH release) and was conducted as previously described (Kumarathasan et al. 2015). Cell proliferation was assessed separately, using the BrdU incorporation assay. All experiments were conducted three times ($n = 3$), with triplicate samples within each experiment. More detailed descriptions of the assays are provided in the supplemental section.

Cytokines/chemokines

Cytokine and chemokine profiles were established from A549, J774A.1 and THP-1 cell supernatants. J774A.1 supernatants were assessed using a Milliplex MAP mouse cytokine 25-plex panel, while a Milliplex MAP 27-plex human cytokine panel (EMD-Millipore, MA) was used for A549 and THP-1 cells. The quantification of cytokines/chemokines was done using the Bio-Plex 200 array reader (Bio-Rad, ON, Canada), according to the supplier-recommended procedure, outlined in more detail in the supplemental section. The baseline levels of the cytokines/chemokines are presented (Table S1).

Particle potency estimates

The dose-response data for cytotoxicity assays and cytokine release were normalized to the mean value of all controls (0 µg dose of particles), to obtain fold-effect (FE) for each particle dose. Potency (β) is derived from

$$FE = (Dose + 1)^{\beta}$$

where, β represents the rate of change of dose with respect to the logarithm of fold-effect for a given endpoint (Vincent et al. 1997). The dose-response data were fitted using CurveExpert v1.4 (D. Hyams, TN).

Cytotoxic potency (β_V) represents the average of the assay-specific potencies for each cell line ($\beta_{V\ A549}$, $\beta_{V\ THP\text{-}1}$, $\beta_{V\ J774A.1}$) and across cell lines ($\beta_{V\ CELLS}$). Similarly, biological reactivity (β_R) of the particles was obtained by averaging the absolute values (to capture deviations from control levels). An average potency for inflammation ($\beta_{I\text{-}V}$) was calculated within each cell line and across the cell lines using $+1*\beta_{I\text{-}V}$ for chemokines and pro-inflammatory cytokines and $-1*\beta_{I\text{-}V}$ for anti-inflammatory cytokines. The mediators IL-1ra, IL-4, IL-9, IL-10 and IL-13 are considered as anti-inflammatory. While IL-6 is a pleiotropic cytokine, it was assumed to be pro-inflammatory for the purposes of this manuscript (Cuneo & Autieri, 2009; Opal & DePalo, 2000). The $\beta_{I\text{-}V}$ (corrected for viability on a dose-by-dose basis) represents an unbiased potency estimate signifying an apparent decrease of cytokine release due to cell death, or an increase in cytokine release due to an increase of cell mass in the wells. Finally, β_R and $\beta_{I\text{-}V}$ were integrated to calculate cell-specific beta potencies (Iβ) within the cell lines ($I\beta_{A549}$, $I\beta_{THP\text{-}1}$, $I\beta_{J774A.1}$) and across the cell lines ($I\beta_{\ CELLS}$). The detailed equations for the integration of the potency estimates are provided in the supplemental section.

Dosimetric adjustment for SiNP aggregates

Sedimentation of nanomaterials in cell culture models is sensitive to particle aggregate size and density. The phenomenon has been discussed in detail by others (Cohen et al., 2013; DeLoid et al., 2014; Pal et al., 2015). In order to assess the sensitivity of our conclusions to dose biases between the different SiNPs, we have made an assumption of higher effective density and increased fractional deposition rate for the SiNP (12 nm) in relation to the trend of lower hydrodynamic diameter, using the worst case scenario for SiNPs extracted from Table 1 of Cohen et al. (2014). Thus for SiNP (12 nm; particle hydrodynamic diameter $d_H = 385$ nm for the 100 ug/cm^2 dose in exposure-equivalent media; Table S2) we assumed a fractional deposition rate of $\alpha = 0.026\ h^{-1}$, and for the SiNP (5–15 nm; $d_H = 576$ nm; Table S2) and SiNP (10–20 nm; $d_H = 805$ nm; Table S2) we assumed a fractional deposition rate of $\alpha = 0.014\ h^{-1}$ (Cohen et al., 2014). Solving

$$f_D(t) = 1 - e^{-\alpha t}$$

for a t = 24 h *in vitro* exposure, the fractional deposited dose, or the ratio of deposited dose to administered dose for SiNP (12 nm), was estimated at 0.46, whereas the fractional deposited dose for SiNP (5–15 nm) and SiNP (10–20 nm) was estimated at 0.28. Thus consequently, we also consider in the data analyses that cells exposed to SiNP (12 nm) could have been exposed to 64% (1.64×) more material after 24 h than the cells exposed to the other two SiNPs.

Statistical analyses. Experimental data (FE) from all assays and cytokine release, as well as the β cytotoxic potency, biological reactivity and inflammatory potency estimates were statistically analyzed by the three-way Analysis of Variance (ANOVA) using SigmaPlot version 12.5 software (Systat Software, San Jose, CA). Tukey's multiple comparisons test was used to elucidate the patterns of significant effects ($\alpha = 0.05$).

Clustering of particles based on their effects on cytokines/chemokines release by the individual cell lines and the visualization of the data were performed using the GenePattern version 3.6.0 (Broad Institute, MIT, Cambridge, MA) webtool (Reich et al., 2006) and Java TreeView plugin version 1.16.r2 (Saldanha, 2004). Principal component analysis (PCA) of the cellular cytokine profiles (significant by ANOVA) was conducted using Minitab v15.1 software (Minitab Inc., PA). The pathways and biological functions impacted by SiNP exposures of the cells were identified using the Ingenuity Pathway Analysis (IPA; Ingenuity

Systems, CA). Further details on the statistical analyses conducted in the present manuscript are provided in the supplemental section.

Results

Characterization of SiNPs

The particle characteristics are shown in Table 1 which contains the data generated by the authors and those provided by the commercial suppliers. Some differences between the two datasets (i.e. author and suppliers) were observed. For example, BET surface area of SiNP (12 nm) determined is ~30% larger than the value provided by the supplier (302 m^2/g vs. 175–225 m^2/g), while those for SiNP (5–15 nm) were similar (613 m^2/g vs. 590–690 m^2/g). The BET surface area for SiNP (10–20 nm) was 840 m^2/g while a measurement was not available from the commercial supplier. All SiNPs had similar external surface areas (SA_{ext}) and total pore volumes (V_t). In contrast, SiNP (10–20 nm) and SiNP (5–15 nm) contained micropores while SiNP (12 nm) did not.

The particle size of all materials was determined by TEM or SEM. Agglomerated, irregularly shaped SiNPs were observed (Figure 1). Based on unit particle size measurements within the agglomerates, SiNP (12 nm), (10–20 nm) and (5–15 nm) showed a mean size of 16.4 nm, 32.2 nm and 19.5 nm respectively in relatively good agreement with the supplier-provided data (Table 1). The SiNPs were agglomerated in dry form (Figure S2A–F), with the highest level observed for SiNP (12 nm), forming large globular agglomerates (Figure S2E, F). The TiO_2 particles formed aggregates of ca. 20 µm, while individual TiO_2 particles were generally spherical (Figure S3A, B). CRI particles were irregularly shaped with approximate size of 5 µm (Figure S3C, D). CRI particles did not tend to aggregate and appeared highly crystalline. The size of the reference particles was in general agreement with that reported by NIST (Table 1).

The TGA of the SiNPs showed two stages of weight loss during calcination; sharp weight loss below 200 °C and a gradual weight loss from ca. 350 °C until 800 °C (Figure S4). The weight loss beyond 200 °C for SiNP (10–20 nm), (5–15 nm), (12 nm) amounted to 5.0%, 2.6%, and 0.29%, respectively, and represents the surface organic content (Table 1).

The quantitation of SiNP surface-associated silanol '–OH' groups from the acid-base titration indicated that the surface acidity of the SiNP (12 nm) is significantly higher (about 2-fold) than that of the SiNP (5–15 nm) and (10–20 nm), both of which were similar (Table 1; two-way ANOVA, SiNP (12 nm) vs. (5–15 nm) and (10–20 nm), $p < 0.001$).

The endotoxin analysis showed that LPS was not present in the SiNP stock suspensions. Only a trace amount of LPS was observed in the SRM stock suspensions (Table 1).

Based on the data provided by the commercial supplier, SiNPs (12 nm) and (10–20 nm) had total trace metal content of ca. 30 ppm while that of SiNP (5–15 nm) was 797 ppm (Table 1). The analyses of trace metals by ICP-MS/-AES (Table S3A) showed a marked difference in metal composition from that indicated by the suppliers (Table S3B). No correlations could be established between the matching elements.

All SiNPs were further characterized in water, DMEM and DMEM +5% FBS using DLS (Table S2). Two SiNP concentrations tested (50, 160 µg/mL) corresponded to the doses of 30 and 100 µg/cm^2 of well surface area, respectively. The DMEM +5% FBS represented the cell exposure media. In all three media, some agglomeration of the SiNPs was observed. However, SiNP (12 nm) agglomerates were consistently smaller than those formed by the (5–15 nm) and (10–20 nm) SiNPs (three-way ANOVA, SiNP (12 nm) across media type, $p < 0.001$). The SiNP (12 nm) in DMEM +5% FBS showed a higher hydrodynamic size, 386 ± 128 nm at 160 µg/mL, compared to 184 ± 7 nm at 50 µg/mL indicating that particle concentration significantly impacts the aggregation in protein-rich media (DMEM +5% FBS; three-way ANOVA; SiNP conc. within media-type; $p = 0.011$).

In liquid media, all SiNPs formed dispersions with negative particle surface charge (Table S2). In water, the SiNP dispersions were

Table 1. Physico-chemical properties of the particles.

Property	SiNP (10–20 nm)	SiNP (5–15 nm)	SiNP (12 nm)	CRI (SRM)	TiO_2 (SRM)
$Size_{man}$ (nm)	20	15	12	2000–6000	<45,000
Mat $State_{man}$	Amorphous	Amorphous	Amorphous	Crystalline	Crystalline, rutile
SA_{man} (m^2/g)	–	590–690	175–225	–	–
$Elem_{man}$ (ppm)	30.0	797.0	30.7	–	–
$Purity_{man}$ (%)	99.5	99.5	99.8	88 ± 0.4	100 ± 0.1
$Size_{part}$ (nm)	32 ± 4.8	20 ± 4.6	16 ± 3.1	5217 ± 1782	18,890 ± 5199
$Size_{agglom}$ (nm)	4592 ± 1988	3577 ± 2431	17,980 ± 7246	NA	18,890 ± 5199
$Size_{wet}$ (nm)	805 ± 152	576 ± 104	385 ± 128	–	–
ζ (mV)	−10.8 ± 0.7	−11.5 ± 0.7	−11.6 ± 1.0	–	–
SA_{BET} (m^2/g)	840 ± 240	613 ± 47	302 ± 25	–	–
SA_{ext} (m^2/g)	388	304	313	–	–
V_t (m^2/g)	0.69 ± 0.2	0.58 ± 0.1	0.56 ± 0.0	–	–
V_m (m^2/g)	0.21 ± 0.1	0.15 ± 0.0	0.01 ± 0.0	–	–
Surf OC (% wt)	5.050	2.550	0.291	–	–
Surf (–OH) (µmol/mg)	1.33 ± 0.2	1.40 ± 0.1	2.54 ± 0.1	–	–
Tot Met (ppm)	4799	11,286	1650	7603	3548
Trans Met (ppm)	342	353	40	2641	155
Biol Act Met (ppm)	2092	8220	912	3971	2753
Endotoxin (ng/mg)	n.d.	n.d.	n.d.	0.019	0.012

Size ($Size_{man}$), material state ($Mat\ State_{man}$), surface area (SA_{man}), elements ($Elem_{man}$) and purity ($Purity_{man}$) were obtained from Sigma-Aldrich or NIST; particle size ($Size_{part}$) was determined by TEM for SiNPs and SEM for SRMs; dry-state agglomerate size ($Size_{agglom}$) was obtained by SEM; hydrodynamic size ($Size_{wet}$) from DLS and zeta potential (ζ) from particle electrophoretic mobility are taken at [0.16 mg/ml] of particles; total surface area (SA_{BET}) was obtained by BET analysis; external surface area (SA_{ext}) and micropore volume (V_m) were calculated by t-plot analysis; total pore volume (V_t) was considered as the volume of N (l) adsorbed at P/Po = ca. 1; surface organic content (Surface OC) was determined by TGA; quantity of surface –OH groups (Surface –OH) was obtained from an acid-base titration; total elemental content (Tot Met) was obtained from ICP-MS/AES; transition metal content (Trans Met) was the total of transition metals (bold text in Table S1) from ICP-MS/AES; biologically active metals (Biol Act Met) represent the total metals from ICP-MS/AES considered to have biological activity based on classification in Nieboer & Richardson (1980), italicized in Table S1; Endotoxin content of the particles (Endotox) was determined using the LAL assay (10 EU/ng; FDA); n.d. denotes data below detection limit; CRI sample did not agglomerate in dry state (NA); "-" is data not available.

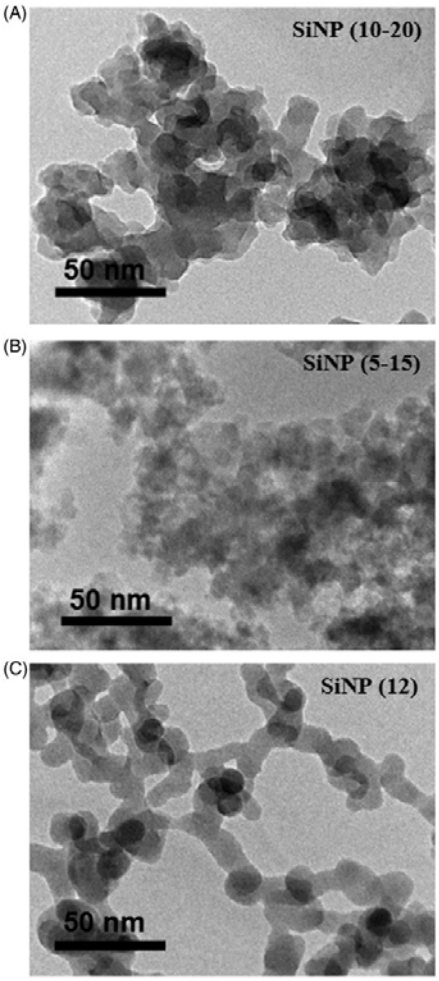

Figure 1. Transmission electron microscopy images of the amorphous SiNP particles. The images of **(A)** SiNP (10–20 nm), **(B)** SiNP (5–15 nm) and **(C)** SiNP (12 nm) are presented. Scale bars are indicated in the lower left corner of each image.

highly stable, with ζ below −25 mV. In DMEM, ζ values became less negative for all particles at both concentrations tested, with SiNP (12 nm) showing the least change. However, in DMEM +5% FBS, SiNP ζ values changed substantially to the range of −9.6 to −10.6 mV at both concentrations (Table S2), indicating an increase in the instability of the particle suspensions (Hunter, 2006), with particles coagulating and flocculating towards the formation of agglomerates.

Cytotoxicity

The SiNPs decreased ATP in a dose-responsive manner (Figure 2(A); three-way ANOVA, *Dose x PM*, $p < 0.001$), with SiNP (12 nm) showing the highest impact on ATP levels in all three cell lines (A549, THP-1, J774A.1), compared to SiNPs (10–20 nm) and (5–15 nm), which showed similar effects. Small elevation above control was observed in ATP levels of A549 cells exposed to the low doses of the SiNPs (three-way ANOVA, *Cells* within *PM*, $p < 0.001$), which was not seen in the macrophages (Figure 2(A)). Overall, the macrophage cell lines were more sensitive to SiNP exposure than A549 cells, with J774A.1 cells most impacted (Figure 2(A); three-way ANOVA, *Dose x Cells*, $p < 0.001$). The ATP levels in the macrophage cell lines were more affected by SiNP exposures than the epithelial cells (Figure 2(A); three-way ANOVA, *Cells* × *PM*, $p < 0.001$). Similar observations were made in the LDH, membrane integrity assay where the cellular responses to the SiNPs were cell type-, particle- and dose-dependent (Figure 2(B); three-way ANOVA, *Dose* × *Cells* × *PM*, $p < 0.001$). J774A.1 cells released most LDH in response to SiNP (12 nm), followed by the other two SiNPs. SiNPs affected the cellular redox status in macrophages but not epithelial cells, as seen by the decreased reduction of resazurin by cells (Figure 2(C); three-way ANOVA, *Dose* × *Cells* × *PM*, $p < 0.001$). SiNP (12 nm) was the most potent, causing the largest decrease in resazurin reduction in J774A.1 cells, followed by THP-1 cells. Cell proliferation in J774A.1 cells was significantly decreased by SiNP (12 nm) but not (5–15 nm) and (10–20 nm) SiNPs (Figure 2(D); three-way ANOVA, *Dose* × *Cells* × *PM*, $p < 0.05$). A549 cell proliferation was not affected by particle exposures. It should be noted, that proliferation of THP-1 cells was not assessed as they lose their proliferative capacity upon PMA-induced differentiation to macrophages (Schwende et al., 1996). The CRI and TiO_2 SRMs did not significantly alter any of the assessed cytotoxicity endpoints, with only marginal changes observed in macrophages.

Cytokines/chemokines

Particle exposures differentially affected the cellular cytokine/chemokine release profiles (Figure 3 (A)–(C), Figures S5–S7). In the three cell lines, SiNP (12 nm) particles induced the release of most of the detected cytokines/chemokines to a higher extent, causing them to cluster separately from the other particles. In A549 cells, the particles affected cytokine release profiles at a lesser magnitude compared to the macrophages. Also in A549 cells, there was a clear contrast in the cytokine profile between SiNP-exposed cells compared to CRI (Figure 3(A)). In THP-1 cells, two distinct groups, one of decreased and the other of increased cytokine release were revealed in response to (SiNP (5–15 nm) and (10–20 nm) exposures, separate from the intermediate effects of CRI and the strong induction of cytokine release by SiNP (12 nm) of the majority of cytokines/chemokines (Figure 3(B)). In J774A.1 cells, an SiNP (12 nm)-driven induction of the majority of the detected cytokines/chemokines formed a cluster separate from the responses induced by the remaining particles. These were separated into two distinct clusters of cytokines/chemokines based on their response to CRI and SiNP (5–15 nm) and (10–20 nm); i.e. markers released at contrasting high and low levels (Figure 3(C)). Based on the cytotoxicity results, both SRMs, CRI and TiO_2 showed similar response. Therefore, cell culture supernatants from CRI-exposed cells only were selected for cytokine analysis. Moreover, CRI was deemed more relevant because of its same elemental composition as the SiNPs.

The inflammatory markers (from 30, 100 μg/cm^2 dose exposures) released by the cell lines at significant levels (based on ANOVA) were analyzed using PCA to identify markers that contribute the most to the overall pattern of the observed particle effects. It was found that the first three PCs (PC1, PC2 and PC3) contributed to 95.7% of the variation in the dataset (Table S4). The analysis revealed a distinct grouping of particles based on the cellular cytokine release patterns, highlighting the unique high inflammatory effects of SiNP (12 nm), the similarity in response of the cell lines to SiNPs (5–15 nm) and (10–20 nm) and the distinct response of the cell lines to CRI (Figure 4). Based on the factor loading of the principal components, the following cytokines were

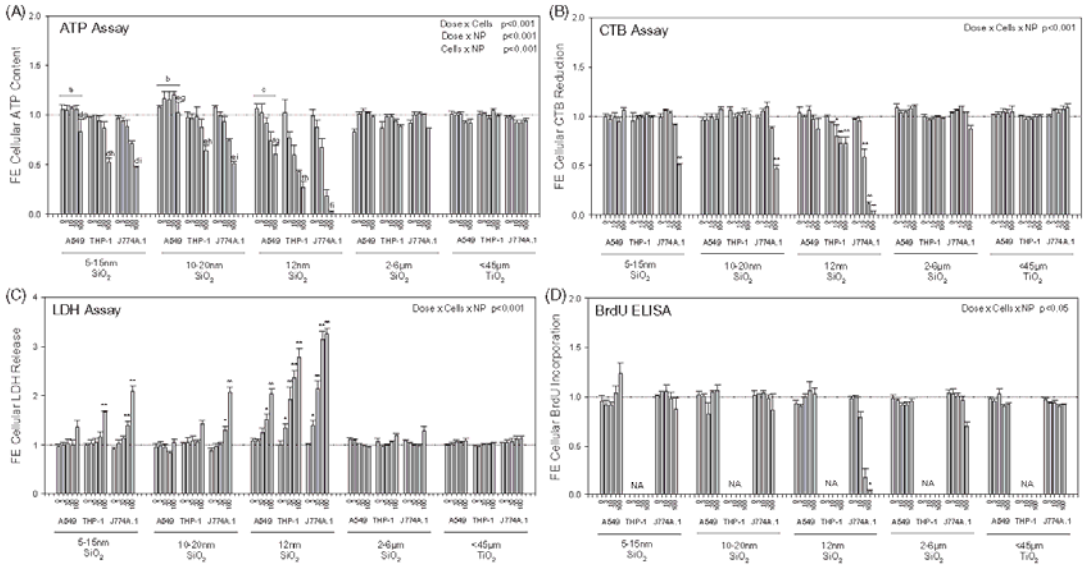

Figure 2. Cytotoxic profile of three mammalian cell lines exposed to 3, 10, 30 and 100 µg/cm^2 of the particles for 24 h. The A549, THP-1 and J774A.1 cell lines were exposed to SiNPs and SRMs (24 h). An integrated bioassay was performed comprising of **(A)** ATP assay, **(B)** LDH assay (release), **(C)** CTB assay and **(D)** BrdU ELISA. **(A)** Three-way ANOVA, two-way interactions: *Cells* × *PM*, *Dose* × *PM*, *Dose* × *Cells*, $p < 0.001$, Tukey comparisons: **(a)** cells treated with SINP (5–15 nm), A549 vs J774A.1 and A549 vs THP-1, $p < 0.001$, **(b)** cells treated with SINP (10–20 nm), A549 vs J774A.1 and A549 vs THP-1, $p < 0.001$, **(c)** cells treated with SINP (12 nm), A549 vs J774A.1 and A549 vs THP-1, $p < 0.001$, **(d)** dose for SINP (5–15 nm), 100 µg/cm^2 different from all other doses, $p < 0.001$, **(e)** dose for SINP (10–20 nm), 100 µg/cm^2 different from all other doses, $p < 0.001$, **(f)** dose for SINP (12 nm), 100 µg/cm^2 different from all other doses, $p < 0.035$, **(g)** dose in A549 cells, 100 µg/cm^2 different from all other doses, $p < 0.012$, **(h)** dose in A549 cells, 100 µg/cm^2 different from all other doses, $p < 0.001$, **(i)** dose in A549 cells, 100 µg/cm^2 different from all other doses, $p < 0.001$; **(B-C)** Three-way ANOVA, three-way interaction: *Dose* × *Cells* × *PM*, $p < 0.001$; **(D)** Three-way ANOVA, three-way interaction: *Dose* × *Cells* × *PM*, $p < 0.05$; **(B–D)** Asterisks indicate effects significantly different from 0 µg dose cells, Tukey comparisons, $^*p < 0.05$, $^{**}p < 0.001$; **(D)** BrdU ELISA was not available for differentiated THP-1 cells. Data were expressed as mean fold-effect (FE) ± SEM for $n = 3$ independent experiments, with three technical replicates within each experiment.

determined to be the main contributors to the contrasting clustering of the particles in the cell lines tested: IL-9 and eotaxin for A549; G-CSF, IP-10, MCP-1, MIP-1α, MIP-1β, RANTES, TNF-α for THP-1; IL-10, IP-10, MIP-2, RANTES, TNF-α in J774A.1 (Figure 4, Table S5).

Particle potency assessment

In order to reduce the complexity of the dataset, the dose-response data from particle exposures were summarized in terms of simplified descriptor Beta (β) derived for each endpoint of cytotoxicity (β_V) or cytokine release (β_{I-V}), as well as averaged across all cytotoxicity assays, or all cytokines to facilitate a rank-based comparison of the overall toxicological profile of each SiNP (Iβ). A plot of β_V values based on all cytotoxicity assays conducted across the three cell lines revealed that SiNP (12 nm) was the most cytotoxic particle, indicated by the highest negative potency values (three-way ANOVA, *PM* main effect, $p < 0.001$), while the SRMs were consistently the least cytotoxic (Figure 5(A), Table S6). Overall, the β_V was correlated between cell lines; THP-1 vs. J774A.1 ($R = 0.998$, $p < 0.001$), THP-1 vs. A549 ($R = 0.897$, $p < 0.05$) and A549 vs. J774A.1 ($R = 0.888$, $p < 0.05$) cells. Based on β_R, SiNP (12 nm) had the highest biological reactivity in each cell line (Table S6). Averaging of the β_V and β_R across cell lines confirmed the highest ranking of SiNP (12 nm) based on the consensus of the cytotoxicity assays (Table 2). Similarly, based on $\beta_{I-V\ CELLS}$, which represents the consensus inflammatory potency of each particle, derived from cellular cytokine profiles and averaged across cell lines, SiNP (12 nm) was ranked highest (Table 2). Some difference was seen in the ranking of the particles compared to the cytotoxicity-based ranking: i.e. SiNP (5–15 nm) and (10–20 nm) were overall less potent in inducing inflammatory mediators than CRI (Table 2).

Despite the contrasting particle ranking based on cytotoxicity and the inflammatory response (Table 2), the β_R and β_{I-V} estimates were marginally correlated ($R = 0.943$, $p = 0.057$). As observed for the β_V profile (Figure 5(A)), SiNP (12 nm) remained the most potent particle, based on β_R and β_{I-V} estimates (Figure 5(B); three-way ANOVA, *PM* main effect, $p < 0.001$), with SiNPs (10–20 nm), (5–15 nm) and CRI grouped together, with a contrast in the inflammatory potency profile of the particles in the epithelial cells vs. the macrophages. Thus, THP-1 and J774A.1 β_{I-V} estimates were significantly correlated ($R = 0.991$, $p = 0.009$), while THP-1 vs. A549 ($R = 0.840$, $p = 0.160$) and A549 vs. J774A.1 ($R = 0.897$, $p = 0.103$) were not associated.

Finally, the biological reactivity and inflammatory response across the cell lines were combined into an integrated potency estimate for each particle. Based on $I\beta_{CELLS}$, SiNP (12 nm) was 6.1×, 8.3× and 10.4× more potent than CRI, SiNP (5–15 nm) and (10–20 nm), respectively (Table 2). The higher potency of SiNP (12 nm) exceeded by far the fold-change which was expected simply from higher deposition (1.64×).

Pathway analysis

Pathway analysis was conducted on the cytokine mediators from SiNP and CRI exposures in the three cell lines. The profiles of the interrogated mediators were associated with a number of common and unique cell type-specific functions (Table 3). The functions common to the three cell lines included cell-to-cell signaling and cellular movement. Cellular development and cell growth and proliferation were highlighted in the macrophages. Note that,

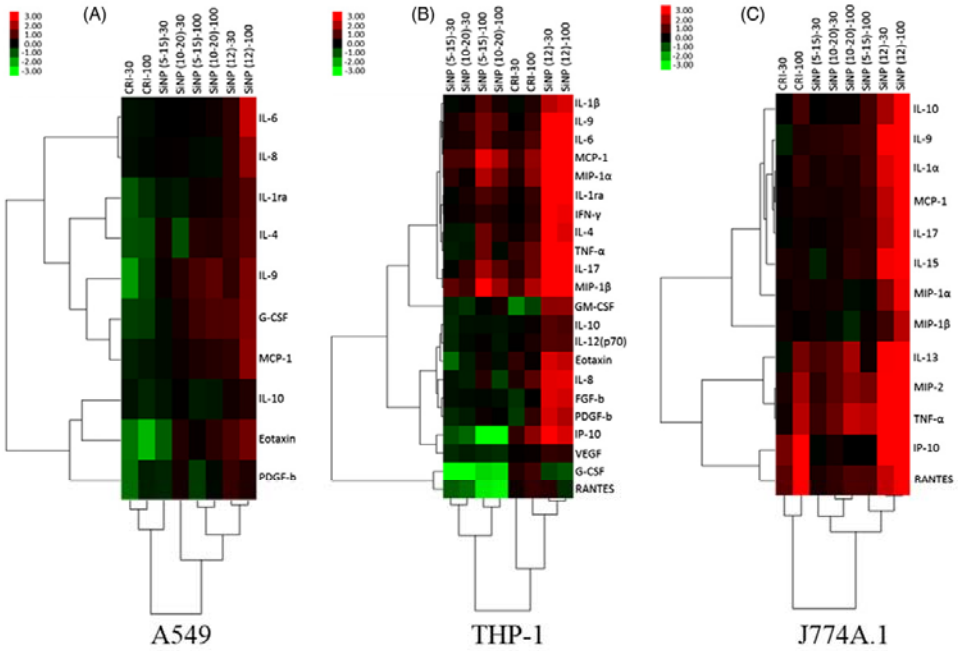

Figure 3. Secretory cytokine profiles of cells exposed to particles. Hierarchical cluster analysis and heatmap of statistically significant cytokines by ANOVA ($p < 0.05$), fold changes in abundance of secretory cytokines in each cell line are presented: **(A)** A549, **(B)** J774A.1 and **(C)** THP-1. All treatments were expressed relative to an untreated control (fold-effect) and adjusted for consensus (average across assays) cytotoxic response at each particle dose level (30 and 100 μg/cm^2). The dataset was log(2) transformed. The bar illustrates the color coding for the cytokines produced by the cells exposed to SiNPs and SRMs. Green indicates decreased cytokine production and red indicates increased cytokine production relative to control groups. The vertical dendrogram represents the clustering of cytokines/chemokines and the horizontal dendrogram represents the clustering of particles. The analysis was based pooled samples of 2–3 wells per sample within each experiment conducted in triplicate experiments ($n = 3$).

since THP-1 cells do not proliferate in their differentiated state, the highlighted cellular function may indicate cellular growth and/or development in the case of this cell line. Other indicated pathways were unique to a particular cell line; lipid metabolism, molecular transport and biochemistry in A549; cell morphology in THP-1; cell death and survival in J774A.1 (Table 3). The cytokine expression profiles and a list of some of the top functional roles underlying the cellular functions are presented (Table S5). The main inflammatory mediators driving the differential response of the cell lines to the silica-based particles, as identified by the PCA (Figure 4, Table S4) were associated with the unique cellular functions identified by the IPA (Table 3 and Table S4).

Correlation of SiNP characteristics with their toxicological profile

Correlations of the integrated consensus potency estimates for biological reactivity ($\beta_{R\ CELLS}$), pro-inflammatory potency ($\beta_{I\text{-}V\ CELLS}$) and integrated potency ($I\beta_{\ CELLS}$) of the individual SiNPs with their physico-chemical characteristics were conducted (Table 4; Table S7). The analysis revealed a significant ($p < 0.05$) positive association of the integrated consensus potency estimates with surface acidity (surface –OH); $\beta_{R\ CELLS}$ ($R = 1.0$, $p = 0.015$), $\beta_{I\text{-}V\ CELLS}$ ($R = 1.0$, $p = 0.019$) and $I\beta_{\ CELLS}$ ($R = 1.0$, $p = 0.018$). Interestingly, a significant negative association was also revealed for the integrated SiNP potency estimates and their transition metal content; $\beta_{R\ CELLS}$ ($R = -0.998$, $p = 0.037$), $\beta_{I\text{-}V\ CELLS}$ ($R = -0.999$, $p = 0.033$) and $I\beta_{\ CELLS}$ ($R = -0.999$, $p = 0.034$). Also, a marginally significant ($0.05 < p < 0.1$) positive association was observed between the integrated consensus SiNP potency estimates and the dry-state particle agglomerate size; $\beta_{R\ CELLS}$ ($R = 0.996$, $p = 0.058$), $\beta_{I\text{-}V\ CELLS}$ ($R = 0.996$, $p = 0.054$) and $I\beta_{\ CELLS}$ ($R = 0.996$, $p = 0.055$), (Table 4). No other physico-chemical characteristics of the SiNPs that were measured were significantly associated with the potency estimates of SiNP exposure (Table S7).

Discussion

The SiNPs induced cytotoxicity and stimulated the release of inflammatory mediators. Despite the similar size of the SiNPs, a difference in their cytotoxic and inflammatory potency was observed across all cell lines. The impact of cellular function and species origin on the toxicological potential of the SiNPs was made apparent in this work. As previously shown, based on a variety of cytotoxicological endpoints, macrophages are more sensitive than epithelial cells to exposures to particles. This has been demonstrated in exposures to urban air particles (Breznan et al., 2016), carbon nanotubes (Kumarathasan et al., 2015), soluble metals from combustion-derived particulates (Riley et al., 2005) or various metallic nanomaterials (Lanone et al., 2009). This type of cellular response is observed irrespective of the type and origin of the particles (e.g. environmental and engineered), suggesting that it may relate to the functional difference of the cell types.

The lower rate of endocytic particle uptake by epithelial cells is consistent with the barrier-type function of the alveolar epithelium, in contrast to the rapid phagocytic uptake of particles by macrophages associated with their clearance function. The J774A.1 macrophages take up polystyrene particles by phagocytosis and micropinocytosis, in contrast to A549 epithelial cell's uptake by clathrin- and caveolae-mediated endocytic pathways

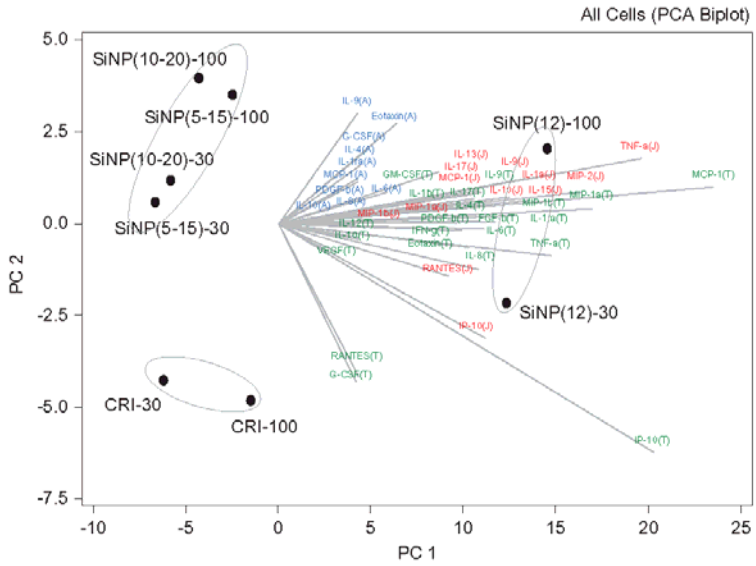

Figure 4. Cytokine drivers of particle effects in A549, THP-1 and J774A.1 cell lines. Principal component analysis was conducted to identify the principal components that explain majority of the variability in the dataset. The cytokine data from cell exposures to particles (30, 100 μg/cm^2) were expressed as fold-effect over control, adjusted for cytotoxicity and log(2) transformed. The bi-plot is a combination of the score plot which shows the score of each PC for each particle observation and the loading plot which shows the load of each cytokine on the identified PC. The letters A, J and T in brackets following the cytokines abbreviate A549, J774A.1 and THP-1 cells, in which the specific analyte was assessed.

(Kuhn et al., 2014). In the present study, cytotoxic potency profile of the SiNPs was correlated between the macrophages and epithelial cells. In contrast, the inflammatory potency profile was only correlated between the J774A.1 and THP-1 cells, but not between these macrophage cell lines and the epithelial A549 cells. Although the cytotoxic ranking of the SiNPs was comparable across the cell lines, the J774A.1 cells were the most sensitive to SiNP exposure. Similarly, rat lung epithelial cells (RLE-6TN) are shown to be more sensitive to metal exposures than A549 cells, while displaying similar cytotoxic trends (Riley et al., 2005). In agreement, pathway analysis of J774A.1 cytokine/chemokine profile highlighted apoptosis/necrosis of blood cells as one of the top functions associated with the silica-based particles. The cell death function was not identified in the THP-1 and A549 profiles.

The cytotoxic and inflammatory potency-based ranking of the particles across the cell lines and the integrated potency estimate $I\beta_{CELLS}$ revealed that SiNP (12 nm) was the most potent particle. While CRI had a low cytotoxic potency ($\beta_{V\ CELLS}$) ranking, it was highly ranked by its inflammatory potency ($\beta_{I-V\ CELLS}$) indicating that it is a potent trigger for cytokine release in macrophages. However, it was inhibitory to a number of cytokines in A549 cells. Similarly, crystalline or amorphous silica-based particles are highly cytotoxic in mouse alveolar macrophages (MH-S), while epithelial cell lines MLE, NIH-3T3, MDCK and HeLa are virtually resistant (Costantini et al., 2011). In the present study, CRI displayed low cytotoxic potency relative to SiNPs, however it had some impact at the highest dose of exposure in the macrophages.

The PCA revealed contrasting cytokine/chemokine profiles across cell lines exposed to particles, highlighting the contributions of IL-9, eotaxin in A549 cells; G-CSF, IP-10, MCP-1, MIP-1α, MIP-1β, RANTES, TNF-α in THP-1 cells; and IL-10, IP-10, MIP-2, RANTES, TNF-α in J774A.1 cells. Although SiNP (12 nm) elicited an increase in IL-9 and eotaxin levels in A549 cells, these markers were inhibited by CRI exposure, while SiNP (5–15 nm) and (10–20 nm) induced an intermediate response. Eotaxin, MIP-1α, MCP-1 and RANTES stimulate the chemotaxis of eosinophils and other leukocytes from circulation to the airways, inducing eosinophilic lung inflammation (Lloyd & Gutierrez-Ramos, 2003). Overexpression of IL-9 in allergen-exposed TG5 mice results in lung eosinophilia, increased serum IgE and bronchial hyperresponsiveness (McLane et al., 1998). Similarly, exogenous IL-9 induces expression of eosinophil chemotactic factors including eotaxin in cultured lung epithelial cells (Dong et al., 1999). The induction of the CC-chemokines in A549 cells suggests that the SiNPs, especially SiNP (12 nm) may uniquely induce a potentially pro-allergic milieu. However, these observations require further *in vivo* study to ascertain the hypothesis. Interestingly, PEG-SiNPs (90 nm) cause innate immune responses at high doses in non-allergic mice and induce Th2/Th17 adjuvant effects at low doses in ovalbumin-sensitized BALB/c mice (Brandenberger et al., 2013).

The pathway analysis also highlighted the likelihood of disturbance in lipid metabolism, release of ROS and changes in cytosolic Ca^{2+} concentrations in the A549 cells. The observations were underscored by the enhanced production of eotaxin, MCP-1 and IL-8 in common between the indicated cellular functions, in addition to other function-specific analytes observed. In fact, amorphous SiNPs have been shown to induce ER stress, dysregulation of Ca^{2+} homeostasis, activation of MAP-kinase and target genes (*cJun*, *cMyc*, *CREB*), induction of oxidative stress and a down-regulation of *p53* in Huh7 human hepatoma cells (Christen et al., 2014). Together, these pathways inhibit apoptosis and induce cell proliferation in response to SiNP exposures. In addition, the association of SiNP effects with lipid metabolism in A549 cells suggests the need to examine potential changes in the synthesis of pulmonary surfactant by the epithelial cells and the levels of eicosanoids, which can act as potent neutrophil chemoattractants (Hurley et al., 2011).

Similarity in the inflammatory response to particles was observed between THP-1 and J774A.1 cells. The cytokine/chemokine profile of the macrophages was indicative of an environment

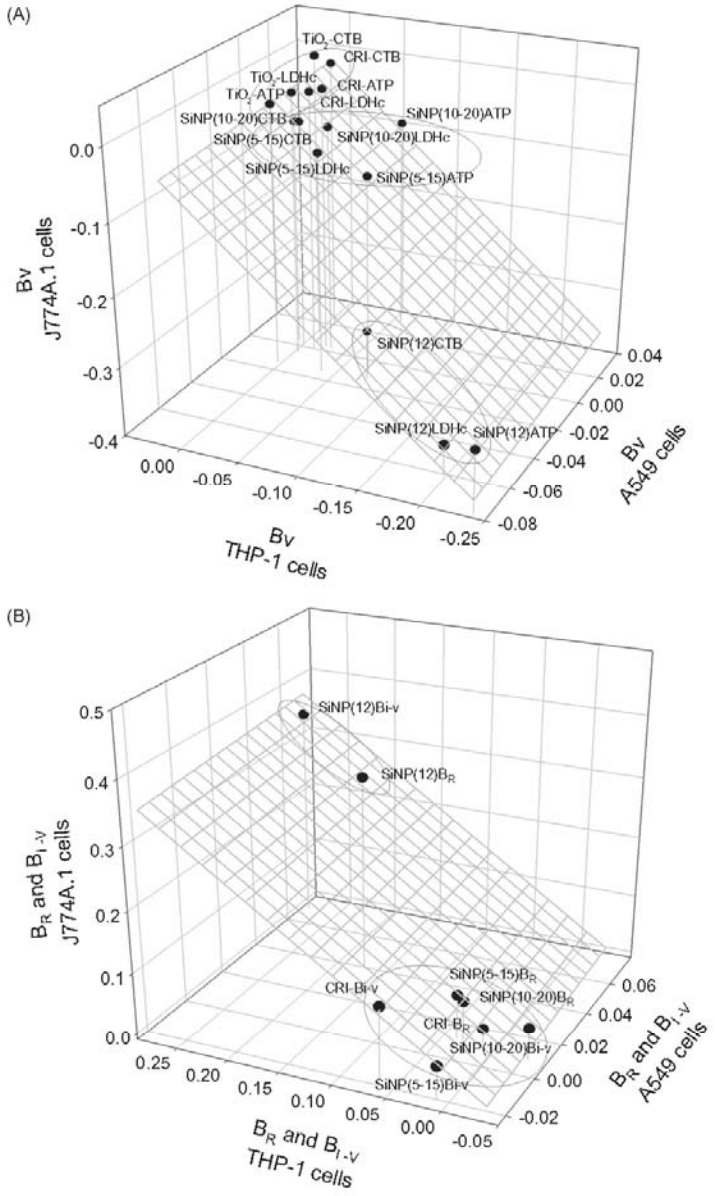

Figure 5. **(A)** Plot showing the distribution of the particles based on their cytotoxic potency (β_v) as measured by CTB, ATP and LDH assay (cell content), with a left to right and top to bottom direction of increasing potency. Three-way ANOVA, *PM* main effect, $p < 0.001$, SINP (12 nm) vs. SINP (10–20 nm), SINP (5–15 nm), SiO_2 and TiO_2, $p < 0.001$; SINP (5–15 nm) vs. SiO_2 and TiO_2, $p < 0.05$; *Cells* main effect, $p < 0.001$, A549 vs. J774A.1 vs THP-1, $p < 0.001$; *Assay* main effect, $p = 0.004$, CTB vs ATP, LDH, $p < 0.05$; **(B)** Plot showing the association of the consensus biological reactivity (β_R; average of absolute values of cytotoxic potency) and consensus inflammatory potency ($\beta_{I\text{-}V}$; average of cytokine potency) of the particles in A549, J774A.1 and THP-1 cells with a right to left and bottom to top direction of increasing potency. Three-way ANOVA, *PM* main effect, $p < 0.001$, SINP (12 nm) vs. SINP (10–20 nm), SINP (5–15 nm) and SiO_2, $p < 0.001$; *Cells* main effect, $p < 0.001$, A549 vs. J774A.1, $p < 0.001$, THP-1 vs. J774A.1, A549, $p < 0.05$; *Potency Estimate*, $p = 0.064$, not significant.

for proliferation, recruitment, differentiation and maturation of leukocytes. Several mediators including G-CSF, IL-10, IP-10, MCP-1, MIP-1α, MIP-1β MIP-2, RANTES and TNF-α were highlighted by the PCA as the main drivers of the contrasting cellular response to the particles. With the exception of TNF-α, IL-10 and G-CSF, these mediators are CC-/CXC-family chemokines, involved in the recruitment of leukocytes and other cell types to sites of inflammation (Comerford & McColl, 2011). Tumor necrosis factor-α is generated primarily by activated macrophages and is involved in the regulation of inflammation, apoptosis, cell proliferation and cell differentiation (Smith et al., 1990), while G-CSF is a glycoprotein growth and survival factor for granulocytes and a potent neutrophil attractant (Metcalf, 1985). Interleukin-10 inhibits monocyte/macrophage and neutrophil cytokine production and Th1-type lymphocyte responses (Cuneo & Autieri, 2009; Opal & DePalo, 2000). Similarly to the present report, a whole-genome microarray

Table 2. Integrated (cytotoxic and inflammatory) particle potency estimates across cell lines (A549, J774A.1 and THP-1).

	Cytotoxic potency				Inflammatory potency			Overall Potency		
Particle	$\beta_{V\ CELLS}$	$\beta_{R\ CELLS}$	Relative Potency (%)	Potency Ranking	$\beta_{I\text{-}V\ CELLS}$	Relative Potency (%)	Potency Ranking	$I\beta_{CELLS}$	Relative Potency (%)	Potency Ranking
SINP (12 nm)	−0.174	0.175	100	1	0.231	100	1	0.203	100	1
CRI (2–6 μm)	−0.009	0.014	7.7	4	0.053	22.9	2	0.034	16.5	2
SINP (5–15 nm)	−0.034	0.038	21.4	2	0.012	5.2	3	0.025	12.1	3
SINP (10–20 nm)	−0.025	0.033	18.8	3	0.006	2.6	4	0.020	9.6	4

Consensus cytotoxic potency $\beta_{V\ CELLS}$ is the average of the cytotoxic potency of the particles in *in vitro* assays from individual cell lines.
Biological reactivity of the particles $\beta_{R\ CELLS}$ represents the average of absolute values of cytotoxic potency β_V.
Consensus inflammatory potency $\beta_{I\text{-}V\ CELLS}$ is the average of cytokine and chemokine levels in cell culture supernatants of individual cell lines.
Integrated potency $I\beta_{CELLS}$ indicates average of potency estimates β_R and $\beta_{I\text{-}V}$ determined for A549, J774A.1 and THP-1 cells.
Relative potency (%) and potency ranking for cytotoxicity are based on $\beta_{R\ CELLS}$.

Table 3. Top cellular function categories from IPA (highest Z-scores) of the cell lines exposed to 30 and 100 μg/cm^2 doses of the particles.

Affected cellular functions	A549	THP-1	J774A.1
Lipid metabolism	√		
Molecular transport	√		
Small molecule biochemistry	√		
Cell morphology		√	
Cell death and survival			√
Cellular growth and proliferation		√	√
Cellular development		√	√
Cellular movement	√	√	√
Cell to cell signaling and interaction	√	√	√

Table 4. Pearson's product moment correlations of the average particle potency estimates *in vitro* and the physico-chemical characteristics of the SiNPs.

Potency estimate	Size agglom	Surface (–OH)	Transition Met
$\beta_{R\ CELLS}$	0.996	1.000	−0.998
	0.058	0.015	0.037
$\beta_{I\text{-}V\ CELLS}$	0.996	1.000	−0.999
	0.054	0.019	0.033
$I\beta_{CELLS}$	0.996	1.000	−0.999
	0.055	0.018	0.034

Top number (R-value), bottom number (*p* value).
Significant correlations ($p \leq 0.05$, 2-tailed) are in bold-type font and the marginal correlation ($0.05 < p < 0.1$, 2-tailed) is in standard-type font Correlations include SINPs only, mineral particles are excluded as their characterization was limited.
Biological reactivity of the particles $\beta_{R\ CELLS}$ represents the average of absolute values of cytotoxic potency β_V.
Consensus inflammatory potency β is the average of cytokine and chemokine levels in cell culture supernatants of individual cell lines.
Integrated potency $I\beta_{CELLS}$ indicates average of potency estimates B_R and $B_{RI\text{-}V}$ determined for A549, J774A.1 and THP-1 cells Transition metal content was the sum total of transition metals (bold text in Table S1) from ICP-MS/AES.
See Table 1 for the abbreviations of the particle properties.

analysis of RAW264.7 macrophages highlighted a number of neutrophil-attracting chemokines, including Ccl3/MIP-1α and Ccl4/MIP-1β among the most robust early gene regulatory events associated with an exposure to a panel of amorphous (7–500 nm) SiNPs (Waters et al., 2009). The inhibition of G-CSF and the induction of IL-1ra, IL-4, IL-10 in THP-1 cells and IL-10, IL-13 in J774A.1 cells, alongside the overwhelmingly pro-inflammatory response in the macrophages highlight the complexity in the inflammatory and compensatory mechanisms in the presence of the silica-based particles. Exposures of macrophages to crystalline SiO_2 and amorphous SiNPs resulted in cell death (Costantini et al., 2011; Thibodeau et al., 2003). The mechanism involves the regulation of caspase-1 activity through the activation of the NALP3/inflammasome and the IL-1α/IL-1β- and TNF-α-induced inflammatory pathways triggered by SiO_2 (Pétrilli et al., 2007; Rabolli et al., 2014). As reported here, IL-1β, TNF-α levels in THP-1 cells and IL-1α, TNF-α in J774A.1 cells were increased in response to CRI and the SINPs, with markedly higher response to SiNP (12 nm), suggesting that the activation of the inflammasome may be anticipated in the macrophages exposed to SiNP (12 nm).

In vitro toxicity assessments using a single cell line and assay can have a limited predictive capability of the toxicity of particle exposures. Thus, we have attempted to circumvent these limitations by integration of multiple assays and cell line responses to obtain a more comprehensive robust potency estimate that is inclusive of a broader range of toxicity effects from particle exposures. The novel approach described in the present work for reducing, integrating and comparing large datasets of cytotoxicity and inflammatory mediators obtained from cells across functions and species provides meaningful results for examining associations between the biological signatures and physico-chemical factors of the particles. The quantity of SiNP surface –OH groups, a measure of particle surface acidity was correlated with biological reactivity β_R, inflammatory potency $\beta_{I\text{-}V}$ and the integrated potency estimate Iβ. The silanol (Si–O–H) groups on the surface of SiNPs have a strong polar interactivity and can readily bond to water, other polar moieties and biomolecules. In agreement with our correlation results, silanol groups have been implicated in increased cell membrane damage and IL-8 release in A549 mono- and co-cultures (with endothelial cells) exposed to amorphous SiNPs. These effects were further augmented in the presence of alveolar surfactant phospholipids, presumably through increased ROS generation (Kasper et al., 2015). In contrast, lipid/protein-based corona formed around the SiNPs in plasma can protect cells from hemolysis (Shi et al., 2012), but will likely not be protective once the complex becomes internalized and processed by the cells. Silanol-associated hydroxyl concentration/density on the surface of pristine SiNPs was shown by others to be associated with their cytotoxic, inflammatory and hemolytic potential (Pavan et al., 2013; Pavan et al., 2014; Zhang et al., 2012). Specifically, strained three-membered silanol groups on fumed amorphous silica surfaces showed the highest potential for cytotoxicity and hemolysis (Zhang et al., 2012). Moreover, in the case of crystalline silica polymorphs, the density of surface geminal (but not single) silanol groups appears to be associated with hemolysis, as shown through molecular modeling (Murashov et al., 2006). Furthermore, acute inflammatory response of C57BL/6 mice to oropharyngeally-instilled SiNPs (16 nm) is attenuated by controlled adjustment of silanol display on the particle surface using calcination and metal (titanium, aluminum) doping (Sun et al., 2015).

Although biological potency estimates did not correlate with total metal content of the SiNPs in the present study, negative correlation with transition metal content was obtained. We observed that SiNPs with higher transition metal content had lower surface acidity and potency (e.g. SiNP (12 nm) vs. (5–15 nm) and

(10–20 nm)). In line with Sun et al. (2015), we hypothesize that increased transition metal content (or specific metals) may contribute to the attenuation of SiNP toxicity by occupying free reactive silanols, reducing silanol display and thereby surface reactivity. We also noted a marginally-significant positive correlation of biological potency with dry-state agglomerate size of the SiNPs, likely a consequence of higher electrostatic interaction of the SiNPs which have higher surface silanol coverage. The density of surface silanols can also be a determinant of electrostatic interaction of fumed SiNPs with membrane phospholipids (Zhang et al., 2012).

Recent reports highlight the importance of characterizing nanoparticle interactions in liquid suspensions and their impact on *in vitro* dosimetry, along with determining sedimentation and diffusion rates of suspended nanoparticle agglomerates and non-agglomerated particles to improve estimates of dose delivered to cells (Cohen et al., 2013; DeLoid et al., 2014; Liu et al., 2015; Pal et al., 2015). Correction of the β potency estimates for the effective delivered dose of the SiNPs in the present study indicated a 64% (1.64×) increase in deposited dose of SiNP (12 nm) relative to the other SiNPs. However, based on the integrated potency estimates, SiNP (12 nm) was 6–10× more potent than the other SiNPs tested (Table 2). Therefore, in the present study, the difference in the SiNP deposition did not account for the marked difference in potency between SiNP (12 nm) and the other SiNPs tested, as well, it did not modify the hazard ranking of the nanoparticles.

Conclusion

Despite similar primary particle size, SiNPs tested had distinct cytotoxicity profiles, comparable across species and cell types. In contrast, the pro-inflammatory potential of the SiNPs in the different cell lines was more nuanced, emphasizing the role of a specific cell type in the toxicological outcome. The pathway analysis revealed distinct cell type-associated cellular functions that may be differentially impacted upon by the particles.

The SiNP (12 nm) was identified as the most potent nanoparticle, with particle surface acidity associated with its cytotoxic and inflammatory potency across the cell lines. Associations with other SiNP properties including dry-state agglomerate size and transition metal components highlight the need for refined understanding of the interrelationships between the various physico-chemical properties. The integration of cytotoxicity and pro-inflammatory endpoints appears to be a promising approach for the derivation of simple but robust potency indices in screening assessment of nanoparticle toxicity. However, due to the heterogeneity of the physico-chemical properties of nanoparticles and their interactions in biological matrices, it remains necessary to test all particles on a case-by-case basis and to conduct targeted validations via *in vivo* animal exposure studies.

Acknowledgements

The authors would like to thank Drs. Daniel Desaulniers and Azam Tayabali for reviewing the manuscript. We are grateful to Andrew Ha, Dawn Jurgens and Tina Tuck for their technical contributions. Drs. Julie S. O'Brien and Surendra Nimesh are recipients of the NSERC Visiting Fellows Award. Ngoc Q. Vuong is a recipient of the Ontario Graduate Scholarship.

Disclosure statement

The authors declare that they have no competing interests. This work was supported by the Chemicals Management Plan (CMP) and the Nanotechnology Section funds, Health Canada.

Funding

This work has been funded by the Chemicals Management Plan and the Nanotechnology Section funds (Health Canada).

References

Brandenberger C, Rowley NL, Jackson-Humbles DN, Zhang Q, Bramble LA, Lewandowski RP, et al. 2013. Engineered silica nanoparticles act as adjuvants to enhance allergic airway disease in mice. Part Fibre Toxicol 10:26.

Breznan D, Karthikeyan S, Phaneuf M, Kumarathasan P, Cakmak S, Denison MS, et al. 2016. Development of an integrated approach for comparison of in vitro and in vivo responses to particulate matter. Part Fibre Toxicol 13:41.

Byrne JD, Baugh JA. 2008. The significance of nanoparticles in particle-induced pulmonary fibrosis. Mcgill J Med 11:43–50.

Chen X, Zhouhua W, Jie Z, Xinlu F, Jinqiang L, Yuwen Q, et al. 2014. Renal interstitial fibrosis induced by high-dose mesoporous silica nanoparticles via the NF-κB signaling pathway. Int J Nanomedicine 10:1–22.

Choi M, Cho WS, Han BS, Cho M, Kim SY, Yi JY, et al. 2008. Transient pulmonary fibrogenic effect induced by intratracheal instillation of ultrafine amorphous silica in A/J mice. Toxicol Lett 182:97–101.

Christen V, Camenzind M, Fent K. 2014. Silica nanoparticles induce endoplasmic reticulum stress response, oxidative stress and activate the mitogen-activated protein kinase (MAPK) signaling pathway. Toxicol Rep 1:1143–51.

Cohen J, Deloid G, Pyrgiotakis G, Demokritou P. 2013. Interactions of engineered nanomaterials in physiological media and implications for *in vitro* dosimetry. Nanotoxicology 7:417–31.

Cohen JM, Teeguarden JG, Demokritou P. 2014. An integrated approach for the *in vitro* dosimetry of engineered nanomaterials. Part Fibre Toxicol 11:20.

Comerford I, McColl SR. 2011. Mini-review series: focus on chemokines. Immunol Cell Biol 89:183–4.

Costantini LM, Gilberti RM, Knecht DA. 2011. The phagocytosis and toxicity of amorphous silica. PLoS One 6:e14647.

Cuneo AA, Autieri MV. 2009. Expression and function of anti-inflammatory interleukins: the other side of the vascular response to injury. Curr Vasc Pharmacol 7:267–76.

Das DD, Harlick PJE, Sayari A. 2007. Applications of pore-expanded MCM-41 silica: 4. synthesis of a highly active base catalyst. Catal Comm 8:829–33.

Das DD, Yang Y, O'Brien JS, Breznan D, Nimesh S, Bernatchez S, et al. 2014. Synthesis and physicochemical characterization of mesoporous SiO_2 nanoparticles. J Nanomater 12:e176015.

Davis GS. 1986. The pathogenesis of silicosis. State of the art. Chest 89:166S–9S.

DeLoid G, Cohen JM, Darrah T, Derk R, Rojanasakul L, Pyrgiotakis G, et al. 2014. Estimating the effective density of engineered nanomaterials for *in vitro* dosimetry. Nat Commun 5:3514.

Ding M, Chen F, Shi X, Yucesoy B, Mossman B, Vallyathan V. 2002. Diseases caused by silica: mechanisms of injury and disease development. Int Immunopharmacol 2:173–82.

Dong Q, Louahed J, Vink A, Sullivan CD, Messler CJ, Zhou Y, et al. 1999. IL-9 induces chemokine expression in lung epithelial cells and baseline airway eosinophilia in transgenic mice. Eur J Immunol 29:2130–9.

Eitan A, Jiang K, Dukes D, Andrews R, Schadler LS. 2003. Surface modification of multiwalled carbon nanotubes: toward the tailoring of the interface in polymer composites. Chem Mater 15:3198–201.

Fruijtier-Pölloth C. 2012. The toxicological mode of action and the safety of synthetic amorphous silica-a nanostructured material. Toxicology 294:61–79.

Golbamaki N, Rasulev B, Cassano A, Marchese, Robinson RL, Benfenati E, et al. 2015. Genotoxicity of metal oxide nanomaterials: review of recent data and discussion of possible mechanisms. Nanoscale 7:2154–98.

Hnizdo E, Sluis-Cremer GK. 1993. Risk of silicosis in a cohort of white South African gold miners. Am J Ind Med 24:447–57.

Hunter RJ. 2006. Electrokinetics of particles. In: Somasundaram P, ed. Encyclopedia of surface and colloid science. Boca Raton: CRC Press, 2220–32.

Hurley BP, Pirzai W, Mumy KL, Gronert K, McCormick BA. 2011. Selective eicosanoid-generating capacity of cytoplasmic phospholipase A2 in *Pseudomonas aeruginosa*-infected epithelial cells. Am J Physiol Lung Cell Mol Physiol 300:L286–94.

Jacobs R, van der Voet H, Ter Braak CJ. 2015. Integrated probabilistic risk assessment for nanoparticles: the case of nanosilica in food. J Nanopart Res 17:251.

Johnston CJ, Driscoll KE, Finkelstein JN, Baggs R, O'Reilly MA, Carter J, et al. 2000. Pulmonary chemokine and mutagenic responses in rats after subchronic inhalation of amorphous and crystalline silica. Toxicol Sci 56:405–13.

Kasper JY, Feiden L, Hermanns MI, Bantz C, Maskos M, Unger RE, et al. 2015. Pulmonary surfactant augments cytotoxicity of silica nanoparticles: Studies on an *in vitro* air-blood barrier model. Beilstein J Nanotechnol 6:517–28.

Kim BY, Rutka JT, Chan WC. 2010. Nanomedicine. N Engl J Med 363:2434–43.

Kuhn DA, Vanhecke D, Michen B, Blank F, Gehr P, Petri-Fink A, et al. 2014. Different endocytotic uptake mechanisms for nanoparticles in epithelial cells and macrophages. Beilstein J Nanotechnol 5:1625–36.

Kumarathasan P, Breznan D, Das D, Salam MA, Siddiqui Y, MacKinnon-Roy C, et al. 2015. Cytotoxicity of carbon nanotube variants: a comparative *in vitro* exposure study with A549 epithelial and J774 macrophage cells. Nanotoxicology 9:148–61.

Kwon JY, Koedrith P, Seo YR. 2014. Current investigations into the genotoxicity of zinc oxide and silica nanoparticles in mammalian models *in vitro* and *in vivo*: carcinogenic/genotoxic potential, relevant mechanisms and biomarkers, artifacts, and limitations. Int J Nanomedicine 9:271–86.

Lanone S, Rogerieux F, Geys J, Dupont A, Maillot-Marechal E, Boczkowski J, et al. 2009. Comparative toxicity of 24 manufactured nanoparticles in human alveolar epithelial and macrophage cell lines. Part Fibre Toxicol 6:14. 30

Lee KP, Kelly DP. 1992. The pulmonary response and clearance of Ludox colloidal silica after a 4-week inhalation exposure in rats. Fundam Appl Toxicol 19:399–410.

Liu R, Liu HH, Ji Z, Chang CH, Xia T, Nel AE, et al. 2015. Evaluation of toxicity ranking for metal oxide nanoparticles via an *in vitro* dosimetry model. ACS Nano 9:9303–13.

Lloyd CM, Gutierrez-Ramos JC. 2003. Regulation of cellular traffic in the asthmatic lung. In: Lambrecht BN, Hoogsteden HC, Diamant Z, eds. The immunological basis of asthma. Boca Raton: CRC Press, 409–38.

McLane MP, Haczku A, van de Rijn M, Weiss C, Ferrante V, MacDonald D, et al. 1998. Interleukin-9 promotes allergen-induced eosinophilic inflammation and airway hyperresponsiveness in transgenic mice. Am J Respir Cell Mol Biol 19:713–20.

Metcalf D. 1985. The granulocyte-macrophage colony-stimulating factors. Science 229:16–22.

Michel K, Scheel J, Karsten S, Stelter N, Wind T. 2013. Risk assessment of amorphous silicon dioxide nanoparticles in a glass cleaner formulation. Nanotoxicology 7:974–88.

Miyata R, van Eeden SF. 2011. The innate and adaptive immune response induced by alveolar macrophages exposed to ambient particulate matter. Toxicol Appl Pharmacol 257:209–26.

Murashov V, Harper M, Demchuk E. 2006. Impact of silanol surface density on the toxicity of silica aerosols measured by erythrocyte haemolysis. J Occup Environ Hyg 3:718–23.

Nadeau D, Vincent R, Kumarathasan P, Brook J, Dufresne A. 1996. Cytotoxicity of ambient air particles to rat lung macrophages: Comparison of cellular and functional assays. Toxicol in Vitro 10:161–72.

Napierska D, Thomassen LC, Lison D, Martens JA, Hoet PH. 2010. The nanosilica hazard: another variable entity. Part Fibre Toxicol 7:39.

Nieboer E, Richardson DHS. 1980. The replacement of the nondescript term 'heavy metals' by a biologically and chemically significant classification of metal ions. Environ Pollut Series B, Chem and Phys 1:3–26.

Opal SM, DePalo VA. 2000. Anti-inflammatory cytokines. Chest 117:1162–72.

Pal AK, Bello D, Cohen J, Demokritou P. 2015. Implications of *in vitro* dosimetry on toxicological ranking of low aspect ratio engineered nanomaterials. Nanotoxicology 9:871–85.

Park JH, Gu L, von Maltzahn G, Ruoslahti E, Bhatia SN, Sailor MJ. 2009. Biodegradable luminescent porous silicon nanoparticles for *in vivo* applications. Nat Mater 8:331–6.

Pavan C, Tomatis M, Ghiazza M, Rabolli V, Bolis V, Lison D, Fubini B. 2013. In search of the chemical basis of the hemolytic potential of silicas. Chem Res Toxicol 26:1188–98.

Pavan C, Rabolli V, Tomatis M, Fubini B, Lison D. 2014. Why does the hemolytic activity of silica predict its pro-inflammatory activity?. Part Fibre Toxicol 11:76.

Pétrilli V, Dostert C, Muruve DA, Tschopp J. 2007. The inflammasome: a danger sensing complex triggering innate immunity. Curr Opin Immunol 19:615–22.

Pope CA 3rd, Burnett RT, Krewski D, Jerrett M, Shi Y, Calle EE, et al. 2009. Cardiovascular mortality and exposure to airborne fine particulate matter and cigarette smoke: shape of the exposure-response relationship. Circulation 120:941–8.

Rabolli V, Thomassen LC, Princen C, Napierska D, Gonzalez L, Kirsch-Volders M, et al. 2010. Influence of size, surface area and microporosity on the *in vitro* cytotoxic activity of amorphous silica nanoparticles in different cell types. Nanotoxicology 4:307–18.

Rabolli V, Thomassen LC, Uwambayinema F, Martens JA, Lison D. 2011. The cytotoxic activity of amorphous silica nanoparticles is mainly influenced by surface area and not by aggregation. Toxicol Lett 206:197–203.

Rabolli V, Badissi AA, Devosse R, Uwambayinema F, Yakoub Y, Palmai-Pallag M, et al. 2014. The alarmin IL-1α is a master cytokine in acute lung inflammation induced by silica micro- and nanoparticles. Part Fibre Toxicol 11:69.

Reich M, Liefeld T, Gould J, Lerner J, Tamayo P, Mesirov JP. 2006. GenePattern 2.0. Nat Genet 38:500–1.

Riley MR, Boesewetter DE, Turner RA, Kim AM, Collier JM, Hamilton A. 2005. Comparison of the sensitivity of three lung derived cell lines to metals from combustion derived particulate matter. Toxicol in Vitro 19:411–19.

Saldanha AJ. 2004. Java Treeview-extensible visualization of microarray data. Bioinformatics 20:3246–8.

Schwende H, Fitzke E, Ambs P, Dieter P. 1996. Differences in the state of differentiation of THP-1 cells induced by phorbol ester and 1,25-dihydroxyvitamin D3. J Leukoc Biol 59:555–61.

Shi J, Hedberg Y, Lundin M, Odnevall Wallinder I, Karlsson HL, Möller L. 2012. Hemolytic properties of synthetic nano- and porous silica particles: the effect of surface properties and the protection by the plasma corona. Acta Biomater 8:3478–90.

Smith CA, Davis T, Anderson D, Solam L, Beckmann MP, Jerzy R, et al. 1990. A receptor for tumor necrosis factor defines an unusual family of cellular and viral proteins. Science 248:1019–23.

Sun B, Pokhrel S, Dunphy DR, Zhang H, Ji Z, Wang X, et al. 2015. Reduction of acute inflammatory effects of fumed silica nanoparticles in the lung by adjusting silanol display through calcination and metal doping. ACS Nano 9:9357–72.

Thibodeau M, Giardina C, Hubbard AK. 2003. Silica-induced caspase activation in mouse alveolar macrophages is dependent upon mitochondrial integrity and aspartic proteolysis. Toxicol Sci 76:91–101.

Vincent R, Goegan P, Johnson G, Brook JR, Kumarathasan P, Bouthillier L, et al. 1997. Regulation of promoter-CAT stress genes in HepG2 cells by suspensions of particles from ambient air. Fundam Appl Toxicol 39:18–32.

Waters KM, Masiello LM, Zangar RC, Tarasevich BJ, Karin NJ, Quesenberry RD, et al. 2009. Macrophage responses to silica nanoparticles are highly conserved across particle sizes. Toxicol Sci 107:553–69.

Zhang H, Dunphy DR, Jiang X, Meng H, Sun B, Tarn D, et al. 2012. Processing pathway dependence of amorphous silica nanoparticle toxicity: colloidal vs pyrolytic. J Am Chem Soc 134:15790–804.

Curriculum Vitae

Ngoc Quang Vuong

---

† EDUCATION †

Ph.D. in Biochemistry 2010 – present
University of Ottawa, Ottawa, Ontario, Canada
Thesis: Fingerprinting the effect of airborne particulate matter via *in vitro* toxicoproteomics.
Research project summary:

The goal of my project was to establish an *in vitro* toxicoproteomic approach that is capable of distinguishing the differences in cellular response to airborne particulate matter (PM) from various environments linked to defined sources of emission, for air regulation purpose.

Technical Works:

-Conducted cyctotoxicity assays such as lactate dehydrogenase (LDH), 5-bromo-2'-deoxyuridine (BrdU), ATP and resazurin reduction are used to determine the toxic potency of the test particles on cells.

-Proteomic analyses (such as two-dimensional gel electrophoresis and mass spectrometry) were conducted to determine the unique changes in the proteome of cells following exposure to particles to elucidate the molecular details delineating the mechanism of toxicity.

-Gene analysis (such as RT-PCR) was performed to further understand the responses of cells to PM at the transcriptional level.

-Carry out statistic and bio-informatic analyses with various softwares such as Excel, R and Ingenuity Pathway Analysis.

Mentor/supervisor duty:

-Supervised and mentored undergraduate students to carry out their honours research projects or co-op work in the field of proteomics and genomics.

-Taught the students how to: search and review the literatures pertinent to their research projects, conduct laboratory work and perform data analysis, report and present their data in a poster or a thesis.

M.Sc. in Biochemistry 2010
University of Ottawa, Ottawa, Ontario, Canada
Thesis: Imaging the nicotinic acetylcholine receptor reconstituted in a POPC membrane.
Research project summary:

Work in collaboration between the University of Ottawa and the National Research Council of Canada on a joint project to image and to assess the interaction between the nicotinic acetylcholine receptor (nAChR) and its reconstituted lipid membrane.

Technical Works:

-Purify the nAChR from the electric organ of the Torpedo electric fish via affinity column chromatography

-Reconstitute the purified receptor in a membrane of defined lipid composition.

-The functionality of the receptor (the ability of the nAChR to gate open the ion channel in response to ligand binding) is characterized by differential Fourier transformed infrared spectroscopy.

-The reconstituted samples are then prepared on an atomically flat mica surface for atomic force microscopy (AFM) imaging.

B.Sc. in Biochemistry

2002 University of Ottawa, Ottawa, Ontario, Canada

Thesis: Elucidation of the lipid composition of rafts isolated from non-capacitated and capacitated pig sperm.

Research project summary:

Work in an in vitro fertilization (IVF) laboratory to dissect the molecular mechanisms that are essential for sperm fertility.

Technical Works:

-Collect sperm and egg from mice for IVF studies.

-Extracted lipids from mouse and pig sperm to characterized the lipid composition and related different lipid species to fertility in sperm.

-Assess lipid contents from the extracts using thin layer chromatography and mass spectrometry.

---

† WORK EXPERIENCE †

Postdoctoral Fellow

Ottawa Hospital Research Institute, Ottawa, Ontario, Canada 2017 – present

Research scope:

Work in a reproductive biology/urology laboratory to assess whether antimicrobial peptides (AMPs) in the semen of male partners contribute significant defence against infection in female genitourinary tract.

Technical works:

-Extract AMPs from semen and urine of humans and animals.

-Culture bacteria from urine of patients that have been contracted with UTI.

-Assess bactericidal potencies of the extracted AMPs against the cultured bacteria.

-Identify the potent AMPs using various proteomic methods such as SDS-PAGE, western blot and mass spectrometry.

Biologist: 2008 – 2010

Health Canada, Ottawa, Ontario Canada

Work in an *Inhaltion Toxicology Laboratory* to investigate the toxic effects of airborne particulate matter (PM) through *in vitro* and *in vivo* models.

Technical Works:

-Prepare clean polyurethane filters such as PM10 (aerodynamic diameter > 10 μm), PM2.5 (10 – 2.5 μm) and PM1 (2.5 – 1.0 μm), and polypropylene ultrafine filter (<1.0 μm) that are used to collect ambient air particles.
-Extract particles from PM10, PM2.5, PM1 and ultrafine filters.
-Prepare the extracted particles for different toxicological studies.
-Examine, collect and process tissues and organs from the particle exposed animals in preparation for downstream studies.
-Organize, analyze and interpret toxicological data through the use of graphical, statistical, and database software including PowerPoint, Excel, Access, R, Word and Sigma Plot.
-Assist in the writing of scientific reports and papers for publication, which include data preparation and literature search and acquisition.
-Develop standard operating protocols for different experiments used in various studies such as preparation of clean polyurethane and polypropylene filters, extraction of particles from filters, and tissues processing and weighing.

Technical Officer 2007 – 2008
National Research Council of Canada, Ottawa, Ontario, Canada
Work in a team of chemist, physicist and biochemist to develop a high-resolution microscopy technique used to examine the molecular organization and/or interaction of lipids and proteins in model and biological membranes.
Technical Works:
-Purify and reconstitute membrane proteins in artificial lipid bilayers for high resolution imaging with atomic force microscopy (AFM).
-Provide microscopic training for new comers and collaborators.
-Maintain and trouble shoot microscopic and analytical instruments such as AFM and HPLC

Teaching Assistant 2005 – 2007
University of Ottawa, Ottawa, Ontario, Canada
Introduction to Organic Chemistry Laboratory
-Supervise and instruct a large group of students to perform and interpret simple experiments such as recrystallization, distillation, extraction, as well as Grignard, E1, SN1 and SN2 reactions.
-Teach the students to write report in a concise manner, and assess their comprehension.
Introduction to Biochemistry Laboratory
-Demonstrate to second year students basic biochemistry experiments such as ion exchange chromatography, amino acid titration and SDS-PAGE in a precise and time efficient manner.
-Constructively criticize lab reports to encourage students to develop critical thinking.
Protein Structure and Function
-Assist third year students to grasp the principles behind modern physics methods use to study protein structures and function, protein folding and engineering, mechanisms of enzyme action, enzyme kinetics, and regulation of enzyme activity.
-Taught the students to view and generate protein structure model from Protein Data Bank with molecular modeling software such as PyMol.

Technical Officer 2003 – 2004

National Research Council of Canada, Ottawa, Ontario, Canada

-Develop a method for the preparation of a solid support bilayer and monolayer.

-Use atomic force microscopy to examine whether the reconstituted rhodopsin has preferential interaction with liquid disordered phase in a domain forming membrane.

-Assist in the photochemistry study of psoralen and coumarin in HSA complexes and DMPC vesicle by UV/Vis and fluorescence spectroscopy.

Student/Research Assistant 2000 – 2003

Ottawa Health Research Institute (OHRI), Ottawa, Ontario, Canada

-Work with mice to study *in vivo* and *in vitro* fertilization.

-Collect and culture sperm from the epididymis of mice, and obtained oocytes from the ovaries of mice by microscopic dissection.

-Investigate the toxicological of air particles such as ozone and airborne PM collected in the Ottawa region on the male reproductive system of rat.

---

† AWARDS †

1) Excellence Scholarship from the University of Ottawa (2010 - 2015)

2) Ontario Graduate Scholarship (2011 - 2012, 2012 - 2013 and 2013 - 2014)

3) Queen Eliziabeth II Graduate Scholarship in Science and Technology (2010 - 2011)

---

† PUBLICATIONS †

1. **Vuong NQ**, Breznan D, Goegan P, O'Brien JS, Williams A, Karthikeyan S, Kumarathasan P and Vincent R. *In vitro* toxicoproteomic analysis of A549 human lung epithelial cells exposed to urban air particulate matter and its water-soluble and insoluble fractions. Particle and Fibre Toxicology. 2017 Oct 2;14(1):39.

2. Breznan D, Das DD, O'Brien JS, MacKinnon-Roy C, Nimesh S, **Vuong NQ**, Bernatchez S, DeSilva N, Hill M, Kumarathasan P, Vincent R. Amorphous silicon dioxide nanoparticles of similar size display differential cytotoxicity in multiple cell lines: Association with surface polarity. Nanotoxicology. 2017 Mar;11(2):223-235.

3. **Vuong NQ**, Goegan P, De Rose F, Breznan D, Thomson E, Williams A, Karthikeyan S, Kumarathasan P and Vincent R. Differential responses of human lung epithelial cells

(A549) to cristobalite and α–quartz identified by *in vitro* toxicoproteomic and toxicogenomic analyses. Journal of Applied Toxicology. 2017 Jun;37(6):721-731.

4. Thomson EM, Breznan D, Karthikeyan S, MacKinnon-Roy C, **Vuong NQ**, Dabek-Zlotorzynska E, Celo V, Charland JP, Kumarathasan P, Brook JR, Vincent R. Contrasting biological potency of particulate matter collected at sites impacted by distinct industrial sources. Particle and Fibre Toxicology. 2016 Dec 1;13(1):65.

5. **Vuong NQ**, Goegan P, Mohattalage S, Breznan D, Ariganello M, Williams A, Elisma F, Karthikeyan S, Vincent R and Kumarathasan P. Proteomic changes in human lung epithelial cells (A549) in response to carbon black and titanium dioxide exposures. Journal of Proteomics. 2016 Oct 21;149:53-63.

6. **Vuong NQ**, Goegan P, Mohattalage S, Breznan D, Ariganello M, Williams A, Elisma F, Karthikeyan S, Vincent R and Kumarathasan P. Human lung epithelial cell A549 proteome data after treatment with titanium dioxide and carbon black. Data in Brief. 2016 Jun 21;8:687-91.

7. Kumarathasan P, Vincent R, Das D, Mohottalage S, Blais E, Blank K, Karthikeyan S, **Vuong NQ**, Arbuckle TE, Fraser WD. Applicability of a high-throughput shotgun plasma protein screening approach in understanding maternal biological pathways relevant to infant birth weight outcome. Journal of Proteomics. 2014 Apr 4;100:136-46.

8. **Vuong N**, Baenziger JE and Johnston JL. Preparation of reconstituted acetylcholine receptor membranes suitable for AFM imaging of lipid-protein interactions. Chemistry and Physics of Lipids. 2010 Feb; 163(2):117-126.

9. Baenziger JE, Ryan SE, Goodreid MM, **Vuong NQ**, Sturgeon RM, and daCosta CJ. Lipid composition alters drug action at the nicotinic acetylcholine receptor. Molecular Pharmacology. 2008 Mar; 73(3):880-90.

10. Bou Khalil M, Chakrabhandu K, Xu H, Weerachatyanukul W, Buhr M, Berger T, Carmona E, **Vuong N**, Kumarathasan P, Wong TTP, Carrier D, and Tanphaichitr N. Sperm Capacitation Induces an Increase in Lipid Rafts Having Zona Pellucida Binding Ability and Containing Sulfogalactosylglycerolipid. Developmental Biology. 2006 Feb; 290(1):220-35.

11. Chen L, Rinco O, Popov J, **Vuong N** and Johnston JL. Psoralen and Coumarin Photochemistry in HSA Complexes and DMPC Vesicle. Photochemistry and Photobiology. 2006 Jan-Feb; 82(1):31-7.

12. Furimsky A, **Vuong N**, Xu H, Kumarathasan P, Xu M, Weerachatyanukul W, Bou Khalil M, Kates M, Tanphaichitr N. Percoll gradient-centrifuged capacitated mouse sperm have increased fertilizing ability and higher contents of sulfogalactosylglycerolipid and docosahexaenoic acid-containing phosphatidylcholine compared to washed capacitated mouse sperm. Biology of Reproduction. 2005 Mar; 72(3):574-83.
